People's Democratic Republic of Algeria

Ministry of Higher Education and Scientific Research

University of Mohamed KhiderBiskra

Faculty of Sciences and Technology

Depratment of Mechanical Engineering

Ref : ……..

جامعة محمد خيضر بسكرة

كلية العلوم والتكنولوجيا

قسم :الهندسة الميكانيكية

المرجع:.....

Thesis Submitted to the Department of Mechanical Engineering to obtain a Doctoral degree

**Option**: Industrial Metals

# *Protection against corrosion of API 5L X70 carbon steel intended to petroleum industry by green inhibitor: SchinusMolle Resin as an eco-friendly inhibitor*

Presented by:

**TAOUI Hicham**

Thesis defended on: 01/07/2020

**Jury committee**

| | | | |
|---|---|---|---|
| BOUMERZOUG Zakaria | Professor | President | University of Biskra |
| CHALA Abdelouahad | Professor | Supervisor | University of Biskra |
| BENTRAH Hamza | MC-A | Co-Supervisor | University of Biskra |
| ABBASSI Ammar | Professor | Examiner | University of Batna 2 |
| NESSARK Belkacem | Professor | Examiner | University of Setif 1 |

# *DEDICATION*

*Every challenging work needs self efforts as well as guidance of elders especially those who are very close to our heart.*

*I dedicate My humble effort to*

*My sweet and loving Father & Mother*

*Whose affection, love, encouragement and prays of day and night made me able to get such success and honor*

*I dedicate this thesis to my*

*Family and friends who have supported meand to my Respected Teachers*

# ***Acknowledgement***

This work was achieved at the Laboratory of Physics of Thin Films and Applications (LPTFA) at the University of Biskra, and the Metallurgy Pedagogical Laboratory of the Department of Mechanical Engineering at the University of Biskra.

Firstly, I would like to express my sincere gratitude to my supervisor Prof CHALA Abdelouahad, for the continuous support of my Ph.D study and related research, and his patience, motivation, and immense knowledge. His guidance helped me all the time of research and writing of this thesis. I could not have imagined having a better advisor and mentor for my Ph.D study.

Besides my supervisor, I would like to thank my co-supervisor Dr.BENTRAH Hamza who has always guided me with his true academic knowledge regarding protection against corrosion. I have been extremely lucky to have such a co-supervisor who cared so much about my work, and who responded to my questions and queries so promptly.

I am extremely thankful to the members of jury, professor ZAKARIA Boumerzoug president, professor AMMAR Abbassi and professor NESSARK Belkacem examiners for serving as my jury members even at hardship. I also want to thank you for letting my defense be an enjoyable moment, and for your brilliant comments and suggestions, thanks to you.

I would like to thank Dr.DJELLAB Mounir for his great help in this thesis. I also want to thank LPCMA laboratory engineer Mr.GASMI Brahim, Mrs.TOUHAMI Hanane and also want to thank the metallurgy laboratory member Mr.SAMIR Dekkiche , Mr.TRIR Boubaker , Mrs.OUAMANE INAS and Mrs.GHANNAI Latifafor their cooperation during the thesis preparation. I would especially like to thank Mrs.TOBBECHE Sana for her encouragement and support.

Last but not the least; I would like to thank my family: my parents, my brothers, sisters, and friends for supporting me spiritually throughout writing this thesis and my life in general.

# *Table of Contents*

# *List of Tables*

## Chapter I:



## Chapter II:



## Chapter III:

# *List of Figures*

## Chapter I:



## Chapter II:

# Chapter III

# *List of Equations*

## Chapter I:



## Chapter II:



## Chapter III:

# *List of Abbreviations*

BRSM: Bark Resin of Shunis Molle

C: Inhibitor concentration

M: Molarity

θ: surface coverage

KI: potassium iodide

$I_{corr}$: corrosion current density

$I_{corr(inh)}$: corrosion current density in presence of inhibitor

$i_{pa}$: anodic peak current

$i_{pc}$ :cathodic peak current

$b_c$: cathodic coefficient

$b_a$: anodic coefficient

$E_{corr}$: corrosion potential

$E_{pa}$: anodic peak potential

$E_{pc}$: cathodic peak potential

$E_{initial}$: Initial potential

$E_{final}$: Final potential

$E_{pas}$: passivation potential

$E_{pit}$: pitting potential

$E_{q=0}$: zero charge potential

OCP: Open Circuit Potential

NHE: Normal Hydrogen Electrode

SCE: Saturated Calomel Electrode

API: American Petroleum Institute

$R_s$: Resistance of solution

$R_p$: Resistance of polarization

$R_t$: Resistance of charge transfer

$\acute{R}_t$ :Resistance of charge transfer in presence of inhibitor

Z: Impedance

$Z_{Im}$: Imaginary part of impedance

$Z_{Re}$: Real part of impedance

EIS: Electrochemical Impedance Spectroscopy

$\eta_{EIS}$: inhibition efficiency calculated from ESI

$\eta_{Pol}$: inhibition efficiency calculated from potentiodynamic polarization

CPE: Constant Phase Element

$C_{dl}$: Double Layer Capacitance

EEC: Equivalent Electrical Circuit

$\Delta G^{\circ}_{ads}$ : Standard adsorption free energy

$K_{ads}$: constant of adsorption

T: Absolute Temperature

R: The universal constant gas

$S_1$: synergistic effect of iodide ions with BRSM

$I_1$: is the inhibition efficiency of the iodide ions

$I_2$: is the inhibition efficiency of BRSM

# *General Introduction*

A study by *National Association of Corrosion Engineers (NACE)* as part of its International Measures of Prevention, *Application and Economic of Corrosion Technologies Study (IMPACT)* revealed that the global cost of corrosion in 2013 was estimated to be US $ 2.5 trillion which was equivalent to 3.4% of the global *Gross Domestic Product* (GDP) in that year [1].

Current economic conditions dictate that oil field operators maximize well/reservoir productivity or injectivity. Achieving the goal of long-term, low-cost sources of hydrocarbons will require significant technology advances in the area of well stimulation.

The first acid treatments for oil wells were performed by Herman Frasch, a chemist at Standard Oil Co.'s Solar Refinery of Lima and his close friend John Van Dyke, manager of the Solar Refinery in 1895. They proposed the use of hydrochloric acid reacts with limestone to produce carbon dioxide (gas) and calcium chloride to remove from the formation as the well fluids are produced. The next significant use of acid in oil wells did not take place until 1928. An inhibitor was used with the acid similar to that used in steel mills to protect the iron from corrosion [2].

Most of corrosion inhibitors used at Petroleum Industry are very toxic, some of them are inorganic and synthetic [3, 4], such as chromates (CrO), molybdate (MoO), silicate (SiO),…etc[5, 6].

Inhibitors must be evaluated in context of health, safety and environmental impact; because environmental agencies in several countries have imposed strict rules and regulation pertaining to toxicity, biodegradability and bioaccumulation [7].

United Nations Environment Assembly (UNEA) and the U.S. Environmental Protection Agency (EPA) are faced with the challenge of efficiently and credibly evaluating chemical safety often with limited or no available toxicity data [8-10]. Hazardous substances and wastes are a public health issue of global concern[11].

There are 12 principles of green chemistry from the book (Green Chemistry :Theory and Practice ) prepared by *Anastas* and *Warner* 1998 , among these principles [12] :

*''It is better to prevent waste than to treat or clean up waste after it has been created ''*.

*''Wherever practicable, synthetic methods should be designed to use and generate substances that possess little or no toxicity to human health and the environment ''.*

Corrosion inhibitors are extensively used for the protection of metals and equipment and they are required to be acceptable, non-toxic, and eco-friendly due to environmental concerns. The cost and harmful effect associated with the commercial organic and inorganic inhibitors have raised considerable awareness in the field of corrosion mitigation. Thus, corrosion scientists and engineers are more inclined towards the implication of green corrosion inhibitors that are inexpensive, readily available, environmentally friendly and ecologically acceptable, and renewable[13].

Several studies have been discussed about natural organic compounds as eco-friendly inhibitors, such as *Gum Arabic(GA)* with inhibition efficiency of 93% [14], *Saponins* Extracted from *Gongronema Latifolium* with inhibition efficiencyof96.5%[15]and *aloes* inhibition efficiency of *Amazonian Tree Alkaloids Extract* was 94%[16]. Most of Green Inhibitors were extracted from plants.

In this study natural organic substance was selected. *The Bark Resin of Schinus Molle (BRSM)* has been studied as green inhibitor. *Schinus Molle* is a tree, it exudessticky latex (Resin) when the peels fissured or damaged.

The present works in this thesis was designed to determine the inhibition efficiency of Resin Schinus Molle on API 5L X70 Steel in Hydrochloric acid (HCl) and Sulfuric acid ($H_2SO_4$) by electrochemical methods and surface analyses. The shape over this thesis reflects that strategy.

**Chapter I:**

Chapter I is addressed to the introduction and literature review on acidification and reservoir formation, corrosion mechanism of carbon steel in acid medium as the first part.

The second part is addressed to literature review of recent publications; a study of the synergistic effect of Halide Ions on inhibition efficiency.

**Chapter II:**

This chapter is an overview of electrochemical techniques and surface analysis used in this study to give essential information to understand the experimental part and to investigate the inhibition efficiency of Bark Resin Schinus Molle.

**Chapter III:**

As a general overview in this chapter, the results obtained from the electrochemical techniques and the surface analysis of API 5L X70 steel is divided into:

The corrosion behavior of API 5L X70 steel has been studied in 0.5M HCl and 0.5M $H_2SO_4$ acid solutions to determine the electrochemical parameters, corrosion type, and also to understand the corrosion mechanism API 5L X70 steel in acid solution.

Bark Resin of Schinus Molle has been investigated for the first time by electrochemical impedance spectroscopy, potentiodynamic polarization, and surface analyses by scanning electronic microscopy (SEM) in the hydrochloric and sulfuric acid solution for understanding the inhibition mechanism of BRSM.

Synergetic effect of the combination BRSM and iodide ions in hydrochloric acid solution has been studied by electrochemical techniques and surface analyses to understand the inhibition efficiency of the system BRSM + iodide ions.

# *Chapter I :Introduction and review of literature*

## I.1. Acidification

Acidizing is the injection of acid into the wellbore to improve well productivity by removing near-well formation damage and other damaging substances. Damaged wells are those which suffer a restriction in flow rate. This may be due to a number of causes, for example, drilling damage or buildup of carbonate scale[17].

Acidizing has been applied to wells in oil and gas bearing rock formations for many years. Acidizing is probably the most widely used work-over and stimulation practice in the oil industry.

Several services companies such as “SCHLUMBERGER” offer some or the whole series of chemical treatments for oil, gas wells as shown in Figure I-1.

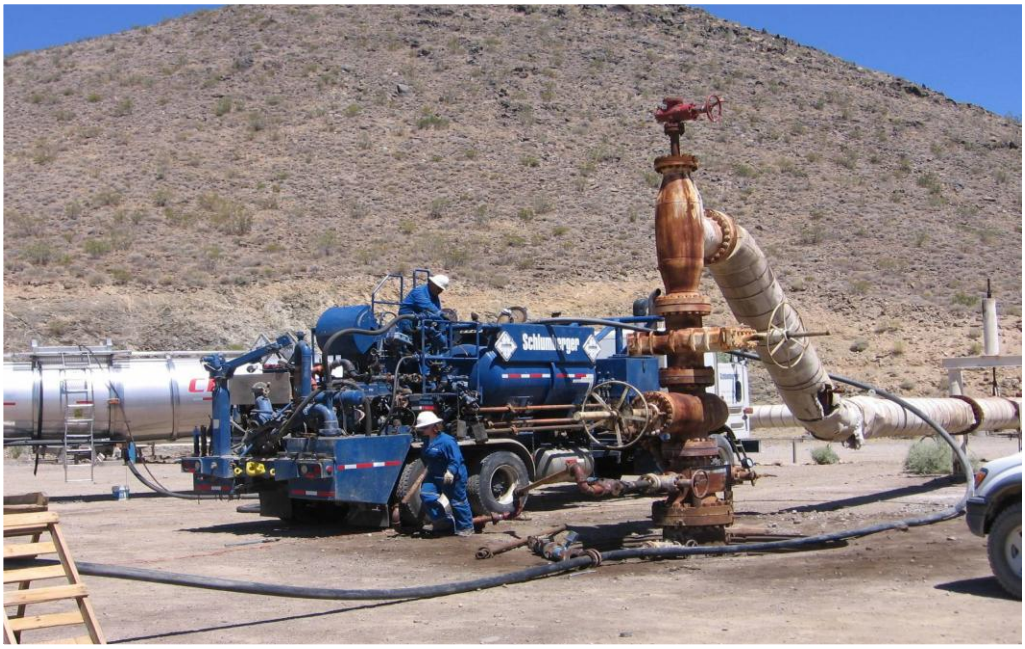

Figure I- 1: Installation of a pumping unit for injection of chemical compounds [18]

***In acid washing:*** The objective is simply tubular and wellbore cleaning. Treatment of the formation is not intended. Acid washing is most commonly performed with hydrochloric acid (HCl) mixtures to clean out scale (such as calcium carbonate), rust, and other debris restricting flow in the well. Matrix and fracture acidizing are both formation treatments.

Figure I-2 illustrates Scale precipitation, the Scale consists of salt, sand, corrosion products, and organic precipitates. It is precipitate due to a chemical reaction with surface of metals.

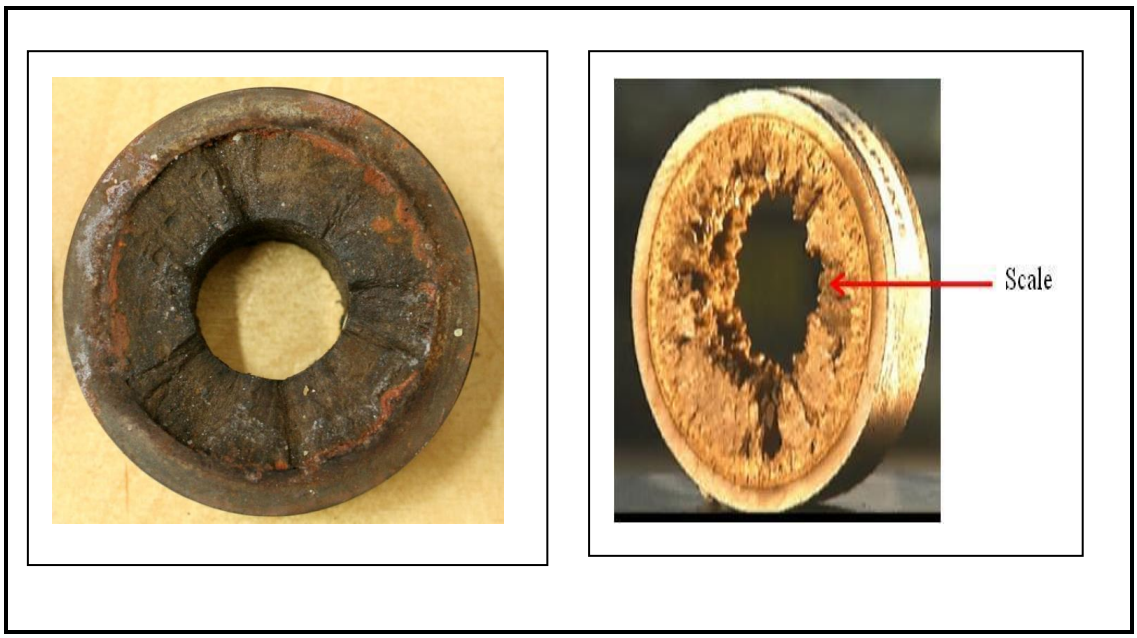


Figure I- 2 : Installation of a pumping unit for injection of chemical compounds [19]

***In matrix acidizing:*** the acid treatment is injected below the formation fracturing pressure. In fracture acidizing, acid is pumped above the formation fracturing pressure.

***Hydraulic fracturing:*** the fluids are injected at a pressure greater than the formation pressure to create channels/fractures through the formation through which the production of oil or gas may increase.

### I.1.1. Formation Type and Reaction with Acids:

Knowing the type of formation being acidized and details of its composition (mineralogy) is critical to achieving positive results

#### I.1.1.1. Carbonate formations

The objective when acidizing carbonate formations is to dissolve carbonate based materials to create new or clean existing pathways or channels that allow the formation fluids (oil, gas, and water) to flow more freely into the well [20].

$$\mathbf{CaCO_3 + 2HCl \rightarrow CaCl_2 + CO_2 + H_2O\ (forcalcite)} \qquad \text{Equ I- 1}$$

$$\mathbf{CaMg(CO_3)_2 + 2HClCaCl_2 + MgCl_2 + 2CO_2 + 2H_2O\ (fordolomite)} \qquad \text{Equ I- 2}$$

#### I.1.1.2. Sandstone Formations:

The most imperative target of sandstone formation acidizing is to dissolve/remove siliceous particles (clay, feldspar and quartz) that restrict the flow of hydrocarbons and reduce permeability around the wellbore [21]. Figure I-3 represents sandstone constituents.

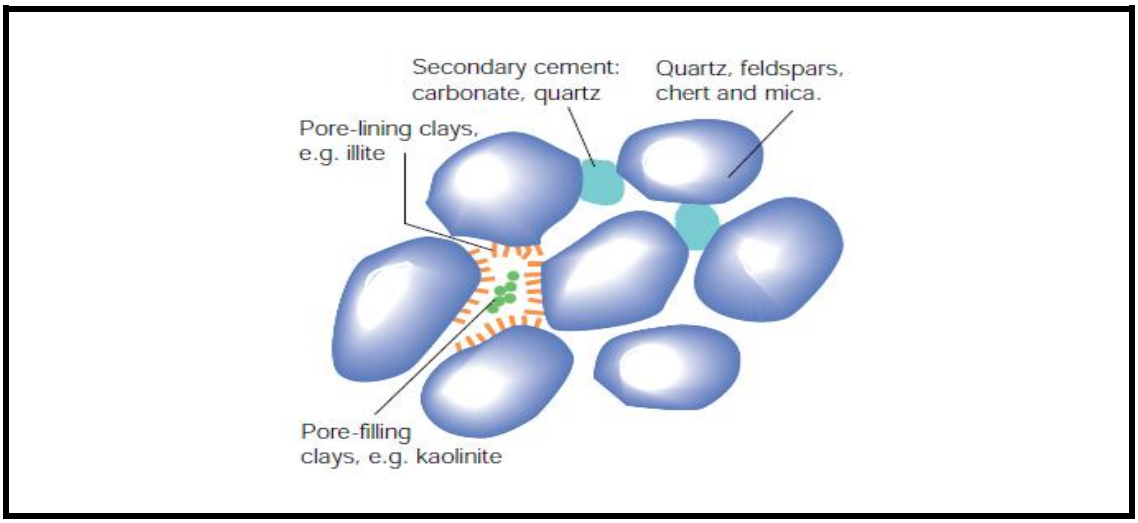


Figure I-3: Constituents of Sandstone [22]

### I.1.2. Stages of acidizing:

- **Pre-flush stage:**

It is employed to dissolve any Na, K and Ca ions that may produce insoluble silicates when reacted with the silica. Pre-flush also provides a low pH region reducing the risk of precipitate formation.

- **Main acid stage:**

It is applied to dissolve the quartz, clay, feldspar and silicates. This acid may also dissolve the remains of carbonates present after the pre-flush stage.

- **An after-flush stage:**

It is used to keep the wet ability of the formation to the original state and it cleans the formation rapidly by removing the spent acid. Mutual solvents, diesel oil, $NH_4Cl$, acetic acid or HCl can be applied at this stage for the efficient displacement of the spent acids [22].

Table I-1: Acidification Guidelines [21]

| Formation | Main acid | Preflush |
|---|---|---|
| Solubility in HCl>15–20% | Avoid use of HF, if possible | 5% NH4Cl |
| Calcite or dolomite | 15% HCl only(1) | 5% NH4Cl + 3% Acetic |
| High iron carbonate (siderite, ankerite) | 15% HCl+ iron control | / |
| High permeability (>100 mD) | 12% HCl–3% HF | 15% HCl |
| High quartz (>80%); low clay (<5%) | 7.5% HCl–1.5% HF | 10% HCl |
| Mod. Clay (5–8%); low feldspar (<10%) | 6.5% HCl–1% HF | 5–10% HCl |
| High clay (>10%) | 13.5% HCl–1.5% HF | 15% HCl |
| High feldspar (>15%) | 9% HCl–1% HF | 10% HCl |
| High feldspar (>15%) and clay (>10%) | 3% HCl–0.5% HF | 5% HCl |
| High iron chlorite (>8%) | 10% acetic–0.5% HF | 5% NH4Cl + 10% Acetic |
| Medium permeability (10–100 mD) | 6% HCl–1% HF | 5–10% HCl |
| High clay ((>5–7%) | 9% HCl–1% HF | 10% HCl |
| Low clay (<5–7%) | 12% HCl–1.5% HF | 10–15% HCl |
| High feldspar (>10–15%) | 9% HCl–1.5% HF | 10% HCl |
| High feldspar (>10–15%) and clay (>10%) | 3% HCl–0.5% HF | 5% HCl |
| High iron chlorite (>8%) | 10% acetic–0.5% HF | 5% NH4Cl +10% Acetic |
| High iron carbonate (>5–7%) | 9% HCl–1% HF | 5% HCl |
| K<25 mD | 5% HCl–0.5% HF | 10% HCl |
| Low permeability (1–10 mD)c,d,e high low clay <5%); low HCl sol. (<10%) | 6% HCl–1.5% HF | 5% HCl |
| High clay (>8–10%) | 3% HCl–0.5% HF | 5% HCl |
| High feldspar (>10%) | 9% HCl–1% HF | 10% HCl |
| High iron chlorite (>5%) | 9% HCl–1% HF | 10% HCl |
| Very low permeability (<1 mD) | Avoid HF acidizing; non-HF matrix stimulation (dictated by damage) or hydraulic fracturing is preferred | |

### I.1.3. Conventional acid systems:

Choice of the acid and any additives for a given situation depends on the underground reservoir characteristics and the specific intention of the treatment, for example near well bore damage removal, dissolution of scale in fractures, etc. A number of different acids are used in conventional acidizing treatments. The most common are [18] :

- Hydrochloric, HCl
- Hydrofluoric, HF
- Acetic, CH3COOH
- Formic, HCOOH
- Sulfamic, H2NSO3H
- Chloroacetic, ClCH2COOH.

## I.2. Carbon Steel Corrosion in Acidic Medium:

Carbon steel materials are widely used in the oil and gas production industry because of its availability, constructability, and relatively low cost [23]. The enormous quantities of steel and other metals used in the petroleum industry are prone to corrosion to a more marked degree than in other industrial environments [24]. Corrosion problems occur in the petroleum industry in at least three general areas [25]:

1- Production.

2- Transportation and Storage.

3- Refinery operations.

### I.2.1. Corrosion Mechanism in Acidic Medium:

The most common form of corrosion in the oil and gas industry occurs when steel comes in contact with an aqueous environment and rusts. When metal is exposed to a corrosive solution (the electrolyte), the metal atoms at the anode site lose electrons, and these electrons are then absorbed by other metal atoms at the cathode site. The cathode, in contact with the anode via the electrolyte, conducts this exchange in an attempt to balance their positive and negative charges. Positively charged ions are released into the electrolyte capable of bonding with other groups of atoms that are negatively charged. The figure I-4 shows the corrosion process:

Anodic Reaction (Oxidation):

$$\mathbf{Fe \rightarrow Fe^{2+} + 2e^{-}} \qquad \text{Equ I- 3}$$

Cathodic Reaction (Reduction):

$$\mathbf{2H^{+} + 2e^{-} \rightarrow H_2} \qquad \text{Equ I- 4}$$

Global Reaction (Oxydo/Reduction):

$$\mathbf{Fe + 2H^{+} \rightarrow Fe^{+2} + H_2} \qquad \text{Equ I- 5}$$

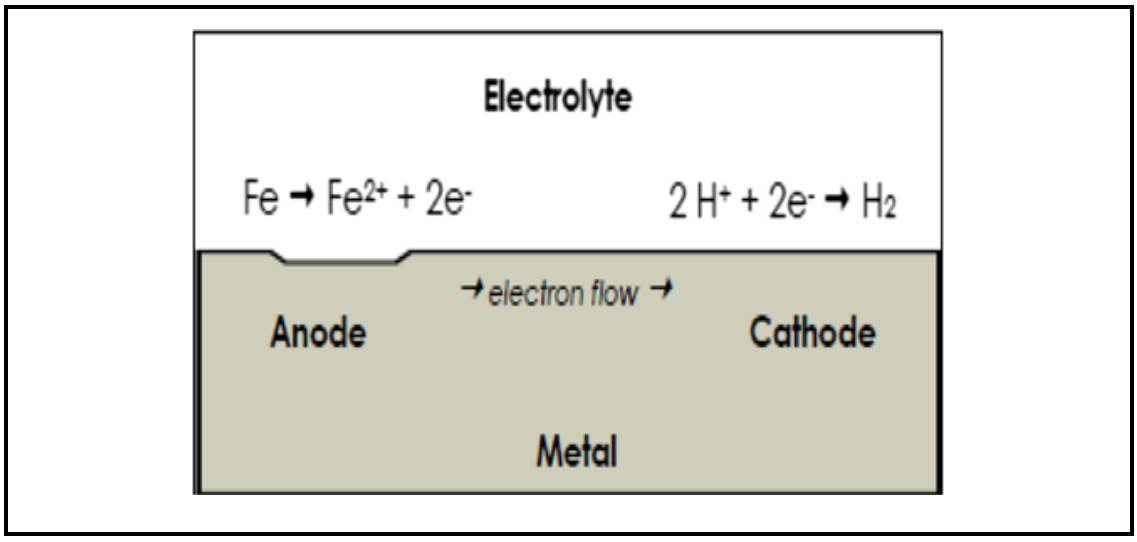


Figure I- 4 : Corrosion Process [26]

## I.3. Corrosion Inhibitors of Carbon Steel in Acidic Medium:

Inhibition is a preventive measure against corrosive attack on metallic materials. Corrosion inhibitors have been frequently studied, since they offer simple solution for protection of metals against corrosion in aqueous environment. Mineral acids like hydrochloric and sulfuric acids are most widely used in pickling baths to remove the metal oxides formed on the surface. The multidisciplinary aspect of corrosion problems combined with the distributed responsibilities associated with such problems only increase the complexity of the subject. Inhibitors are used in industrial and commercial processes to minimize both the metal loss and acid consumption [27].

### I.3.1. Inorganic Inhibitors:

Inorganic elements or metals have a crucial role in living organisms, when they are at trace amounts. The higher concentrations of many metals cause toxicity to all forms of lives. It is also applicable for the derivatives of metals. For example, chromium compounds, mainly chromates were widely used as potential corrosion inhibitors in aqueous systems due to their high efficiency [28-30]. Besides the high inhibition efficiency, chromates exhibit high toxicity and consequently prohibited to use for industrial applications[31].

### I.3.2. Organic Inhibitors:

Large numbers of organic compounds were studied and are being studied to investigate their corrosion inhibition potential. All these studies reveal that organic compounds especially those with N, S and O showed significant inhibition efficiency. But, unfortunately most of these compounds are not only expensive but also toxic to living beings. It is needless to point out the importance of cheap, safe inhibitors of corrosion. Plant extracts have become important as an environmentally acceptable, readily available and renewable source for wide range of inhibitors. They are the rich sources of ingredients which have very high inhibition efficiency [32].

### I.3.2.1. Inhibition Mechanism of Organic Inhibitors:

The organic inhibitors are composed of numerous formulations: aromatic molecules, linear or branched chain macromolecules, etc. They contain a non-polar , hydrophobic part consisting mainly of carbon and hydrogen atomes and a polar hydrophilic part consisting of one or more functional groups such as amines (-NH2), mercaptants (-SH), hydroxyls (-OH), carboxyls (-COOH), phosphates (-PO3) or their derivatives .The inhibitor is attached to the surface by its hydrophilic functional group, while its larger non polar part partially blocks the active surface [33].

### I.3.2.2. Adsorption of Organic Inhibitor:

Adsorption is the selective transfer of certain components of a fluid phase, called solutes to the surface of an insoluble solid. The adsorbed solutes are referred to as adsorbates, and the solid material as adsorbent. When an adsorbent is exposed to a fluid phase, molecules in the fluid phase diffuse to its surface, where they are either chemically bond with the solid surface or are held there physically by weak van der Waals intermolecular forces. When adsorption is caused by van der Waals forces, it is referred to as physical adsorption or physisorption, whereas it is called chemical adsorption or chemisorption if it is caused by chemical forces [34]. The table I-2 summarizes the different properties between chemisorptiona and physisorption.

Table I-2: Chemisoption and physisorption properties [35].

| Physisorption : physical adsorption | Chemisorption : Chemical adsorption |
|---|---|
| -Low heat adsorption usually <**40 kj.mol$^{-1}$** | -high heat adsorption usually **>40 kj.mol$^{-1}$** |
| -Force of attraction are Van der waal's forces | -Force of attraction are chemical bond forces |
| -It usually takes place at low temperature and decreases with increasing temperature | -It takes place at high temperature |
| -It is reversible | -It is irreversible |
| -It is related to the ease liquification of the gas | -The extent of adsorption is generally not related to liquification of the gas |
| -It is not very specific | -It is highly specific |
| -It forms multi-molecular layers | -It forms mono-molecular layers |
| -It does not require any activation energy | -It requires activation energy |

### I.4. The Use of organic Inhibitors in Acidic Medium:

H.Elabbasy et al.[36] studied the inhibition effect of Ambrosia Maritima, which was also named after (Damsissa) extract, towards the corrosion of carbon steel in 1M HCl solution was investigated utilizing potentiodynamic polarization, electrochemical impedance spectroscopy (EIS) and electrochemical frequency modulation (EFM) methods. The process of adsorption obeyed Langmuir adsorption isotherm. Damsissa extract was found to act as a mixed-type in 1M HCl. The computed adsorption thermodynamic parameters demonstrated that the adsorption was a spontaneous, endothermic process accompanied by an increase in the entropy. The maximum value of the inhibition approached 92.6% within the presence of 300 ppm Damsissa extract utilizing Tafel polarization procedure. The results obtained from the various electrochemical processes were in a great agreement. The inhibition of the extract was assumed to occur through the adsorption of active ingredients on the metal surface. Morphology of the surface was analyzed utilizing scanning electron microscopy (SEM), Fourier transforms infrared (FTIR) and atomic force microscopy (AFM) which confirmed the presence of a protective film of extract molecule on carbon steel 1018 surface.

H.Bentrah et al.[14] investigated the influence of temperature (25-65°C) on the adsorption and the inhibition efficiency of gum arabic (GA) for the corrosion of API 5L X42 pipeline steel in 1M HCl. The Inhibition behavior on steel in HCl has been studied in relation to the concentration of the inhibitor and the temperature using potentiodynamic polarization curves and electrochemical impedance spectroscopy. Thermodynamic parameters of adsorption were calculated from the viewpoint of adsorption theory. The results show that at a temperature range from 25 to 65°C, GA was a good inhibitor for API 5L X42 pipeline steel, and its inhibition efficiency was significantly stable. The maximum inhibition efficiency (93 per cent) is obtained at 4 g $L^{-1}$. In absence and presence of GA, there is almost no change in the corrosion mechanism regardless of the temperature. The adsorption of GA on steel surface is an exothermic process. The adsorption of GA involves physical adsorption. The use of GA as an eco-friendly corrosion inhibitor is practical for carbon steel in HCl.

The stability of inhibition efficiency of GA at a temperature range from 25 to 65°C could find possible applications in acid pickling, industrial acid cleaning and acid descaling.

M.Mobin et al.[37] evaluated the anticorrosion behavior of bromelain on low carbon steel (LCS) in 1 M HCl solution was studied employing weight loss, potentiodynamic polarization measurement (PDP), electrochemical impedance spectroscopy (EIS), UV-visible spectrophotometry, and surface assessment techniques like scanning electron microscopy (SEM) and energy dispersive X-ray analysis (EDAX) at 308 K - 338 K. The obtained results suggest that bromelain is an excellent corrosion inhibitor and its inhibition efficiency (% η) is both concentration and temperature dependent. %η is observed to increase with an increase in bromelain concentration and an increase in electrolyte temperature. The maximum %η of 97.6% is observed at bromelain concentration of 1000 ppm at 338 K. The inhibitor adsorption on the LCS surface is in accordance with the Langmuir adsorption isotherm.

A.Ruiz et al.[38] revealed the soluble extract from Opuntia ficus-indica (Nopal extract) as a green inhibitor due to its component called mucilage, which has the ability to retain water; for this reason, it has been used as metal corrosion protection in machinery pieces, tools and other metallic components that need to be stored for short periods. In this way, three industrial carbon steels (AISI 1018, 1045 and 4140) have been exposed in sulfuric acid (H2SO4) to evaluate the corrosion behavior with or without Nopal extract (NE). Some electrochemical techniques have been implemented to evaluate the corrosion inhibition efficiency (IE) such as DC linear polarization resistance (LPR) and AC electrochemical impedance spectroscopy (EIS). Results indicated a considerable superficial modification of steel in terms of dielectric constant and ion charge capacity. When the NE was added, the corrosion mechanism changed from localized to general attack, decreasing the corrosion rate in all cases. More susceptibility to fail by corrosion was observed in the 1045 carbon steel in comparison with the other two studied steels; these results were confirmed by the percentage of inhibitor's efficiency of about 95%.

It has been found that the inhibition performance and mechanism of loquat leaves extract (LLE) for the corrosion of mild steel in 0.5 M H2SO4 were investigated using weight loss method, electrochemical measurements and scanning electron microscope (SEM). The results revealed that LLE acted as a modest cathodic inhibitor, its inhibition efficiency increased with the concentration of LLE and reached a maximum value of 96% at the 100% V/V concentration, but decreased with incremental temperature. Besides, it was found that the adsorption of LLE on steel surface obeyed Langmuir adsorption isotherm, and then the thermodynamic and kinetic parameters were further determined accordingly. Furthermore, LLE was preliminarily separated by pH-gradient sedimentation and the synergistic inhibition between the isolates was investigated[39].

The studies carried out many inhibitor additives during acidizing treatment in order to prevent excessive corrosion, prevent sludge and emulsions, prevent iron precipitation, improve cleanup, improve coverage of the zone, and prevent precipitation of reaction products. Foremost among acid additives are corrosion inhibitors; therefore compatibility of other additives with corrosion inhibitor is very critical to the success of acidizing treatment. Any additive that alters the tendency of the corrosion inhibitor to adsorb on casing and tubing will also change its effectiveness. In present work, the inhibitive action of henna extract on corrosion of N80 API steel in regular mud acid (HCL/HF 12/3 wt%) at 28 °C was investigated through electrochemical technique. After determining the optimum concentration of henna extract, effect of acid additives on inhibitive action of henna extract on corrosion behavior of N80 steel in regular mud acid was investigated through polarization measurement and electrochemical impedance spectrometry methods. Inhibition efficiency of henna extract as a corrosion inhibitor for N80 API steel in regular mud acid at 28 °C is 85.98% (average of three methods). The results show that except iron control additive, all additives decrease the performance of henna extract as corrosion inhibitor [40] .Large of organic inhibitors used to protect carbon steel in acidic medium, some of them present in table I-3.

Table I-3: Natural inhibitors properties in acid medium

| Inhibitors | Concentration | Acid Medium | Adsorption Mode | (η %) | Refe |
|---|---|---|---|---|---|
| pomegranate peels extract (PPE) | 15 vol.% | 1M HCl | / | 96 | [41] |
| Mangiferaindica (mango) | 1000 ppm | 1 M HCl | Langmuir | 92 | [42] |
| Cephapirin Drug | 600 ppm | 2 M HCl | Temkin | 83 | [28] |
| Saracaashoka seeds extract | 100 mg/L | 0.5M H2SO4 | Langmuir | 95.48 | [29] |
| Alkaloid extract | 200 mg/L | 0.5M H2SO4 | Langmuir | 93 | [30] |
| Lavandula and Ricinuscommunisoils | 2ml/ 200 ml | 0.5M H2SO4 | / | 96.35 | [43] |
| Gum Arabic (GA) | 2g/l | 1M HCl | Langmuir | 92 | [44] |

### I.5. Polymer as Inhibitor:

The use of polymers as corrosion inhibitors has attracted considerable attention recently. Polymers are used as corrosion inhibitors because, through their functional groups they form complexes with metal ions and on the metal surface these complexes occupy a large surface area, thereby blanketing the surface and protecting the metal from corrosive agents present in the solution [8]. The inhibitive power of these polymers is related structurally to the cyclic rings, heteroatom (oxygen and nitrogen) that are the major active centers of adsorption[45]. A number of naturally occurring polymers have shown promising results as metal corrosion inhibitors in different corrosive environments [46].

### I.5.1. Examples of inhibition with polymer:

I.Nadi, et al.[47] studied the inhibition effect of the invasive brown seaweed Sargassum muticum extract (ESM),harvested from the Atlantic coast of Morocco, against the corrosion of carbon steel (CS) in 1 M HCl medium was studied for the first time using gravimetric, electrochemical and surface techniques. The methanolic crude extract of Sargassum muticum (ESM) is rich in alginate biopolymer. The evaluation corrosion tests showed that this algal extract acts as a good mixed corrosion inhibitor for CS substrate in 1 M HCl since inhibition efficiency of 97 % was reached with 1 g/L of ESM at 303 K. AC impedance findings showed that the seaweed extract adding in the corrosive electrolyte increases the polarisation resistance and conversely decreases the charge capacitance at the interface. Adsorption of ESM on the substrate surface followed the Langmuir adsorption isotherm. X-ray photoelectron spectroscopy analyses (XPS) demonstrated that the corrosion inhibition mechanism of CS substrate in 1 M HCl environment by the investigated algal extract is typical of the chemisorption process and the protective barrier is mainly formed by the adsorbed biological macromolecules.

M.Messali, et al.[48] investigated the Guar gum as a water-soluble, nonionic, nontoxic, biodegradable and biocompatible hetero polysaccharide with unlimited number of industrial applications. In this study, guar gum was evaluated as a natural inhibitor of carbon steel (CS) corrosion in 2 M H3PO4 solution. The characteristic effect of guar gum on the steel corrosion was studied at concentration ranges from 0.1 to 1.0 g/L at 298 to 328 K by weight loss and electrochemical methods. Obtained results showed that, the inhibition efficiency (η%) of guar gum decreased slightly when the temperature increased and increased by increasing the inhibitor concentration reaching the maximum value at 1.0 g/L. The adsorption of guar gum on steel surface was studied by the Temkin adsorption model. EIS measurements indicate that the values of the polarization resistance (Rp) of CS in presence of guargum are significantly higher than that of the untreated surface. Steel surface coated with guar gum was analyzed by SEM, FTIR and XRD.

### I.6. Synergistic Effect of Halide Ions on the Corrosion Inhibition:

M.Djellab, et al.[49] revealed the inhibition efficiency of Gum Arabic (GA) for the corrosion of API5L X70 pipeline steel in sulfuric acid through the addition of halide ions (potassium iodide [KI], potassium chloride [KCl], and potassium bromide [KBr]). The synergistic effect of GA and halide ions has been studied using potentiodynamic polarization curves, electrochemical impedance spectroscopy, and surface analysis by scanning electron microscope (SEM). The results show that substantial corrosion inhibition (99%) using 2 g $L^{-1}$ GA and 0.5mMKI can be obtained in synergistic manner. The adsorption of GA in combination with iodide ions follows Langmuir adsorption isotherm. GA combined with KI acts as a mixed type inhibitor in sulfuric acid.

The corrosion inhibition of rice husk extract for bio-corrosion in mild steel in 1 M of H2SO4 solution and the effect of adding potassium iodide were investigated using the weight-loss method with a variable solution temperature and various bio-inhibitor concentrations. The addition of potassium iodide can significantly increase the efficiency of rice husk extract. The highest efficiency is 95.89% at 1,250 ppm of inhibitor concentration at a temperature of 313 K. The inhibition efficiency of rice husk extract is synergistically increased with the addition of potassium iodide. The characteristics of the adsorption inhibitors were assessed using the Langmuir isotherm adsorption approach at all studied concentrations and temperatures. The synergy of rice husk extract and potassium iodide was examined using thermodynamic and kinetic parameters [50].

A.Ridhwan, et al.[51] studied the inhibitive effect of mangrove tannin (MT) on mild steel (MS) corrosion in 0.5 M hydrochloric acid solution was studied using electrochemical techniques and gravimetric method. The influence of halides viz., KCl, KBr and KI on the corrosion inhibition of MT were also investigated. Results show that MT alone provided satisfactory inhibition on the corrosion of MS and it was also found that the inhibition efficiency increased synergistically in the presence of halide ions. The synergistic effect of halide ions was found to follow the order: KI>KBr>KCl. The inhibitor reduced the corrosion rate through adsorption process and obeyed the Langmuir's adsorption isotherm.

## I.7. Conclusion

Steel is the most important metal used in every part of the oil and gas industry from production and processing to the distribution of refined products.

Protection against corrosion during the acidification of oil wells is very important in the petroleum industry. Basically, this kind of protection is by using corrosion inhibitors at low concentration in the corrosive medium, but most of these inhibitors are toxic.

There is an increasing concern about the toxicity, biodegradability, and bioaccumulation of corrosion inhibitors discharged into the environment. For this reason, the United Nations Environment Assembly **(UNEA)** and the U.S. Environmental Protection Agency **(EPA)** are concerned with the importance of protecting and preservation of the ecosystem under the slogan of **'' Green Chemistry ''**.

Therefore, great efforts have been made about searching for new corrosion inhibitors. Organic substances from natural sources have also been studied in different media. In the case of extracts from plants, studies have demonstrated that they are good alternatives. The literature reviews have shown that natural organic polymers are the best choice for the protection of carbon steel in acidic medium.

# *Chapter II :Experimental Techniques*

This chapter is an overview of the Electrochemical Technique used in this study; it also contains essential information to understand the experimental part.

## II.1. Techniques of studies

There are two main methods to investigate the corrosion phenomenon and inhibitor efficiency in a different corrosive medium.

The first one is **electrochemical method** to evaluate the inhibition efficiency and inhibition mechanism of selected inhibitor in a different corrosive medium.

The second one is **surface analysis** used to determine the state of the sample (working electrode) and the nature of the layer on the sample surface. Thus, it confirms the inhibition efficiency.

### II.1.1. Electrochemical Methods

The electrochemical method is a branch of chemistry concerned with the interaction of electrical and chemical effects; it is originated from the study of the movement of electrons in an oxidation-reduction reaction.

The electrochemical method is an analytical technique that uses a measurement of potential, charge or current. It is divided into many methods, some these methods are:

Electrochemical Impedance Spectroscopy

Potentiodynamic Polarization

Cyclic Voltammetry Technique

### II.1.1.1. Electrochemical Impedance spectroscopy

Electrochemical impedance spectroscopy (EIS) is a powerful technique for characterizing a wide variety of electrochemical systems and for determining the contribution of electrode or electrolytic processes in these systems [52].

Electrochemical Impedance spectroscopy (EIS) is a general term that subsumes the small-signal measurement of the linear electrical response of a material of interest (including electrode effects) and the subsequent analysis of the response to yield useful information about the physicochemical properties of the system [53].

EIS data is commonly analyzed by fitting it to an equivalent electrical circuit model. Most of the circuit elements in the model are common electrical elements such as **resistors**, **capacitor**s, and **inductors**. To be useful, the elements in the model should have a basis in the physical electrochemistry of the system.

As an example, most models contain a resistor that models the cell's solution resistance. Some knowledge of the impedance of the standard circuit components is therefore quite useful. Table II-1 lists the common circuit elements, the equation for their current versus voltage relationship, and their impedance [54]. Figure 2 illustrate the Nyquist plot with equivalent electrical circuits.

Table II-1: Common Electrical Elements

| Component | Current Vs. Voltage | Impedance |
|---|---|---|
| resistor | E= IR | Z = R |
| inductor | E = L di/dt | Z = jωL |
| capacitor | I = C dE/dt | Z = 1/jωC |

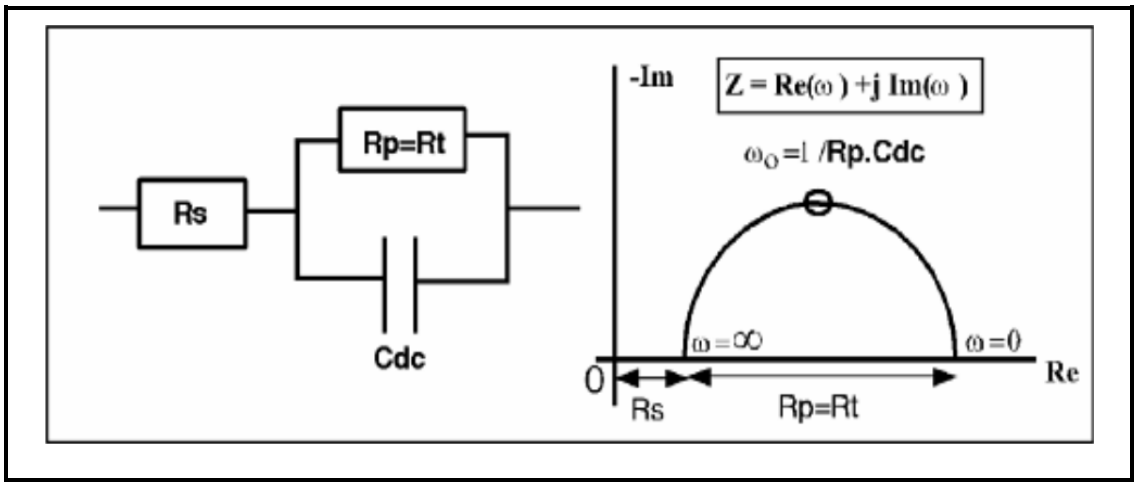


Figure II- 1: Circuit comprising the resistance of the $R_S$ solution, in series with the assembly (bias resistor $R_P$, here confused with the charge transfer resistor $R_t$, in parallel with the double layer capacite $C_{dl}$) [55].

Figure II-2 illustrates the Bode and Nyquist plots of steel samples exposed to the blank acidic solution .The resulting data were fitted using the proposed equivalent electrical circuits (EEC) shown in Nyquist plots. In the suggested $R_t$, $R_p$, and $R_s$ are defined as the resistance of double layer against the transfer of charge, polarization resistance.

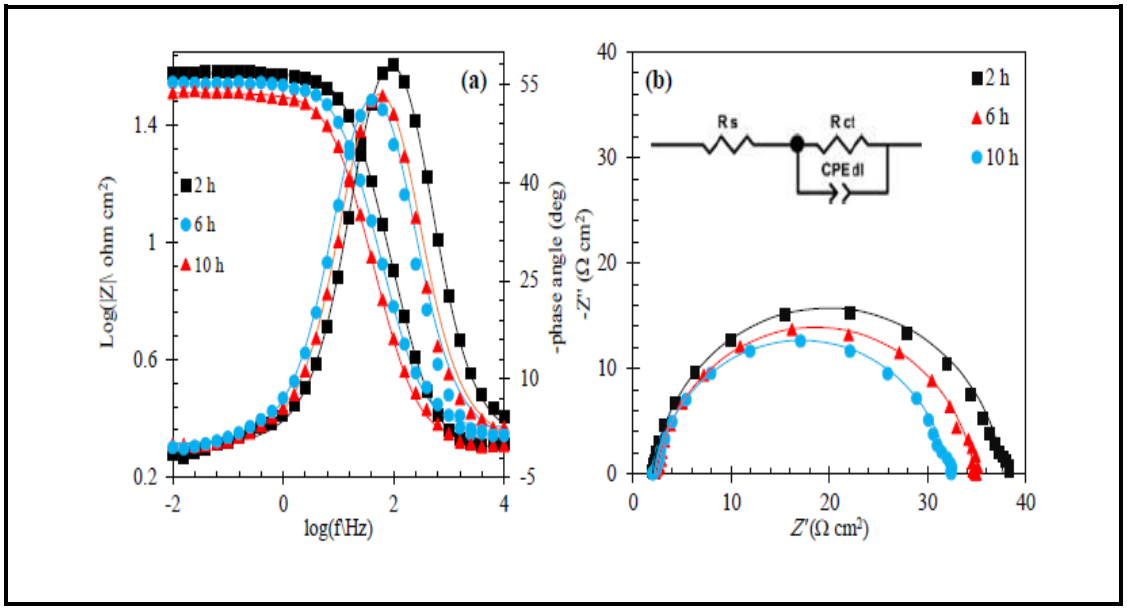


Figure II- 2: The (a) Bode and (b) Nyquist plots obtained for blank sample immersed in 1 M HCl solution [56].

### II.1.1.2. Potentiodynamic polarization

In a potentiodynamic experiment, the current represents the rate with which the anodic or cathodic reactions are taking place on the working electrode. Typically, the current is expressed in terms of the current per unit area of the working electrode, or the current density. Numerous variables will influence the rate of a given electrochemical reaction, including the temperature, the surface condition of the surface being interrogated, as well as the chemical environment in which the experiment is performed. In general, cathodic currents are considered to be negative and anodic currents to be positive. It should be noted that in an Evans diagram (a plot of E vs log(I)) the absolute value of the current density is plotted (i.e., both anodic and cathodic currents are plotted as positive values) [57].

The Tafel extrapolation method provides a direct measurement of the corrosion rate and of the corrosion potential, and it is very useful in predicting the corrosion properties of various corrosion systems. It is possible to measure extremely low corrosion rates. The rapid determination of corrosion rates with Tafel plots can be advantageous for the evaluation of inhibitors and the comparison of alloys. The cathodic and anodic polarization data are obtained by using a three-electrode electrochemical cell containing **working**, c**ounter**, and **reference electrodes**. The corrosion measurements are performed by using a potentiostat that is connected to the electrochemical cell [58]. As shown in figure II-3, the anodic and cathodic current of Tafel polarization curves.

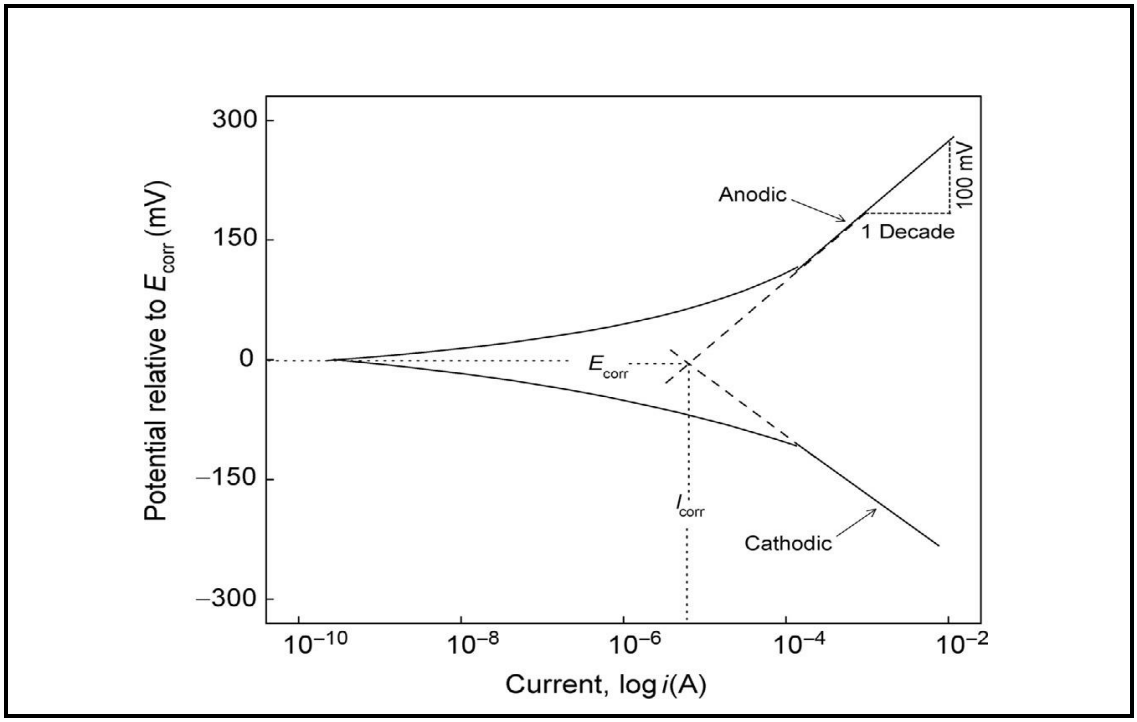


Figure II- 3: Corrosion rate determination [54]

### II.1.1.3. Cyclic Voltametry Technique

Cyclic voltametry is a powerful and popular electrochemical technique commonly employed to investigate the reduction and oxidation processes of molecular species[59]. It is used to analyze the corrosion behavior and passive films formed on metal and metal alloys surfaces.

The potential is scanned linearly between an initial potential $E_{initial}$ to a final potential value $E_{final}$ followed by reversal of the potential scan back to the initial potential value as seen in figure II-4.The sweep rate might range from a few mV/s to thousands mV/s. The anodic peak current ($i_{pa}$), the cathodic peak current ($i_{pc}$), the anodic peak potential ($E_{pa}$), and the cathodic peak potential ($E_{pc}$) values can be obtained and can be used to identify the diffusion coefficient of the ionic species involved [60].

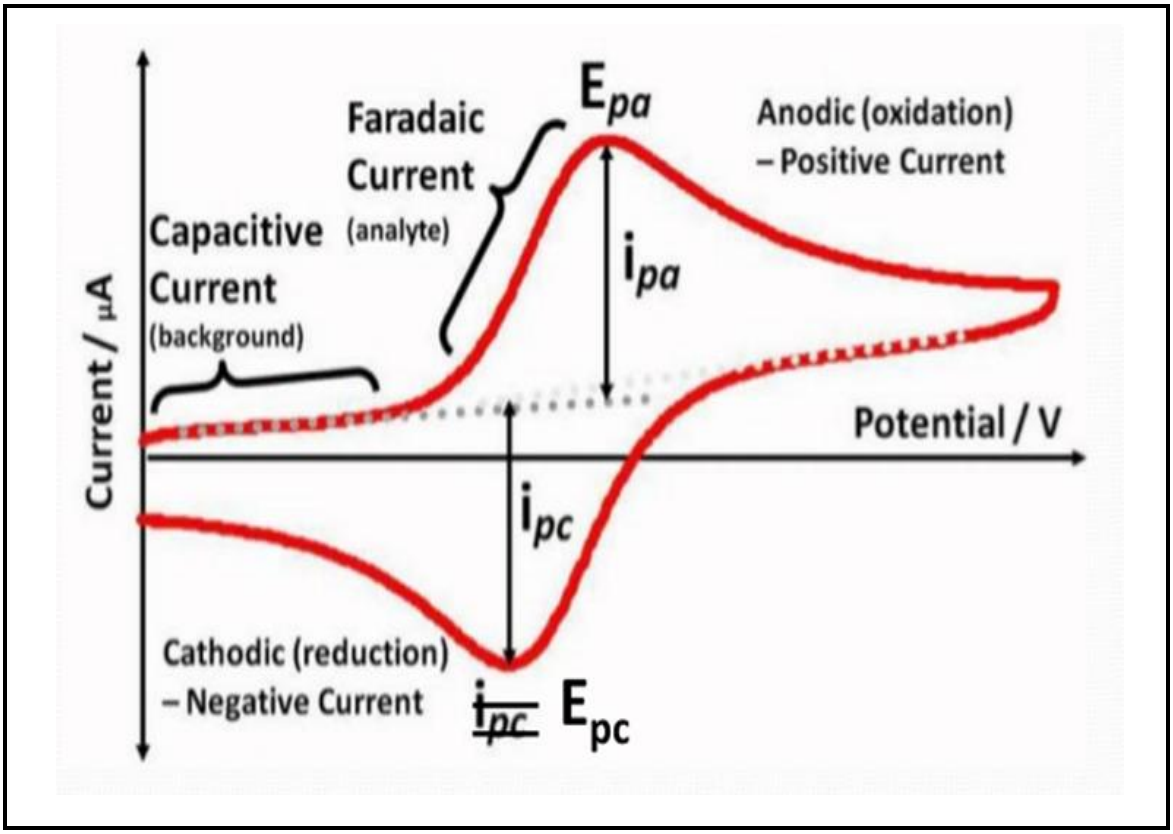


Figure II- 4: : Cyclic voltammetry for a reversible charge transfer, $\mathbf{E_{pc}}$:cathodic peak potential, $\mathbf{E_{pa}}$ :anodic peak potential, $\mathbf{i_{pc}}$ :cathodic peak current, $\mathbf{i_{pa}}$ : anodic peak current [61].

### II.1.2. Surface analysis

SEM-EDX is one of the main techniques used for examining and analyzing elemental surface component of corrosion related samples. The SEM examination provides information about the steel surface, specifically with regard to the morphology and corrosion type, while EDX is used for elemental analysis[62].

## II.2. Experimental Conditions:

### II.2.1. Material (working electrode)

The working electrodes (API 5L X70 pipeline steel), for electrochemical experiments, were cut into 3 × 3 × 1 $cm^3$. The chemical composition of API 5L X70 pipeline is showing in table II-2.

API 5L means: Pipeline

X70 means: Steel grade (example: A25, A, B, X42, X60, X80)

The number 70 means: 70 000 psi, elastic limit or yield point in psi (pound per square inch).

Table II-2: Chemical composition of API 5L X70 (weight percentage)

| C (Max) | Mn (Max) | Si (Max) | P (Max) | S (Max) | Cr (Max) | Ni (Max) | Nb (Max) | Ti (Max) | Fe |
|---|---|---|---|---|---|---|---|---|---|
| 0.12 | 1.68 | 0.27 | 0.012 | 0.05 | 0.051 | 0.04 | 0.003 | 0.03 | Bal |

The samples were mounted in the electrochemical cell, and the surface area of each electrode exposed to the electrolyte was 2.85 $cm^2$. Exposed surface of each sample was prepared by wet grinding with silicon carbide abrasive papers (grade 320 -500-600-800), rinsed with distilled water and degreased with acetone.

### II.2.1.1. Metallographic

To determine the metallographic structure of the API 5L X42 steel, a sample was polished on SiC abrasive discs of different granulometry (P120, P180, P400, P600, P800, P1000, and P1200, then rinsed with distilled water, cleaned with ethanol and well dried. After the metallographic attack of the surface of the steel API 5L X70, the different constituent phases of the material could be highlighted. The etching was carried out by plunging (20 seconds) the previously polished steel into a solution of "nital 4%" (mix of nitric acid 4% and alcohol (ethanol) 96%). An optical microscope analysis reveals that this steel has a microstructure characteristic of ferrito-perlitic steel. Figure II-5 shows the metallographic structure of API 5L X70.

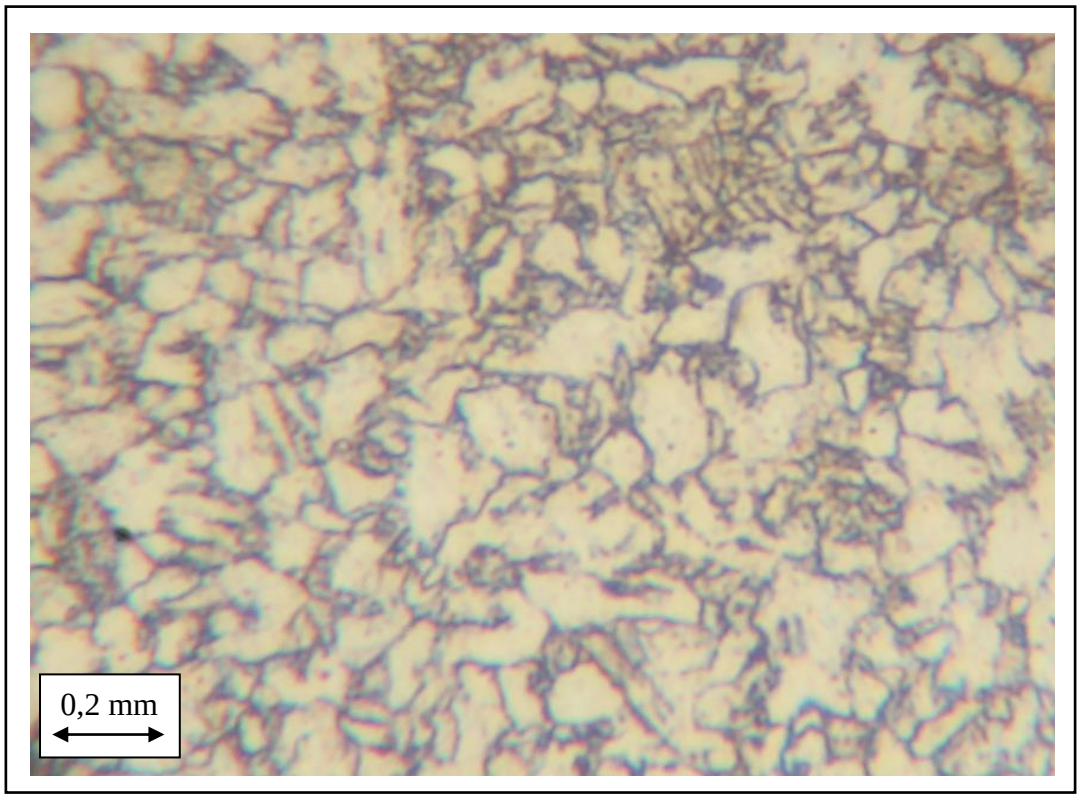


Figure II-5: (X400) metallographic structure of API 5L X70 steel after 20 seconds etched by "4%Nital" (Ferrito-Perlitic Microstructure)

### II.2.2. Medium (electrolyte)

Two types of the aggressive solution have been used in this study Hydrochloric acid was prepared by dilution of 36% HCl acid with distilled water. Sulfuric acid was prepared by dilution of 96% $H_2SO_4$acid with distilled water.

### II.2.3. Inhibitor

The bark resin of Schinus molle was collected in March 2018 from Biskra Algeria and the species were identified as "***S. molleL., Anacardiaceae***". Figure II-6 shows Schinus molle tree.

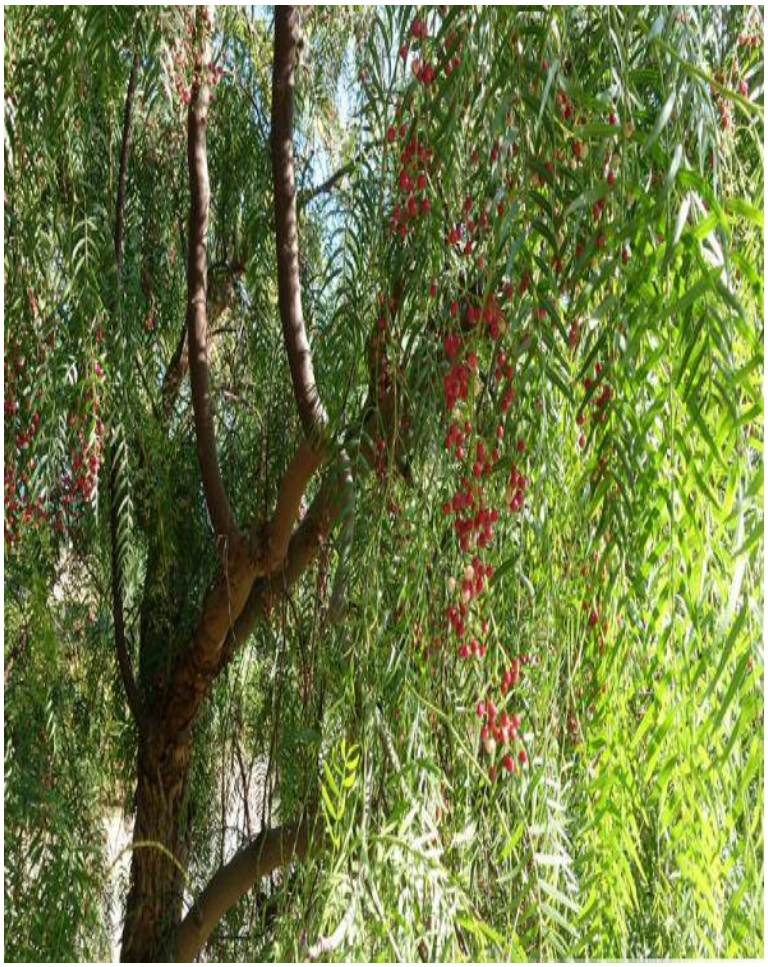

Figure II- 6: Schinus molle tree

Dried bark resin of S. molle powder was selected for the present study with the molecular structure shown in figure II-7.

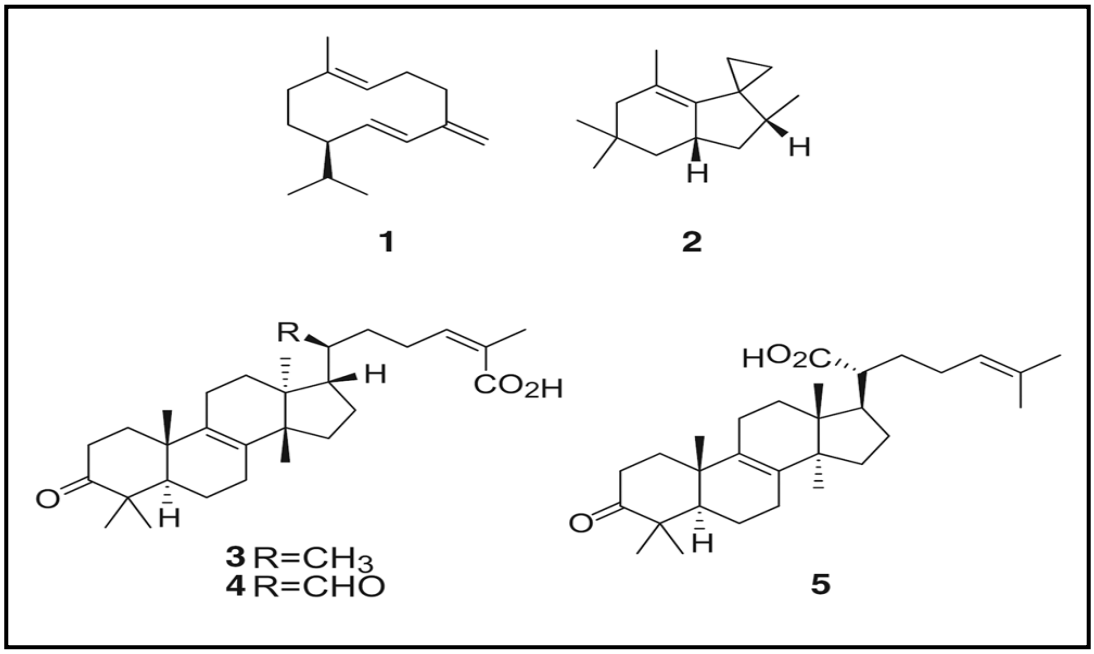


Figure II-7: The molecular structure of bark resin of schinus molle: germacrene-D (1), terebinthene (2), isomasticadienoic acid (3), isomasticadienonalic acid (4), and pinicolic acid (5)

### II.2.3.1. Fourier-transform infrared spectroscopy (FTIR) of BRSM

The solid bark resin of S.molle was characterized by Fourier transform infrared spectroscopy. FTIR spectra were recorded in an FTIR830 spectrophotometer (SHIMADZU Company, Japan), which extended from 4000 to 400 $cm^{-1}$, using the KBr disk technique.

### II.2.4. Electrochemical Methods

Two electrochemical techniques, namely, electrochemical impedance spectroscopy (EIS) and potentiodynamic polarization, were used to study the inhibition efficiency of BRSM for API 5LX70 in 0.5M hydrochloric acid. Electrochemical measurements were performed using a Gamry Ref 3000 with Gamry Instruments Framework (version 7.05) commercial software.

A Gamry Paracell (Electrochemical Cell) with a standard three-electrode configuration consisting of Ag/AgCl reference electrode (the potential of Ag/AgCl electrode is the same of the saturated calomel electrode and equal to 240 mV vs.NHE), graphite block for Paracell as counter electrode and the sample acted as the working electrode. The working electrode was connected with a copper wire on the backside and installed in customized Teflon assembly and exposed on the solution side to about 2.85 $cm^2$ working area.

All experiments were performed in stagnant aerated solutions at 30 °C. The working electrode was immersed in test solution at the open circuit potential (OCP) for 1 h to be sufficient to attain a stable state.

The analyses were performed using Gamry Echem Analyst (version 7.05) commercial software developed by Gamry.

#### II.2.4.1. Potentiodynamic polarization

Potentiodynamic polarization studies were carried out from the cathodic potential of −0.3 V to anodic potential of+0.3 V with respect to the corrosion potential ($E_{corr}$) at a scan rate of 0.3 mV $s^{-1}$. The corrosion current densities ($I_{corr}$) were determined graphically from the cathode part of polarization curve. Similar method has been previously employed for non-Tafel dependence curves with acceptable deviation of less than 10% from other methods of corrosion rate determination.[ 24] Because of the presence of a degree of nonlinearity in the Tafel slope part of the

obtained polarization curves, the Tafel constants were calculated as a slope of the points after($E_{corr}$) by ±80 mV.

The values of inhibition efficiency $\eta_{pol}$ were calculated using the following equation:

$$\eta_{pol}\,\% = \frac{I_{corr} - I_{corr}\,(inh)}{I_{corr}} \times 100 \qquad \text{Equ II. 1}$$

Where $I_{corr}$ and $I_{corr}$ (inh) represent corrosion current density values without and with inhibitor, respectively.

### II.2.4.2. Electrochemical impedance spectroscopy

Electrochemical impedance spectroscopy (EIS) was carried out at OCP in the frequency range of 100 kHz to100 mHz using a 10 mV peak-to-peak voltage excitation. Inhibition efficiency $\eta_{EIS}$ is calculated on the basis of the equation:

$$\eta_{ESI} = \frac{R_t - \acute{R}_t}{R_t} \times 100 \qquad \text{Equ II. 2}$$

Where $\acute{R}_t$ is charge transfer resistance value without the presence of BRSM in acid medium, and $R_t$ is charge transfer resistance value in the presence of BRSM.

### II.2.5. Surface analysis

The API 5L X70 steel surface was prepared both without (blank) and with inhibitor; 2 g $L^{-1}$BRSM was used. After60 h waiting time, the electrodes were removed from the cells and dried. An electron microscope, TESCAN VEGA3, was used for SEM-EDX study.

# *Chapter III :Results and Discussion*

## III.1. Part one: Studying corrosion of API 5L X70 steel in HCl and H2SO4 medium

The purpose of this part is to investigate the corrosion of API 5L X70 steel in different acidic medium (hydrochloric acid and sulfuric acid). For that, a series of electrochemical techniques have been realized to determine the electrochemical parameters such as corrosion rate, corrosion potential, charge transfer resistance, and double-layer capacity.The surface has been analyzed by scanning electron microscopy (SEM) after removing the corrosion products to determine the corrosion type and the damage of steel surface in HCl and $H_2SO_4$acid medium

### III.1.1. Electrochemical techniques of API 5L X70 steel

#### III.1.1.1. Cyclic voltammetry technique

Concerning to clarifying the electrochemical behavior of API 5L X70 steel in different acids (HCl, $H_2SO_4$), cyclic voltammetry was applied. The investigation was to show the different domains of potential and a passivation domain in the cyclic voltammograms.

***API 5L X70 steel in HCl medium:***

There are two different zones in Figure III-1. It represents the cyclic voltammogram of API 5L X70 steel in 0.5M HCl.

Zone I: represents the cathodic domain

Reduction reaction: $\mathbf{2H^+ + 2e^- \rightarrow H_2}$

Zone II: represents the anodic domain (active dissolution).

Oxidation reaction: $\mathbf{Fe \rightarrow Fe^{+2} + 2e^-}$ Reduction reaction: $\mathbf{2H^+ + 2e^- \rightarrow H_2}$

The noticeable is the absence of the passivation zone in the HCl acid medium.

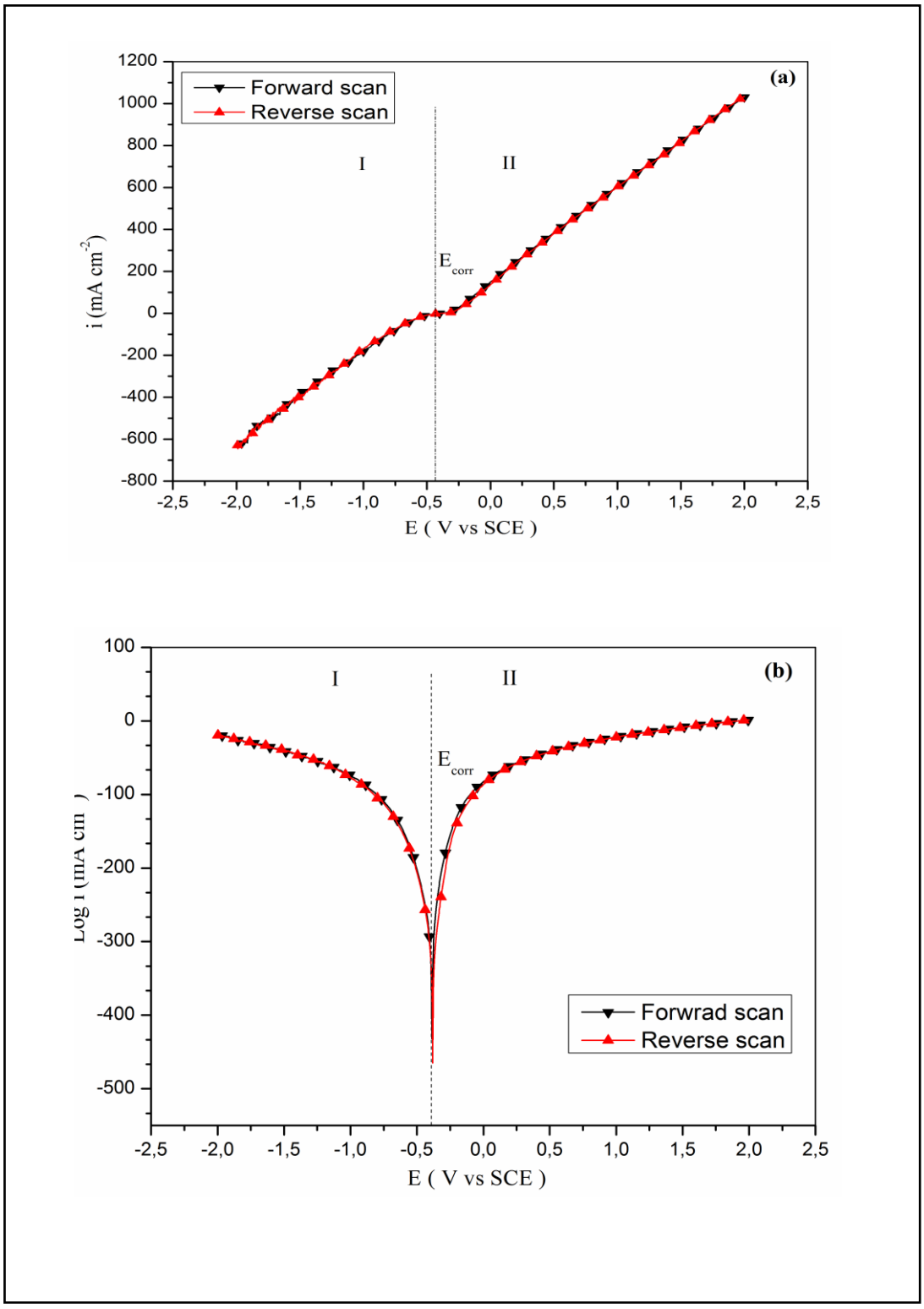


Figure III-1: Cyclic voltammogram of API 5L X70 steel in 0.5M HCl, (a) linear curve and (b) logarithmic curve at 20°C.

***API 5L X70 carbon steel in $H_2SO_4$ medium:***

Figure III-2 represents different zones of potential in the cyclic voltammogram of API 5L X70 steel in 0.5M $H_2SO_4$.

Zone I:represents the cathodic domain

Reduction reaction: $\mathbf{2H^+ + 2e^- \rightarrow H_2}$

Zone II: represents the anodic domain (active dissolution).

Oxidation reaction: $\mathbf{Fe \rightarrow Fe^{+2} + 2e^-}$ Reduction reaction: $\mathbf{2H^+ + 2e^- \rightarrow H_2}$

Zone III: The metal goes from the active state to the passive state with a drop in the current density. The corrosion potential is located in the passive domain:

$\mathbf{E_{pas} < E_{cor} < E_{pit}}$, a film ($FeSO_4$) was formed on a steel surface.

Zone IV: the trans-passive potential $E_{pit}$ indicates the end of the current level which corresponds to the passive domain. At this point, the density of the anodic partial increases due to the trans-passive dissolution. The trans-passive potential is called the pitting potential.

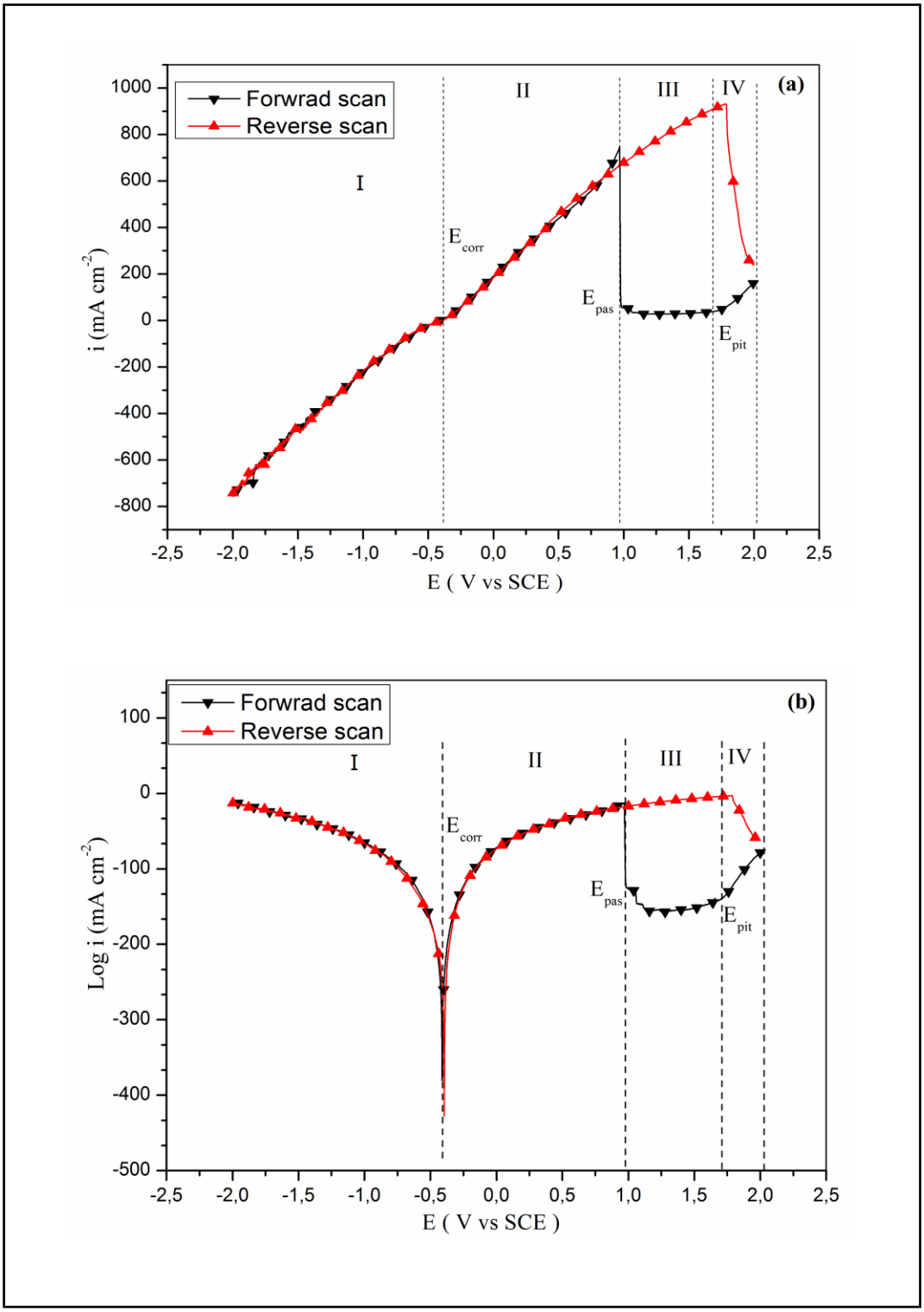


Figure III-2: Cyclic voltammogram of API 5L X70 steel in 0.5M $H_2SO_4$, (a) linear curve and (b) logarithmic curve at 20°C.

### III.1.1.2. Potentiodynamic polarization technique

Anodic and cathodic polarization of some millivolts around the corrosion potential was plotted to determine the corrosion rate and different parameters, with a scanning rate of 0.3 mv /s, at 30°C and 1 hour of immersion time.

Figure III-3 represents the logarithmic polarization curves of API 5L X70 steel in 0.5M HCl and 0.5M $H_2SO_4$ acid media at 30°C.

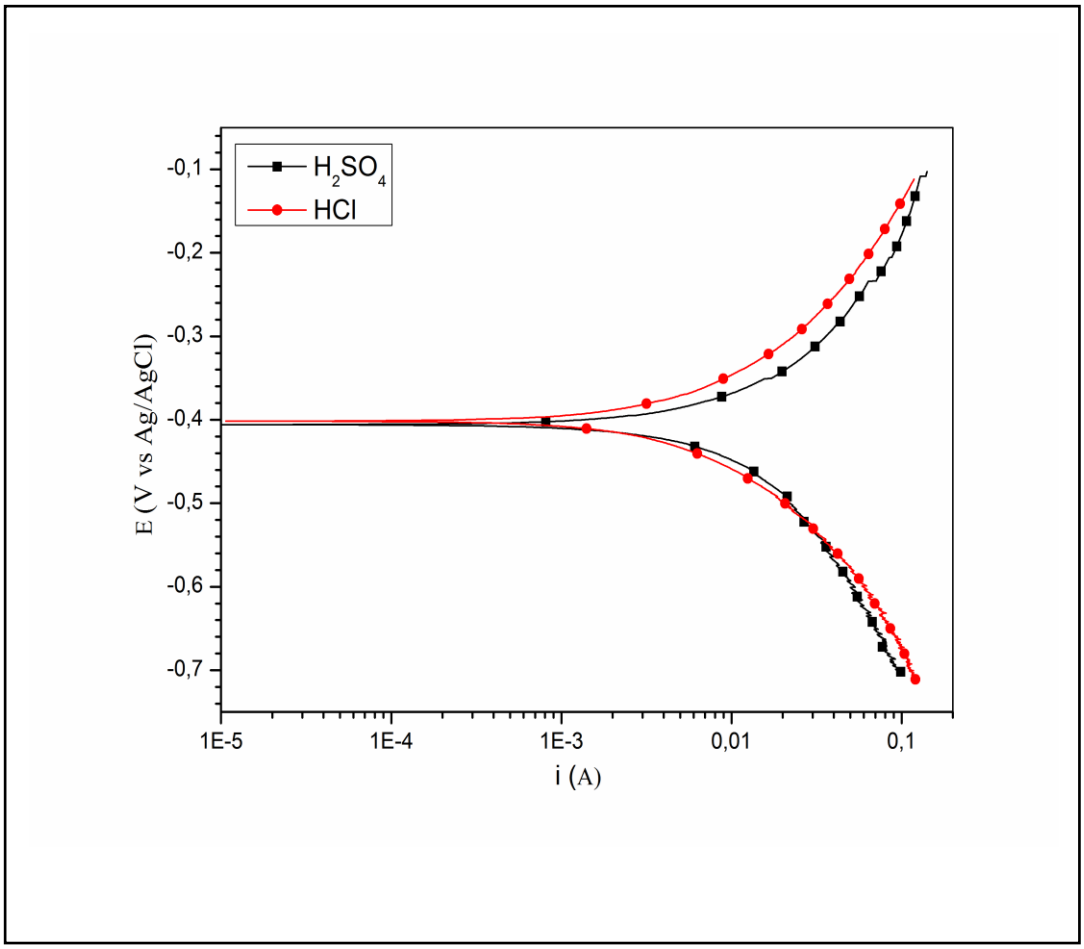


Figure III-3: Polarization curves of API 5L X70 carbon steel in 0.5M HCl and 0.5M $H_2SO_4$ at 30°C.

The corrosion reactions contain at least one partial anodic reaction and one partial cathodic reaction. It is apparent that the cathodic and anodic currents in $H_2SO_4$ medium are higher than the cathodic and anodic current in HCl medium. It means that the corrosion rate of API 5L X70 in the 0.5M $H_2SO_4$ solution is bigger than 0.5M HCl solution.

All values of the electrochemical parameters determined from the polarization test are summarized in table III-1.

Table III-1: Potentiodynamic polarization parameters for API5L X70 in 0.5M HCl solution and 0.5M $H_2SO_4$solution at 30 °C.

| Media | $E_{corr}$ (mV) | $I_{corr}$ ($\mu A\ cm^{-2}$) | - bc ($mV\ dec^{-1}$) | ba ($mV\ dec^{-1}$) |
|---|---|---|---|---|
| 0.5M HCl | -472 | 265 | 128 | 100 |
| 0.5M $H_2SO_4$ | -406 | 1661 | 126 | 102 |

From the table III-1, the corrosion rate of API 5L X70 steel in the 0.5M $H_2SO_4$ solution ($I_{corr}$= 1661$\mu A\ cm^{-2}$) is bigger than the corrosion rate API 5L X70 carbon steel in the 0.5M HCl solution ($I_{corr}$ = 265$\mu A\ cm^{-2}$),which means that 0.5M $H_2SO_4$acid solution is more aggressive than 0.5M HCl acid solution.

### III.1.1.3. Electrochemical impedance spectroscopy technique

Figures (III-4 and III-5) represent the Nyquist plots diagram and Bode plots respectively; ESI has been achieved to determine different electrochemical parameters of API 5L X70 steel in 0.5M HCl acid solution and 0.5M $H_2SO_4$ at 30°C and 1 hour of immersion time.

The table III-2 summarizes the different electrochemical parameters obtained from electrochemical impedance spectroscopy of API 5L X70 steel in 0.5M HCl solution and 0.5M $H_2SO_4$ solution.

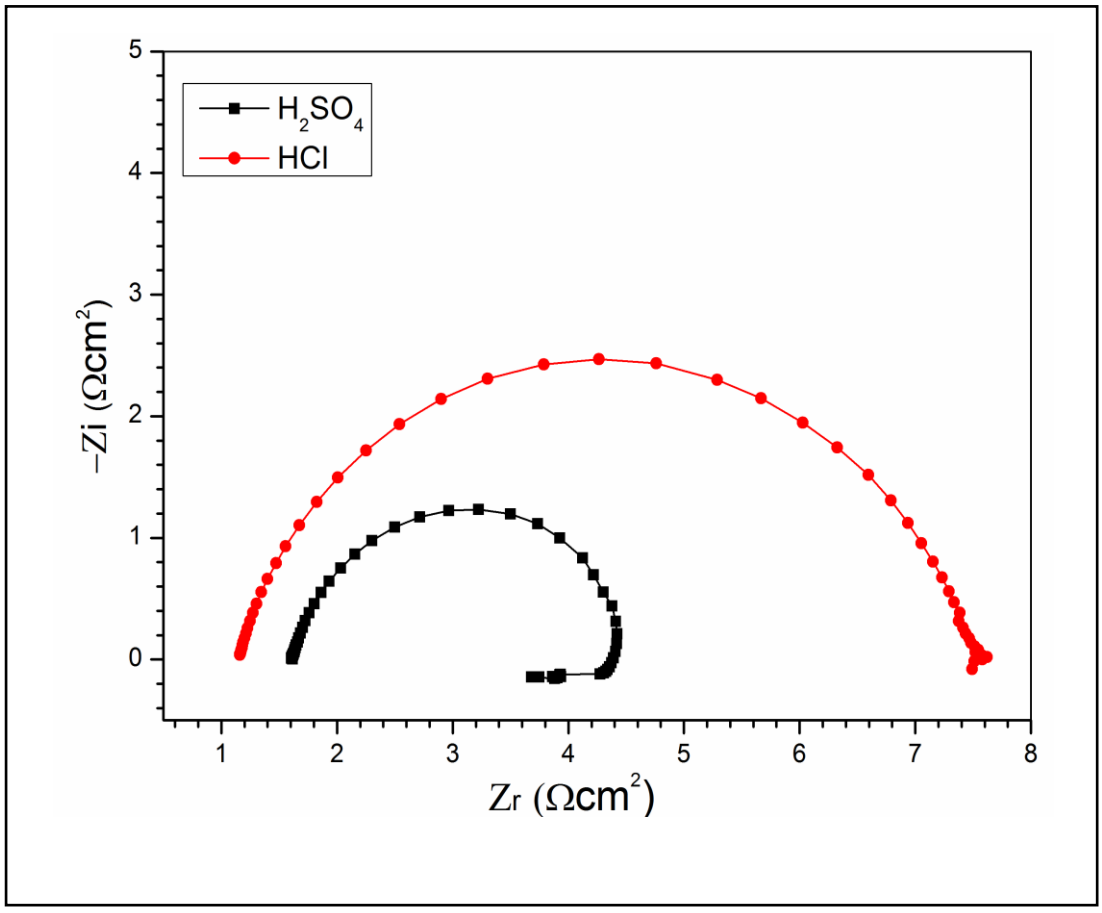


Figure III-4: Nyquist plots for API 5L X70 steel in 0.5M HCl and 0.5M $H_2SO_4$ at 30 °C

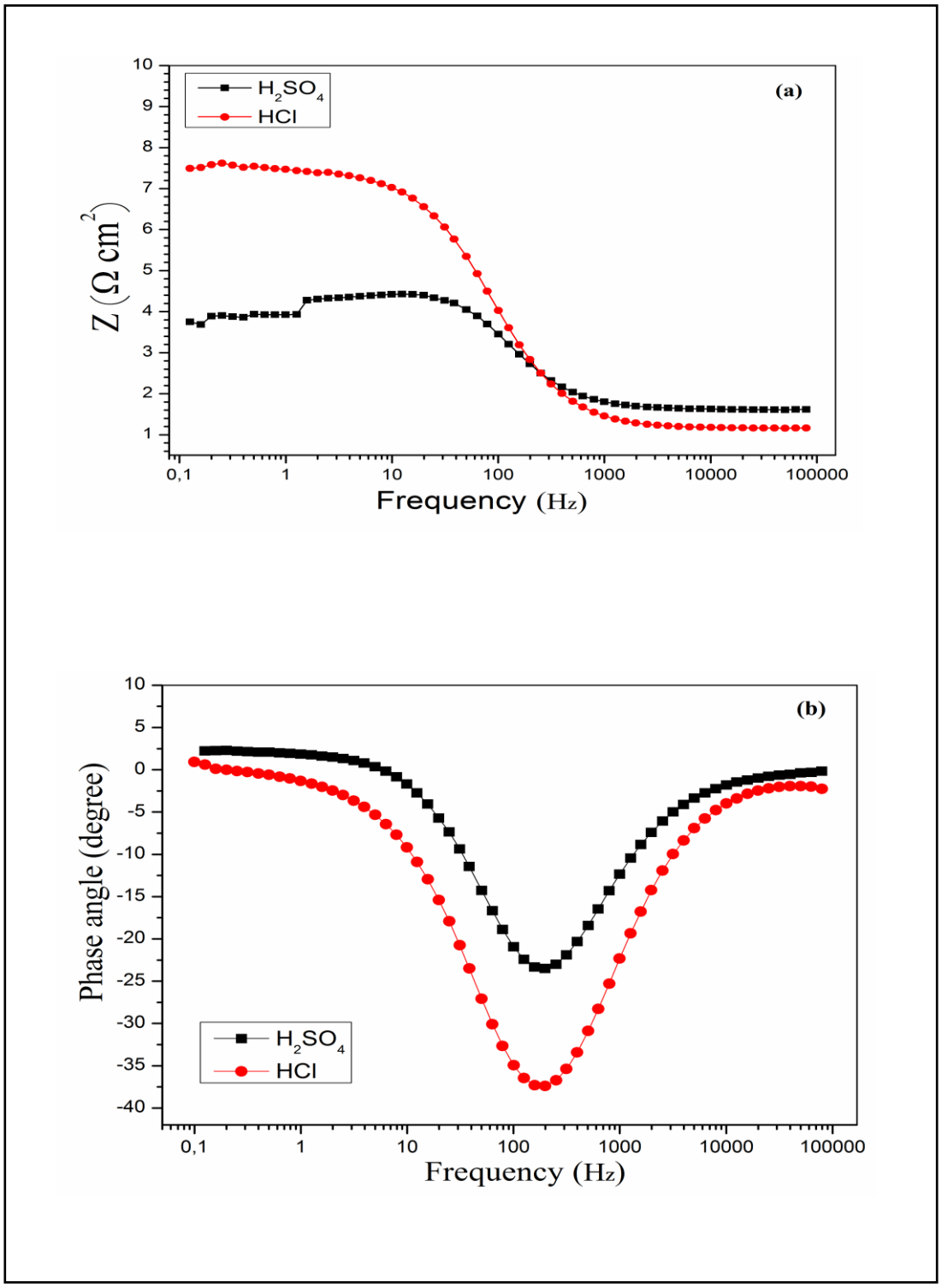


Figure III-5:Bode plots for API 5L X70 steel in 0.5M HCl and 0.5M $H_2SO_4$ at 30 °C (a)Bode modulus and (b) Bode phase angle .

Table III-2: Electrochemical impedance parameters for API 5L X70 in 0.5M HCl and 0.5M $H_2SO_4$ solution at 30 ° C.

| Media | $R_s$ $\Omega cm^2$ | $Y_0$ $\mu\Omega\ S^n\ cm^{-2}$ | n | $R_t$ ($\Omega\ cm^2$) | L ($H\ cm^2$) | $R_L$ ($\Omega cm^2$) | $C_{dl}$ ($\mu F\ cm^{-2}$) |
|---|---|---|---|---|---|---|---|
| 0.5 M $H_2SO_4$ | 1.6 | 934 | 0.89 | 2.86 | 1.17 | 9.97 | 473 |
| 0.5 M HCl | 2 | 2501 | 0.90 | 7.3 | - | - | 1344 |

Electrochemical impedance spectroscopy is a powerful technique to determine different parameters, in this study the main object is to compare between the electrochemical behavior of API 5L X70 steel in hydrochloric acid solution and sulfuric acid solution.

Based on table III-2, the electrochemical parameters of the steel in 0.5M $H_2SO_4$ acid are much lower than electrochemical parameters of the steel in 0.5M HCl acid. For example, the transfer charge resistance ($R_t$) equals 2.86 ($\Omega\ cm^2$) and the double layer capacitance $C_{dl}$ equals 473 ($\mu F\ cm^{-2}$)in 0.5M $H_2SO_4$, while in the 0.5M HCl acid solution the transfer charge resistance equals 7.3 ($\Omega\ cm^2$) and double layer capacitance equals 1344 ($\mu F\ cm^{-2}$).

From these results we can say that the 0.5M $H_2SO_4$ acid solution is more aggressive than 0.5M HCl acid solution during the reaction with API 5L X70 steel at 30°C.

There is a great arrangement between potentiondynamic polarization test and electrochemical impedance spectroscopy; both of them have the same result that the sulfuric acid is more aggressive than hydrochloric acid.

### III.1.2. Immersion test of API 5L X70 steel in HCl and $H_2SO_4$ acid medium

Immersion test was achieved to investigate the corrosion type of API 5L X70 steel in 0.5M HCl and 0.5M $H_2SO_4$ medium after 72 hours of immersion. The surface has been analyzed by using **SEM** microscopy after removing the corrosion products by polishing the surface with 1200 paper and tissue paper for 30 second as shown in figure III-6

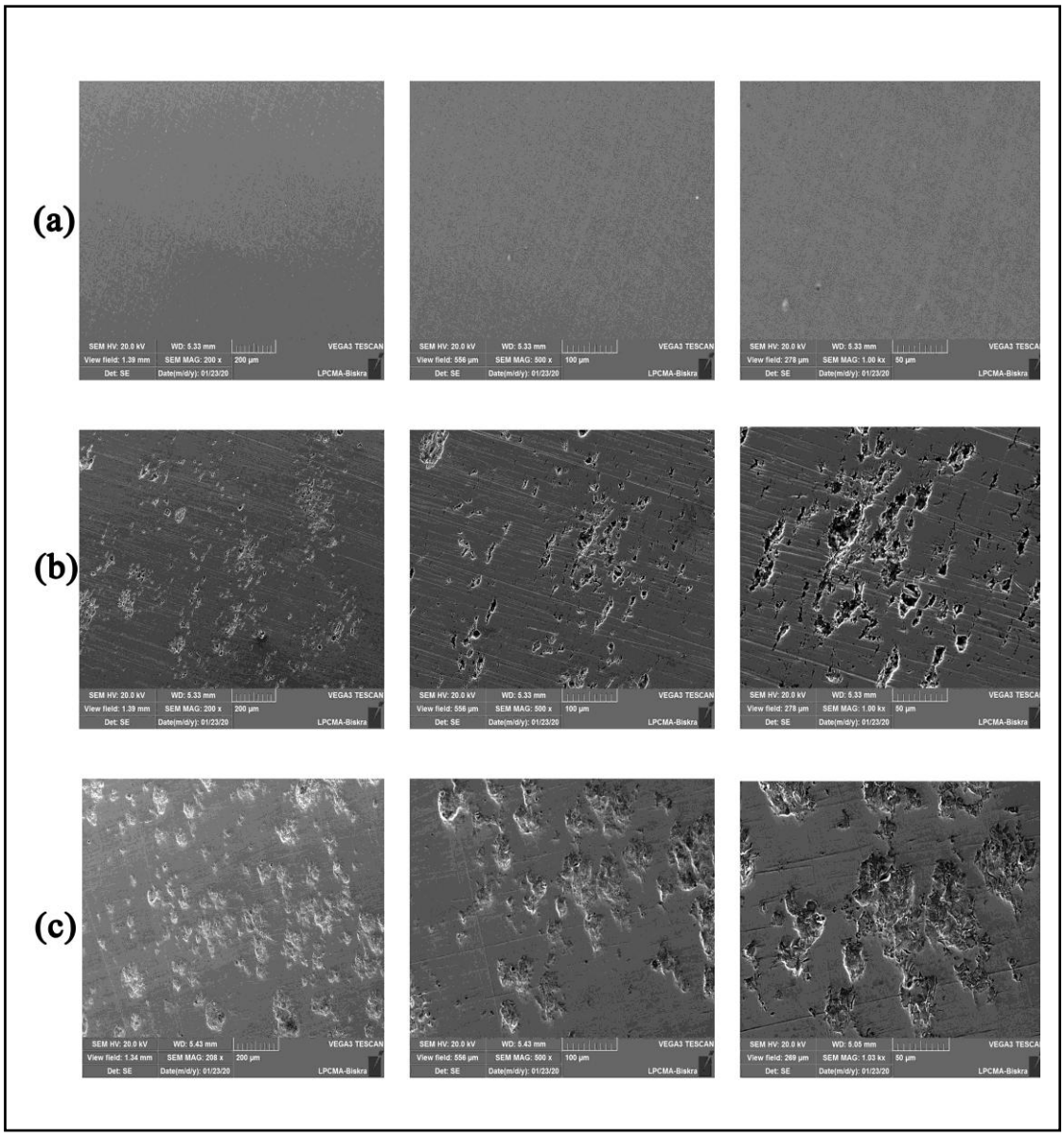


Figure III-6: SEM images of the API 5L X70 steel surface after removing the corrosion products (a) before corrosion, (b) after immersion in 0.5 M HCl, (c) after immersion in 0.5M $H_2SO_4$ at 30°C for 72 h.

Hydrochloric and sulfuric solution can be described as strongly acidic solution due to the great number of hydrogen ions and concentration in the solution.

General corrosion or uniform corrosion is the type of corrosion of carbon steel in hydrochloric and sulfuric acid solution. It is characterized by corrosive attack proceeding evenly over the entire surface area, or a large fraction of the total area[63].

From the figure III-6,the SEM morphologies (b) and (c) of API 5L X70 steel were immersed in 0.5M HCl and 0.5M $H_2SO_4$, the surface of the specimens seem completely attacked and corroded at 200µm of magnification in both acid solutions the damage on the API 5L X70 steel surface is due to the oxidation reaction and dissolution of iron.

In more focalization, the SEM morphologies at 50µm of magnification are easy to see the pitting corrosion. The appearance of pits on steel surface refers to the anions $Cl^-$ in the hydrochloric acid solution from SEM morphology (b), and $SO_4^{-2}$ in sulfuric acid solution in SEM morphology (c), pits shape and size in HCl solution is different from $H_2SO_4$ solution, it is 20 µm in HCl solution and 40µm in $H_2SO_4$,the corrosion pits grow when the immersion time increases.

The results obtained from the SEM analyses of API 5L X70 steel specimens after immersion test in 0.5M HCl and 0.5M $H_2SO_4$ acid solutions conformed the results obtained from the electrochemical impedance spectroscopy and potentiondynamic polarization.

## III.2. Part two : Effect of BRSM on Inhibition Efficiency of API 5L X70 steel in 0.5M HCl acid solution

### III.2.1. Fourier-transform infrared spectroscopy (FTIR) of BRSM

FTIR spectrum of BRSM is shown in Figure III-7. Original absorption band at3438 $cm^{-1}$(associated hydroxyl) was overlapped by the strong stretching mode of N–H. The strong band at 1705 $cm^{-1}$is due to C=O stretching band (cyclic ketone). The strong band at 2940 $cm^{-1}$is due to O–H stretching band, it indicates the presence of carboxylic acid group in the inhibitor.

The peak at 1455 $cm^{-1}$is due to aromatic C–C stretching band. The C–N asymmetric stretching band is observed at1390 $cm^{-1}$.There is absorption band at1055 $cm^{-1}$, which can be ascribed to the C–N or C–O stretching vibration. These observations confirmed that the bark resin of S. molle contains a mixture of natural products. These results indicate that BRSM contains O and probably N atoms in functional groups(O–H, N–H, C=O (ketone), C–N, C–O) and aromatic ring.

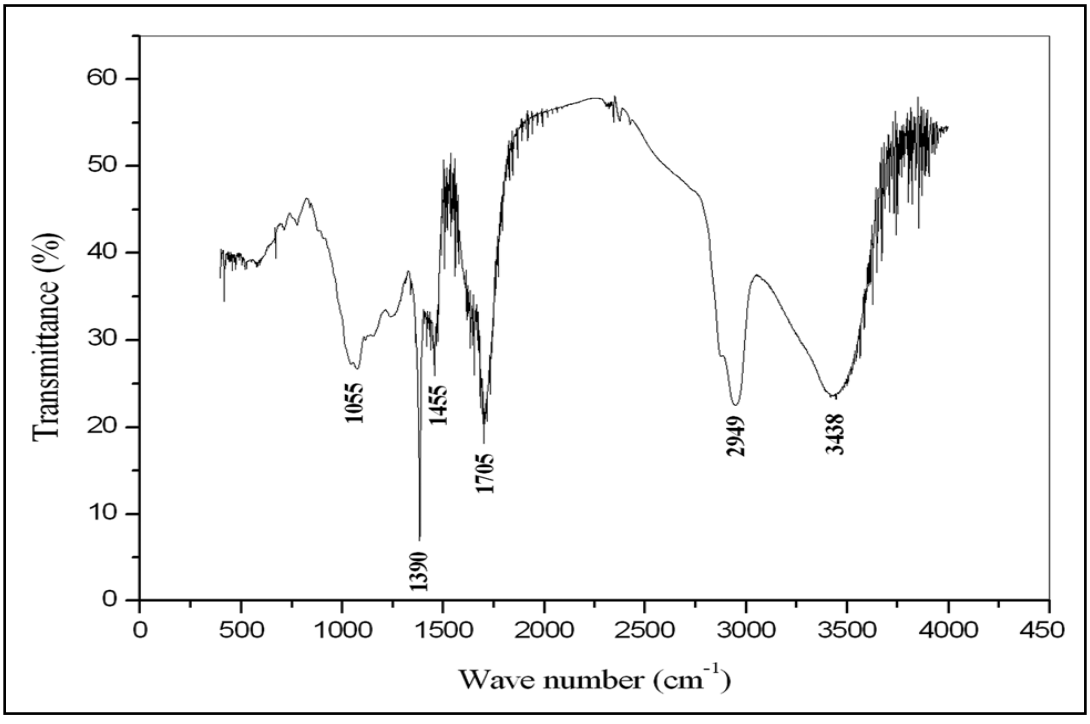


Figure III-7 : FTIR spectra of BRSM

### III.2.2. Potentiodynamic polarization measurements of API 5L X70 steel in 0.5 M HCl media

The effect of bark resin of S. molle on the anodic and cathodic behavior of API 5L X70 steel in 0.5Mhydrochloric acid solution has been studied by polarization measurements and the Tafel plots are shown in Figure III-8.The values of corrosion current density ($I_{corr}$), corrosion potential ($E_{corr}$), cathodic Tafel slope ($b_c$), anodic Tafel slope ($b_a$), and inhibition efficiency ($\eta_{pol}$) are presented in Table III-3.

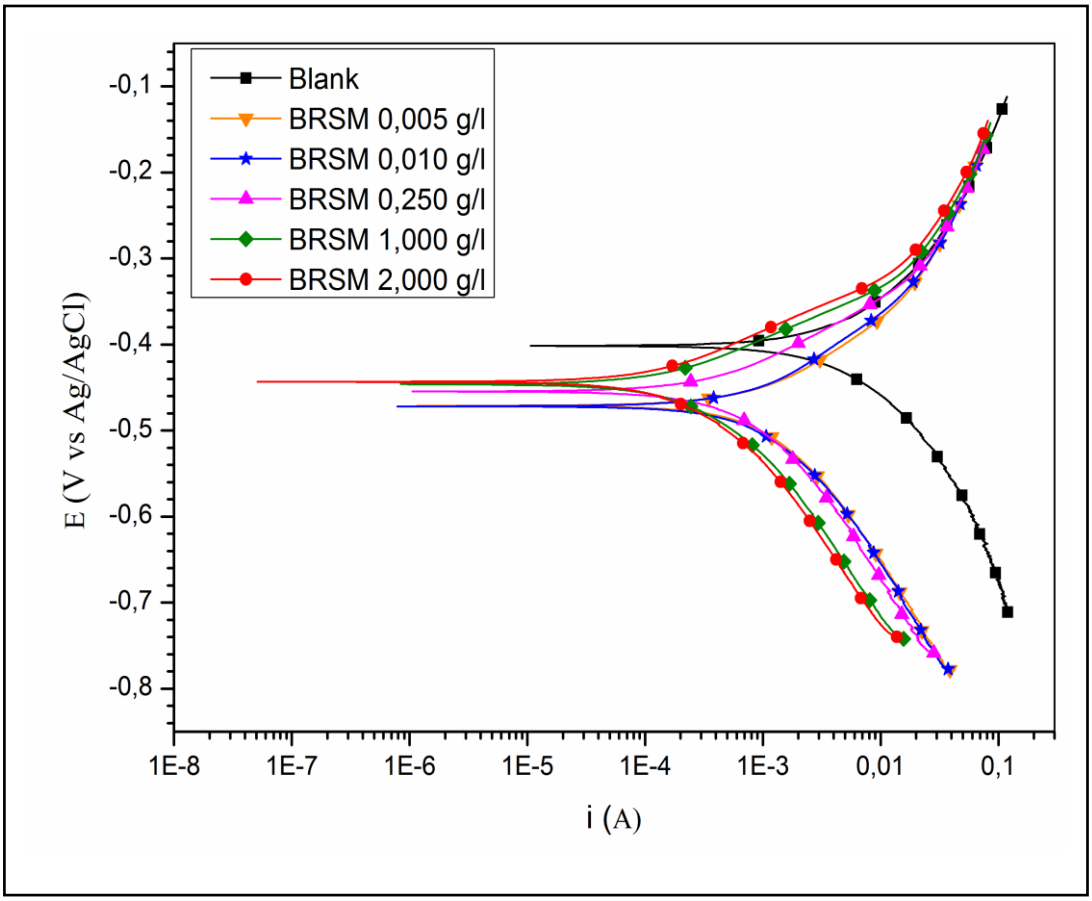


Figure III-8: Potentiodynamic polarization curves for API 5L X70 pipeline steel in 0.5M HCl without and with different concentrations of BRSM at 30 °C (immersion time is 1 h)

Both anodic and cathodic current were decreased in Figure III-8 indicating that BRSM suppressed both the anodic and cathodic reactions through adsorption on the carbon steel surface.

Table III-3: Potentiodynamic polarization parameters for API 5L X70 in 0.5 M HCl solution in the absence and the presence of BRSM at 30 °C.

| Concentration | $E_{corr}$ (mV) | $I_{corr}$ ($\mu A\ cm^{-2}$) | $-b_c$ ($mV\ dec^{-1}$) | $b_a$ ($mV\ dec^{-1}$) | $\eta_{pol}$ % |
|---|---|---|---|---|---|
| Blank | -472 | 265 | 128 | 100 | - |
| 0.005 gL-1 BRSM | -472 | 96 | 142 | 91 | 63 |
| 0.010 gL-1 BRSM | -472 | 79 | 125 | 90 | 70 |
| 0.250 gL-1 BRSM | -452 | 51 | 125 | 76 | 80 |
| 1.000 gL-1 BRSM | -448 | 30 | 130 | 72 | 88 |
| 2.000 gL-1 BRSM | -442 | 22 | 125 | 76 | 91 |

From Table III-3 it is evident that the corrosion current density ($I_{corr}$) value decreases from 265 to 22 $\mu A\ cm^{-2}$with the highest concentration of BRSM (2 $g\ L^{-1}$). The addition of BRSM does not alter the value of $E_{corr}$ significantly indicating the mixed type of inhibiting behavior of the inhibitor. Generally, if the displacement in $E_{corr}$ is >85 mV with respect to $E_{corr}$ in uninhibited solution, the inhibitor can be seen as a cathodic or anodic type[64, 65].In our study the maximum displacement is 30 mV, which confirms that BRSM acts as a mixed-type inhibitor. The similar results were also reported with Rollinia occidentalis extract [66] and Gum Arabic [67].

Cao[68],explained that if the shift of corrosion potential due to addition of an interface inhibitors negligible, the inhibition is most probably caused by a geometric blocking effect of the adsorbed inhibitive species on the surface of the corroding metal. From the polarization results, it could be concluded that the inhibition of BRSM may be mainly due to the geometric blocking effect.

From Table III-3, $I_{corr}$ decreases and $\eta_{pol}$ increases with the increase in inhibitor concentration. The maximum value of 91% of $\eta_{pol}$ also indicates that BRSM is a good inhibitor for API 5L X70 steel in 0.5M hydrochloric acid.

### III.2.3. Electrochemical impedance spectroscopy measurements of API 5L X70 steel in 0.5 M HCl media

Figure III-9 shows the Nyquist diagrams for BRSM in 0.5M hydrochloric acid at 30 °C (immersion time is 1 h).Obviously, all impedance spectra have typical characteristics that have been widely reported for steel in strong acid media. As shown in Figure III-9, in uninhibited and inhibited 0.5M hydrochloric acid solutions, the impedance spectra exhibit one single capacitive loop, which indicates that the corrosion of steel is mainly controlled by the charge transfer process[69, 70].

In the case of the geometric blocking effect, the EIS display will be a single capacitive loop if the inhibition efficiency is high and similar to that in the blank solution if the inhibition efficiency is low [14, 68], which suggests that the geometric blocking effect is the inhibition mode of BRSM.

The same mode was also reported with Rollinia occidentalis extract [66]. It is noted that these capacitive loops are not perfect semicircles which can be attributed to the inhomogeneity of the electrode surface arising from surface roughness or interfacial phenomena [71]. Furthermore, the diameter of the capacitive loop in the presence of inhibitor (BRSM) is larger than that in blank solution, and enlarges with the inhibitor concentration. This indicates that the impedance of inhibited substrate increases with the inhibitor concentration, and leads to good inhibitive performance.

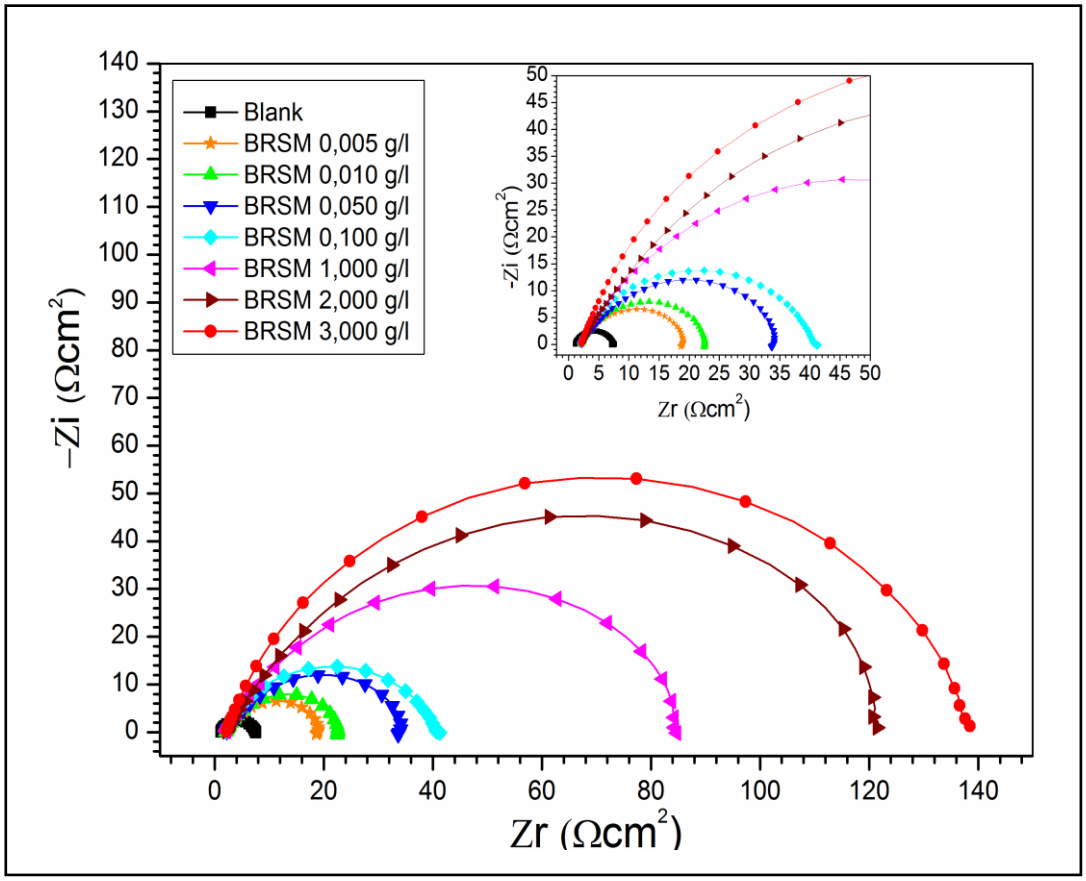


Figure III-9: Nyquist plots of the corrosion of API 5L X70 in 0.5M HCl without and with different concentrations of BRSM at 30 °C (immersion time is 1 h)

The experimental EIS are presented as Bode plots in Figure III-10. According to the Bode plot of impedance module |Z| versus frequency (Figure III-10 (a)), the |Z| of API 5L X70 steel is clearly found to depend on the inhibitor concentration. An increase in inhibitor concentration leads to an increase in the |Z| value. The phase angle plots (Figure III-10 (b)) show one time constant.

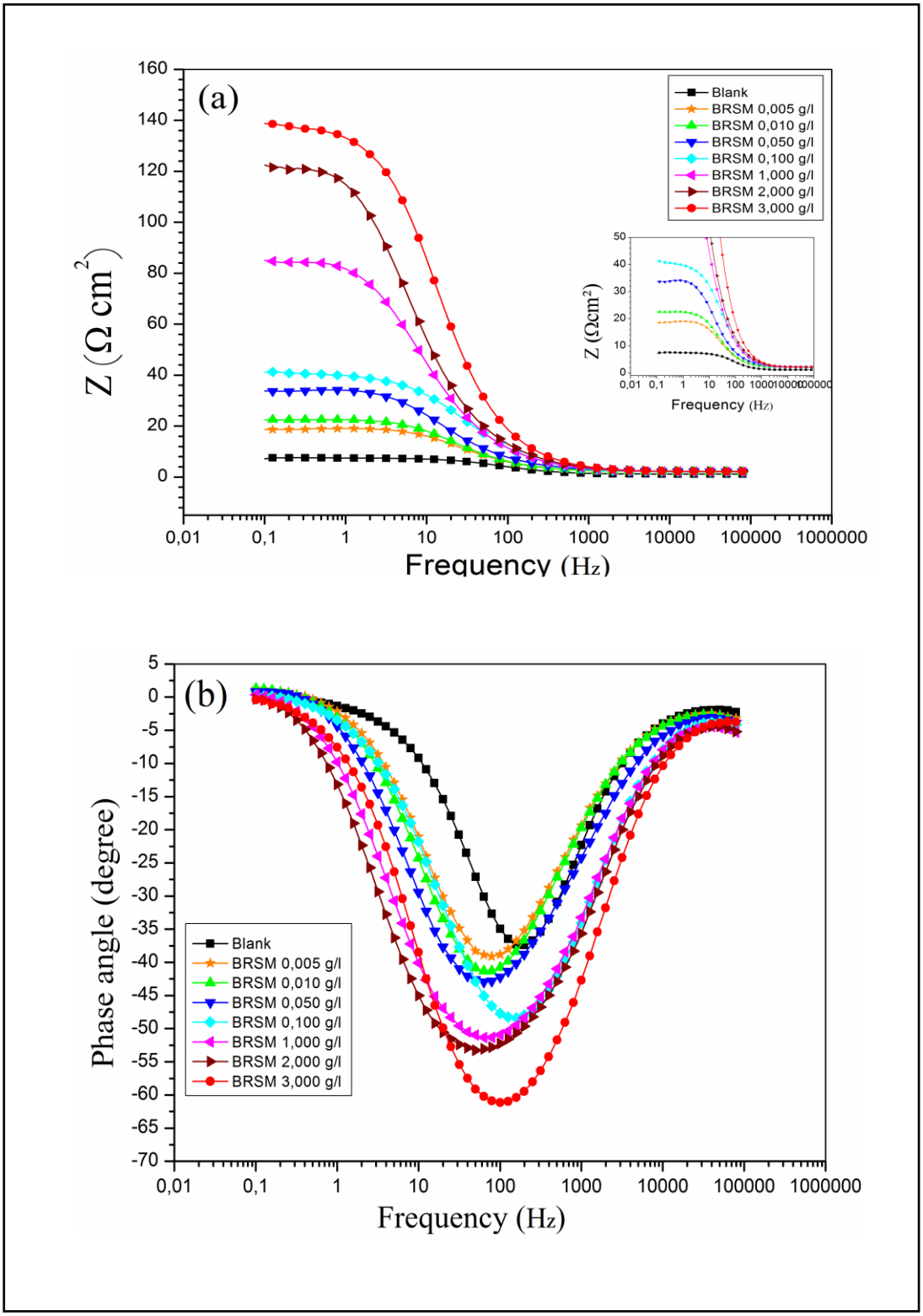


Figure III-10**:** Bode plots for API 5L X70 steel in 0.5 M HCl without and with different concentrations of BRSM at 30 °C, (a)Bode modulus and (b) Bode phase angle .

## ***Equivalent circuit model:***

A model of equivalent circuit has been attempted to fit these experimental data using the software Impedance Model Editor designed by Gamry Echem Analyst. Figure III-11 shows simulated and experimentally generated impedance diagrams for API5L X70 steel immersed in 0.5Mhydrochloric acid solution in the presence of 3 g $L^{-1}$BRSM.Excellent fit with this model was obtained for all experimental data. The circuit consists of the solution resistance $R_s$, the constant phase element representing the double-layer capacitance ($CPE_{dl}$) and the charge transfer resistance $R_t$.

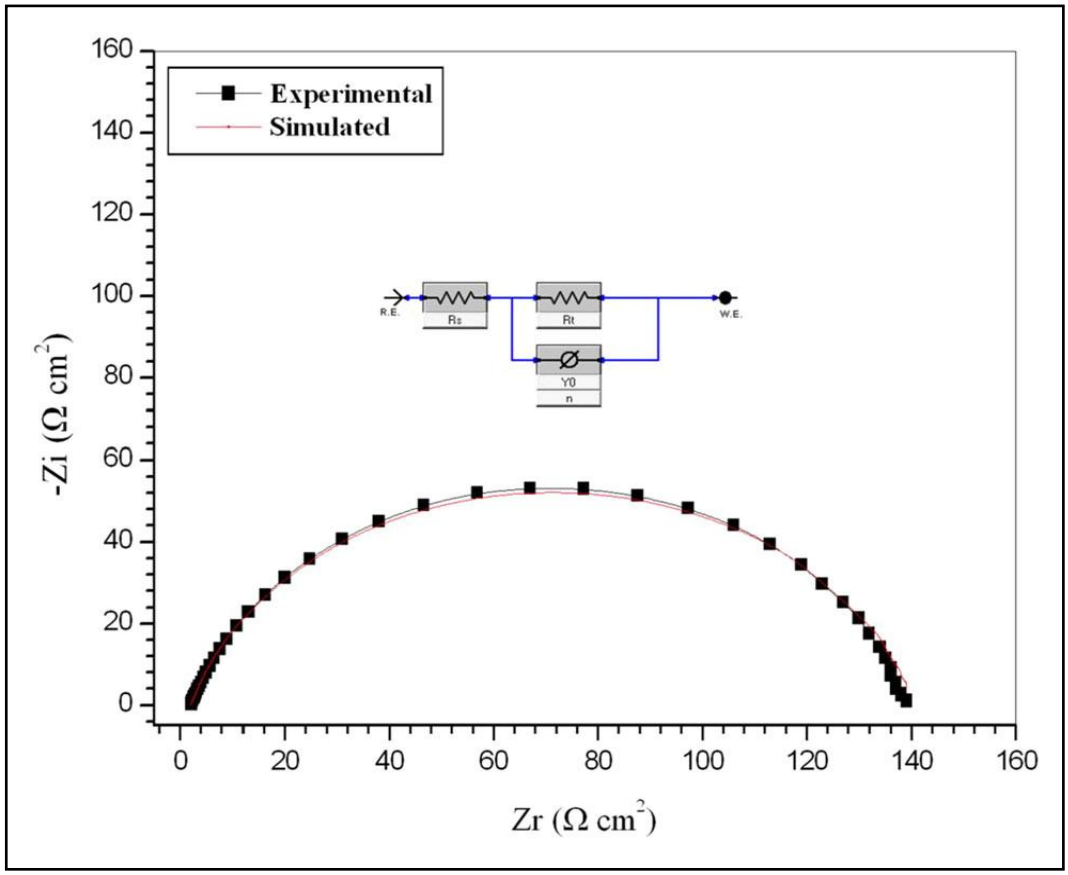


Figure III-11:Nyquist plot of experimental data and simulated data, together with the equivalent circuit used to fit the impedance data ,recorded for API 5L X70 steel in 0.5M HCl containing 3 $gL^{-1}$ BRSM.

Table III-4 shows representative parameter values of the fitting results to EIS data obtained for API 5L X70 steel using the equivalent circuits of figure III-11. The solution resistance $R_s$ is constant; it is equal to 2 Ω $cm^2$ in all experiences in this part.

Table III-4: Electrochemical impedance parameters for API 5L X70 in 0.5 M HCl solution in the absence and the presence of BRSM at 30 ° C.

| Concentration | $Y_0$ ($\mu\Omega S^n cm^{-2}$) | n | $R_t$ ($\Omega cm^2$) | $C_{dl}$ ($\mu F cm^{-2}$) | $\eta_{EIS}$ % |
|---|---|---|---|---|---|
| Blank | 2501 | 0.90 | 7.3 | 1344 | - |
| 0.005 g $L^{-1}$ BRSM | 1186 | 0.78 | 17.4 | 410 | 58 |
| 0.010 g $L^{-1}$ BRSM | 1179 | 0.78 | 21.2 | 407 | 65 |
| 0.050 g $L^{-1}$ BRSM | 1148 | 0.74 | 33.4 | 369 | 78 |
| 0.250 g $L^{-1}$ BRSM | 900 | 0.80 | 39.0 | 342 | 81 |
| 1.000 g $L^{-1}$ BRSM | 680 | 0.76 | 87.0 | 281 | 91 |
| 2.000 g $L^{-1}$ BRSM | 659 | 0.74 | 127.6 | 253 | 94 |
| 3.000 g $L^{-1}$ BRSM | 259 | 0.82 | 138.0 | 123 | 94 |

$R_t$ values remarkably increased from the value of 7.3 Ω$cm^2$ for the solution without BRSM to 138 Ω$cm^2$ for the highest concentration of BRSM (3 g $L^{-1}$) in the solution at 30 °C. This indicates that the corrosion resistance of API 5L X70 steel was increased with increasing BRSM concentration. It should be noted that when the inhibitor concentration reaches about 2 g $L^{-1}$, $R_t$ value reaches certain data and does not change markedly.

In order to give more accurate fit results, the constant phase elements (CPE) were submitted for the capacitors [72]. The impedance value of the CPE is a function of frequency, but its phase is independent of frequency. Its impedance is defined as [73, 74]

$$Z_{CPE} = Y_0^{-1}(j\omega)^{-n} \qquad \text{Equ III. 1}$$

where $Z_{CPE}$ represents the impedance of a CPE, $Y_0$ is a proportional factor that indicates the combination of properties related to both the surfaces and electro active species in dependent of frequency, j is imaginary number,ω is the angular frequency, and ω equal to 2πf, where f is the frequency; and n has the meaning of a phase shift and is related to a slope of the log |Z| versus log f plots and usually is in the range between 0.5 and 1.

The double layer capacitance $C_{dl}$ was calculated using Equ III.2 [75]

$$C_{dl} = Y0\ (2\pi F_{max})^{n-1} \qquad \text{Equ III. 2}$$

Where $f_{max}$ is the frequency at which the imaginary component of the impedance is maximum. On the contrary to the charge transfer resistance, better protection provided by an inhibitor can be associated with a decrease in capacitance of the metal. $C_{dl}$ values remarkably decreased from the value of 1344 μF $cm^{-2}$ for the solution without BRSM to 123 μF $cm^{-2}$ for the highest concentration of BRSM (3 g $L^{-1}$) in the solution at 30 °C.

Good agreement between electrochemical impedance spectroscopy and potentiodynamic polarization curves is obtained.

## ***Inhibition efficiency variation:***

Based on the values of $R_t$ in table III-2 the variation of inhibition efficiency ($\eta_{EIS}$) for carbon steel in the 0.5M hydrochloric acid solution as a function of BRSM concentration is shown in Figure III-12. When the concentration of BRSM is less than 2 $gL^{-1}$, $\eta_{EIS}$ increases sharply with an increase in concentration, while a further increase causes no appreciable change in performance. At 2 g $L^{-1}$of BRSM, $\eta_{EIS}$ value is higher than 94%, which indicates that BRSM is a good inhibitor for API 5L X70 steel in HCl solution.

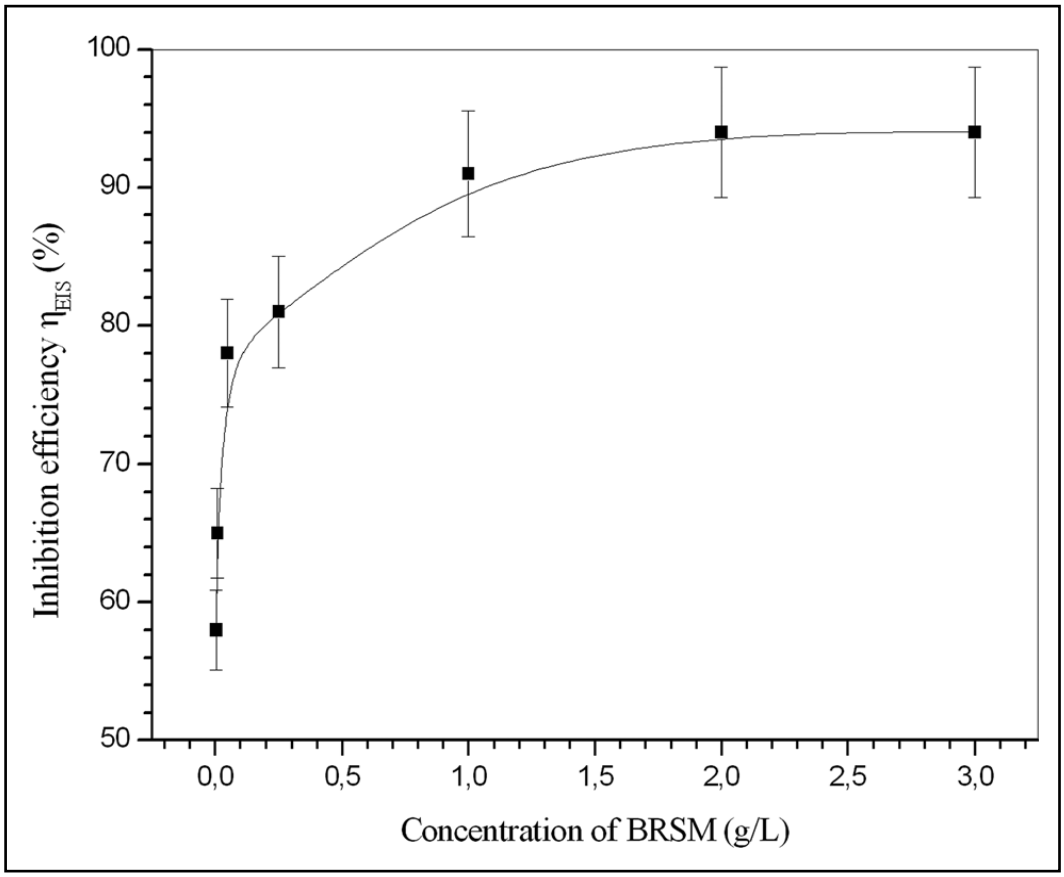


Figure III-12: Relationship between inhibition efficiency ($\eta_{EIS}$) and concentration of BRSM in 0.5M HCl at 30 °C (Electrochemical impedance spectroscopy method, immersion time is 1 h).

### III.2.4. Adsorption isotherm and standard adsorption free energy

In the present study, several adsorption isotherms were assessed, and the Langmuir adsorption isotherm was found to give the best description of the adsorption behavior of the studied inhibitor (Figure III-13). A correlation between surface coverage ($\theta = \eta_{EIS}\%/100$) and the concentration of inhibitor (C) in the electrolyte can be represented by the Langmuir adsorption isotherm [76].

$$\frac{C}{\theta} = \frac{1}{K_{ads}} + C \qquad \text{Equ III. 3}$$

Where the $K_{ads}$ is constant of adsorption. By plotting C/θ versus C, straight line with slope value close to 1 was obtained. From the value of the adsorption constant, the standard free energy of adsorption $\Delta G^{\circ}_{ads}$ is determined usingthe following equation [14, 49, 77]:

$$\Delta G^{\circ}_{ads} = -RT\ln(1 \times 10^{6} K_{ads}) \qquad \text{Equ III. 4}$$

Where $1 \times 10^{6}$ is the concentration of water molecules expressed in mg $L^{-1}$, R is the universal gas constant and T is the absolute temperature. The values of $\Delta G^{\circ}_{ads}$ and $K_{ads}$ are listed in Table III-3. Generally, values of $\Delta G^{\circ}_{ads}$ up to $-20$ kJ $mol^{-1}$are consistent with electrostatic interaction between charged molecules and a charged metal (which indicates physical adsorption) while those more negative than $-40$ kJ $mol^{-1}$involves charge sharing or transfer from the inhibitor components to the metal surface to form a coordinate type of bond (which indicates chemisorption) [78-80]. It is difficult to distinguish between chemisorptions and physisorption only based on these criteria, especially when charged species are adsorbed.

The possibility of Coulomb interactions between adsorbed cations and specifically adsorbed anions can increase the Gibbs energy even if no chemical bond appears[68].Of the two possibilities, the physisorption mode is likely to predominate due to the obtained value of $\Delta G^{\circ}_{ads}$ (-24.76 kJ $mol^{-1}$). Similar results were also reported with Sunflower seed hull extract [81].

Table III-5: Parameters of Langmuir adsorption isotherm for API 5L X70 in 0.5M HCl solution containing BRSM at 30 °C

| Isotherm mode | Linear correlation coefficient | Slope | $K_{ads}$ (L $g^{-1}$) | $\Delta G°_{ads}$ (kJ $mol^{-1}$) |
|---|---|---|---|---|
| Langmuir | 0,99991 | 1,05 | 54.85 | -24.76 |

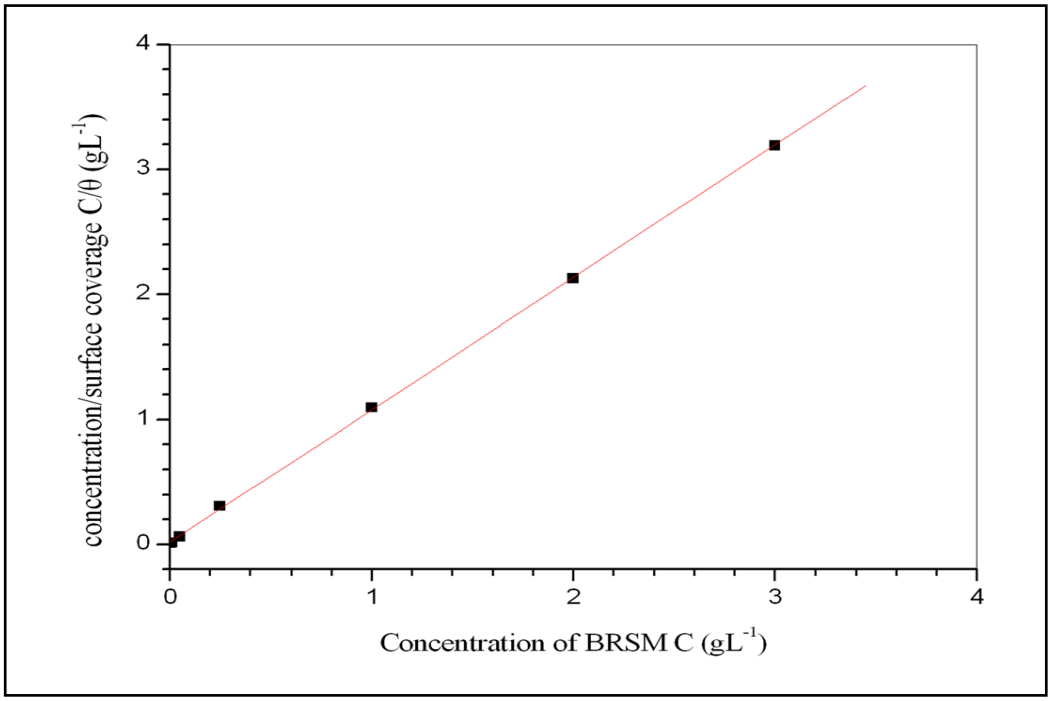


Figure III-13: Langmuir isotherm adsorption mode of BRSM on the API 5L X70 steel surface in 0.5M HCl at 30 °C (from EIS measurements).

### III.2.5. SEM-EDX analysis

Figure III-14 shows the microstructure and the corresponding chemical analysis for the polished metal, in the presence and absence of the inhibitor (BRSM), to confirm the efficiency of BRSM obtained by the EIS and polarization curves methods. The polished steel consists principally of the iron element (Figure III-14(a)). When the metal was submerged in hydrochloric acid, it was observed that in addition to the iron element, the oxygen element and the chlorine element are present as a consequence of the corrosion phenomenon (Figure III-14(b)).

In the microstructure corresponding to the sample with the inhibitor (Figure III-14(c)), a decrease in corrosion can be observed. To determine the elements present in API 5L X70 steel surface after 60 h of exposure to 0.5M hydrochloric acid, EDX analysis were used.

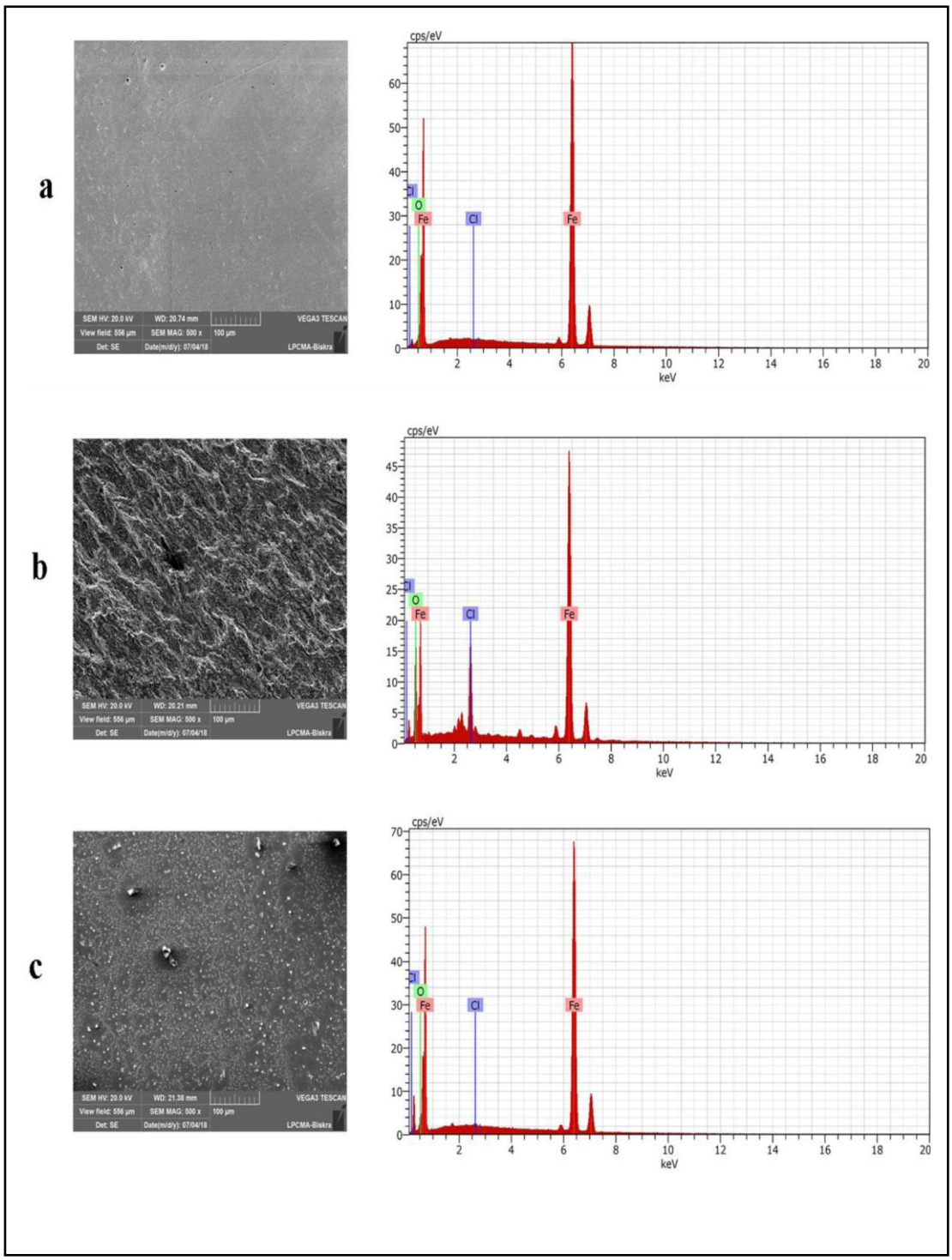


Figure III-14: SEM-EDX spectra of API 5L X70 steel: polished steel (a), in presence of corroding medium (b), and in presence of 2 $gL^{-1}$ BRSM (c)

Before the corrosion test, the peaks are related only to the iron element present in the API 5L X70 steel (Table III-6). In the absence of inhibitor, the spectra exhibit the peaks of the oxygen element and the chlorine element which polished API 5L X70 does not have.

The spectra of API 5L X70 steel immersed in 0.5M hydrochloric acid containing 2 g $L^{-1}$BRSM shows that the amount of oxygen and chlorine decreases, probably due to the adsorption of BRSM on the surface of API 5L X70 steel.

Table III-6: Content of elements obtained from EDX spectra for API 5L X70 steel

| Element | % atomic | | |
|---|---|---|---|
| | Steel | Steel + HCl | Steel + HCl + 2 g/L BRSM |
| iron | 96.47 | 58.95 | 93.42 |
| oxygen | 3.53 | 32.66 | 6.26 |
| chlorine | 0.00 | 8.39 | 0.32 |

The figure III-15 shows SEM images of API 5L X70 steel immersion in hydrochloric acid medium with and without BRSM inhibitor after removing the corrosion products. The metal specimens were immersed in 0.5M HCl in the presence and absence optimum concentration of BRSM inhibitor for 72 hours at 20°C.

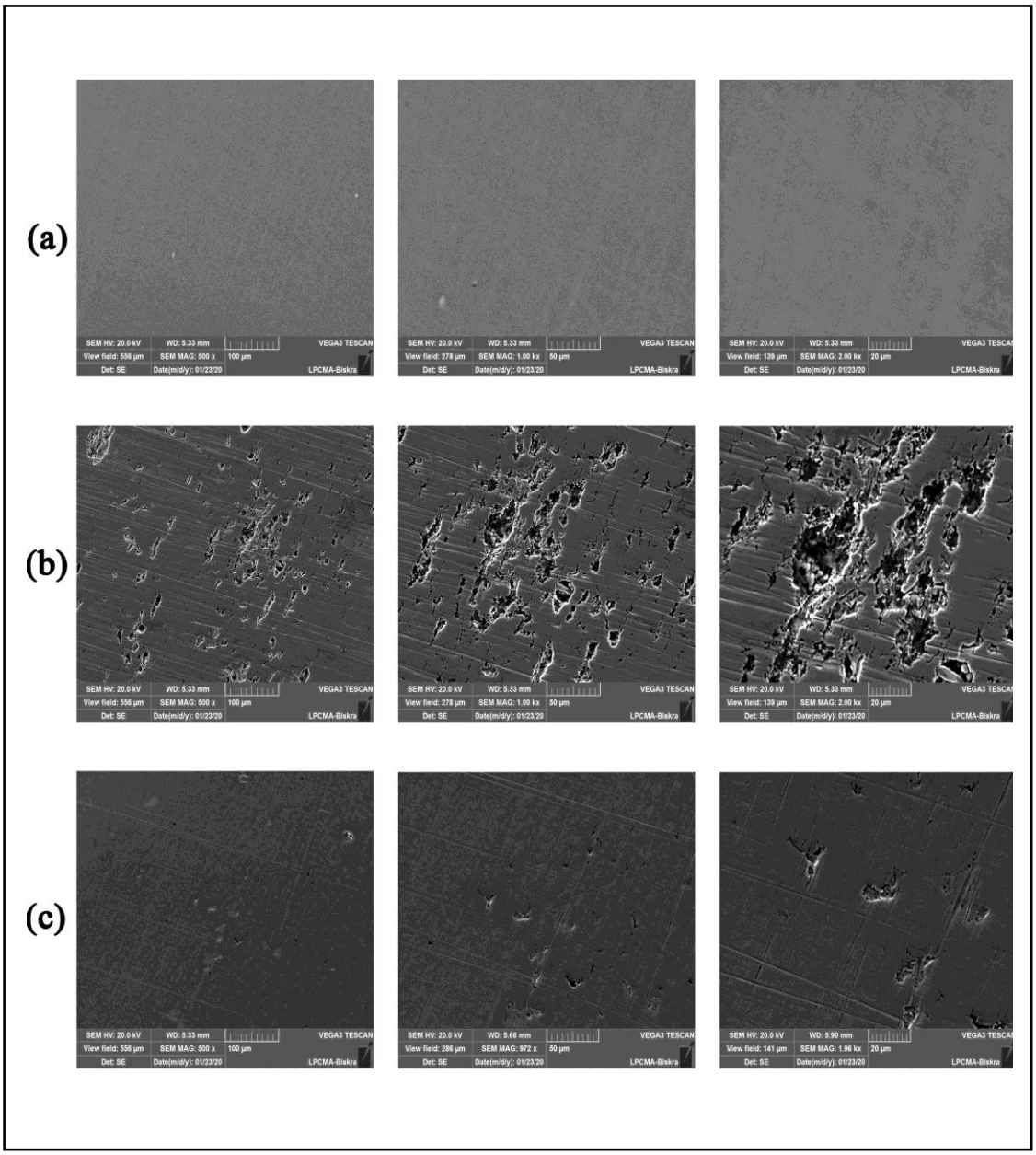


Figure III-15:SEM images of the API 5L X70 steel surface after removing the corrosion products (a) before corrosion, (b) after immersion in 0.5 M HCl, (c) after immersion in 0.5M HCl + 2g/L BRSM at 20°C for 72 h.

The specimens were removed and polished with abrasive paper (1200 grade) to 10 seconds and tissue paper to 20 seconds for removing the corrosion products on steel surface and rinsed with acetone and dried and used for taking the images with different magnifications.

Based on the result obtained from figure III-15, the comparative analysis of the SEM images shows that the solution is without and with inhibitor. It presents a generalized type of corrosion and dissolution of iron material (figure b), this is evident in the 100µm image magnification .The formation of pits is observed most often in the presence of $\mathbf{Cl^-}$ ions [82], and also the development of these pits is due to the immersion time.

On the other hand, when the API 5L X70 steel was immersed in 0.5M HCl solution containing the optimal concentration (2 g/L) of BRSM (figure c), the specimen surface seems almost intact and the degree of damage and dissolution of the iron is reduced. The size of corrosion pits in absence of BRSM is 20µm while in presence of 2 g/L BRSM, the corrosion pits are reduced on all steel surface.

The results obtained from the immersion test are conformed the results of electrochemical impedance spectroscopy and potentiodynamic polarization where the inhibition efficiency equals 94% at 2 g/L BRSM.

Figure III-15 conformed the inhibition mechanism, the interaction between the inhibitor and metal surface shows of the formation of true physical barriers.

## III.3. Part three: Synergistic effect of Iodide ions and BRSM for the corrosion inhibition of API 5L X70 steel in 0.5M HCl

The synergistic effect of iodide ions and BRSM has been investigated for the corrosion inhibition by using different electrochemical techniques to determine the electrochemical parameters such as corrosion rate and corrosion potential, SEM and EDX technique have also been used to analyze to the surface of steel.

### III.3.1. Potentiodynamic polarization measurements of API 5L X70 steel in 0.5M HCl in presence of BRSM and KI

The potentiodynamic polarization behavior of API 5L X70 steel in 0.5 M HCl with 3mM KI and with the different concentrations of BRSM is shown in Figure III-16. It is clear from the figure that the addition of BRSM has reduced both the anodic iron dissolution and cathodic hydrogen evolution reactions. Corrosion current densities reduced markedly in the presence of 0.5g/L BRSM + 3mM KI compared to 0.05g/L + 3mM KI. The related electrochemical parameters such as $I_{corr}$, $E_{corr}$, the cathodic Tafel slope ($b_c$) and anodic Tafel slope ($b_a$) obtained from the polarization curves are listed in Table III-7.

The results in the tables indicated that $I_{corr}$ decreased significantly when 0.5g/L BRSM was combined with 3mM Iodide ions. The $E_{corr}$ values were not remarkably shifted in the presence of the combination of BRSM + KI; therefore the combination BRSM + KI could be regarded as a mixed-type inhibition.

The inhibition efficiencies for the combination BRSM with KI were calculated and also listed in the tables. The addition of BRSM concentration has slightly improved the value of inhibition efficiency (from 86% up to 94% in 3mM KI). Although the anodic and cathodic currents were significantly reduced when both BRSM and Iodide ions were present, a low polarization current was observed, indicating a synergistic effect occurred between BRSM and Iodide ions[83].

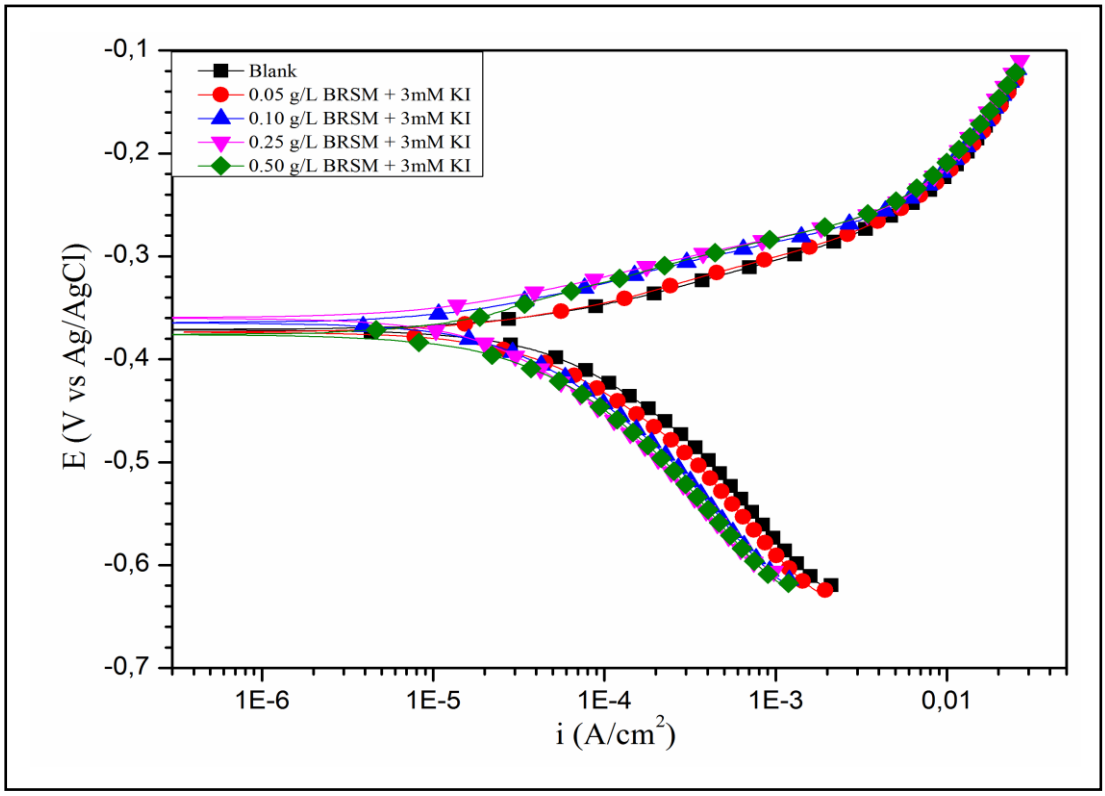


Figure III-16: Potentiodynamic polarization curves for API 5L X70 pipeline steel in 0.5M HCl with different concentrations of BRSM and 3mM KI at 20 °C (immersion time is 1 h).

Table III-7: Potentiodynamic polarization parameters for API 5L X70 in 0.5 M HCl solution in the absence and the presence of BRSM + 3mM KI at 20 °C.

| Concentration | $E_{corr}$ (mV) | $I_{corr}$ ($\mu A\ cm^{-2}$) | - bc ($mV\ dec^{-1}$) | ba ($mV\ dec^{-1}$) | $\eta_{pol}$ % |
|---|---|---|---|---|---|
| Blank | -401 | 339.5 | 106 | 84.5 | - |
| 0.05 gL-1 BRSM + 3mM KI | -370 | 46.41 | 132 | 50 | 86 |
| 0.01 gL-1 BRSM + 3mM KI | -374 | 38 | 128 | 52 | 89 |
| 0.25 gL-1 BRSM + 3mM KI | -365 | 21.3 | 118 | 46 | 93 |
| 0.50 gL-1 BRSM + 3mM KI | -358 | 20.2 | 134 | 44.5 | 94 |

### III.3.2. Electrochemical impedance spectroscopy measurements of API 5L X70 steel in 0.5 M HCl media in presence of BRSM and KI

The impedance data recorded on API 5L X70 steel immersed in 0.5M HCl acid solution with 3mM KI and with the different concentrations of BRSM are shown in figure III-17 Nyquist diagram and figure III-18 Bode plots.

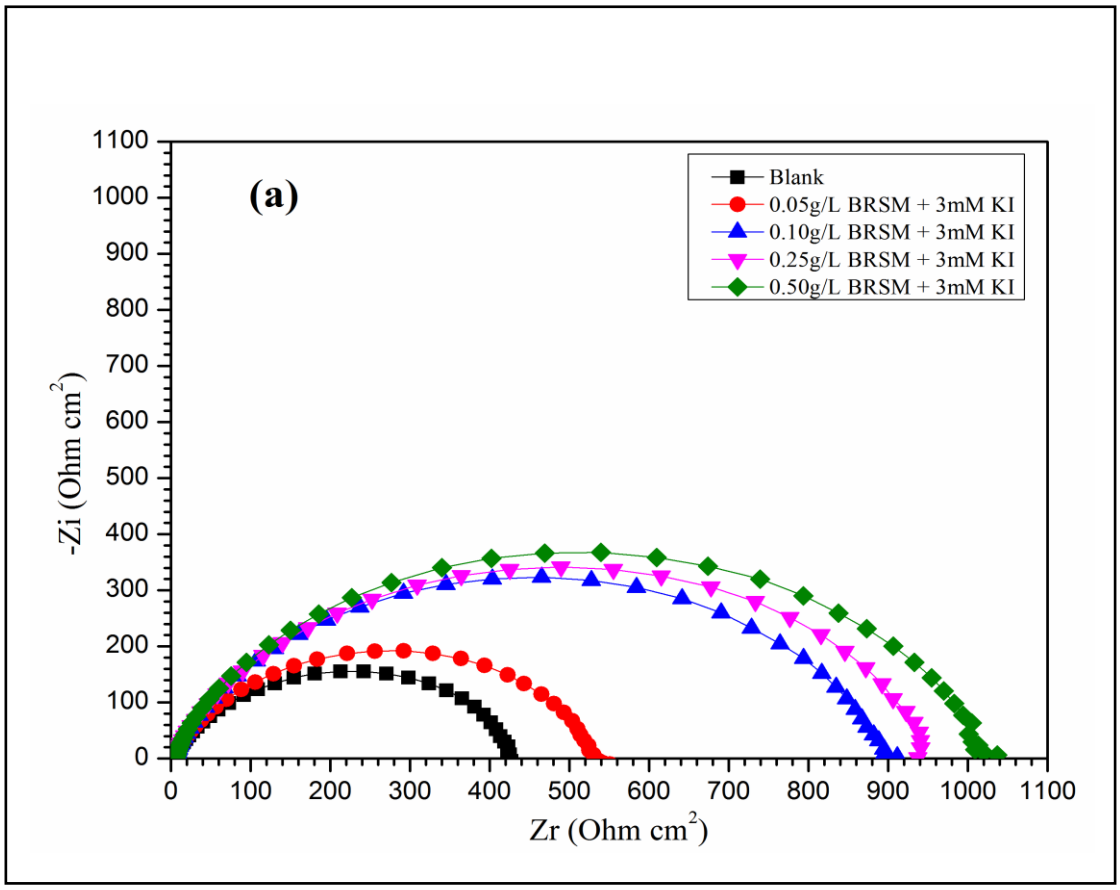


Figure III-17: Nyquist plots of the corrosion of API 5L X70 in 0.5M HCl with 3mM KI + different concentrations of BRSM at 20 °C (immersion time is 30 min)

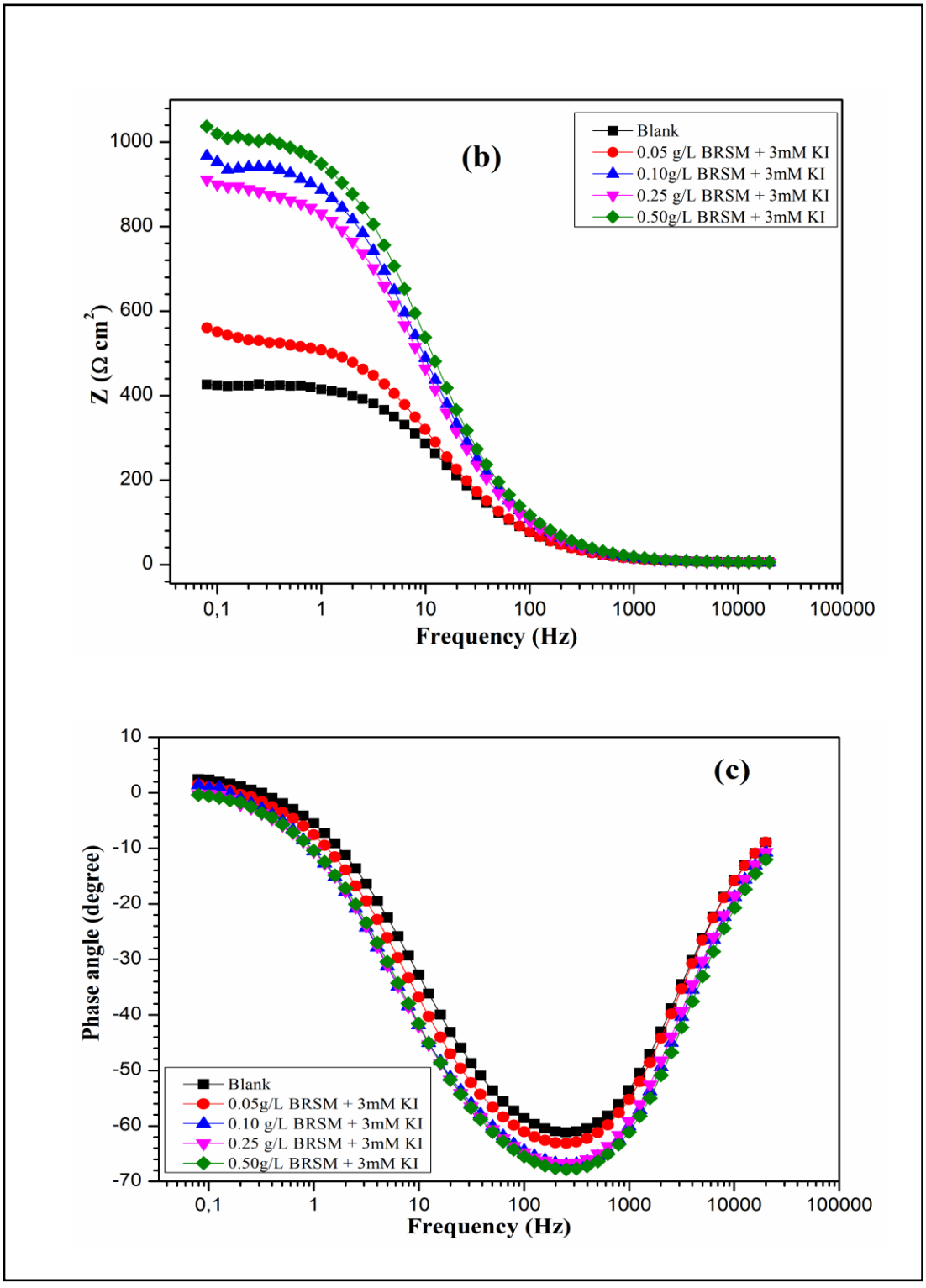


Figure III-18: Bode plots for API 5L X70 steel in 0.5M HCl with 3mM KI +different concentrations of BRSM at 20 °C, (a) Bode modulus and (b) Bode phase angle .

As can be seen from the figure. The spectra obtained without and with combination of (BRSM + 3mM KI) consist of one depressed capacitive loop corresponding to one time constant in the Bode plots. The high-frequency part of the impedance and phase angle describes the behavior of an inhomogeneous surface layer, where as the low-frequency component depicts the kinetic response for the charge transfer reaction [84]. It is observed that increasing the concentration of the combination of (BRSM+ 3mM KI) results in an increase in the size of the semicircle in figure III-17, in the impedance of the interface in figure III-18 (a), and in the maximum phase angle in figure III-18 (b), which indicate inhibition of the corrosion process. The impedance spectra for the Nyquist plots were analyzed by fitting to the equivalent circuit model shown in figure III-11, which has been used previously to model the carbon steel/acid interface[71, 85].The capacitive loop observed in all EIS diagrams can be related to the charge transfer reaction and the electrical double layer formed on the metal surface[86]. Table III-8 gives the values of the charge transfer resistance $R_t$ double layer capacitance $C_{dl}$ and inhibition efficiency obtained from the above plots. The solution resistance $R_s$ is constant; it is equal to 5Ω $cm^2$ in all experiences in this part.

Table III-8: Electrochemical impedance parameters for API 5L X70 in 0.5M HCl solution with 3mM KI + different concentrations of BRSM at 20 °C

| Concentration | $Y_0$ ($\mu\Omega\ S^n\ cm^{-2}$) | n | $R_t$ ($\Omega\ cm^2$) | $C_{dl}$ ($\mu F\ cm^{-2}$) | $\eta_{EIS}$ % |
|---|---|---|---|---|---|
| Blank | 227.5 | 0.80 | 49.46 | 75.93 | - |
| 0.05 g $L^{-1}$ BRSM + 3mM KI | 85.95 | 0.81 | 423.5 | 37.57 | 88 |
| 0.10 g $L^{-1}$ BRSM + 3mM KI | 69.69 | 0.81 | 525 | 33.15 | 91 |
| 0.25 g $L^{-1}$ BRSM + 3mM KI | 48.35 | 0.83 | 878.8 | 25.86 | 94 |
| 0.50 g $L^{-1}$ BRSM + 3mM KI | 45.56 | 0.83 | 932.5 | 24.37 | 95 |

The addition of KI to the BRSM further enhances $R_t$ values (start from 49.46Ωcm$^2$ to 932.5Ωcm$^2$) and reduces $C_{dl}$ values (start from 75.93μF cm$^{-2}$ to24.37μFcm$^{-2}$) without and with the combination of (BRSM + 3mM KI) respectivelyand the inhibition efficiency $\eta_{EIS}$ value 88% in the presence of 0.05 g/L BRSM + 3mM KI and as maximum inhibition efficiency $\eta_{EIS}$ value 95% in the presence of 0.5 g/L BRSM + 3mM KI. This can be attributed to the enhanced adsorption of BRSM in the presence of KI because of the synergistic effect of iodide ions.

***Inhibition efficiency variation:***

The variation of inhibition efficiency ($\eta_{EIS}$) for API 5L X70 steel in the 0.5M hydrochloric acid solution with different concentrations of BRSM in presence of 3mM KI is depicted in figure III-19. The inhibition efficiencies ($\eta_{EIS}$) were calculated from the values of $R_t$ in the table III-8. It can be seen from the figure that the inhibition efficiency increases with increasing the concentrations of the BRSM. The maximum value of inhibition efficiency ($\eta_{EIS}$) is 95% in presence of the combination 0.5 g/L BRSM + 3mM KI.

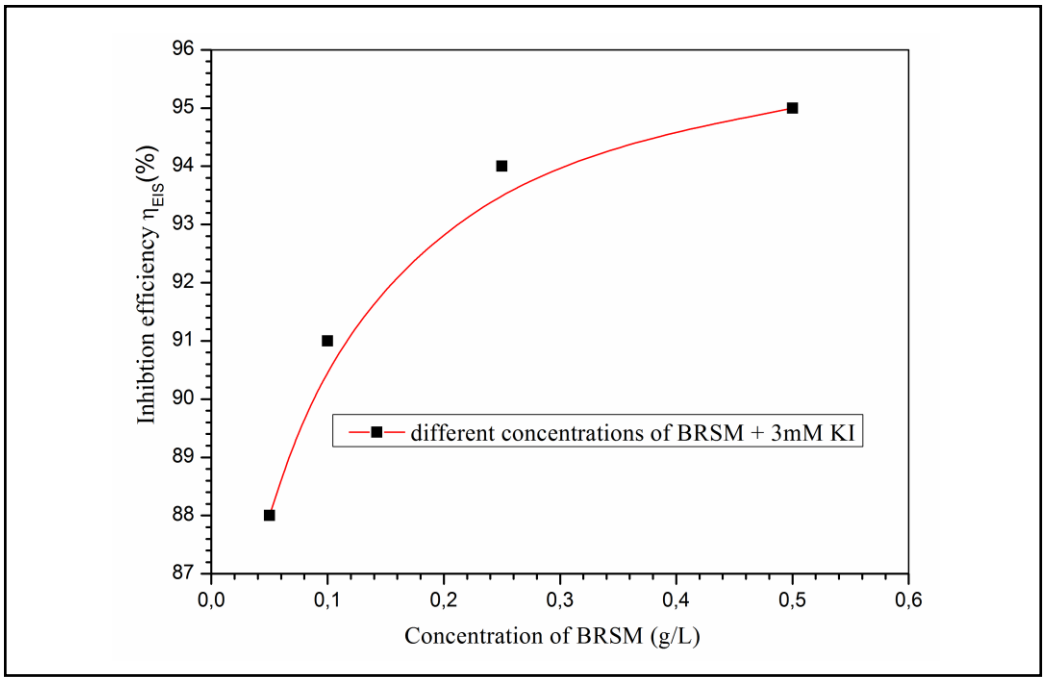


Figure III- 19: Relationship between inhibition efficiency ($\eta_{EIS}$) and different concentration of BRSM + 3mM KI in 0.5M HCl at 20 °C

### III.3.3. Adsorption isotherm and standard adsorption free energy

In order to evaluate the mode of adsorption of BRSM and combined inhibitor BRSM + KI on API 5L X70 steel in 0.5M hydrochloric acid, Langmuir, Temkin, and Frumkin adsorption isotherms were evaluated. According to Equ III-3, the Langmuir isotherm is the best fitting for the data, as shown in Figure III-20.

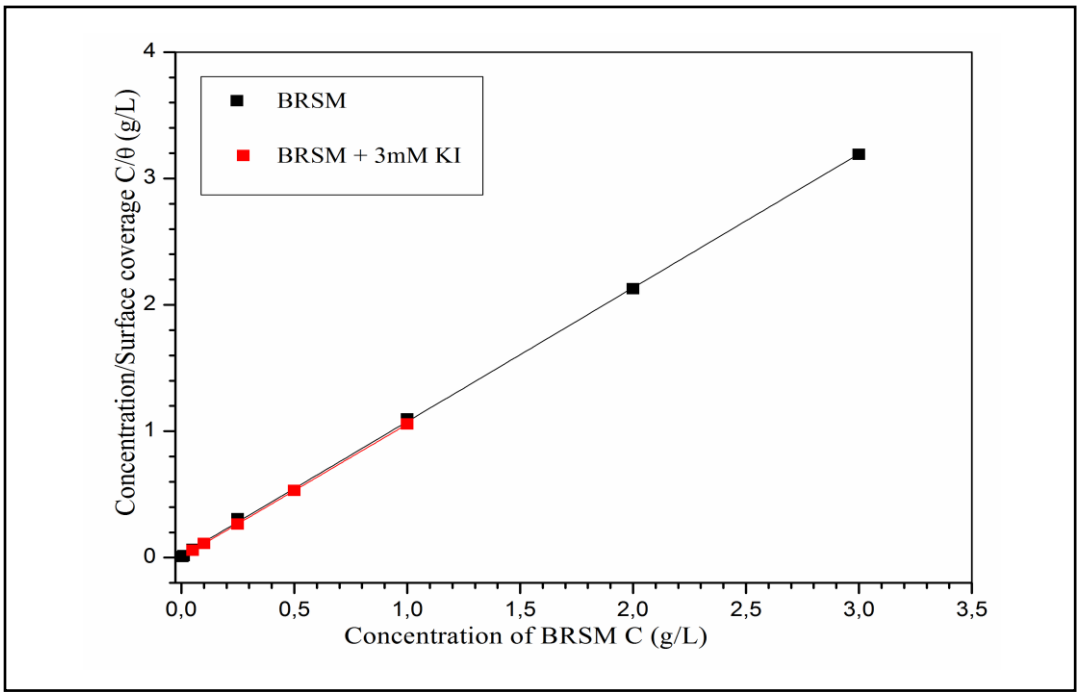


Figure III- 20: Langmuir isotherm adsorption mode of BRSM and BRSM + KI on the API 5L X70 steel surface in 0.5M HCl.

It is found that the slope is very close to 1 which indicates the adsorption of BRSM in combination with KI on API 5L X70 steel surface in 0.5M hydrochloric acid obeys Langmuir adsorption isotherm. The value of $K_{ads}$ can be calculated from intercept of straight lines C/θaxis and the $\Delta G^{o}_{ads}$ value was calculated using Equ III-5. The linear regression parameters are listed in table III-9.

Table III- 9: Parameters of Langmuir adsorption isotherm for API 5L X70 in 0.5M HCl solution of BRSM and BRSM+KI.

| Inhibitor | Isotherm mode | L C coefficient | Slope | $K_{ads}$ (L $g^{-1}$) | $\Delta G°_{ads}$ (kJ $mol^{-1}$) |
|---|---|---|---|---|---|
| BRSM | Langmuir | 0,99991 | 1,22 | 54,85 | -25,49 |
| BRSM+KI | Langmuir | 0.99999 | 1.05 | 207,46 | -30,85 |

In the present study, the value of $\Delta G°_{ads}$ ($-30.85$ kJ $mol^{-1}$) is found to be within the range $-40$ to$-20$ kJ $mol^{-1}$; probably means that the adsorption of BRSM combined with KI on API 5L X70 steel surface involves both physical adsorption and chemical adsorption. The extent of synergism between iodide ions and BRSM molecules has been analyzed by estimating the synergism parameter $S_1$which is given by Aramaki and Hackermann in1964 and used by some authors[87, 88]:

$$S_1 = \frac{1 - I_{1+2}}{1 - \grave{I}_{1+2}}$$

Where $I_{1+2} = I_1 + I_2$,$I_1$is the inhibition efficiency of the iodide ions, The value of inhibition efficiency of 3mM KI for API 5L X70 steel in 0.5M HCl acid was 85%[89]. $I_2$ is the inhibition efficiency of BRSM, $\grave{I}_{1+2}$ is the measured inhibition efficiency for the BRSM in combination with the iodide ions. $S_1$ approaches unity when no interaction between the inhibitor molecules exists, while $S_1>1$ indicates a synergistic effect. In case of $S_1< 1$, antagonistic behavior prevails which may lead to competitive adsorption. The $S_1$ was 1.89 for 3mM KI in presence of 2 g $L^{-1}$ BRSM in 0.5M HCl acid, suggesting the synergistic action of iodide ions with BRSM.

### III.3.4. SEM-EDX analysis

The API 5L X70 steel specimens were immersed after been polished in the hydrochloric acid solution for 60 hours immersion time in the absence and presence of optimum concentration of the BRSM and 3mM KI. After the elapsed time, the specimens were taken out and their surface morphology was determined by SEM and EDX. FigureIII-21(a) represents the SEM micrograph of the API 5L X70 steel specimen before immersion in the hydrochloric acid. Figure III-21(b) represents the specimen immersion in 0.5M HCl solution in absence of the inhibitor which is characterized by highly corroded and damaged surface. However, in the presence of optimum concentrations 0.5 g $L^{-1}$ BRSM + 3mM KI the surface morphologies of the specimens (figure III-21 c) have been remarkably improved owing to the formation of the protective film on the metallic surface. This finding further suggests that the combination of BRSM and iodide inhibit API 5L X70 steel corrosion in 0.5M HCl solution by the adsorption process. The EDX spectra of the API 5L X70 steel used to investigate the steel surface in the absence and the presence of optimum concentration 0.5 $gL^{-1}$ BRSM + 3mM KI are shown in figure III-21 Spectra, (a) represents the EDX spectrum of the polished steel before corrosion test, the peaks are related only to the iron element present in the API 5L X70 steel (Table III-10). In the absence of inhibitor, the spectra (b) exhibit the peaks of the oxygen element and the chlorine element which the polished API 5L X70 does not have. The spectra (c) of API 5L X70 steel immersed in 0.5M hydrochloric acid containing the combination of 0.5 $gL^{-1}$ BRSM + 3mM KI shows that the appearance of new peak of iodide and decreases of the peaks of both oxygen and chlorine, probably due to the adsorption of the combination BRSM and iodide on the surface of API 5L X70steel. These results confirm the results obtained from the electrochemical techniques.

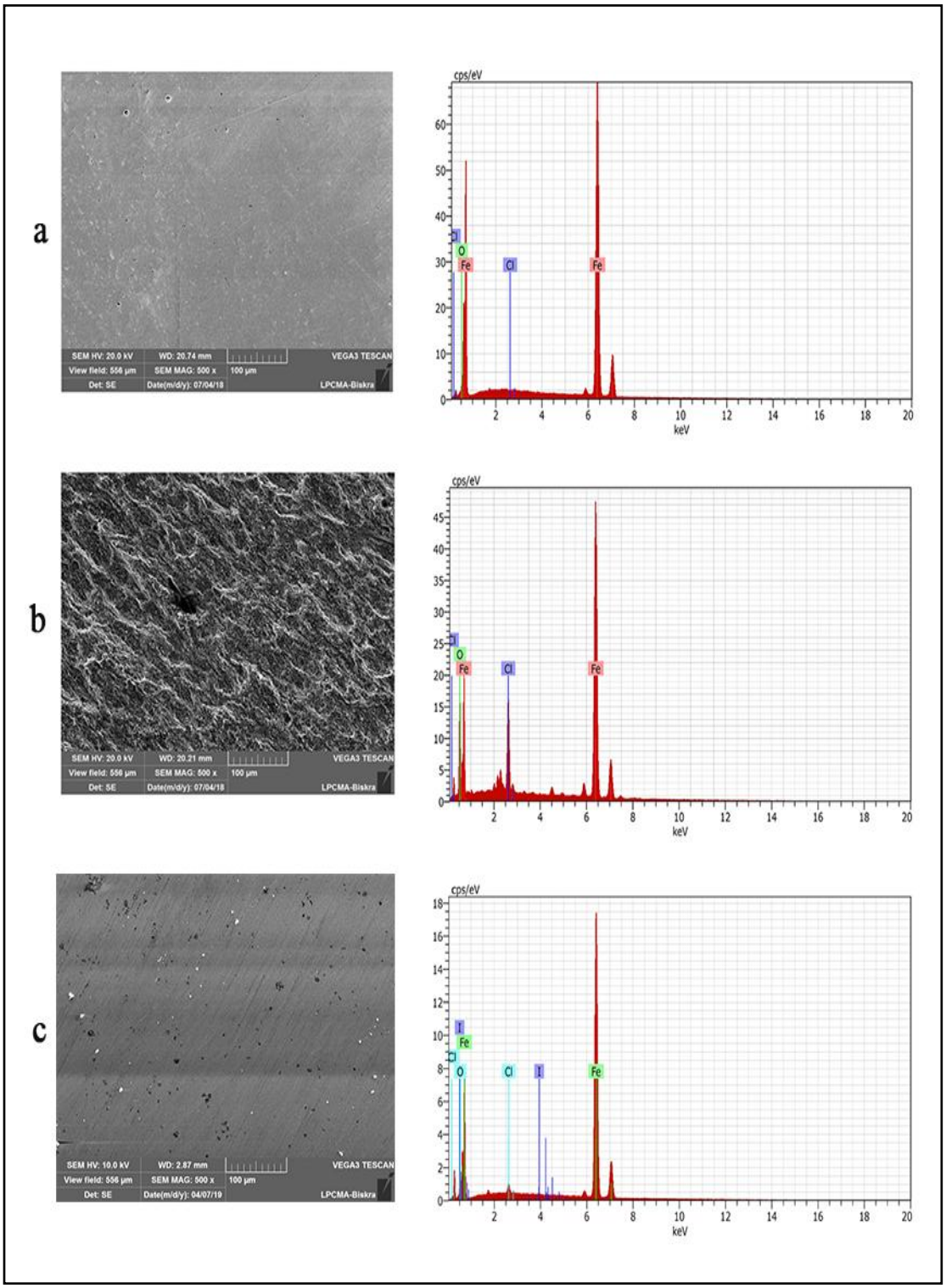


Figure III-21: SEM-EDX spectra of API 5L X70 steel: polished steel (a), in presence of corroding medium (b), and in presence of 0.5 $gL^{-1}$ BRSM + 3mM KI (c)

Table III-10: Content of elements obtained from EDX spectra for API 5L X70 steel

| Element | % atomic | | |
|---|---|---|---|
| | Steel | Steel + HCl | Steel + HCl + 0.5 g/L BRSM+3mM KI |
| iron | 96.47 | 58.95 | 87.09 |
| oxygen | 3.53 | 32.66 | 11.48 |
| chlorine | 0.00 | 8.39 | 1.40 |
| Iodide | 0.00 | 0.00 | 0.03 |

## III.4. Part four: Effect of BRSM on Inhibition Efficiency of API 5L X70 steel in 5% HCl as a real case

In the oil/gas industry, different concentrations of hydrochloric acid are used in the acidification process; for that the chosen 5% HCl concentration as a real case to investigate the inhibition efficiency effect of BRSM on API 5L X70 steel. The electrochemical techniques were used to determine the electrochemical parameters such as the corrosion rate and inhibition efficiency and the surface analyses method to confirm the result obtained from the electrochemical techniques.

### III.4.1. Potentiodynamic polarization measurements of API 5L X70 steel in 5%HCl

The anodic and cathodic polarization graphs obtained from API 5L X70 steel in 5%HCl solution in absence and presence of varying concentrations of BRSM are shown in Figure III-22.

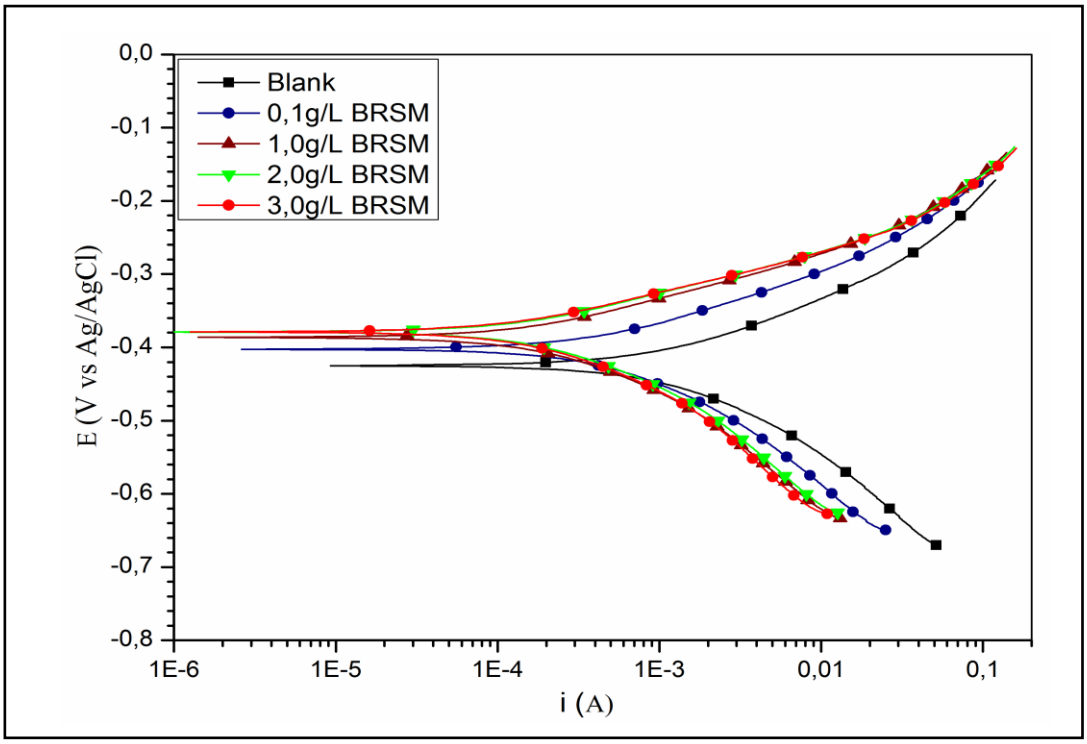


Figure III-22: Potentiodynamic polarization curves for API 5L X70 steel in 5% HCl without and with different concentrations of BRSM at 30 °C (immersion time is 1 h).

It is clearly seen from figure III-22 that in presence of BRSM the current density of the cathodic and anodic branch of polarization curves are displaced towards lower values than those recorded in the free acid solution [90].

The parameters such as $E_{corr}$, $I_{corr}$, $b_a$ and $b_c$, and $\eta_{pol}$% obtained from polarization plots are depicted in Table III-11.

Table III-11: Potentiodynamic polarization parameters for API 5L X70 steel in 5% HCl solution in the absence and the presence of BRSM at 30 °C.

| Concentration | $E_{corr}$ (mV) | $I_{corr}$ ($\mu A\ cm^{-2}$) | - bc ($mV\ dec^{-1}$) | ba ($mV\ dec^{-1}$) | $\eta_{pol}$ % |
|---|---|---|---|---|---|
| Blank | -424 | 280 | 101 | 82 | - |
| 0.10 $gL^{-1}$ BRSM | -402 | 119 | 99 | 71 | 57 |
| 0.50 $gL^{-1}$ BRSM | -386 | 51 | 89 | 62 | 81 |
| 1.00 $gL^{-1}$ BRSM | -380 | 49 | 85 | 59 | 82 |
| 3.00 $gL^{-1}$ BRSM | -379 | 48 | 93 | 59 | 82 |

The displacement in $I_{corr}$ is more pronounced with the increase in BRSM concentration. $\eta_{pol}$% inhibition is calculated by $I_{corr}$ value. Also, it can be seen that the $\eta_{pol}$% increases with a rise in BRSM concentration. This behavior shows that BRSM acts as an effective corrosion inhibitor for the API 5L X70 steel in 5% HCl medium.

Values of $b_a$ and $b_c$ changes with inhibitor concentration, however, their shift is not recognized to follow a definite trend. Slight variation in $b_a$ and $b_c$ values in presence of different concentrations of BRSM indicates that both the anodic iron dissolution and cathodic hydrogen evolution processes are inhibited.

### III.4.2. Electrochemical impedance spectroscopy measurements of API 5L X70 steel in 5%HCl

EIS measurement was conducted to study the corrosion processes that occur at the API 5L X 70 steel surfaces as well as at the interface of electrode/electrolyte without and with inhibitor. Nyquist plots and Bode diagrams for API 5L X70 steel electrode immersed in uninhibited and BRSM inhibited HCl solution at 30°C at the OCP is presented in figure III-23 and figure III-24 respectively.

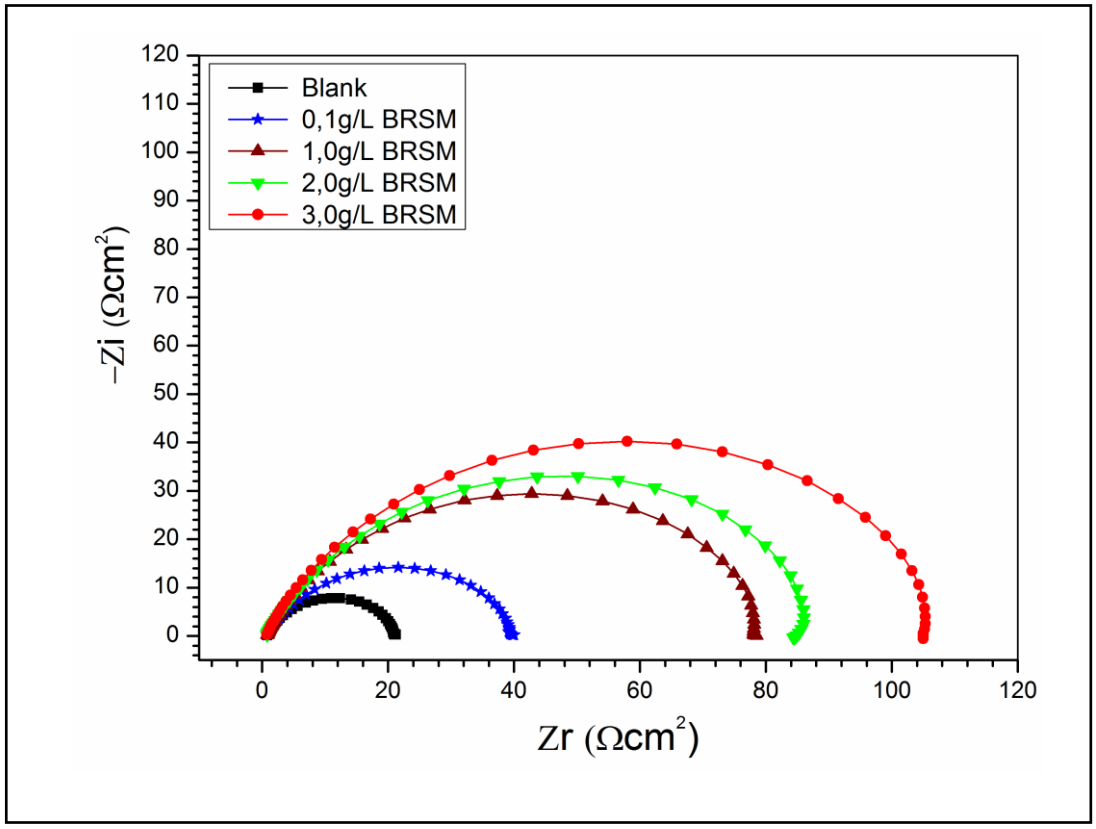


Figure III-23: Nyquist plots of the corrosion of API 5L X70 steel in 5% HCl without and with different concentrations of BRSM at 30 °C (immersion time is 1 h).

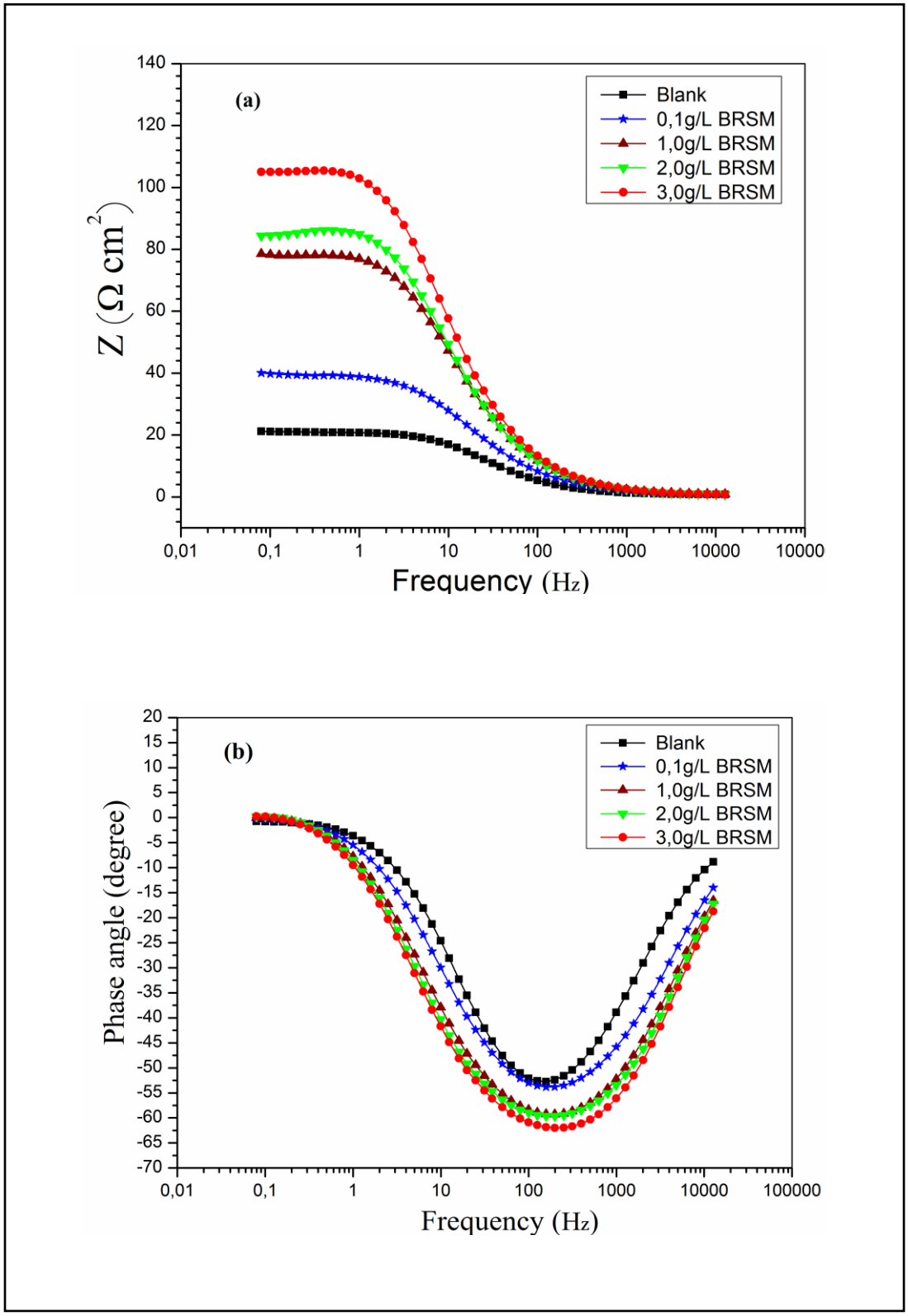


Figure III-24: Bode plots for API5L X70 steel in 5% HCl without and with different concentrations of BRSM at 30 °C, (a) Bode modulus and (b) Bode phase angle .

The impedance spectra (figure III-23) obtained without and with BRSM exhibit a single capacitive loop, which suggest that a single charge transfer process occurred during the dissolution of API 5L X70 in 5% HCl in absence and presence of BRSM [91]. Further, an increase in the diameter of the capacitive loop was noticed with increasing the BRSM concentration. This reflects the effectualness of BRSM at higher concentrations [92]. The continuous increase in the diameter of the loop with increasing concentration of BRSM suggests that the impedance of API 5L X70 increases due to increased coverage by the BRSM molecules adsorbed on the electrode surface [93]. BRSM molecules are adsorbed on the surface of API 5L X70 forming an inhibitive film covering the reaction sites and hence increases the impedance. The shape of the impedance diagrams in presence of BRSM is identical with that of blank solution which suggests that there is no change in the corrosion mechanism on the addition of inhibitor [94]. The equivalent circuit with one time constant is fitted as presented in figure III-11. The double layer capacitance $C_{dl}$ calculated using Equ III.2. Values of $R_t$ were obtained from the equivalent circuit and listed in Table III-12. This table also contains values of $C_{dl}$. The value of $R_t$ increases whereas the $C_{dl}$ value decreases in inhibited media. Increase in $R_t$ is due to an increase in surface coverage by the inhibitor. The decrease in $C_{dl}$ with an increase in the thickness of the adsorbed layer is due to adsorption of BRSM at the metal/solution interface which in turn decrease in local dielectric constant [95].

Nyquist plots demonstrated that the inhibition effect of BRSM is increased by increasing concentration, which is further confirmed by Bode diagrams. The Bode plots imply only one phase maxima revealing that the process of corrosion is occurring through one step corresponding to one time constant. In Bode modulus diagram, the impedance modulus was observed to increase with increasing BRSM concentration for the entire frequency range which indicates reduced corrosion rates in inhibited acid solutions. The phase angle at high frequencies gave a general idea of the anticorrosion behavior of inhibitor. More negative value of phase angle tells the capacitive nature of the electrochemical process. A more negative value of the phase angle at high frequency was observed with increasing BRSM concentration which indicates excellent inhibitive behavior at higher BRSM concentration [40].

The solution resistance $R_s$ is constant; it is equal to 0.7 $\Omega cm^2$ in all experiences in this part.

Table III-12: Electrochemical impedance parameters for API 5L X70 in 5% HCl solution in the absence and the presence of BRSM at 30 ° C.

| Concentration | $Y_0$ ($\mu\Omega\ S^n\ cm^{-2}$) | n | $R_t$ ($\Omega\ cm^2$) | $C_{dl}$ ($\mu F\ cm^{-2}$) | $\eta_{EIS}$ % |
|---|---|---|---|---|---|
| Blank | 1024 | 0.799 | 20.76 | 388 | - |
| 0.100 g $L^{-1}$ BRSM | 875 | 0.754 | 40.15 | 293 | 48 |
| 1.000 g $L^{-1}$ BRSM | 553 | 0.776 | 80.66 | 225 | 74 |
| 2.000 g $L^{-1}$ BRSM | 552 | 0.775 | 88.96 | 230 | 76 |
| 3.000 g $L^{-1}$ BRSM | 460 | 0.787 | 108.7 | 240 | 81 |

***Inhibition efficiency variation:***

Figure shows the inhibition efficiency ($\eta_{EIS}$) variation for the API 5L X70 steel in the 5% hydrochloric acid solution with different concentrations of BRSM.

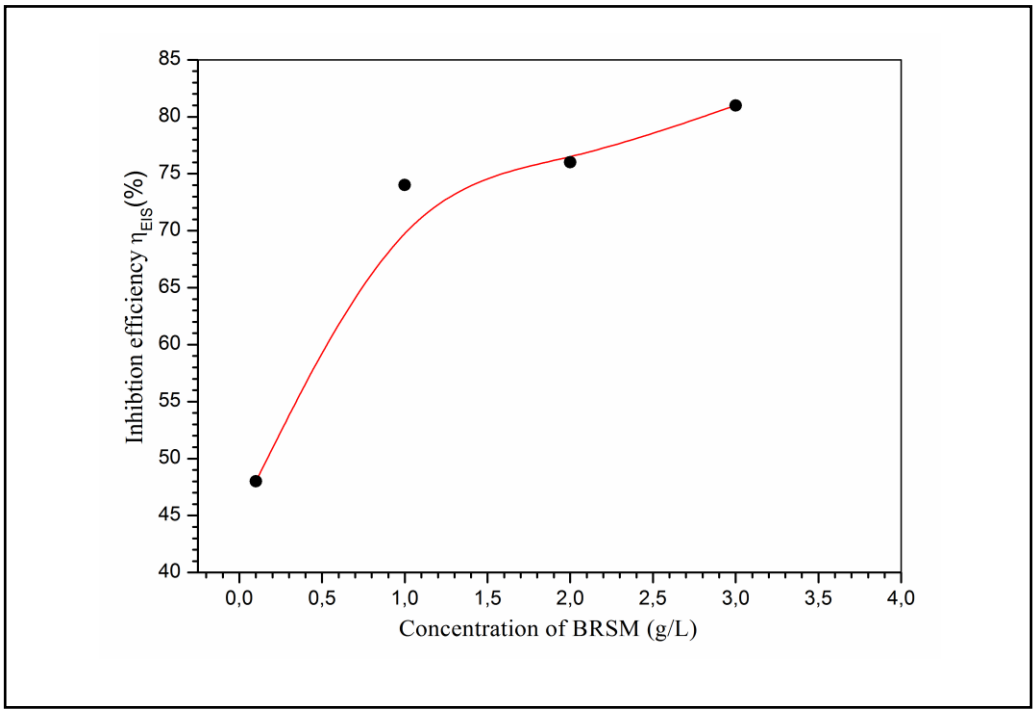


Figure III-25: Relationship between inhibition efficiency ($\eta_{EIS}$) and concentration of BRSM in 5 % HCl at 30 °C.

The inhibition efficiencies ($\eta_{EIS}$) were calculated from the values of $R_t$ in the table III-12. It can be seen from the figure III-25 that the inhibition efficiency increases with increasing the concentrations of the BRSM. The maximum value of inhibition efficiency ($\eta_{EIS}$) is 81% in presence of 3 g/L BRSM.

### III.4.3. Adsorption isotherm and standard adsorption free energy

Corrosion inhibition by organic compounds is, mainly, due to their ability to adsorb onto a metal surface to form a protective film. The establishment of isotherms that describe the adsorption behavior of corrosion inhibitor is important as they provide important clues about the nature of metal/inhibitor interaction. Values of degree of surface coverage (**θ**) corresponding to different BRSM concentrations at 30°C after 1 h of immersion were used to determine which isotherm best described the adsorption process. A straight line was obtained on plotting C/θ vs. C (mol $L^{-1}$) as shown in Figure III-26. The Langmuir adsorption isotherm was found to fit best with our experimental data.

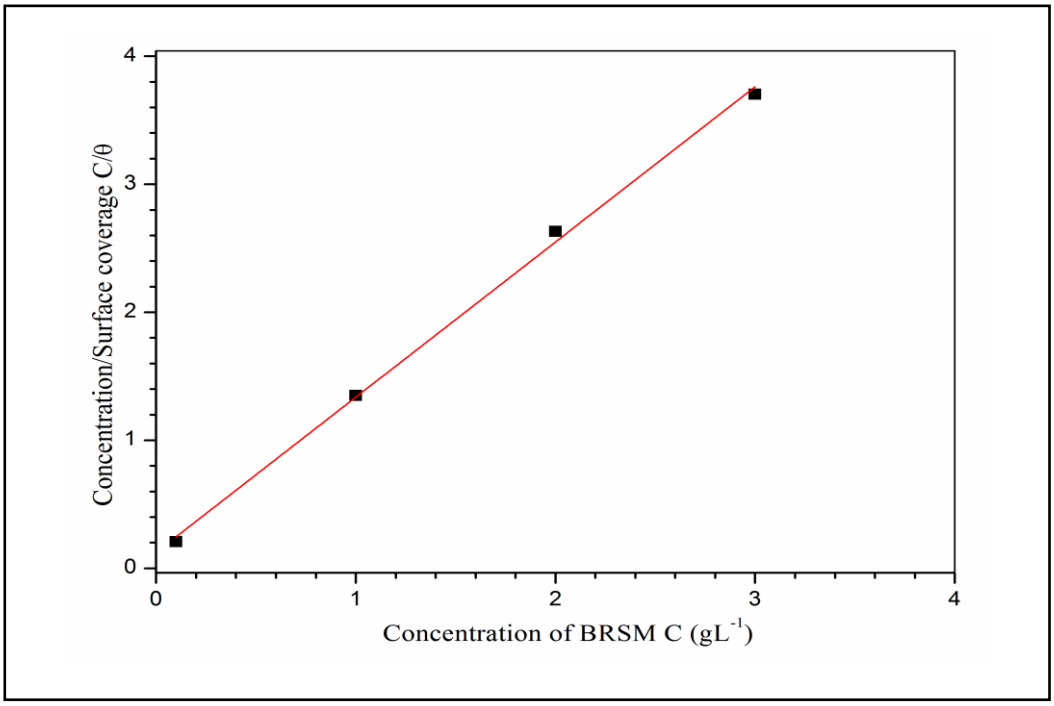


Figure III-26: Langmuir isotherm adsorption mode of BRSM on the API 5L X70 steel surface in 5%HCl at 30 °C (from EIS measurements).

The value of $K_{ads}$ obtained can be used to calculate the standard free energy ($\Delta G_{ads}$) via the equation; calculated values of $K_{ads}$ and $\Delta G_{ads}$ are listed in table III-13.

Table III- 13: Parameters of Langmuir adsorption isotherm for API 5L X70 steel in 5% HCl solution containing BRSM at 30 °C.

| Media | Isotherm mode | Linear correlation coefficient | Slope | $K_{ads}$ (L $g^{-1}$) | $\Delta G°_{ads}$ (kJ $mol^{-1}$) |
|---|---|---|---|---|---|
| 5% HCl | Langmuir | 0.99746 | 1.21 | 8,01 | -22,65 |

In the case of BRSM, $\Delta G_{ads}$ value of the inhibitor was found to be -22,65 kJ $mol^{-1}$, this indicates the phenomena of adsorption of inhibitor on the metal surface by physical adsorption process.

### III.4.4. SEM analysis of the API 5L X70 steel immersion in 5% HCl acid medium with and without BRSM

The API 5L X70 steel has been immersed in the 5% HCl acid solution in absence and presence of the optimum concentration of inhibitor (3 g/L BRSM) for 72 hours at 20°C; the specimens have been polished with abrasive paper (1200 grade) to 10 seconds and tissue paper to 20 seconds for removing the corrosion products on steel surface and rinsed with acetones and dried used for taking the image with different magnifications, as shown in the figure III-27.

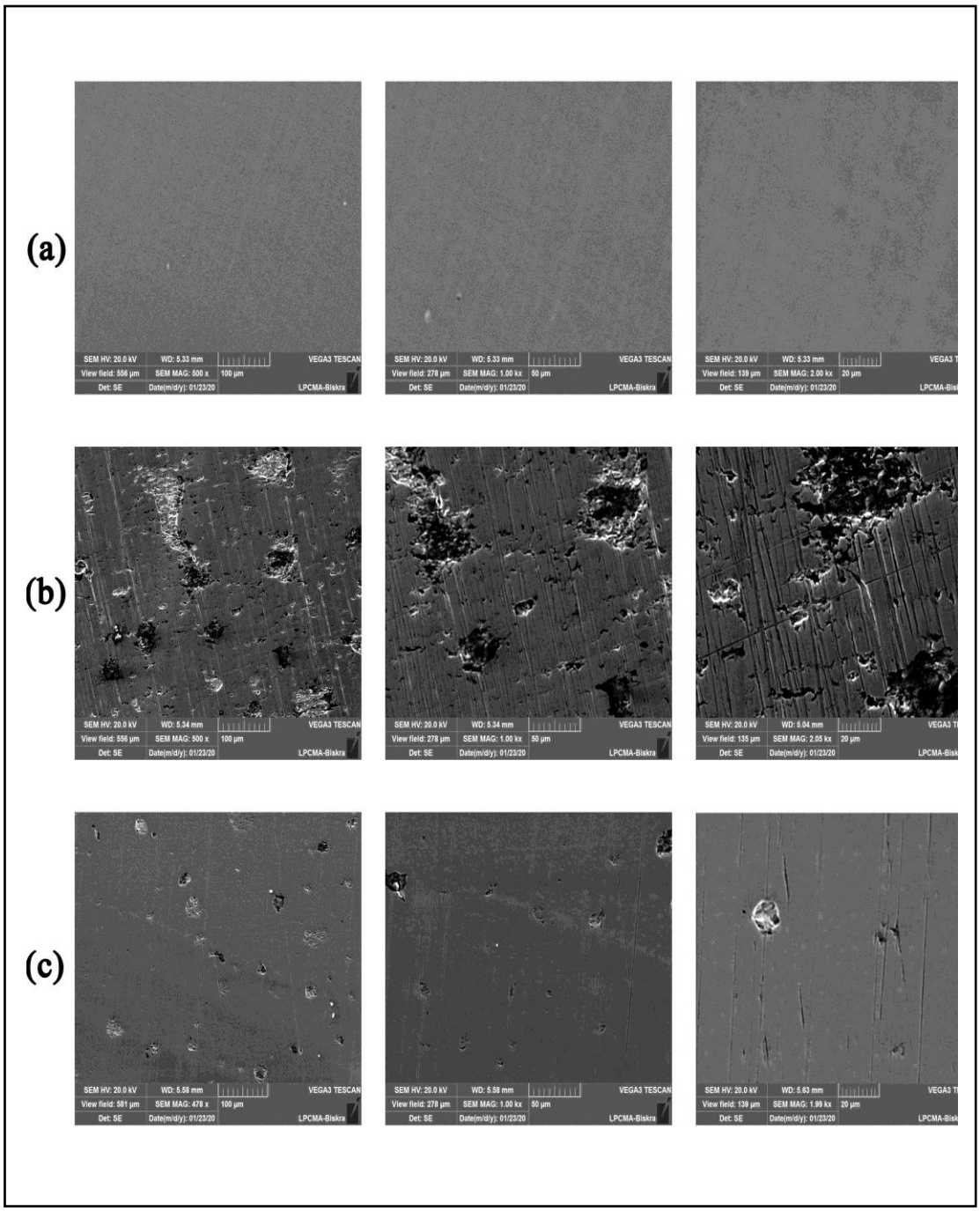


Figure III-27: SEM images of the API 5L X70 steel surface after removing the corrosion products (a) before corrosion, (b) after immersion in 5% HCl, (c) after immersion in 5% HCl + 3 g/L BRSM at 20°C for 72 h.

From figure (b) in the absence of BRSM, it's clear that the specimen surface of API 5L X70 was completely damaged and the steel was dissolved due to the oxidation reaction between the **$H^+$** and **Fe** ,with generalized type of corrosion.

However, when the API 5L X70 steel is immersed in 5% HCl solution containing the optimum concentration (3 g/L) of BRSM (figure c), the specimen surface seems a little bit attacked and the degree of damage and dissolution of the steel surface is reduced. The size of corrosion pits in absence of BRSM is 40µm while, in presence of 2 g/L BRSM the corrosion pits are reduced on all steel surface.

The results obtained from the immersion test are conformed those results of electrochemical impedance spectroscopy and potentiodynamic polarization where the inhibition efficiency equal 81% at 3 g/L BRSM.

## III.5. Part five: Effect of BRSM on Inhibition Efficiency of API 5L X70 steel in 0.5M $H_2SO_4$ acid solution

The corrosion inhibitors are widely used in different acidic media; for that, the sulfuric acid medium was selected in this part. To investigate the properties of BRSM in 0.5M $H_2SO_4$ by using the electrochemical techniques to determine the electrochemical parameters such as the corrosion rate and inhibition efficiency and the surface analyses method to confirm the result obtained from the electrochemical techniques.

### III.5.1. Potentiodynamic polarization measurements of API 5L X70 steel in 0.5 M $H_2SO_4$ media

Figure III-28 shows the polarization curves of steel in 0.5M $H_2SO_4$ blank solution and in the presence of different concentrations of BRSM.

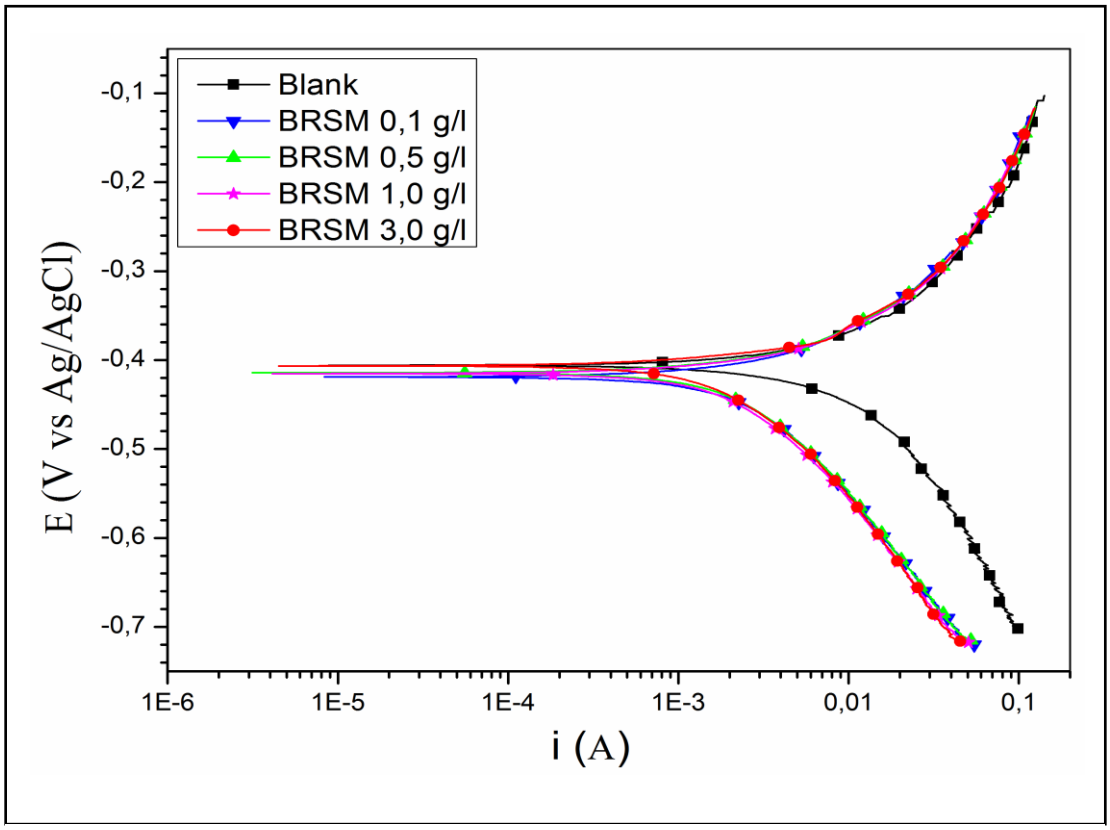


Figure III-28: Potentiodynamic polarization curves for API 5L X70 steel in 0.5M $H_2SO_4$ without and with different concentrations of BRSM at 30 °C (immersion time is 1 h)

With the increase in BRSM concentration, both the anodic and cathodic currents were inhibited, this result shows that the addition of BRSM inhibitor reduced anodic dissolution and also retarded the rate of the hydrogen evolution reaction.

The values of various electrochemical parameters are summarized in table III-14. This table gives the values of kinetic corrosion parameters as the corrosion potential $E_{corr}$, corrosion current density $I_{corr}$, Tafel slopes ($b_c$,$b_a$) and inhibition efficiency $\eta_{pol}$ for the corrosion of steel in 0.5M $H_2SO_4$with different concentrations of BRSM.

The corrosion current densities were estimated by Tafel extrapolation of the cathodic and anodic curves to the open circuit corrosion potential. From this table III-14, it can be concluded that:

From the table III-14 the $E_{corr}$ values do not alter significantly in the presence of the inhibitor. This observation shows clearly that the inhibition of corrosion was mixed

The $I_{corr}$ values decreases and $\eta_{pol}$ increases in the presence of different concentrations of BRSM.

Table III-14: Potentiodynamic polarization parameters for API 5L X70 in 0.5 M $H_2SO_4$ solution in the absence and the presence of BRSM at 30 °C.

| Concentration | $E_{corr}$ (mV) | $I_{corr}$ ($\mu A\ cm^{-2}$) | - bc ($mV\ dec^{-1}$) | ba ($mV\ dec^{-1}$) | $\eta_{pol}$ % |
|---|---|---|---|---|---|
| Blank | -406 | 1661 | 126 | 102 | - |
| 0.10 $gL^{-1}$ BRSM | -419 | 556 | 142 | 62 | 66 |
| 0.50 $gL^{-1}$ BRSM | -415 | 473 | 130 | 52 | 71 |
| 1.00 $gL^{-1}$ BRSM | -415 | 440 | 130 | 46 | 73 |
| 3.00 $gL^{-1}$ BRSM | -407 | 381 | 120 | 34 | 77 |

### III.5.2. Electrochemical impedance spectroscopy measurements of API 5L X70 steel in 0.5 M $H_2SO_4$ media

The impedance data recorded on API 5L X70 steel immersed in 0.5M sulfuric acid solution without and with different concentrations of BRSM are shown in figure III-29 in Nyquist diagram and figure III-30 Bode plots.

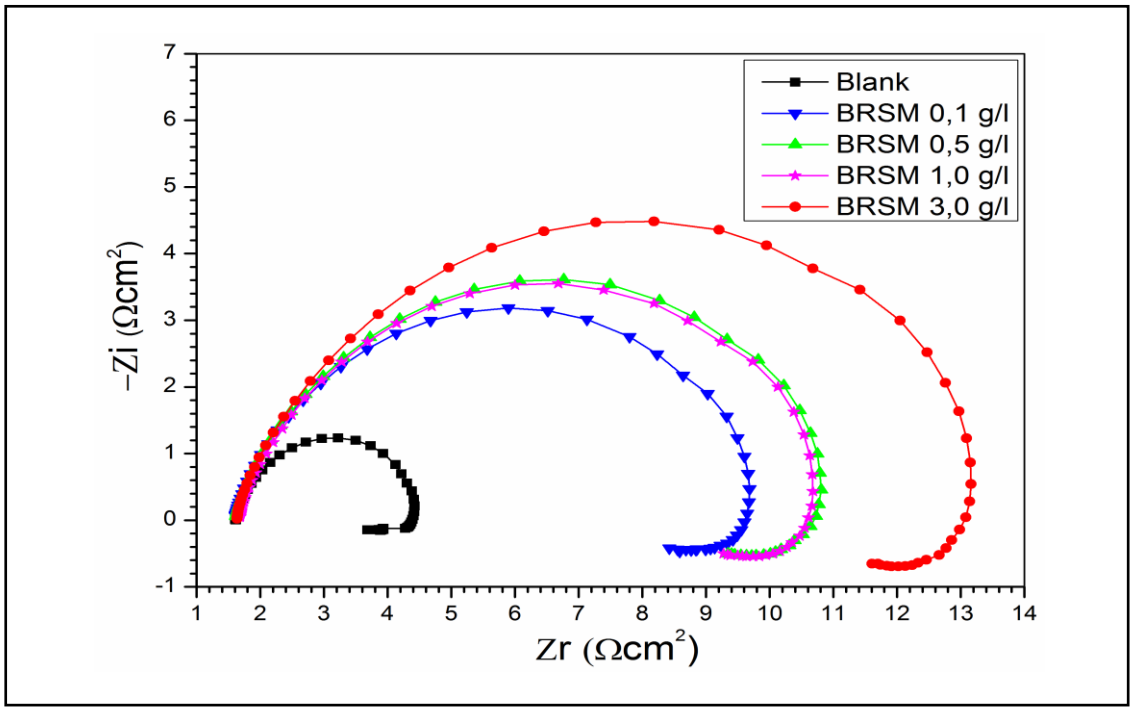


Figure III-29: Nyquist plots of the corrosion of API 5L X70 in 0.5M $H_2SO_4$without and with different concentrations of BRSM at 30 °C (immersion time is 1 h).

Inspection of the plots revealed that the shape of Nyquist plots in the absence and presence of inhibitor is similar which indicates an unchanged mechanism of corrosion. This depressed form of semicircles has been attributed to the inhomogeneity of the electrode surface arising from surface roughness or interfacial phenomena [71].

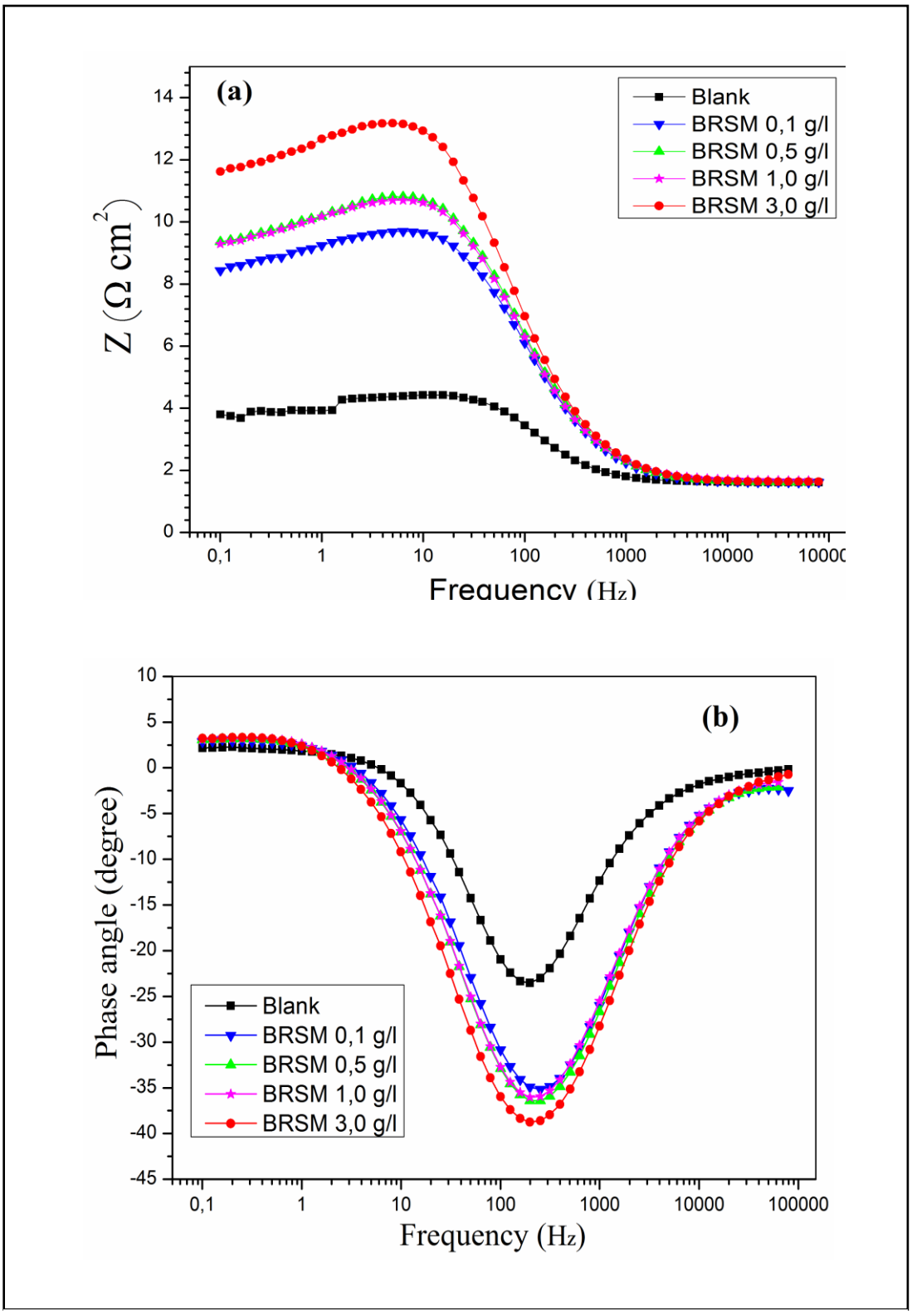


Figure III-30: Bode plots for API 5L X70 steel in 0.5M $H_2SO_4$ without and with different concentrations of BRSM at 30 °C, (a)Bode modulus and (b) Bode phase angle .

The Nyquist plots reveal that each impedance diagram consists of a large capacitive loop at high frequencies (HF) and an inductive loop at low frequencies (LF) both in the absence and presence of inhibitor. The presence of two time constants for iron dissolution at $E_{corr}$ in the absence of inhibitor has been reported in the literature [96, 97].

The HF capacitive loop could be attributed to the double layer capacity in parallel with the charge transfer resistance ($R_t$). The LF inductive loop may be originated from the relaxation process obtained by adsorption species as $H^+_{ads}$ and $SO_4^{-2}$ on the surface of the metal. It mayalso be attributed to the re-dissolution of the passivated surfaceat low frequencies [98]. Figure III-31 shows simulated and experimentally generated impedance diagrams for API 5L X70 steel immersed in 0.5Msulfuric acid solution in the presence of 3 g $L^{-1}$ BRSM. Excellent fit with this model was obtained for all experimental data.

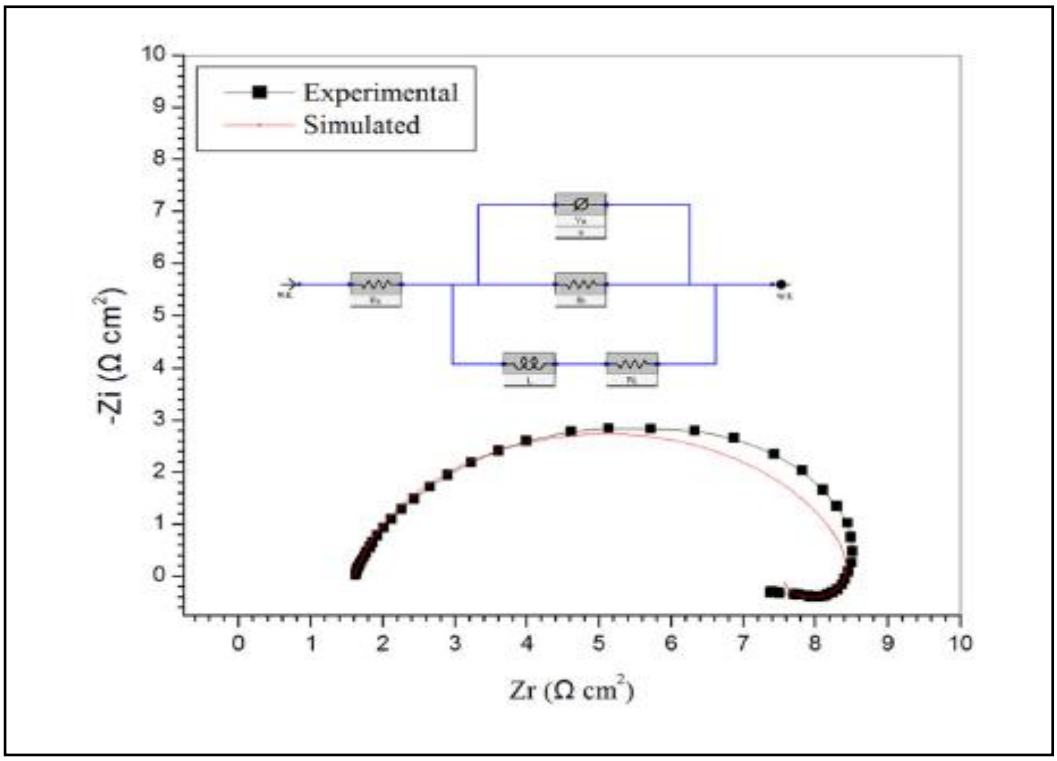


Figure III-31: Nyquist plot of experimental data and simulated data, together with the equivalent circuit used to fit the impedance data, recorded for API 5L X70 steel in 0.5M $H_2SO_4$ containing 3 $gL^{-1}$ BRSM.

From the figure III-31, it is very clear that the measured impedance plot is in accordance with the one calculated by the equivalent circuit. The circuit consists of the solution resistance $R_s$, the charge transfer resistance $R_t$, the constant phase element (CPE), the inductive elements, $R_L$, and L.

For the description of a frequency independent phase shift between an applied AC potential and its current response, a constant phase element (CPE) is used. CPE is an element whose impedance value is a function of the frequency and whose phase is independent of the frequency and its impedance (Equ III-1) [99, 100].The double layer capacitance $C_{dl}$ was calculated using (Equ III-2) [101, 102].

Examination of the impedance plots clearly shows that the introduction of BRSM affected the impedance responses of the system (steel/sulfuric acid); notably an increase in the diameter of the semicircle (Figure III-29), impedance modulus of the interface at the low frequency region (Figure III-30 (a)). Also the phase angle plots (Figure III-30 (b)) show a wide peak. Similar results were obtained by Refs [103, 104].

The values of the electrochemical parameters derived from Nyquist plots are given in Table III-15.It can be observed that the values of $R_t$ increase while the values of $C_{dl}$ decrease with increase in concentration of BRSM. The decrease in $C_{dl}$ on the introduction of BRSM to the acid solution indicates the presence of a protective layer that covers the surface of the electrode. The adsorption of BRSM on the API 5L X70 steel surface decreases $C_{dl}$ because they displaced the water molecules and other ions that were originally adsorbed on the surface.

With higher concentration of inhibitor (BRSM), either the thickness of the protective layer or the surface coverage by inhibitor increased due to more inhibitor electrostatically adsorbed on the electrode surface[98, 105]. The values of inhibition efficiency given in table III-15show that inhibition efficiency increases with increase

in concentration of BRSM with the highest value of 70% obtained at BRSM concentration of 3 g $L^{-1}$.The solution resistance $R_s$ is constant; it is equal to 1.6Ω $cm^2$ in all experiences in this part.

Table III-15: Electrochemical impedance parameters for API 5L X70 in 0.5M $H_2SO_4$ solution in the absence and the presence of BRSM at 30 ° C.

| Concentration | $Y_0$ μΩ $S^n$ $cm^{-2}$ | n | $R_t$ (Ω $cm^2$) | L (H $cm^2$) | $R_L$ (Ωcm$^2$) | $C_{dl}$ (μF $cm^{-2}$) | $\eta_{EIS}$ % |
|---|---|---|---|---|---|---|---|
| Blank | 940 | 0.89 | 2.86 | 1.17 | 10 | 472 | - |
| 0.10 g $L^{-1}$ BRSM | 695 | 0.82 | 8.34 | 7.4 | 41.2 | 226 | 65 |
| 0.50 g $L^{-1}$ BRSM | 735 | 0.8 | 9 | 7.3 | 42 | 229 | 68 |
| 1.00 g $L^{-1}$ BRSM | 738 | 0.81 | 9.46 | 8.3 | 41.5 | 236 | 70 |
| 3.00 g $L^{-1}$ BRSM | 728 | 0.81 | 9.4 | 9.5 | 41.7 | 235 | 70 |

***Inhibition efficiency variation:***

Figure III-32 shows the inhibition efficiency ($\eta_{EIS}$) variation for the API 5L X70 steel in the 0.5M sulfuric acid solution with different concentrations of BRSM. The inhibition efficiencies ($\eta_{EIS}$) were determined from the values of $R_t$ in the table III-15. It can be seen from the figure that the inhibition efficiencies are very close and the maximum value of inhibition efficiency ($\eta_{EIS}$) is 70% in presence of 1g/L BRSM.

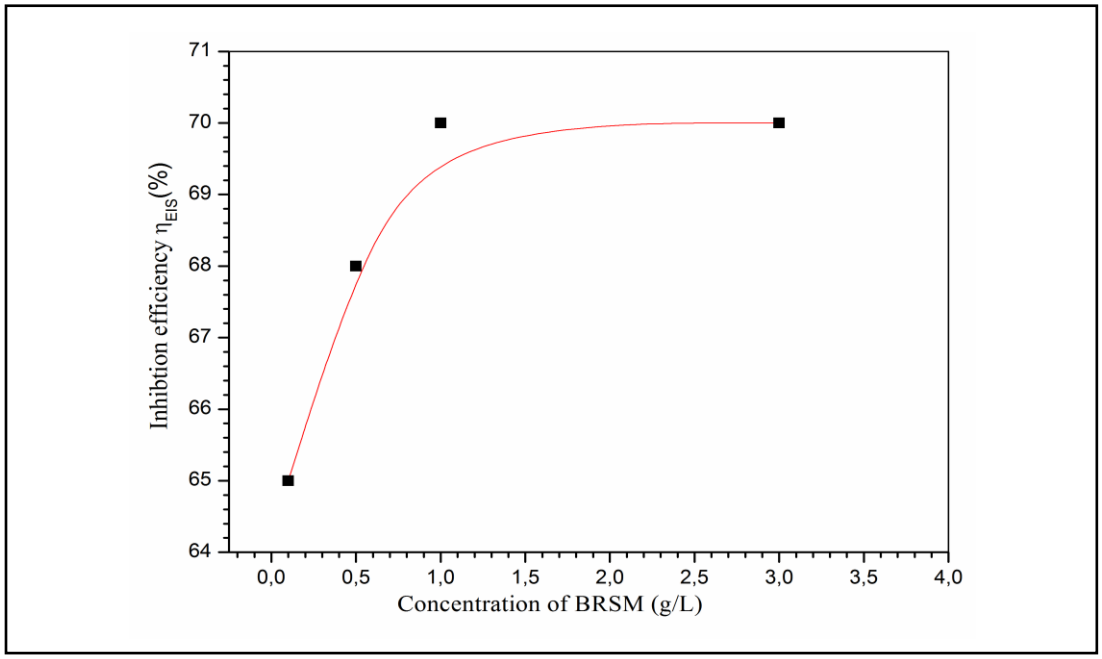


Figure III-32: Relationship between inhibition efficiency ($\eta_{EIS}$) and concentration of BRSM in 0.5M $H_2SO_4$ at 30 °C.

### III.5.3. Adsorption isotherm and standard adsorption free energy

Adsorption isotherm was employed to understand the interaction between inhibitor and the surface of API 5L X70 steel substrate in the 0.5M sulfuric acid. The degree of surface coverage**θ**obtained from the EIS method (**θ= $\eta_{EIS}$ % /100**). Langmuir, Freundlich and Temkin were employed to establish the isotherm most appropriate to experimental data. The linear correlation coefficient with $R^2$value which is nearer to unity was taken to define the type of adsorption process. Langmuir isotherm model which shows good fit with the value was considered for the current study. Langmuir adsorption process speaks only about the interaction between the inhibitor molecules and the metal substrates and not between the inhibitor molecules.

The plot of **C/θ**versus **C** yielded linear graph that is shown in figure III-33.

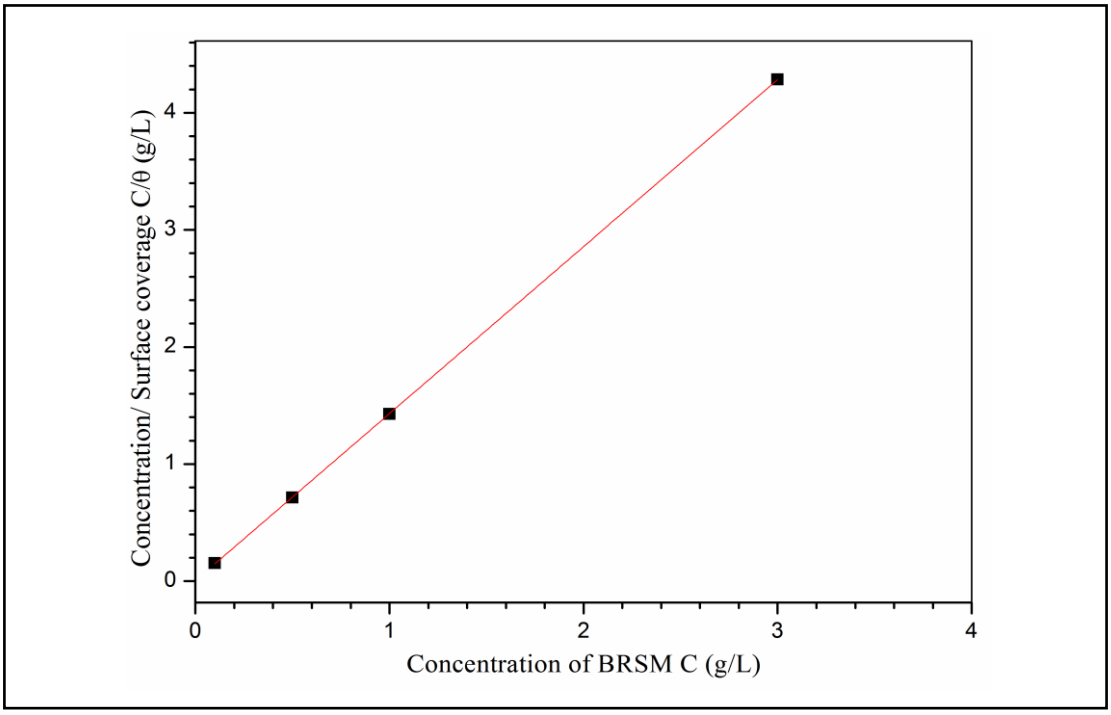


Figure III-33: Langmuir isotherm adsorption mode of BRSM on the API 5L X70 steel surface in 0.5M $H_2SO_4$ at 30 °C.

This explains that the adsorption of the inhibitor molecules on the mild steel surface is reliable on Langmuir adsorption isotherm model and the correlation coefficient ($R^2$) obtained are near to unity.

The value of $K_{ads}$ obtained can be used to calculate the standard free energy ($\Delta G_{ads}$) via the equation; calculated values of $K_{ads}$ and $\Delta G°_{ads}$ are listed in table

Table III-16: Langmuir isotherm adsorption mode of BRSM on the API 5L X70 steel surface in 0.5M $H_2SO_4$ at 30 °C.

| Isotherm mode | Linear correlation coefficient | Slope | $K_{ads}$ (L $g^{-1}$) | $\Delta G°_{ads}$ (kJ $mol^{-1}$) |
|---|---|---|---|---|
| Langmuir | 0,99999 | 1,42 | 206,185 | -30,185 |

The negative value of $\Delta G°_{ads}$ indicates that the adsorption of inhibitor on the API 5L X70 steel substrates occurs spontaneously. Usually, values of standard free energy values less or closer to −20 kJ $mol^{-1}$ are reliable with electric charges between molecules in inhibitor and surface charged steel substrate (physisorptions) while those more negative than –40 kJ $mol^{-1}$ involves sharing of electrons from the inhibitor molecules to the metal surface to form a chemical bonding (chemisorptions) [106, 107].

Based on the literature[108], the obtained $\Delta G°_{ads}$ (-30.185 kJ/mol) in this work indicates that the adsorption mechanism of BRSM on API 5L X70 steel surface involves two types of interactions, predominant physisorption (ionic) and weak chemisorption (molecular).

### III.5.4. SEM analysis of the API 5L X70 steel immersion in $H_2SO_4$acid medium with and without BRSM

The API 5L X70 steel has been immersed in the 0.5M $H_2SO_4$ acid solution in absence and presence the of optimum concentration of inhibitor (3 g/L BRSM) for 72 hours at 20°C; the specimens have been polished with abrasive paper (1200 grade) to 10 seconds and tissue paper to 20 seconds for removing the corrosion products on steel surface and rinsed with acetones and dried used for taking the image with different magnifications, as shown figure III-34.

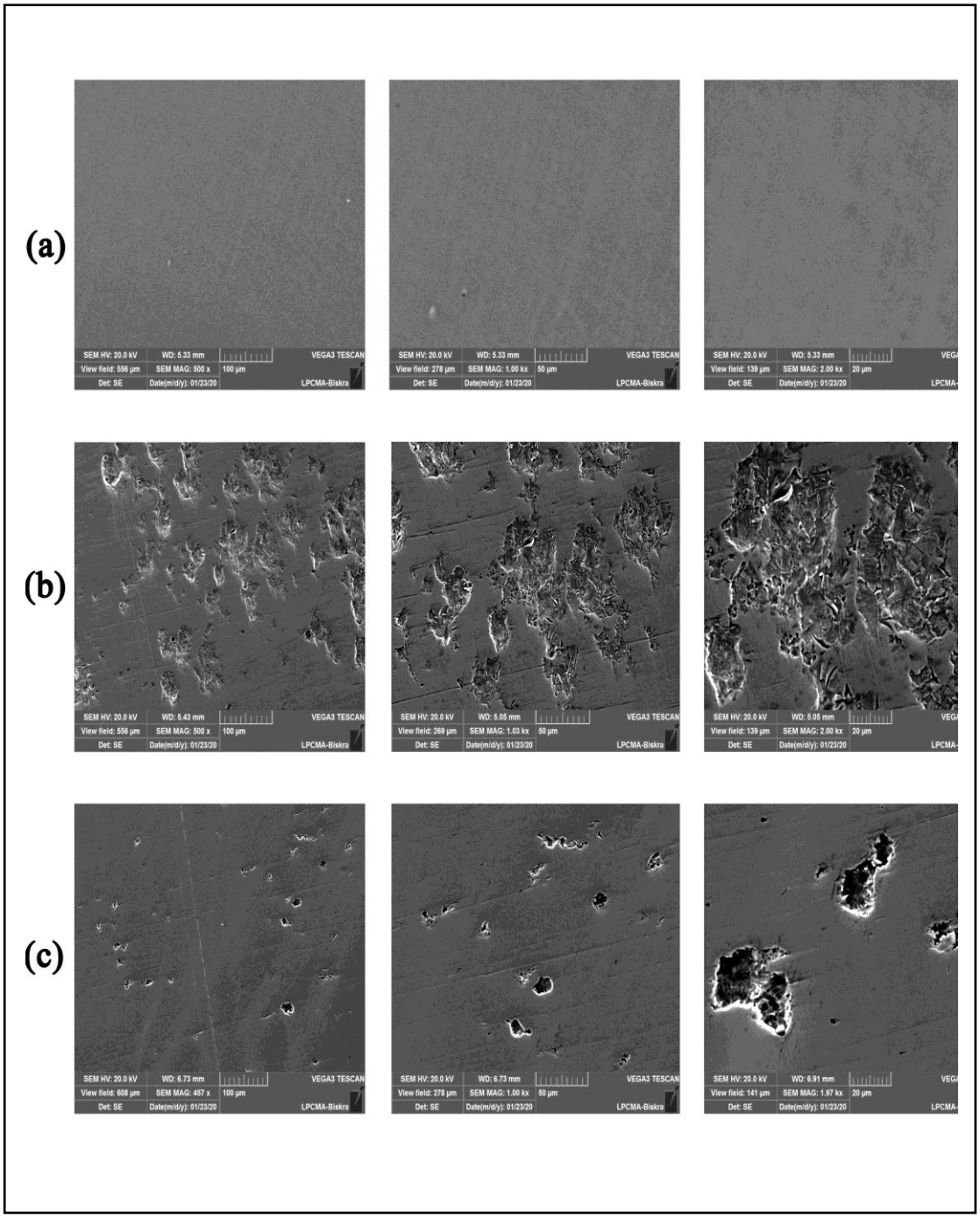


Figure III-34: SEM images of the API 5L X70 steel surface after removing the corrosion products (a) before corrosion, (b) after immersion in 0.5M $H_2SO_4$, (c) after immersion in 0.5M $H_2SO_4$ + 3 g/L BRSM at 20°C for 72 h.

From figure (b) in the absence of BRSM, it's clear that the specimen surface of API 5L X70 was completely damaged and steel was dissolved due to the oxidation reaction with generalized type of corrosion.

However, when the API 5L X70 steel was immersed in 0.5M $H_2SO_4$ solution containing the optimum concentration (3 g/L) of BRSM (figure c), the specimen surface seems attacked and the degree of damage and dissolution of the steel surface is a little reduced. The size of corrosion pits in absence of BRSM is 40µm while, in presence of 3 g/L BRSM the corrosion pits are slightly reduced on all steel surface.

The results obtained from the immersion test conformed those results of electrochemical impedance spectroscopy and potentiodynamic polarization where the inhibition efficiency is 70 % at 3 g/L BRSM.

### III.6. Explanation for the inhibition of BRSM

Corrosion inhibition of API 5L X70 steel in hydrochloric acid and sulfuric acid by BRSM can be explained by adsorption of the major constituents of bark resin of S. molle such as isomasticadienoic acid, isomasticadienonalic acid and pinicolic acid. Two main types of interaction can describe the adsorption of these molecules: chemisorption and physisorption.

In aqueous acidic solutions, the BRSM exists either as neutral molecules or in the form of cations (protonated BRSM) as follows:

$$BRSM + x\ H^+ \leftrightarrow [BRSMHx]^{x+1} \qquad \text{Equ III. 5}$$

The neutral BRSM may be adsorbed on the metal surface via the chemisorption mechanism involving the displacement of water molecules from the metal surface and adsorption most probably takes place through the ketone functions.

The transfer of a lone pair of electrons on the oxygen atom in the oxygenated monoterpens (isomasticadienoic acid, isomasticadienonalic acid, and pinicolic acid) to the surface forms a coordinate bond. The BRSM molecules can be adsorbed also on the metal surface on the basis of donor–acceptor interactions between p-electrons of the heterocycle and vacant dorbitals of iron. On the other hand, in aqueous hydrochloric and sulfuric acid medium, the BRSM molecules, particularly, the oxygenated monoterpen derivatives (isomasticadienoic acid, isomasticadienonalic acid, and pinicolic acid) can easily be protonated at the oxygen heteroatom in the ketone function.

However, the charge of the metal surface can be determined from the value of $E_{corr}- E_{q=0}$(zero charge potential)[109].The $E_{q=0}$ of iron is −530 mV versus SCE in hydrochloric acid[110] and -550 mV versus SCE in sulfuric acid [111].In the present system, the value of $E_{corr}$ obtained in0.5M hydrochloric acid is −472 mV and the value of $E_{corr}$ obtained in 0.5M $H_2SO_4$−406 mV. So the steel surface charges positive charge in hydrochloric and sulfuric solution because of $E_{corr}- E_{q=0}$ (zero charge potential)> 0.

Since the anions of chloride ions could be specifically adsorbed on the steel surface, thereby given rise to negatively charged steel surface[112].The formation of positively charged protonated species facilitates adsorption of the compound on the metal surface through electrostatic interaction between the BRSM molecule and the carbon steel surface (physisorption). Thus, the metal complexes of $Fe^{+2}$and BRSM or protonated BRSM mightbe formed as follows:

$$\mathrm{BRSM} + \mathrm{Fe}^{+2} \leftrightarrow [\mathrm{BRSM}-\mathrm{Fe}]^{2+} \qquad \text{Equ III. 6}$$

$$[BRSMHx]^{x+1} + Fe^{+2} \leftrightarrow [BRSMHx - Fe]^{(2+x)+} \qquad \text{Equ III. 7}$$

These complexes might be adsorbed on API 5L X70steel surface by the Van der Waals force to form the coating that aid in isolating the metal surface. Similar mechanism has been documented with Lannea coromandelica leaf extract[113]and Artemisia Mesatlantica essential oil [114].

In the case of addition of KI to BRSM, KI helps BRSM get adsorbed onto the iron surface, thus increasing the coverage of the API 5L X70 steel surface, hence maintaining good corrosion inhibition efficiency, and at the same time, decreases the amount of BRSM used. Because the API 5L X70 steel surface has extra positive charges in blank solution from $E_{q=0}$ analysis, $I^-$ will firstly be adsorbed on the metal surface[115]. In acid solution, the carbonyl oxygen (C=O) may be protonated and the molecule exists as a polycation. So BRSM will form positively charged molecules in hydrochloric acid solution[116]. Since the anions of Iodide could be specifically adsorbed on the steel surface, thereby given rise to negatively charged steel surface. The formation of positively charged protonated species facilitates adsorption of the compound on the metal surface through electrostatic interaction between the BRSM molecule and the steel surface (physisorption).

The interaction of protonated BRSM with $I^-$ anions might be formed as follows:

$$I_{ads}^- + BRSM_s^+ \leftrightarrow (IBRSM)_{ads} \qquad \text{Equ III. 8}$$

# *General Conclusion*

Protection against corrosion in the petroleum industry is very important. Inorganic and synthetic compounds have already been used as inhibitors. However, these inhibitors are characterized by having high toxicity on the human body and a negative impact on the environment and they are also not easy to decompose. Many national and international organizations are seeking to protect the environment by using ***green chemistry.***

The main objective of this thesis was to evaluate the inhibition properties of a natural organic compound proposed as an alternative to the chemical inhibitors in the petroleum industry. This organic inhibitor is characterized by non-toxicity, and by having no negative impact to the environment, biodegradability and available from renewable sources.

Fourier-transform infrared spectroscopy (FTIR) analysis indicated that Bark Resine of Schunis Molle (BRSM) contains O and probably N atoms in functional groups (O–H, N–H, C=O (ketone), C–N, C–O) and aromatic ring. The inhibition efficiency of BRSM has been investigated by electrochemical measurements (polarization curves and electrochemical impedance spectroscopy) and surface analyses (SEM – EDX) in acidic solutions.

First of all in the absence of BRSM inhibitor, the corrosion of API 5L X70 steel has been studied in hydrochloric and sulfuric acid medium to understand the different electrochemical parameters.From the potentiodynamic polarization, the elctrochmical results showed that the corrosion rate of API 5L X70 steel in 0.5 M HCl was 265 $\mu A.cm^{-2}$ And in 0.5 M $H_2SO_4$ was 1661 $\mu A.cm^{-2}$. From the EIS, the charge transfer resistance in HCl higher than $H_2SO_4$, the Nyquist plots reveals that the impedance diagram was consisted of a large capacitive loop at high frequency and an inductive loop at law frequency in sulfuric acid, and one capacitive loop in hydrochloric acid. That means sulfuric acid solution is more aggressive than hydrochloric acid solution.

The SEM micrograph has showed general corrosion type in the both solutions and the pits on the steel surface due to $Cl^-$ and $SO_4^{-2}$.

The evaluation of BRSM in 0.5M HCl acid medium provided the following results, the potentiodynamic polarization data indicates that the inhibitor affects both cathodic and anodic processes, which means that the inhibitor acts as a mixed type and the corrosion rate of API 5L X70 steel in absence of BRSM is 265 $\mu Acm^{-2}$ and in presence of the optimum concentration (2g/L BRSM) it decreases significantly to 22 $\mu Acm^{-2}$and in same time, the inhibition efficiency increases to reach the maximum value of 92%. From the EIS, the charge transfer resistance increases with the increase of the concentration of the inhibitor and the inhibition efficiency ($\eta_{EIS}$) is 94% in 2 g/L. The results obtained from SEM-EDX analysis after 60 hours of immersion in 0.5M HCl with and without BRSM; in absence of BRSM the corrosion products were appeared on the surface of API 5L X70 steel, they were consist from chlorine and oxygen elements, in presence of BRSM the remarkable thing is the absence of the corrosion products. After removing the corrosion products, the SEM micrograph are shown significantly reduced of the corrosion in presence of BRSM. These results obtained from the SEM-EDX analysis are in good arrangement with electrochemical techniques.

The synergetic effect between BRSM and iodide halogen has been studied in 0.5M HCl acid solution. From the potentiodynamic polarization, the inhibition efficiency is 94% in the presence of the combination (0.5g/L BRSM + 3mM KI) and addition of the different concentrations of BRSM has reduced both the anodic iron dissolution and the cathodic hydrogen evolution reactions. From the EIS, the value of inhibition efficiency $\eta_{EIS}$ is 88% in the presence of 0.05 g/L BRSM + 3mM KI and increases as maximum inhibition efficiency $\eta_{EIS}$ value 95% in the presence of 0.5 g/L BRSM + 3mM KI. This can be attributed to the enhanced adsorption of BRSM in the presence of KI because of the synergistic effect of iodide ions. From SEM micrograph of the API 5L X70 steel, the specimen immersion in 0.5M HCl solution in absence of the inhibitor is characterized by highly corroded and damaged surface. However, in the presence of optimum concentrations 0.5 g $L^{-1}$ BRSM + 3mM KI the surface morphology of the specimen has been remarkably improved owing to the formation of the protective film on the metallic surface. From the EDX spectra, the appearance

of new peak of iodide and decreases of the peaks of the both oxygen and chloride, probably due to the adsorption of the combination BRSH and iodide on the surface of API 5L X70steel.These results are confirmed the results obtained from the electrochemical techniques.

The use of 5% HCl acid medium as a real case, the results obtained from potentiodynamic polarization showed that the cathodic and the anodic branch are displaced towards lower values and the inhibition efficiency $\eta_{pol}$ increases with the increase of the BRSM concentrations the maximum value is 82% at 3g/L BRSM. The anodic iron dissolution and the cathodic hydrogen evolution processes are inhibited. BRSM acts as an effective inhibitor for the API 5L X70 steel in 5% HCl medium. From the EIS, the increase in the loop is due to the increase coverage by the BRSM molecules adsorbed on the steel surface. The surface analysis of API 5L X70 steel were immersed in 5% HCl with and without BRSM by SEM. The morphology of specimen is highly attacked and damaged in the absence of BRSM; in the presence of 3g/L BRSM the degree of the damage is reduced. The electrochemical techniques are in good arrangement with the surface analysis.

Sulfuric acid medium was selected to study the inhibition efficiency of BRSM. The results obtained from potentiondynamic polarization of API 5L X70 steel in 0.5M $H_2SO_4$ with addition of BRSM has shown the reduced of anodic dissolution and retarded in the rate of the hydrogen evolution reaction. The maximum value of the inhibition efficiency $\eta_{pol}$ was 77% at 3 g/L BRSM. From the EIS, the values of transfer charge resistance ($R_t$) increase while the values of double layer capacitor ($C_{dl}$) decrease during the increase of BRSM concentration. The inhibition efficiency ($\eta_{EIS}$) increases with the increase of BRSM the highest value is 70% at 3 g/L BRSM. From SEM images, the specimen is aggressively attacked in absence of BRSM and in presence of 3 g/L BRSM the damage is little bit reduced. The results obtained from the surface analysis are comforted those results of electrochemical impedance spectroscopy and potentiodynamic polarization.

***In this research, there are similar results obtained from all experiments:***

- The Langmuir isotherm was found to describe the type of adsorption of BRSM on the surface of API 5L X70 steel.
- The standard free energy adsorption ($\Delta G_{ads}^{0}$) indicates that the adsorption mechanism of BRSM on API 5L X70 steel surface involves two types of interaction, predominant physisorption (ionic) and weak chemisorption (molecular).
- The inspection of the plots revealed that the shape of Nyquist plot in absence and presence of the BRSM is similar. That indicates unchanged mechanism of corrosion.

***As perspectives, we plan to do the following work:***

- It would be more judicious to study the influence of hydrodynamic conditions, under the same operating conditions, on the effectiveness of Bark Resin Schinus Molle.
- It would also be desirable for this study to use surface characterization techniques such as XPS photoelectron spectroscopy (X-Ray Photoelectron Spectroscopy) and Raman spectroscopy in order to establish more precisely the formation of corrosion products and their interaction.

# *References*


[1]. G, K., et al., *International Measures of Prevention,Application, and Economics of Corrosion Technologies Study.* NACE International, 2016: p. 216.

[2]. Robertson, J.O. and G.V. Chilingarian, *Chapter 5 Acidizing Oilwells.* 1989. **19**: p. 161-190.

[3]. Díaz-Cardenas, M.Y., et al., *Electrochemical and chemical quantum studies of a natural alkaloid compound: Boldine, as green corrosion behaviour on carbon steel and Copper in sulfuric acid.* Journal of Materials and Environmental Sciences, 2019. **10**(10): p. 1011-1024.

[4]. Marciales, A., et al., *Performance of green corrosion inhibitors from biomass in acidic media.* Corrosion Reviews, 2018. **36**(3): p. 239-266.

[5]. Ahmad, A., R. Kumar, and A. Kumar, *Effect of sodium molybdate and sodium tungstate in concrete rebar corrosion.* Anti-Corrosion Methods and Materials, 2019. **66**(3): p. 253-263.

[6]. El-Meligi, A.A., *Corrosion Preventive Strategies as a Crucial Need for Decreasing Environmental Pollution and Saving Economics.* Corrosion Science, 2010. **2**: p. 22-33.

[7]. Bharatiya, U., et al., *Effect of Corrosion on Crude Oil and Natural Gas Pipeline with Emphasis on Prevention by Ecofriendly Corrosion Inhibitors: A Comprehensive Review.* Journal of Bio- and Tribo-Corrosion, 2019. **5**(2).

[8]. Lisa P. Jackson, *Citizen Petition under Toxic Substances Control Act Regarding the Chemical Substances and Mixtures Used in Oil and Gas Exploration or Production.* Environmental Protection Agency "EARTHJUSTICE", 2011.

[9]. Thomas, R.S., et al., *The next generation blueprint of computational toxicology at the U.S. Environmental Protection Agency.* Oxford University, 2019.

[10]. IPEN and WECF, *Beyond 2020: Green chemistry and sustainable chemistry*. 2017.

[11]. Nations, U., *Report of the Special Rapporteur on the implications for human rights of the environmentally sound management and disposal of hazardous substances and wastes, Başkut Tuncak*. 2015.

[12]. Anastas, P.T. and J.C. Warner, *Green chemistry : theory and practice*. 1998, New York : Oxford University Press.

[13]. Goni, L.K.M.O. and M.A.J. Mazumder, *Green Corrosion Inhibitors*. 2019, Chemistry Department, King Fahd University of Petroleum & Minerals, Dhahran,Saudi Arabia: Intechopen.

[14]. Bentrah, H., et al., *The influence of temperature on the corrosion inhibition of API 5L X42 pipeline steel in HCl medium by gum arabic.* Anti-Corrosion Methods and Materials, 2017. **4**: p. 409-417.

[15]. Ikeuba, A.I. and P.C. Okafor, *Green corrosion protection for mild steel in acidic media: saponins and crude extracts of Gongronema latifolium.* Pigment & Resin Technology, 2019. **48**(1): p. 57-64.

[16]. Chevalier, M., *Investigation of Corrosion Inhibition Efficiency of Amazonian Tree Alkaloids Extract for C38 steel in 1M Hydrochloric Media.* International Journal of Electrochemical Science, 2019: p. 1208-1223.

[17]. Speight, J.G., *Rules of thumb for petroleum engineers*. 2017: John Wiley & Sons.

[18]. Portier, S., L. André, and F.-D. Vuataz, *Review on chemical stimulation techniques in oil industry and applications to geothermal systems*, in *Centre for Geothermal Research, Neuchâtel, Switzerland*. 2007.

[19]. ABBAS, A.J., *Descaling of Petroleum Production Tubing utilising Aerated High Pressure Flat Fan Water Sprays*, in *School of Computing, Science and Engineering, College of Science and Technology,*. 2014, Salford, Manchester, UK.

[20]. NA Mumallah, P., *Factors Influencing the Reaction Rate of Hydrochloric Acid and Carbonate Rock.* Society of Petroleum Engineers, 1991.

[21]. Shafiq, M.U. and H.B. Mahmud, *Sandstone matrix acidizing knowledge and future development.* Journal of Petroleum Exploration and Production Technology, 2017. **7**(4): p. 1205-1216.

[22]. Crowe, C., J. Masmonteil, and R. Thomas, *Trends in matrix acidizing.* Oilfield Review, 1992. **4**(4): p. 22-40.

[23]. Mutahhar, F., et al., *Mechanistic modeling of erosion–corrosion for carbon steel.* 2017: p. 749-763.

[24]. Sastri, V.S., *Corrosion processes and the use of corrosion inhibitors in managing corrosion in underground pipelines.* 2014: p. 127-165.

[25]. Prabha, S.S., R.J. Rathish, and R. Dorothy, *CORROSION PROBLEMS IN PETROLEUM INDUSTRY AND THEIR SOLUTION.* European Chemical Bulletin, 2014. **3**: p. 300-307.

[26]. Popoola, L.T., et al., *Corrosion problems during oil and gas production and its mitigation.* International Journal of Industrial Chemistry, 2013. **4**: p. 35.

[27]. Palanisamy, G., *Corrosion Inhibitors*. 2019: intechopen. 2-20.

[28]. El-Haddad, M.N., A.S. Fouda, and A.F. Hassan, *Data from Chemical, electrochemical and quantum chemical studies for interaction between Cephapirin drug as an eco-friendly corrosion inhibitor and carbon steel surface in acidic medium.* Chemical Data Collections, 2019. **22**: p. 100251.

[29]. Saxena, A., et al., *Use of Saraca ashoka extract as green corrosion inhibitor for mild steel in 0.5 M H2SO4.* Journal of Molecular Liquids, 2018. **258**: p. 89-97.

[30]. Ngouné, B., et al., *Performances of Alkaloid Extract from Rauvolfia macrophylla Stapf toward Corrosion Inhibition of C38 Steel in Acidic Media.* ACS Omega, 2019. **4**(5): p. 9081-9091.

[31]. Kesavan, D., M. Gopiraman, and N. Sulochana, *Green_Inhibitors_for_Corrosion_of_Metals_A_Review.* Chemical Science Review and Letters, 2012: p. 1-8.

[32]. Raja, P.B. and M.G. Sethuraman, *Natural products as corrosion inhibitor for metals in corrosive media — A review.* Materials Letters, 2008. **62**(1): p. 113-116.

[33]. Ropital, F., *Corrosion and degradation of metallic materials*. 2010: Editions Technip.

[34]. Erkey, C., *Thermodynamics and Dynamics of Adsorption of Metal Complexes on Surfaces from Supercritical Solutions.* 2011. **1**: p. 41-77.

[35]. Mccafferty, E., *Introduction to Corrosion Science.* Springer, 2010.

[36]. Elabbasy, H., S. Zidan, and A. El-Aziz, *Inhibitive behavior of Ambrosia Maritima extract as an eco-friendly corrosion inhibitor for carbon steel in 1M HCl.* Zastita materijala, 2019. **60**(2): p. 129-146.

[37]. Mobin, M., M. Basik, and J. Aslam, *Pineapple stem extract (Bromelain) as an environmental friendly novel corrosion inhibitor for low carbon steel in 1 M HCl.* Measurement, 2019. **134**: p. 595-605.

[38]. Ruiz, A.M., et al., *Opuntia ficus-indica (Nopal Extract) as Green Inhibitor for Corrosion Protection in Industrial Steels.* Corrosion Inhibitors, Principles and Recent Applications, 2018: p. 145.

[39]. Zheng, X., et al., *Corrosion inhibition of mild steel in sulfuric acid solution by loquat (Eriobotrya japonica Lindl.) leaves extract.* Scientific Reports, 2018. **8**(1).

[40]. Abdollahi, R. and S.R. Shadizadeh, *Effect of acid additives on anticorrosive property of henna in regular mud acid.* Scientia Iranica, 2012. **19**(6): p. 1665-1671.

[41]. Ait Aghzzaf, A., D. Veys-Renaux, and E. Rocca, *Pomegranate peels crude extract as a corrosion inhibitor of mild steel in HCl medium: Passivation and hydrophobic effect.* Materials and Corrosion, 2019.

[42]. Ramezanzadeh, M., et al., *Corrosion inhibition of mild steel in 1 M HCl solution by ethanolic extract of eco-friendly Mangifera indica (mango) leaves: Electrochemical, molecular dynamics, Monte Carlo and ab initio study.* Applied Surface Science, 2019. **463**: p. 1058-1077.

[43]. A.Loto, C. and R. T.Loto, *Effects of Lavandula and Ricinus Communis Oil as Inhibitors of Mild Steel Corrosion in HCL and H2SO4 Media.* Procedia Manufacturing, 2019. **35**: p. 407-412.

[44]. Bentrah, H., Y. Rahali, and A. Chala, *Gum Arabic as an eco-friendly inhibitor for API 5L X42 pipeline steel in HCl medium.* Corrosion Science, 2014. **82**: p. 426-431.

[45]. Umoren, S.A., *Polymers as Corrosion Inhibitors for Metals in Different Media* The Open Corrosion Journal, 2009: p. 175-188.

[46]. Umoren, S.A. and M.M. Solomon, *Recent Developments on the Use of Polymers as Corrosion Inhibitors.* The Open Materials Science Journal, 2014: p. 39-54.

[47]. Nadi, I., et al., *Sargassum muticum extract based on alginate biopolymer as a new efficient biological corrosion inhibitor for carbon steel in hydrochloric acid pickling environment: Gravimetric, electrochemical and surface studies.* International Journal of Biological Macromolecules, 2019. **141**: p. 137-149.

[48]. Messali, M., et al., *Guar gum as efficient non-toxic inhibitor of carbon steel corrosion in phosphoric acid medium: Electrochemical, surface, DFT and MD simulations studies.* Journal of Molecular Structure, 2017. **1145**: p. 43-54.

[49]. Djellab, M., et al., *Synergistic effect of halide ions and gum arabic for the corrosion inhibition of API5L X70 pipeline steel in H2SO4.* Materials and Corrosion, 2019. **70**(1): p. 149-160.

[50]. Pramudita, M., S. Sukirno, and M. Nasikin, *Synergistic Corrosion Inhibition Effect of Rice Husk Extract and KI for Mild Steel in H2SO4 Solution.* Bulletin of Chemical Reaction Engineering & Catalysis, 2019. **14**(3): p. 697.

[51]. Ridhwan, A.M., A.A. Rahim, and A.M. Shah, *Synergistic Effect of Halide Ions on the Corrosion Inhibition of Mild Steel in Hydrochloric Acid using Mangrove Tannin.* International Journal of Electrochemical Science, 2012. **7**: p. 8091 - 8104.

[52]. Ribeiro, D.V., C.A.C. Souza, and J.C.C. Abrantes, *Use of Electrochemical Impedance Spectroscopy (EIS) to monitoring the corrosion of reinforced concrete.* Revista IBRACON de Estruturas e Materiais, 2015. **8**(4): p. 529-546.

[53]. Macdonald, J.R., *Impedance Spectroscopy.* Annals of Biomedical Engineering, 1992. **20**: p. 289-305.

[54]. *Gamry Instruments Software Tutorials and Primers.* 2005.

[55]. Normand, B., *Prévention et lutte contre la corrosion: une approche scientifique et technique.* Presses polytechniques et universitaires romandes, 2004:.

[56]. Majd, M.T., et al., *Green method of carbon steel effective corrosion mitigation in 1 M HCl medium protected by Primula vulgaris flower aqueous extract via experimental, atomic-level MC/MD simulation and electronic-level DFT theoretical elucidation.* Journal of Molecular Liquids, 2019. **284**: p. 658-674.

[57]. Enos, D.G. and L.L. Scribner, *The Potentiodynamic Polarization Scan*. 1997.

[58]. Popov, B.N., *Basics of Corrosion Measurements.* 2015: p. 181-237.

[59]. Elgrishi, N., et al., *A Practical Beginner's Guide to Cyclic Voltammetry.* Journal of Chemical Education, 2017. **95**(2): p. 197-206.

[60]. Taher, A.M., *Evaluating Corrosion and Passivation by Electrochemical Techniques.* International Journal of Mechanical Engineering and Robotics Research, 2016. **7**(2): p. 131-135.

[61]. Khan, M.S., et al., *Dopamine detection using mercaptopropionic acid and cysteamine for electrodes surface modification.* Journal of Electrical Bioimpedance, 2018. **9**(1): p. 3-9.

[62]. Fytianos, G., et al., *Corrosion Evaluation of MEA Solutions by SEM-EDS, ICP-MS and XRD.* Energy Procedia, 2016. **86**: p. 197-204.

[63]. Davis, J.R. and D. Associates, *Corrosion Understanding the Basics*. 2000: ASM International.

[64]. Ituen, E., O. Akaranta, and A. James, *Green anticorrosive oilfield chemicals from 5-hydroxytryptophan and synergistic additives for X80 steel surface protection in acidic well treatment fluids.* Journal of Molecular Liquids, 2016. **224**: p. 408-419.

[65]. Li, W., et al., *Experimental and quantum chemical studies on two triazole derivatives as corrosion inhibitors for mild steel in acid media.* Materials and Corrosion, 2011. **62**(11): p. 1042-1050.

[66]. Alvarez, P.E., et al., *Rollinia occidentalis extract as green corrosion inhibitor for carbon steel in HCl solution.* Journal of Industrial and Engineering Chemistry, 2018. **58**: p. 92-99.

[67]. Azzaoui, K., et al., *Eco friendly green inhibitor Gum Arabic (GA) for the corrosion control of mild steel in hydrochloric acid medium.* Corrosion Science, 2017. **129**: p. 70-81.

[68]. Cao, C., *On electrochemical techniques for interface inhibitor research.* corrosion science, 1996. **38**(12): p. 2073-2082.

[69]. Hegazy, M.A. and F.M. Atlam, *Three novel bolaamphiphiles as corrosion inhibitors for carbon steel in hydrochloric acid: Experimental and computational studies.* Journal of Molecular Liquids, 2016. **218**: p. 649-662.

[70]. Chaouiki, A., et al., *Understanding corrosion inhibition of mild steel in acid medium by new benzonitriles: Insights from experimental and computational studies.* Journal of Molecular Liquids, 2018. **266**: p. 603-616.

[71]. Kissi, M., et al., *Establishment of equivalent circuits from electrochemical impedance spectroscopy study of corrosion inhibition of steel by pyrazine in sulphuric acidic solution.* Applied Surface Science, 2006. **252**(12): p. 4190-4197.

[72]. Kaczerewska, O., et al., *Efficiency of cationic gemini surfactants with 3-azamethylpentamethylene spacer as corrosion inhibitors for stainless steel in hydrochloric acid.* Journal of Molecular Liquids, 2017. **247**: p. 6-13.

[73]. Karthik, N. and M. Sethuraman, *A robust method of enhancement of protection ability of electrodeposited silane film over copper surface using H2O2.* Materials and Corrosion, 2014. **65**(10): p. 982-990.

[74]. Meeusen, M., et al., *The use of odd random phase electrochemical impedance spectroscopy to study lithium-based corrosion inhibition by active protective coatings.* Electrochimica Acta, 2018. **278**: p. 363-373.

[75]. Feng, L., et al., *The synergistic corrosion inhibition study of different chain lengths ionic liquids as green inhibitors for X70 steel in acidic medium.* Materials Chemistry and Physics, 2018. **215**: p. 229-241.

[76]. Salinas-Solano, G., et al., *Development and evaluation of a green corrosion inhibitor based on rice bran oil obtained from agro-industrial waste.* Industrial Crops and Products, 2018. **119**: p. 111-124.

[77]. Solomon, M.M., et al., *Synergistic inhibition of aluminium corrosion in H2SO4 solution by polypropylene glycol in the presence of iodide ions.* Pigment & Resin Technology, 2016. **45**(4): p. 280-293.

[78]. Singh, P., V. Srivastava, and M. Quraishi, *Novel quinoline derivatives as green corrosion inhibitors for mild steel in acidic medium: electrochemical, SEM, AFM, and XPS studies.* Journal of Molecular Liquids, 2016. **216**: p. 164-173.

[79]. Tao, Z., et al., *4-Chloro-benzoic acid [1, 2, 4] triazol-1-ylmethyl ester as an effective inhibitor of mild steel corrosion in HCl solution.* Materials and Corrosion, 2010. **61**(10): p. 877-884.

[80]. Fekry, A. and R.R. Mohamed, *Acetyl thiourea chitosan as an eco-friendly inhibitor for mild steel in sulphuric acid medium.* Electrochimica Acta, 2010. **55**(6): p. 1933-1939.

[81]. Hassannejad, H. and A. Nouri, *Sunflower seed hull extract as a novel green corrosion inhibitor for mild steel in HCl solution.* Journal of Molecular Liquids, 2018. **254**: p. 377-382.

[82]. Kolotyrkin, J.M., *Pitting corrosion of metals.* Corrosion, 1963. **19**(8): p. 261t-268t.

[83]. Feng, Y., et al., *The synergistic effects of propargyl alcohol and potassium iodide on the inhibition of mild steel in 0.5 M sulfuric acid solution.* Corrosion Science, 1999. **41**(5): p. 829-852.

[84]. Khaled, K. and N. Hackerman, *Investigation of the inhibitive effect of ortho-substituted anilines on corrosion of iron in 1 M HCl solutions.* Electrochimica Acta, 2003. **48**(19): p. 2715-2723.

[85]. Sayed, S., et al., *Synergistic effects of benzotriazole and copper ions on the electrochemical impedance spectroscopy and corrosion behavior of iron in sulfuric acid.* The Journal of Physical Chemistry B, 2003. **107**(23): p. 5575-5585.

[86]. Markhali, B., et al., *Electrochemical impedance spectroscopy and electrochemical noise measurements as tools to evaluate corrosion inhibition of azole compounds on stainless steel in acidic media.* Corrosion Science, 2013. **75**: p. 269-279.

[87]. Usman, B.J., S.A. Umoren, and Z.M. Gasem, *Inhibition of API 5L X60 steel corrosion in CO2-saturated 3.5% NaCl solution by tannic acid and synergistic effect of KI additive.* Journal of Molecular Liquids, 2017. **237**: p. 146-156.

[88]. Zhang, Z., et al., *Inhibition of carbon steel corrosion in phase-change-materials solution by methionine and proline.* Corrosion Science, 2016. **111**: p. 675-689.

[89]. Mounir, D., *Corrosion des installations pétrolières : Effet de la synergie des ions iodures et des inhibiteurs naturels sur la protection contre la corrosion de l'acier API 5L X70 en milieux acides. Doctorat thesis,(2019)*, in *mechanical departement, University of Biskra*.

[90]. Gerengi, H. and H.I. Sahin, *Schinopsis lorentzii extract as a green corrosion inhibitor for low carbon steel in 1 M HCl solution.* Industrial & Engineering Chemistry Research, 2012. **51**(2): p. 780-787.

[91]. Singh, M.R., P. Gupta, and K. Gupta, *The litchi (Litchi Chinensis) peels extract as a potential green inhibitor in prevention of corrosion of mild steel in 0.5 M H2SO4 solution.* Arabian Journal of Chemistry, 2015.

[92]. Ahamad, I., R. Prasad, and M.A. Quraishi, *Experimental and theoretical investigations of adsorption of fexofenadine at mild steel/hydrochloric acid interface as corrosion inhibitor.* Journal of Solid State Electrochemistry, 2010. **14**(11): p. 2095-2105.

[93]. Parveen, M., M. Mobin, and S. Zehra, *Evaluation of L-tyrosine mixed with sodium dodecyl sulphate or cetyl pyridinium chloride as a corrosion inhibitor for mild steel in 1 M HCl: experimental and theoretical studies.* RSC advances, 2016. **6**(66): p. 61235-61248.

[94]. Labjar, N., et al., *Corrosion inhibition of carbon steel and antibacterial properties of aminotris-(methylenephosphonic) acid.* Materials Chemistry and Physics, 2010. **119**(1-2): p. 330-336.

[95]. Thanapackiam, P., et al., *Electrochemical evaluation of inhibition efficiency of ciprofloxacin on the corrosion of copper in acid media.* Materials Chemistry and Physics, 2016. **174**: p. 129-137.

[96]. Umoren, S., Y. Li, and F. Wang, *Synergistic effect of iodide ion and polyacrylic acid on corrosion inhibition of iron in H2SO4 investigated by electrochemical techniques.* Corrosion Science, 2010. **52**(7): p. 2422-2429.

[97]. Okafor, P.C. and Y. Zheng, *Synergistic inhibition behaviour of methylbenzyl quaternary imidazoline derivative and iodide ions on mild steel in H2SO4 solutions.* Corrosion Science, 2009. **51**(4): p. 850-859.

[98]. Qian, B., et al., *Synergistic effect of polyaspartic acid and iodide ion on corrosion inhibition of mild steel in H2SO4.* Corrosion Science, 2013. **75**: p. 184-192.

[99]. Zarrouk, A., et al., *New 1H-pyrrole-2, 5-dione derivatives as efficient organic inhibitors of carbon steel corrosion in hydrochloric acid medium: electrochemical, XPS and DFT studies.* Corrosion Science, 2015. **90**: p. 572-584.

[100]. Arockiasamy, P., et al., *Evaluation of corrosion inhibition of mild steel in 1 M hydrochloric acid solution by Mollugo cerviana.* International Journal of Corrosion, 2014. **2014**.

[101]. Li, X., S. Deng, and H. Fu, *Inhibition of the corrosion of steel in HCl, H2SO4 solutions by bamboo leaf extract.* Corrosion Science, 2012. **62**: p. 163-175.

[102]. Hegazy, M., *Novel cationic surfactant based on triazole as a corrosion inhibitor for carbon steel in phosphoric acid produced by dihydrate wet process.* Journal of Molecular Liquids, 2015. **208**: p. 227-236.

[103]. Umoren, S.A., *Polypropylene glycol: A novel corrosion inhibitor for× 60 pipeline steel in 15% HCl solution.* Journal of Molecular Liquids, 2016. **219**: p. 946-958.

[104]. Liu, F., et al., *Electrochemical behavior of Q235 steel in saltwater saturated with carbon dioxide based on new imidazoline derivative inhibitor.* Corrosion Science, 2009. **51**(1): p. 102-109.

[105]. Zhao, J. and G. Chen, *The synergistic inhibition effect of oleic-based imidazoline and sodium benzoate on mild steel corrosion in a CO2-saturated brine solution.* Electrochimica Acta, 2012. **69**: p. 247-255.

[106]. Krishnaveni, K. and J. Ravichandran, *Effect of aqueous extract of leaves of Morinda tinctoria on corrosion inhibition of aluminium surface in HCl medium.* Transactions of Nonferrous Metals Society of China, 2014. **24**(8): p. 2704-2712.

[107]. Eduok, U., S. Umoren, and A. Udoh, *Synergistic inhibition effects between leaves and stem extracts of Sida acuta and iodide ion for mild steel corrosion in 1 M H2SO4 solutions.* Arabian Journal of Chemistry, 2012. **5**(3): p. 325-337.

[108]. Fouda, A., et al., *Tobacco plant extracts as save corrosion inhibitor for carbon steel in hydrochloric acid solutions.* Int J Adv Res, 2014. **2**: p. 817-832.

[109]. Schweinsberg, D. and V. Ashworth, *The inhibition of the corrosion of pure iron in 0.5 M sulphuric acid by n-alkyl quaternary ammonium iodides.* Corrosion science, 1988. **28**(6): p. 539-545.

[110]. Banerjee, G. and S. Malhotra, *Contribution to adsorption of aromatic amines on mild steel surface from HCl solutions by impedance, UV, and Raman spectroscopy.* Corrosion, 1992. **48**(1): p. 10-15.

[111]. Deng, S. and X. Li, *Inhibition by Ginkgo leaves extract of the corrosion of steel in HCl and H2SO4 solutions.* Corrosion Science, 2012. **55**: p. 407-415.

[112]. Li, X., S. Deng, and H. Fu, *Synergism between red tetrazolium and uracil on the corrosion of cold rolled steel in H2SO4 solution.* Corrosion Science, 2009. **51**(6): p. 1344-1355.

[113]. Muthukrishnan, P., B. Jeyaprabha, and P. Prakash, *Adsorption and corrosion inhibiting behavior of Lannea coromandelica leaf extract on mild steel corrosion.* Arabian Journal of Chemistry, 2017. **10**: p. S2343-S2354.

[114]. Boumhara, K., et al., *Artemisia Mesatlantica essential oil as green inhibitor for carbon steel corrosion in 1 M HCl solution: Electrochemical and XPS investigations.* Journal of Industrial and Engineering Chemistry, 2015. **29**: p. 146-155.

[115]. Kokalj, A., et al., *What determines the inhibition effectiveness of ATA, BTAH, and BTAOH corrosion inhibitors on copper?* Journal of the American Chemical Society, 2010. **132**(46): p. 16657-16668.

[116]. Solomon, M., et al., *Inhibitive and adsorption behaviour of carboxymethyl cellulose on mild steel corrosion in sulphuric acid solution.* Corrosion science, 2010. **52**(4): p. 1317-1325.

# *Annexes*

Received: 12 August 2018 | Accepted: 17 September 2018
DOI: 10.1002/maco.201810477

ARTICLE

Materials and Corrosion

# Bark resin of *Schinus molle* as an eco-friendly inhibitor for API 5L X70 pipeline steel in HCl medium

**Hicham Taoui** | **Hamza Bentrah** | **Abdelouahad Chala** | **Mounir Djellab**

Laboratoire de Physique des Couches Minces et Applications, Université de Biskra, B.P. 145, Biskra R.P. 07000, Algeria

**Correspondence**
Hamza Bentrah, Laboratoire de Physique des Couches Minces et Applications, Université de Biskra, B.P. 145, Biskra R.P. 07000, Algeria.
Email: hamzacorrsci@gmail.com

The inhibition effect of bark resin of *Schinus molle* (BRSM) on the corrosion of API 5L X70 pipeline steel in hydrochloric acid solution has been studied for the first time by potentiodynamic polarization and electrochemical impedance spectroscopy (EIS) measurements; also, surface morphology has been analyzed by SEM-EDX. The inhibitor (BRSM) has been characterized by Fourier transform infrared spectroscopy (FTIR). The results show that BRSM is a good inhibitor in hydrochloric acid solution. The maximum percentage inhibition efficiency is equal to 94% at 2 $gL^{-1}$. The adsorption of BRSM on API 5L X70 pipeline steel surface obeys Langmuir adsorption isotherm, and involves physical adsorption. Polarization curves reveal that BRSM acts as a mixed-type inhibitor in hydrochloride acid.

**KEYWORDS**
acid inhibition, API5L X70 pipeline steel, bark resin of *Schinus molle*, EIS, hydrochloric acid

## 1 | INTRODUCTION

Carbon steel is the most widely used engineering material. Despite its relatively limited corrosion resistance, carbon steel is used in large tonnages in petroleum production, refining,[1,2] and pipelines.[3,4] In the petroleum industry, carbon steel pipelines are susceptible to corrosion by acidic solutions. As acidic media, hydrochloric acid[5,6] and sulfuric acid[7,8] are often used as industrial acid cleaners and pickling acids. The use of corrosion inhibitors has been found to be one of the best know methods available for the protection of metals against corrosion and one of the most useful in the industry.[9] This method is following stand up due to low cost. The role of inhibitors is to form a surface coating one or several molecular layers thick that serves as a barrier. Many effective organic inhibitors have a reactive group (such as N, S, P, O, as well as aromatic rings) attached to a hydrocarbon. The reactive group interacts with the metal surface, and the hydrocarbon portion of the molecule is in contact with the environment. Excellent corrosion inhibitors are considered to be such organic compounds which not only provide offer electrons to unoccupied d orbitals of carbon steel surface to form coordinate covalent bond, but also can accept the free electrons from the surface of carbon steel as well, by using their antibond orbital to form feedback bonds in turn.[10] It is reported also that organic compounds having −OH, −COOH, $NH_2$, etc., are excellent corrosion inhibitors, especially in acidic media.[11] Indeed, polyaspartic acid[12] (carboxyl functional group), 2-amino thiazole[13] ($NH_2$ functional group) and gum agum rabic[14] (hydroxyl functional group) act as good corrosion inhibitors for the corrosion of carbon steel in acidic medium. However, some of these corrosion inhibitors are either too toxic to the environment,[15] not biodegradable or very expensive. The new generation of environmental regulation requires the replacement of toxic inhibitors with non-toxic inhibitors.[16,17] An important number of papers have been published with the intention to develop environmentally friendly corrosion inhibitors and a lot of research has been doing to the development of the called "green" corrosion inhibitors, Neem extract,[18] *Griffonia simplicifolia* extract,[19] *Asparagus racemosus* extract,[20] *Morus alba* pendula leaves extract,[21] and xanthan gum.[22] From the ongoing discussion

  

it can be concluded that natural products, such as plant extracts, essential oils, and purified compounds are ideal candidates to replace traditional expensive and toxic inorganic and synthetic organic corrosion inhibitors. The aim of the present work is to determine for the first time the inhibition effect of bark resin of *Schinus molle* (BRSM) on the corrosion of carbon steel in 0.5 M hydrochloric acid solution by electrochemical methods. Meanwhile, the adsorption mode of BRSM on API 5L X70 pipeline steel surface was obtained, and the adsorption standard free energy $\Delta G^{\circ}_{ads}$ was calculated and discussed. A probable inhibitive mechanism is proposed from the viewpoint of adsorption theory.

## 2 | EXPERIMENTAL

### 2.1 | Material

The working electrodes (API5L X70 pipeline steel), for electrochemical experiments, were cut into 3 × 3 × 1 cm, with the following chemical composition (weight percentage): C 0.12 max, Mn 1.68 max, P 0.012 max, Si 0.27 min, Cr 0.051 max, S 0.005 max, Ni 0.04 max, Ti 0.03 max, Nb 0.033 max, and the balance Fe. The samples were mounted in the electrochemical cell, and the surface area of each electrode exposed to the electrolyte was 2.85 $cm^2$. Exposed surface of each sample was prepared by wet grinding with silicon carbide abrasive papers (grade 320–500–600–800), rinsed with distilled water and degreased with acetone.

### 2.2 | Medium

The aggressive solution of 0.5 M hydrochloric acid was prepared by dilution of AR grade 36% hydrochloric acid with distilled water.

### 2.3 | Inhibitor

The bark resin of *S. molle* was collected in March 2018 from Biskra-Algeria and the species was identified as *S. molle* L., Anacardiaceae. Dried bark resin of *S. molle* powder was selected for the present study. In earlier studies, the main components of BRSM are germacrene-D, terebinthene, isomasticadienoic acid, isomasticadienonalic acid, and pinicolic acid (Figure 1).[23]

### 2.4 | Electrochemical techniques

Two electrochemical techniques, namely, electrochemical impedance spectroscopy (EIS) and potentiodynamic polarization, were used to study the inhibition efficiency of BRSM for API 5L X70 in 0.5 M hydrochloric acid. Electrochemical measurements were performed using a Gamry Ref 3000 with Gamry Instruments Framework (version 7.05) commercial software.

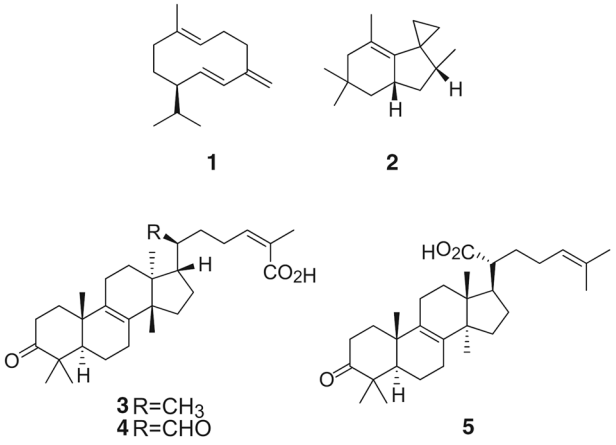


**FIGURE 1** The molecular structure of bark resin of *Schinus molle*: germacrene-D (1), terebinthene (2), isomasticadienoic acid (3), isomasticadienonalic acid (4), and pinicolic acid (5)

A Gamry Paracell (Electrochemical Cell) with a standard three-electrode configuration consisting of Ag/AgCl reference electrode (the potential of Ag/AgCl electrode is the same of the saturated calomel electrode and equal to 240 mV vs. NHE), graphite block for Paracell as counter electrode and the sample acted as the working electrode. The working electrode was connected with a copper wire on the backside and installed in customized Teflon assembly and exposed on the solution side to about 2.85 $cm^2$ working area.

All experiments were performed in stagnant aerated solutions at 30 °C. The working electrode was immersed in test solution at the open circuit potential (OCP) for 1 h to be sufficient to attain a stable state.

The analyses were performed using Gamry Echem Analyst (version 7.05) commercial software developed by Gamry.

Potentiodynamic polarization studies were carried out from the cathodic potential of −0.3 V to anodic potential of +0.3 V with respect to the corrosion potential (Ecorr) at a scan rate of 0.3 mV $s^{-1}$. The corrosion current densities ($I_{corr}$) were determined graphically from the cathode part of polarization curve. Similar method has been previously employed for non-Tafel dependence curves with acceptable deviation of less than 10% from other methods of corrosion rate determination.[24] Because of the presence of a degree of nonlinearity in the Tafel slope part of the obtained polarization curves, the Tafel constants were calculated as a slope of the points after ($E_{corr}$) by ±80 mV.

The values of inhibition efficiency $\eta_{pol}$ were calculated using the following equation:

$$\eta_{pol}\% = \frac{I_{corr} - I_{corr}(inh)}{I_{corr}} \times 100 \qquad (1)$$

where $I_{corr}$ and $I_{corr}$(inh) represent corrosion current density values without and with inhibitor, respectively.

Electrochemical impedance spectroscopy (EIS) was carried out at OCP in the frequency range of 100 kHz to 100 mHz using a 10 mV peak-to-peak voltage excitation. Inhibition efficiency $\eta_{EIS}$ is calculated on the basis of the equation:

$$\eta_{EIS}\% = \frac{R_t - \acute{R}_t}{R_t} \times 100 \quad (2)$$

where $\acute{R}_t$ is charge transfer resistance value in 0.5 M hydrochloric acid, and $R_t$ is charge transfer resistance value in the presence of BRSM.

## 2.5 | Surface analysis

### 2.5.1 | Surface study by scanning electron microscopy (SEM)

The API 5L X70 steel surface was prepared both without (blank) and with inhibitor; 2 g $L^{-1}$ BRSM was used. After 60 h waiting time, the electrodes were removed from the cells and dried. An electron microscope, TESCAN VEGA3, was used for SEM-EDX study.

### 2.5.2 | Fourier-transform infrared spectroscopy (FTIR) of BRSM

The solid bark resin of *S. molle* was characterized by Fourier transform infrared spectroscopy. FTIR spectra was recorded in an FTIR830 spectrophotometer (SHIMADZU Company, Japan), which extended from 4000 to 400 $cm^{-1}$, using the KBr disk technique.

## 3 | RESULTS AND DISCUSSION

FTIR spectrum of BRSM is shown in Figure 2. Original absorption band at 3438 $cm^{-1}$ (associated hydroxyl) was overlapped by the strong stretching mode of N–H. The strong band at 1705 $cm^{-1}$ is due to C═O stretching band (cyclic ketone). The strong band at 2940 $cm^{-1}$ is due to O–H stretching band, it indicates the presence of carboxylic acid group in the inhibitor.

The peak at 1455 $cm^{-1}$ is due to aromatic C–C stretching band. The C–N asymmetric stretching band is observed at 1390 $cm^{-1}$.There is absorption band at 1055 $cm^{-1}$, which can be ascribed to the C–N or C–O stretching vibration. These observations confirmed that the bark resin of *S. molle* contains a mixture of natural products. These results indicate that BRSM contains O and probably N atoms in functional groups (O–H, N–H, C═O (ketone), C–N, C–O) and aromatic ring.

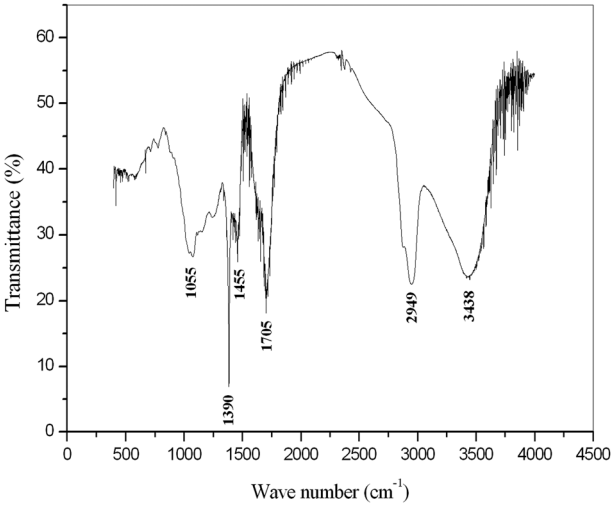


**FIGURE 2** FTIR spectra of BRSM

## 3.1 | Effect of BRSM on inhibition efficiency

### 3.1.1 | Electrochemical impedance spectroscopy measurements

Figure 3 shows the Nyquist diagrams for BRSM in 0.5 M hydrochloric acid at 30 °C (immersion time is 1 h). Obviously, all impedance spectra have typical characteristics that have been widely reported for steel in strong acid media. As shown in Figure 3, in uninhibited and inhibited 0.5 M hydrochloric acid solutions, the impedance spectra exhibit one single capacitive loop, which indicates that the corrosion of steel is mainly controlled by the charge transfer process.[25,26] In the case of the geometric blocking

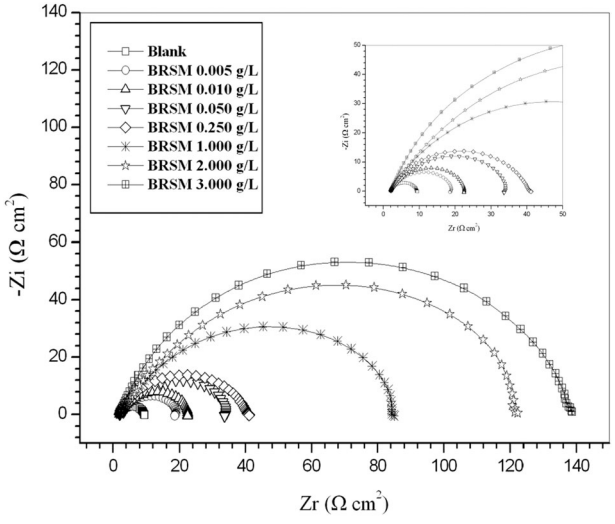


**FIGURE 3** Nyquist plots of the corrosion of API 5L X70 in 0.5 M HCl without and with different concentrations of BRSM at 30 °C (immersion time is 1 h)

effect, the EIS display will be a single capacitive loop if the inhibition efficiency is high and similar to that in the blank solution if the inhibition efficiency is low,[14,27] which suggests that the geometric blocking effect is the inhibition mode of BRSM. The same mode was also reported with *Rollinia occidentalis* extract.[28] It is noted that these capacitive loops are not perfect semicircles which can be attributed to the inhomogeneity of the electrode surface arising from surface roughness or interfacial phenomena.[29] Furthermore, the diameter of the capacitive loop in the presence of inhibitor (BRSM) is larger than that in blank solution, and enlarges with the inhibitor concentration. This indicates that the impedance of inhibited substrate increases with the inhibitor concentration, and leads to good inhibitive performance.

The experimental EIS are presented as Bode plots in Figure 4. According to the Bode plot of impedance module |Z| versus frequency (Figure 4a), the |Z| of API 5L X70 steel is clearly found to depend on the inhibitor concentration. An increase in inhibitor concentration leads to an increase in the |Z| value. The phase angle plots (Figure 4b) show one time constant.

A model of equivalent circuit has been attempted to fit these experimental data using the software Impedance Model Editor designed by Gamry Echem Analyst. Figure 5 shows simulated and experimentally generated impedance diagrams for API5L X70 pipeline steel immersed in 0.5 M hydrochloric acid solution in the presence of 3 g $L^{-1}$ BRSM. Excellent fit with this model was obtained for all experimental data. The circuit consists of the solution resistance $R_s$, the constant phase element representing the double-layer capacitance (CPEdl) and the charge transfer resistance $R_t$.

Table 1 shows representative parameter values of the fitting results to EIS data obtained for API 5L X70 pipeline steel using the equivalent circuits of Figure 5.

$R_t$ values remarkably increased from the value of 7.3 Ω $cm^2$ for the solution without BRSM to 138 Ω $cm^2$ for the highest concentration of BRSM (3 g $L^{-1}$) in the solution at 30 °C. This indicated that the corrosion resistance of API 5L X70 pipeline steel was increased with increasing BRSM concentration. It should be noted that when the inhibitor concentration reaches about 2 g $L^{-1}$, $R_t$ value reaches certain data and does not change markedly. Based on the values of $R_t$ in Table 1, the variation of inhibition efficiency ($\eta_{EIS}$) for carbon steel in the 0.5 M hydrochloric acid solution as a function of BRSM concentration is shown in Figure 6. When the concentration of BRSM is less than

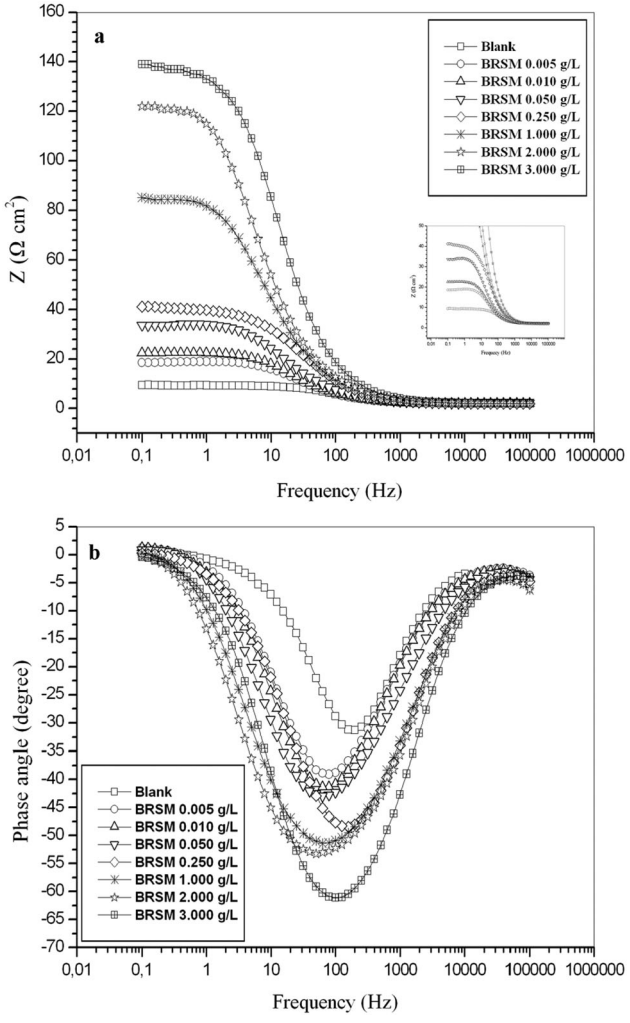


**FIGURE 4** Bode plots for API5L X70 pipeline steel in 0.5 M HCl without and with different concentrations of BRSM at 30 °C, (a) Bode modulus and (b) Bode phase angle representations

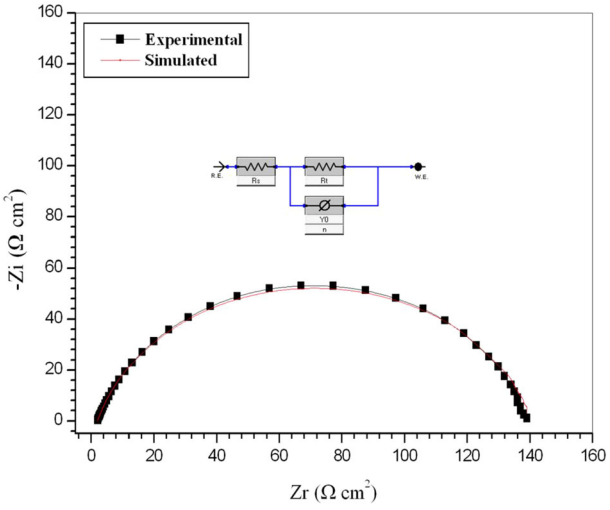


**FIGURE 5** Nyquist plot of experimental data and simulated data, together with the equivalent circuit used to fit the impedance data, recorded for API5L X70 pipeline steel in 0.5 M HCl containing 3 g $L^{-1}$ BRSM [Color figure can be viewed at wileyonlinelibrary.com]

**TABLE 1** Electrochemical impedance parameters for API5L X70 in 0.5 M HCl solution in the absence and the presence of BRSM at 30 °C

| Concentration | $R_s$ ($\Omega\,cm^2$) | $Y_0$ ($\mu\Omega\,S^n\,cm^{-2}$) | $n$ | $R_t$ ($\Omega\,cm^2$) | $C_{dl}$ ($\mu F\,cm^{-2}$) | $\eta_{EIS}$ % |
|---|---|---|---|---|---|---|
| Blank | 2 | 2501 | 0.90 | 7.3 | 1344 | - |
| 0.005 g $L^{-1}$ BRSM | 2 | 1186 | 0.78 | 17.4 | 410 | 58 |
| 0.010 g $L^{-1}$ BRSM | 2 | 1179 | 0.78 | 21.2 | 407 | 65 |
| 0.050 g $L^{-1}$ BRSM | 2 | 1148 | 0.74 | 33.4 | 369 | 78 |
| 0.250 g $L^{-1}$ BRSM | 2 | 900 | 0.80 | 39.0 | 342 | 81 |
| 1.000 g $L^{-1}$ BRSM | 2 | 680 | 0.76 | 87.0 | 281 | 91 |
| 2.000 g $L^{-1}$ BRSM | 2 | 659 | 0.74 | 127.6 | 253 | 94 |
| 3.000 g $L^{-1}$ BRSM | 2 | 259 | 0.82 | 138.0 | 123 | 94 |

2 g $L^{-1}$, $\eta_{EIS}$ increases sharply with an increase in concentration, while a further increase causes no appreciable change in performance. At 2 g $L^{-1}$ of BRSM, $\eta_{EIS}$ value is higher than 94%, which indicates that BRSM is a good inhibitor for API 5L X70 pipeline steel in HCl solution.

In order to give more accurate fit results, the constant phase elements (CPE) were submitted for the capacitors.[30] The impedance value of the CPE is a function of frequency, but its phase is independent of frequency. Its impedance is defined as[31,32]

$$Z_{CPE} = Y_0^{-1}(j\omega)^{-n} \quad (3)$$

where $Z_{CPE}$ represents the impedance of a CPE, $Y_0$ is a proportional factor that indicates the combination of properties related to both the surfaces and electroactive species independent of frequency, $j$ is imaginary number; $\omega$ is the angular frequency, and $\omega$ equal to $2\pi f$, where $f$ is the frequency; and n has the meaning of a phase shift and is related to a slope of the log |Z| versus log $f$ plots and usually is in the range between 0.5 and 1.

The double layer capacitance $C_{dl}$ was calculated using Eq. (4).[33]

$$C_{dl} = Y0\ (2\pi f_{max})^{n-1} \quad (4)$$

where $f_{max}$ is the frequency at which the imaginary component of the impedance is maximum.

On the contrary to the charge transfer resistance, better protection provided by an inhibitor can be associated with a decrease in capacitance of the metal. $C_{dl}$ values remarkably decreased from the value of 1344 $\mu F\,cm^{-2}$ for the solution without BRSM to 123 $\mu F\,cm^{-2}$ for the highest concentration of BRSM (3 g $L^{-1}$) in the solution at 30 °C.

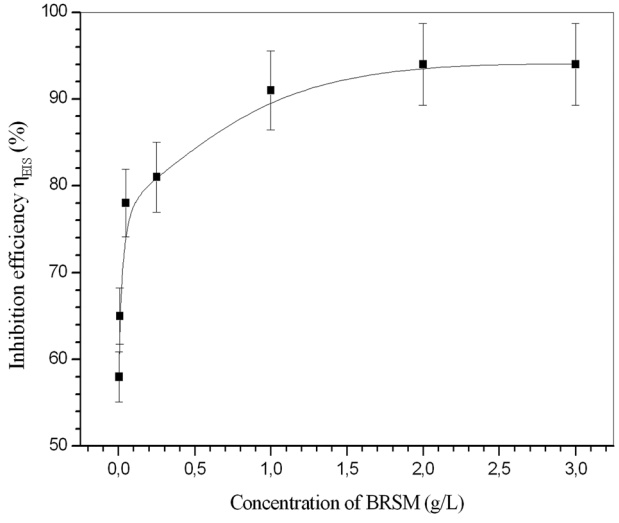


**FIGURE 6** Relationship between inhibition efficiency ($\eta_{EIS}$) and concentration of BRSM in 0.5 M HCl at 30 °C (Electrochemical impedance spectroscopy method, immersion time is 1 h)

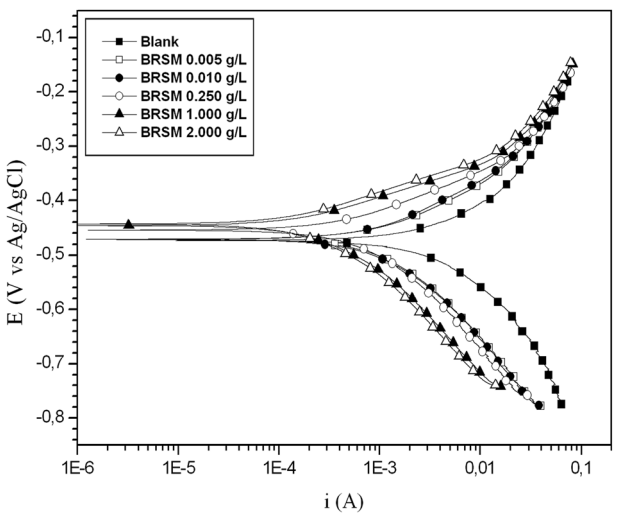


**FIGURE 7** Potentiodynamic polarization curves for API 5L X70 pipeline steel in 0.5 M HCl without and with different concentrations of BRSM at 30 °C (immersion time is 1 h)

**TABLE 2** Potentiodynamic polarization parameters for API5L X70 in 0.5 M HCl solution in the absence and the presence of BRSM at 30 °C

| Concentration | $E_{corr}$ (mV) | $I_{corr}$ (μA cm$^{-2}$) | - $b_c$ (mV dec$^{-1}$) | $b_a$ (mV dec$^{-1}$) | $\eta_{pol}$ % |
|---|---|---|---|---|---|
| Blank | −472 | 265 | 128 | 100 | - |
| 0.005 g L$^{-1}$ BRSM | −472 | 96 | 142 | 91 | 63 |
| 0.010 g L$^{-1}$ BRSM | −472 | 79 | 125 | 90 | 70 |
| 0.250 g L$^{-1}$ BRSM | −452 | 51 | 125 | 76 | 80 |
| 1.000 g L$^{-1}$ BRSM | −448 | 30 | 130 | 72 | 88 |
| 2.000 g L$^{-1}$ BRSM | −442 | 22 | 125 | 76 | 91 |

### 3.1.2 | Potentiodynamic polarization measurements

The effect of bark resin of *S. molle* on the anodic and cathodic behavior of API 5L X70 pipeline steel in 0.5 M hydrochloric acid solution has been studied by polarization measurements and the Tafel plots are shown in Figure 7. The values of corrosion current density ($I_{corr}$), corrosion potential ($E_{corr}$), cathodic Tafel slope ($b_c$), anodic Tafel slope ($b_a$), and inhibition efficiency ($\eta_{pol}$) are presented in Table 2.

Both the anodic and cathodic current were decreased in Figure 7 indicating that BRSM suppressed both the anodic and cathodic reactions through adsorption on the carbon steel surface.

From Table 2 it is evident that the corrosion current density ($I_{corr}$) value decreases from 265 to 22 μA cm$^{-2}$ with the highest concentration of BRSM (2 g L$^{-1}$). The addition of BRSM does not alter the value of $E_{corr}$ significantly indicating the mixed type of inhibiting behavior of the inhibitor. Generally, if the displacement in $E_{corr}$ is >85 mV with respect to $E_{corr}$ in uninhibited solution, the inhibitor can be seen as a cathodic or anodic type.[34,35] In our study the maximum displacement is 30 mV, which confirms that BRSM acts as a mixed-type inhibitor. The similar results were also reported with *Rollinia occidentalis* extract[28] and gum arabic.[36] Cao[27] explained that if the shift of corrosion potential due to addition of an interface inhibitor is negligible, the inhibition is most probably caused by a geometric blocking effect of the adsorbed inhibitive species on the surface of the corroding metal. From the polarization results, it could be concluded that the inhibition of BRSM may be due in the main to the geometric blocking effect. Good agreement with electrochemical impedance spectroscopy is obtained from Table 2, $I_{corr}$ decreases and $\eta_{pol}$ increases with the inhibitor concentration. The maximum value 91% of $\eta_{pol}$ also indicates that BRSM is good inhibitor for API 5L X70 pipeline steel in 0.5 M hydrochloric acid. Good agreement between electrochemical impedance spectroscopy and potentiodynamic polarization curves is obtained.

### 3.1.3 | Adsorption isotherm and standard adsorption free energy

In the present study, several adsorption isotherms were assessed, and the Langmuir adsorption isotherm was found to give the best description of the adsorption behavior of the studied inhibitor (Figure 8). A correlation between surface coverage ($\theta = \eta_{EIS}\%/100$) and the concentration of inhibitor ($C$) in the electrolyte can be represented by the Langmuir adsorption isotherm.[37]

$$\frac{C}{\theta} = \frac{1}{K_{ads}} + C \tag{5}$$

where $K_{ads}$ is constant of adsorption. By plotting $C/\theta$ versus $C$, straight line with slope value close to 1 was obtained. From the value of the adsorption constant, the standard free energy of adsorption $\Delta G^{\circ}_{ads}$ is determined using

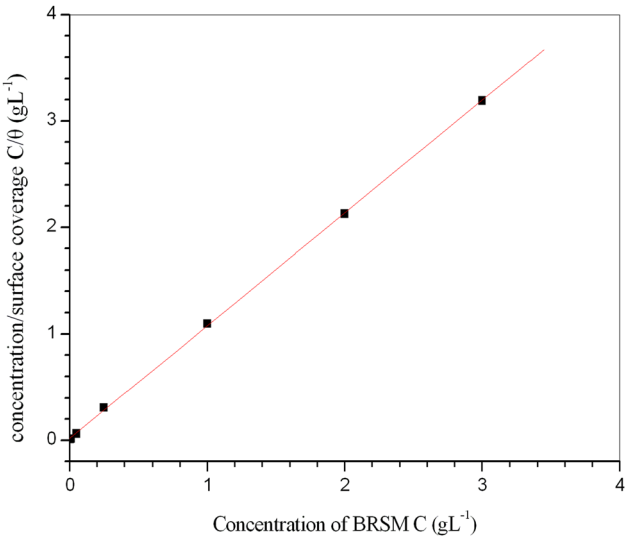


**FIGURE 8** Langmuir isotherm adsorption mode of BRSM on the API 5L X70 pipeline steel surface in 0.5 M HCl at 30 °C (from EIS measurements) [Color figure can be viewed at wileyonlinelibrary.com]

**TABLE 3** Parameters of Langmuir adsorption isotherm for API5L X70 in 0.5 M HCl solution containing BRSM at 30 °C

| Isotherm mode | Linear correlation coefficient | Slope | $K_{ads}$ (L $g^{-1}$) | $\Delta G^{\circ}_{ads}$ (kJ $mol^{-1}$) |
|---|---|---|---|---|
| Langmuir | 0.99991 | 1.05 | 54.85 | −24.76 |

the following equation[17,38,39]:

$$\Delta G^{\circ}_{ads} = -RT \ln (1 \times 10^{6} K_{ads}) \quad (6)$$

where $1 \times 10^{6}$ is the concentration of water molecules expressed in mg $L^{-1}$, $R$ is the universal gas constant and $T$ is the absolute temperature. The values of $\Delta G^{\circ}_{ads}$ and $K_{ads}$ are listed in Table 3. Generally, values of $\Delta G^{\circ}_{ads}$ up to −20 kJ $mol^{-1}$ are consistent with electrostatic interaction between charged molecules and a charged metal (which indicates physical adsorption) while those more negative than −40 kJ $mol^{-1}$ involves charge sharing or transfer from the inhibitor components to the metal surface to form a coordinate type of bond (which indicates chemisorption).[40–42] It is difficult to distinguish between chemisorption and physisorption only based on these criteria, especially when charged species are adsorbed. The possibility of Coulomb interactions between adsorbed

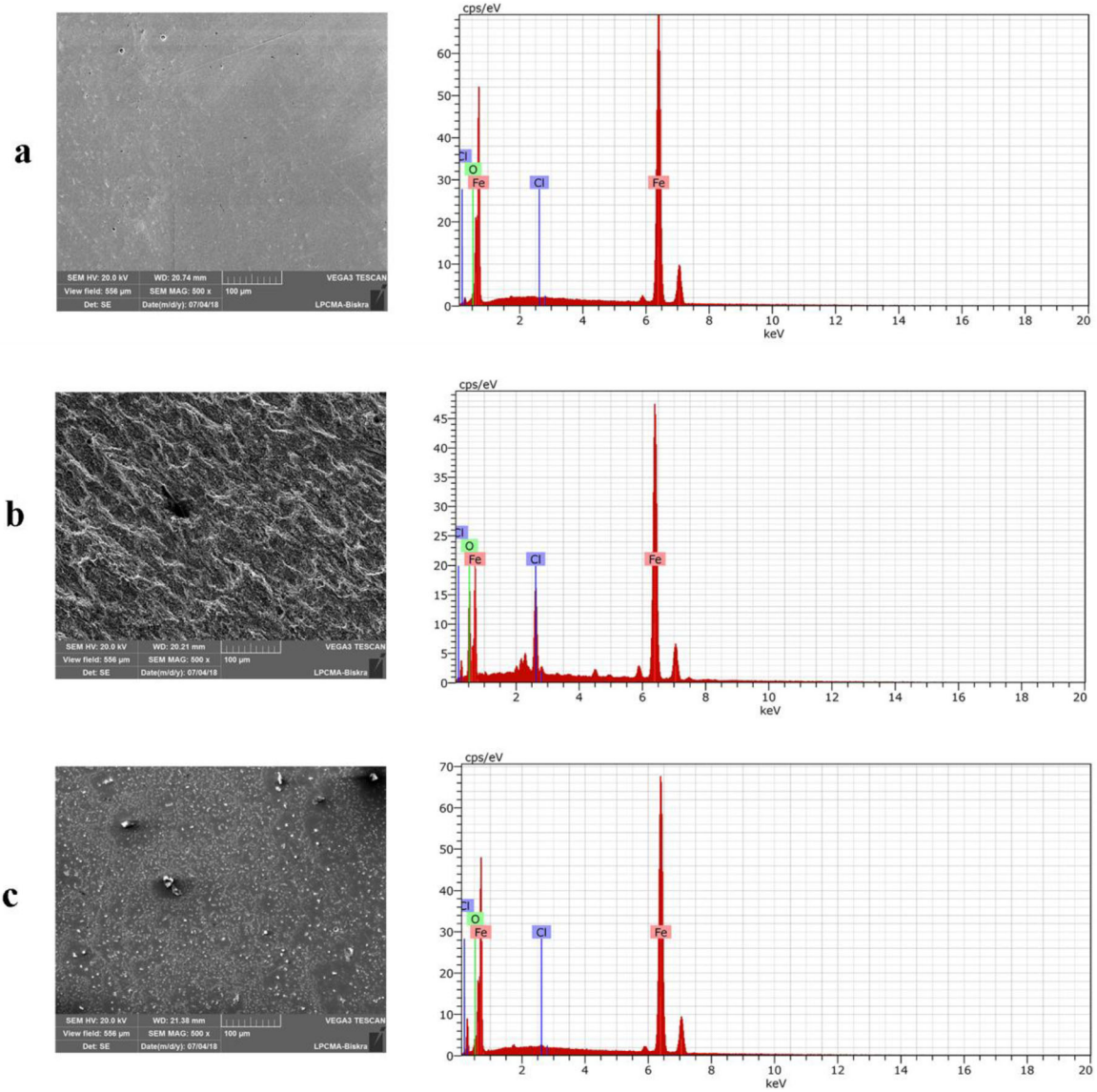


**FIGURE 9** SEM-EDX spectra of API 5L X70 pipeline steel: polished steel (a), in presence of corroding medium (b), and in presence of 2 g $L^{-1}$ BRSM (c) [Color figure can be viewed at wileyonlinelibrary.com]

cations and specifically adsorbed anions can increase the Gibbs energy even if no chemical bond appears.[27] Of the two possibilities, the physisorption mode is likely to predominate due to the obtained value of $\Delta G^{\circ}_{ads}$ ($-24.76\,kJ\,mol^{-1}$). Similar results were also reported with Sunflower seed hull extract.[43]

## 3.2 | SEM-EDX analysis

Figure 9 shows the microscopy pictures and the corresponding chemical analysis for the polished metal, in the presence and absence of the inhibitor (BRSM), to confirm the efficiency of BRSM obtained by the EIS and polarization curves methods. The polished steel consists principally of the element iron (Figure 9a). When the metal was submerged in hydrochloric acid, it was observed that in addition to the element iron, the element oxygen and the element chlorine are present as a consequence of the corrosion phenomenon (Figure 9b). In the microscopy picture corresponding to the sample with the inhibitor (Figure 9c), a decrease in corrosion can be observed. To determine the elements present in API 5L X70 pipeline steel surface after 60 h of exposure to 0.5 M hydrochloric acid, EDX analysis were used. Before the corrosion test, the peaks are related only to the element iron present in the API 5L X70 steel (Table 4). In the absence of inhibitor, the spectra exhibit the peaks of the element oxygen and the element chloride which polished API 5L X70 does not have. The spectra of API 5L X70 steel immersed in 0.5 M hydrochloric acid containing $2\,g\,L^{-1}$ BRSM shows that the amount of oxygen and chloride decreases, probably due to the adsorption of BRSH on the surface of API 5L X70 pipeline steel.

**TABLE 4** Content of elements obtained from EDX spectra for API 5L X70 pipeline steel

| | % atomic | | |
|---|---|---|---|
| Element | Steel | Steel + HCl | Steel + HCl + 2 g $L^{-1}$ BRSM |
| Iron | 96.47 | 58.95 | 93.42 |
| Oxygen | 3.53 | 32.66 | 6.26 |
| Chlorine | 0.00 | 8.39 | 0.32 |

## 3.3 | Explanation for inhibition of BRSM

Corrosion inhibition of API 5L X70 in 0.5 M hydrochloric acid by BRSM can be explained by adsorption of the major constituents of bark resin of *S. molle* such as isomasticadienoic acid, isomasticadienonalic acid and pinicolic acid. Two main types of interaction can describe the adsorption of these molecules: chemisorption and physisorption.

In aqueous acidic solutions, the BRSM exists either as neutral molecules or in the form of cations (protonated BRSM) as follows:

$$BRSM + xH^{+} \leftrightarrow [BRSMHx]^{x+1}$$

The neutral BRSM may be adsorbed on the metal surface via the chemisorption mechanism involving the displacement of water molecules from the metal surface and adsorption most probably takes place through the ketone functions. The transfer of a lone pair of electrons on the oxygen atom in the oxygenated monoterpens (isomasticadienoic acid, isomasticadienonalic acid, and pinicolic acid) to the surface forms a coordinate bond. The BRSM molecules can be adsorbed also on the metal surface on the basis of donor–acceptor interactions between p-electrons of the heterocycle and vacant d-orbitals of iron. On the other hand, in aqueous hydrochloric acid medium, the BRSM molecules, particularly, the oxygenated monoterpen derivatives (isomasticadienoic acid, isomasticadienonalic acid, and pinicolic acid) can be easily protonated at the oxygen heteroatom in the ketone function. However, the charge of the metal surface can be determined from the value of $E_{corr} - E_{q=0}$ (zero charge potential).[44] The $E_{q=0}$ of iron is $-530$ mV versus SCE in hydrochloric acid.[45] In the present system, the value of Ecorr obtained in 0.5 M hydrochloric acid is $-472$ mV. So the steel surface charges positive charge in hydrochloric solution because of $E_{corr} - E_{q=0}$ (zero charge potential) $> 0$. Since the anions of chloride ions could be specifically adsorbed on the steel surface thereby given rise to negatively charged steel surface.[46] The formation of positively charged protonated species facilitates adsorption of the compound on the metal surface through electrostatic interaction between the BRSM molecule and the carbon steel surface (physisorption). Thus, the metal complexes of $Fe^{2+}$ and BRSM or protonated BRSM might be formed as follows:

$$BRSM + Fe^{2+} \leftrightarrow [BRSM - Fe]^{2+}$$

$$[BRSMHx]^{x+1} + Fe^{2+} \leftrightarrow [BRSMHx - Fe]^{(2+x)+}$$

These complexes might be adsorbed on API 5L X70 pipeline steel surface by the Van der Waals force to form the coating that aid in isolating the metal surface. Similar mechanism has been documented with *Lannea coromandelica* leaf extract[47] and *Artemisia Mesatlantica* essential oil.[48]

## 4 | CONCLUSIONS

The main conclusions are as follows:

1. FTIR analysis indicated that BRSM contains O and probably N atoms in functional groups (O–H, N–H, C═O (ketone), C–N, C–O) and aromatic ring.
2. BRSM acts as a good inhibitor for the corrosion of API 5L X70 pipeline steel in 0.5 M hydrochloric acid. Inhibition efficiency increases with the inhibitor concentration, and the maximum value is 94% at 2 g $L^{-1}$.
3. Langmuir adsorption isotherm was found to give the best description of the adsorption behavior of the studied inhibitor.
4. Two main types of interaction can describe the adsorption of BRSM: physical adsorption and chemisorption. Of the two possibilities, the physisorption mode is likely to predominate due to the obtained value of $\Delta G^{\circ}_{ads}$.
5. The potentiostatic polarization data indicate that the inhibitor affects both cathodic and anodic processes, that is, the inhibitor acts as a mixed type.
6. Results of polarization and EIS studies suggest that the mode of the inhibition effect of bark resin of *S. molle* is geometric blocking effect.
7. Results of EIS study suggests that the corrosion of API 5L X70 pipeline steel, in presence of BRSM, is mainly controlled by the charge transfer process.

## ACKNOWLEDGMENTS

We would like to thank Mr. Samir, Mrs. Inas, and Mrs. Latifa for their help.

## ORCID

*Hamza Bentrah* http://orcid.org/0000-0002-9199-317X
*Mounir Djellab* http://orcid.org/0000-0003-0541-9217

## REFERENCES

[1] K. P. V. Kumar, M. S. N. Pillai, G. R. Thusnavis, *J. Mater. Sci. Technol*. **2011**, *27*, 1143.
[2] M. A. Migahed, *Prog. Org. Coat*. **2005**, *54*, 91.
[3] H. H. Almahamedh, *Proc. Eng*. **2015**, *114*, 34.
[4] M. A. Deyab, S. S. Abd El-Rehim, *Electrochim. Acta* **2007**, *53*, 1754.
[5] M. A. Migahed, E. M. S. Azzam, S. M. I. Morsy, *Corros. Sci*. **2009**, *51*, 1636.
[6] M. Farsak, H. Keleş, M. Keleş, *Corros. Sci*. **2015**, *98*, 223.
[7] X. Li, S. Deng, H. Fu, *Corros. Sci*. **2011**, *53*, 302.
[8] Z. Panossian, N. L. D. Almeida, R. M. F. D. Sousa, G. D. S. Pimenta, L. B. S. Marques, *Corros. Sci*. **2012**, *58*, 1.
[9] B. M. Prasanna, B. M. Praveen, N. Hebbar, T. V. Venkatesha, H. C. Tandon, S. B. Abd Hamid, *J. Assoc. Arab Univ. Basic Appl. Sci*. **2017**, *22*, 62.
[10] M. A. Migahed, E. G. Zaki, M. M. Shaban, *RSC Adv*. **2016**, *6*, 71384.
[11] L. Hamadi, S. Mansouri, K. Oulmi, A. Kareche, *Egypt. J. Petrol*. **2018**, https://doi.org/10.1016/j.ejpe.2018.04.004
[12] R. Cui, N. Gu, C. Li, *Mater. Corros*. **2011**, *62*, 362.
[13] F. Y. Cui, L. Guo, S. T. Zhang, *Mater. Corros*. **2014**, *65*, 1194.
[14] H. Bentrah, Y. Rahali, A. Chala, *Corros. Sci*. **2014**, *82*, 426.
[15] S. Hooshmand Zaferani, M. Sharifi, D. Zaarei, M. R. Shishesaz, *J. Environ. Chem. Eng*. **2013**, *1*, 652.
[16] L. Guo, S. T. Zhang, W. P. Li, G. Hu, X. Li, *Mater. Corros*. **2014**, *65*, 935.
[17] M. Djellab, H. Bentrah, A. Chala, H. Taoui, *Mater. Corros*. **2018**, https://doi.org/10.1002/maco.201810203
[18] P. Parthipan, J. Narenkumar, P. Elumalai, P. S. Preethi, A. Usha Raja Nanthini, A. Agrawal, A. Rajasekar, *J. Mol. Liq*. **2017**, *240*, 121.
[19] E. Ituen, O. Akaranta, A. James, S. Sun, *Sustain. Mater. Technol*. **2017**, *11*, 12.
[20] A. Saxena, D. Prasad, R. Haldhar, *J. Mater. Sci*. **2018**, *53*, 8523.
[21] M. Jokar, T. S. Farahani, B. Ramezanzadeh, *J. Taiwan Inst. Chem. Eng*. **2016**, *63*, 436.
[22] M. Mobin, M. Rizvi, *Carbohydr. Polym*. **2016**, *136*, 384.
[23] G. R. Malca-García, L. Hennig, M. L. Ganoza-Yupanqui, A. Piña-Iturbe, R. W. Bussmann, *Rev. Bras. Farmacogn*. **2017**, *27*, 67.
[24] M. Behpour, S. M. Ghoreishi, M. Khayatkashani, N. Soltani, *Corros. Sci*. **2011**, *53*, 2489.
[25] M. A. Hegazy, F. M. Atlam, *J. Mol. Liq*. **2016**, *218*, 649.
[26] A. Chaouiki, H. Lgaz, I.-M. Chung, I. H. Ali, S. L. Gaonkar, K. S. Bhat, R. Salghi, H. Oudda, M. I. Khan, *J. Mol. Liq*. **2018**, *266*, 603.
[27] C. Cao, *Corros. Sci*. **1996**, *38*.
[28] P. E. Alvarez, M. V. Fiori-Bimbi, A. Neske, S. A. Brandán, C. A. Gervasi, *J. Ind. Eng. Chem*. **2018**, *58*, 92.
[29] M. Kissi, M. Bouklah, B. Hammouti, M. Benkaddour, *Appl. Surf. Sci*. **2006**, *252*, 4190.
[30] O. Kaczerewska, R. Leiva-Garcia, R. Akid, B. Brycki, *J. Mol. Liq*. **2017**, *247*, 6.
[31] C. Kamal, M. G. Sethuraman, *Mater. Corros*. **2014**, *65*, 846.
[32] M. Meeusen, P. Visser, L. Fernández Macía, A. Hubin, H. Terryn, J. M. C. Mol, *Electrochim. Acta* **2018**, *278*, 363.
[33] L. Feng, S. Zhang, Y. Qiang, S. Xu, B. Tan, S. Chen, *Mater. Chem. Phys*. **2018**, *215*, 229.
[34] E. Ituen, O. Akaranta, A. James, *J. Mol. Liq*. **2016**, *224*, 408.
[35] W. Li, L. Hu, Z. Tao, H. Tian, B. Hou, *Mater. Corros*. **2011**, *62*, 1042.
[36] K. Azzaoui, E. Mejdoubi, S. Jodeh, A. Lamhamdi, E. Rodriguez-Castellón, M. Algarra, A. Zarrouk, A. Errich, R. Salghi, H. Lgaz, *Corros. Sci*. **2017**, *129*, 70.
[37] G. Salinas-Solano, J. Porcayo-Calderon, L. M. Martinez de la Escalera, J. Canto, M. Casales-Diaz, O. Sotelo-Mazon, J. Henao, L. Martinez-Gomez, *Ind. Crops Prod*. **2018**, *119*, 111.
[38] B. Hamza, C. Abdelouahad, D. Mounir, R. Youssouf, T. Hicham, *Anti-Corros. Methods Mater*. **2017**, *64*, 409.
[39] M. Solomon, S. Umoren, A. Israel, I. Etim, *Pigm. Resin Technol*. **2016**, *45*, 280.
[40] P. Singh, V. Srivastava, M. A. Quraishi, *J. Mol. Liq*. **2016**, *216*, 164.
[41] Z. Tao, S. Zhang, W. Li, B. Hou, *Mater. Corros*. **2010**, *61*, 877.

[42] A. M. Fekry, R. R. Mohamed, *Electrochim. Acta* **2010**, *55*.
[43] H. Hassannejad, A. Nouri, *J. Mol. Liq*. **2018**, *254*, 377.
[44] D. P. Schweinsberg, V. Ashworth, *Corros. Sci*. **1988**, *28*, 539.
[45] G. Banerjee, S. N. Malhotra, *Corrosion* **1992**, *48*, 10.
[46] X. Li, S. Deng, H. Fu, *Corros. Sci*. **2009**, *51*, 1344.
[47] P. Muthukrishnan, B. Jeyaprabha, P. Prakash, *Arab. J. Chem*. **2017**, *10*, S2343.
[48] K. Boumhara, M. Tabyaoui, C. Jama, F. Bentiss, *J. Ind. Eng. Chem*. **2015**, *29*, 146.

**How to cite this article:** Taoui H, Bentrah H, Chala A, Djellab M. Bark resin of *Schinus molle* as an eco-friendly inhibitor for API 5L X70 pipeline steel in HCl medium. *Materials and Corrosion*. 2018;1–10. https://doi.org/10.1002/maco.201810477

Received: 19 January 2020 | Accepted: 4 February 2020

DOI: 10.1002/maco.202011533

ARTICLE

Materials and Corrosion

# Synergistic effect of iodide ions and bark resin of *Schinus molle* for the corrosion inhibition of API5L X70 pipeline steel in $H_2SO_4$

**Mounir Djellab**[1,2] | **Hamza Bentrah**[1,2] | **Abdelouahad Chala**[2,3] | **Hicham Taoui**[1,2] | **Slimane Kherief**[1,2] | **Bouzid Bouamra**[2,3]

[1]Laboratory of Metallurgy, Department of Mechanical Engineering, Faculty of Science and Technology, Mohamed Khider University of Biskra, Biskra, Algeria

[2]Laboratoire de Physique des Couches Minces et Applications, Mohamed Khider University of Biskra, Biskra, Algeria

[3]Department of Materials Science, Mohamed Khider University of Biskra, Biskra, Algeria

**Correspondence**
Mounir Djellab, Laboratoire de Physique des Couches Minces et Applications, Mohamed Khider University of Biskra, B.P. 145, Biskra R.P. 07000, Algeria.
Email: mounircorrsci@gmail.com

**Funding information**
General Directorate of Scientific Research and Technological Development, Algeria

**Abstract**

The synergistic effect of bark resin of *Schinus molle* (BRSM) and iodide ions in 0.5 M sulfuric acid has been studied for the first time by potentiodynamic polarization and electrochemical impedance spectroscopy measurements; also, the surface morphology has been analyzed by scanning electron microscopy–energy-dispersive X-ray spectroscopic analysis in the present work. The results show that the BRSM and iodide ions have an evident synergistic inhibition effect in a 0.5-M sulfuric acid solution. The adsorption of the BRSM/iodide ion system follows the Langmuir adsorption isotherm and acts as a mixed-type inhibitor in sulfuric acid. The BRSM/iodide ion system is an effective inhibitor for API5L X70 pipeline steel in the 0.5-M sulfuric acid solution. The maximum percentage inhibition efficiency is equal to 99% at 1 g/L BRSM + 2 mM KI.

**KEYWORDS**

bark resin of *Schinus molle*, carbon steel, corrosion inhibition, eco-friendly inhibitor, EIS, iodide ion, sulfuric acid, synergistic effect

## 1 | INTRODUCTION

Due to its relatively high strength, low cost, and widespread availability, large infrastructure items such as storage tanks and pipelines use mild steel.[1] However, low resistance of carbon steel to acid corrosion has been the major hurdle in its applications, and there remains a need to prolong the lifetimes of steel items. Among the various approaches employed to minimize steel corrosion in an acidic environment, the usage of inorganic/organic inhibitors is well-established and the cheapest method.[2,3] Corrosion inhibitors can be incorporated into paint coatings or added to water tanks, pipelines, and so forth. Generally, inhibitors form passive or almost impermeable films on the metal surface to reduce the rate of corrosion.[1]

Over the past few decades, chromates were the most commonly used inhibitive pigments. However, the adversely affecting chemicals and the recent increase in environmental awareness have geared the research activities toward the development of nontoxic, cheap, environment-friendly, and biodegradable substances as inhibitors.[4,5] These prerequisites are fulfilled by the natural polymers that efficiently protect metals in diverse degrading environments. A few natural polymers, which have been studied as green and eco-friendly inhibitors for carbon steel corrosion in acid solutions in the recent past, include guar gum,[6] gum arabic,[7–9] carboxymethyl cellulose,[10–12] pectin,[13,14] xanthan gum,[15–17] Boswellia Serrata gum,[18] fenugreek gum,[19] tragacanth gum,[2] starch,[20,21] and chitosan.[22–24]

  

On the contrary, the inhibition efficiency of corrosion inhibitors can be synergistically improved by the addition of halide ions in the corrosive medium. Recently, several scientific studies have been taken into account to clarify the role of synergism on the mechanism of corrosion inhibition of steel in sulfuric acid.[25,26]

This synergism has been reported to be due to the increased surface coverage as a result of ion-pair interactions between an organic cation and the halide anion. The halide ion present in an inhibiting solution first adsorbs on the corroding surface by creating oriented dipoles, and thus, it facilitates the adsorption of inhibitor cations on the dipoles.[27–29] In the literature, the inhibitive effects of halides have been reported to be in the order: $I^- > Br^- > Cl^-$.[25,30,31] The highest synergistic effect of iodide ions is reported to be due to chemisorption with the metal surface due to its larger size and ease of polarizability.[32,33]

The aim of this investigation is to assess the improvement of corrosion inhibition of bark resin of *Schinus molle* (BRSM), in a synergistic manner with iodide ions, for API5L X70 pipeline steel in 0.5 M sulfuric acid at 20°C using electrochemical measurements, and surface analyses to clarify its inhibition mechanism. The main components of BRSM are germacrene-D, terebinthene, isomasticadienoic acid, isomasticadienonalic acid, and pinicolic acid.[34,35] The structure of BRSM is as shown in Figure 1.[35]

## 2 | EXPERIMENTAL

### 2.1 | Material

API5L X70 pipeline steel was used as a working electrode in this investigation. The samples (API5L X70 pipeline steel), for electrochemical experiments, were cut as cylinders with diameter of 1.4 cm, with the following chemical composition (weight percentage): C 0.12 max, Mn 1.68 max., Si 0.27 min., P 0.012 max., S 0.005 max., Cr 0.051 max., Ni 0.04 max., Nb 0.033 max., Ti 0.03 max., and the balance Fe. The surface area of each electrode exposed to the electrolyte was 0.785 $cm^2$. The exposed surface of each sample was prepared by wet grinding with silicon carbide-abrasive papers (grade 320–500–600–800), rinsed with distilled water, and degreased with acetone.

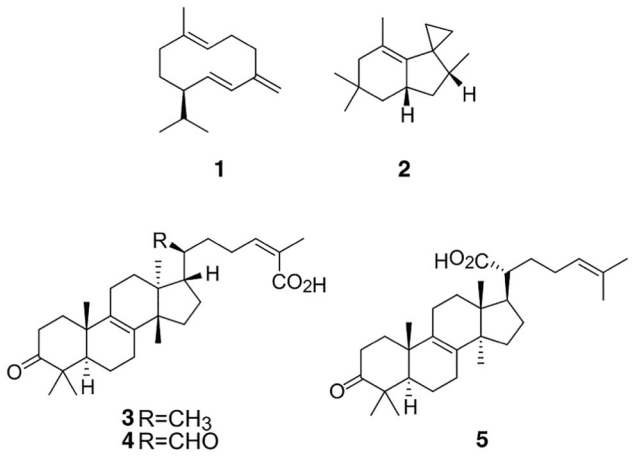


**FIGURE 1** The molecular structure of bark resin of *Schinus molle*: germacrene-D (1), terebinthene (2), isomasticadienoic acid (3), isomasticadienonalic acid (4), and pinicolic acid (5)

### 2.2 | Medium

The concentration of the corrosive medium was 0.5 M sulfuric acid prepared from analytical reagent grade 95% sulfuric acid. All preparations were made using distilled water.

### 2.3 | Inhibitor

The BRSM was collected from trees at Biskra (southeast Algeria), in April 2019. The species was identified as *Schinus molle* L., Anacardiaceae, The dried BRSM powder was selected for the present study and used as corrosion inhibitor.

### 2.4 | Electrochemical techniques

Two electrochemical techniques, namely, potentiodynamic polarization (PDP) and electrochemical impedance spectroscopy (EIS), were used to study the inhibition effect of the BRSM and BRSM/iodide ion system for API5L X70 steel in 0.5 M sulfuric acid at 20°C.

All experiments were performed in a one-compartment cell with three electrodes connected to a Gamry Instruments Potentiostat/Galvanostat/ZRA (Reference 3000) with Gamry Instruments Framework (version 7.05) commercial software.

The Gamry applications included software DC105 for corrosion, EIS300 for EIS measurements, and Echem Analyst 7.05 software package for data fitting.

The working electrode was carbon steel with an exposed surface area in the corrosive environment of 0.785 $cm^2$. A graphite block was used as the counter electrode, and a standard Ag/AgCl electrode (the potential of the Ag/AgCl electrode is the same as the saturated calomel electrode and equal to 240 mV vs. NHE) was used as the reference electrode.

All electrochemical experiments of the API5L X70 steel were carried out in 0.5 M sulfuric acid medium without

(blank) and with inhibitor (BRSM or BRSM/iodide ion system) after 30 min of immersion at 20°C. Three replicate samples were used for each test condition.

Tafel curves were obtained by changing the electrode potential automatically from −0.25 to +0.25 V versus open-circuit potential at a scan rate of 0.5 mV/s.

The linear Tafel segments of the anodic and cathodic curves were extrapolated to corrosion potential to obtain the corrosion current densities ($I_{corr}$). Due to the presence of a degree of nonlinearity in the Tafel slope part of the obtained polarization curves, the Tafel constants were calculated as a slope of the points after ($E_{corr}$) by ±80 mV. The values of inhibition efficiency ($\eta_{pol}$) were calculated using the following equation:

$$\eta_{pol}\% = \frac{I_{corr} - I_{corr\,(inh)}}{I_{corr}} \times 100, \quad (1)$$

where $I_{corr}$ and $I_{corr(inh)}$ represent corrosion current density values without and with inhibitor, respectively.

EIS measurements were performed under potentiostatic conditions over a frequency range from 20 kHz to 50 MHz, with an amplitude of 10 mV peak-to-peak. Inhibition efficiency values ($\eta_{EIS}$) from the EIS data were computed by comparing the values of the charge transfer resistance in the absence and presence of BRSM or BRSM/iodide ion system as follows:

$$\eta_{EIS}\% = \frac{R_t - \acute{R}_t}{R_t} \times 100, \quad (2)$$

where $\acute{R}_t$ is charge transfer resistance value in 0.5 M sulfuric acid, and $R_t$ is the charge transfer resistance value in the presence of the BRSM or BRSM/iodide ion system.

## 2.5 | Surface analysis

Morphological studies of the API5L X70 carbon steel electrode surface were undertaken using scanning electron microscopy (SEM) and energy-dispersive X-ray spectroscopic analysis (EDX) examinations of electrode surfaces exposed to different test solutions using a TESCAN VEGA3 scanning electron microscope. API5L X70 carbon steel specimens with dimensions of 1 × 1 × 1 cm were abraded successively with silicon carbide paper of different grades (320–500–600–800) and thereafter using a cloth with 3-μm diamond paste to a near-mirror finished surface. The cleaned coupons were immersed for 72 hr in 0.5 M sulfuric acid without (blank) and with inhibitor (BRSM or BRSM/iodide ion system) at 20°C and then rinsed with distilled water, dried in warm air, and submitted for SEM–EDX surface examination.

# 3 | RESULTS AND DISCUSSION

## 3.1 | Inhibition effect of BRSM

### 3.1.1 | Electrochemical impedance spectroscopy measurements

The corrosion behavior of API5L X70 pipeline steel in 0.5 M sulfuric acid at 20°C, without and with different concentrations of BRSM, was investigated using electrochemical impedance spectroscopy. EIS plots of API5L X70 pipeline steel in uninhibited and inhibited acidic solutions containing various concentrations of BRSM are given in Figure 2 in (a) Nyquist, (b) Bode modulus, and (c) Bode phase angle. The electrochemical parameters calculated from the Nyquist plots are given in Table 1. Inspection of the plots revealed that the shape of Nyquist plots contains depressed semicircles with their center located under the real axis, and their size increases with inhibitor concentration, indicating a charge transfer process, mainly controlling the corrosion of carbon steel.[36,37] Such a behavior is typical of solid electrodes and often referred to as frequency dispersion, attributed to the surface heterogeneity due to surface roughness, impurities, or dislocations,[38,39] fractal structures, distribution of activity centers, adsorption of inhibitors, and formation of porous layers.[40–42]

From Figure 2a, all spectra obtained are similar in shape and consist of a large capacitive loop at high frequencies (HF) and an inductive loop at low frequencies (LF) both in the absence and in presence of inhibitor. The presence of two-time constants for iron dissolution at $E_{corr}$ in the absence of inhibitors has been reported in the literature.[43,44] The HF capacitive loop could be attributed to the double-layer capacity in parallel with $R_t$. The LF inductive loop may originate from the relaxation process obtained by adsorption species as $H^+_{ads}$ and $SO^{2-}_4$ on the surface of the metal. It may also be attributed to the re-dissolution of the passivated surface at low frequencies.[45]

The Bode and phase-angle plots for API5L X70 pipeline steel in 0.5 M sulfuric acid at 20°C with and without inhibitor are given in Figure 2. From Figure 2b, the increase of impedance plots at low frequencies in Bode plots confirms an increase in the inhibition efficiency with increasing the concentration of inhibitor, which is related to the adsorption of BRSM compounds on the API5L X70 steel surface in 0.5 M sulfuric acid.[46,47] According to the appearance of phase-angle

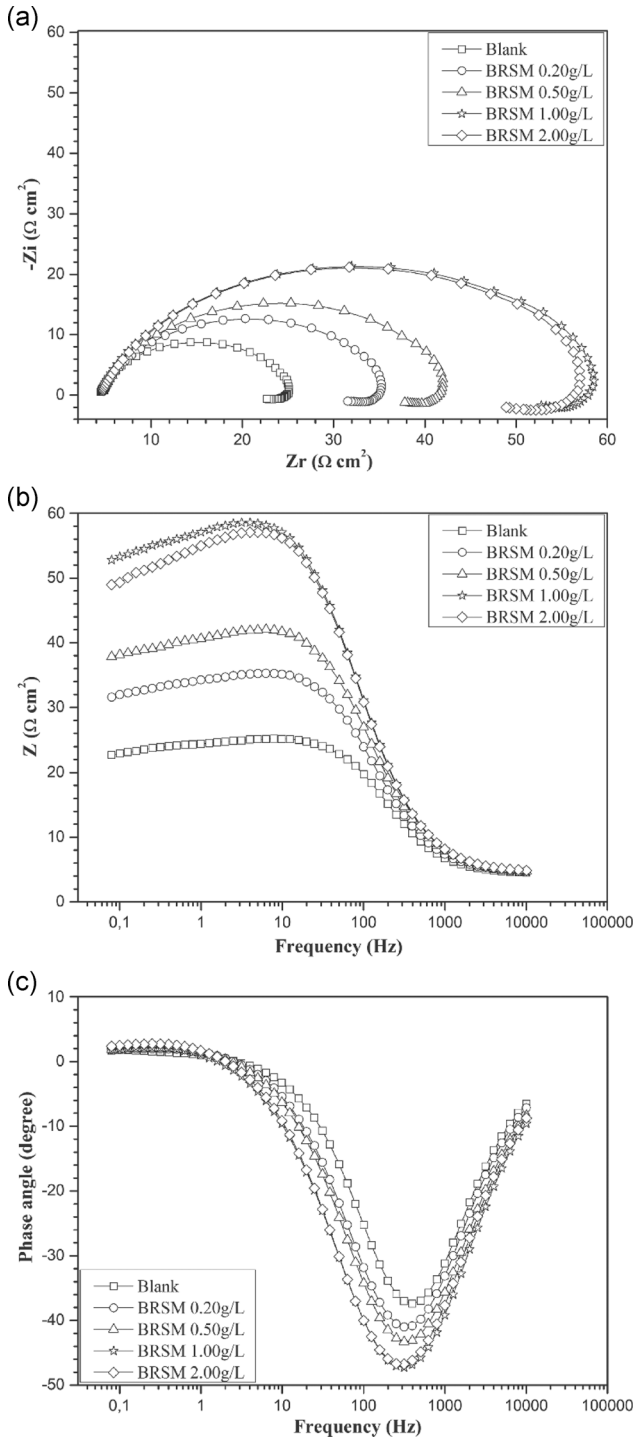


**FIGURE 2** Electrochemical impedance spectroscopy plots for API5L X70 pipeline steel in 0.5 M $H_2SO_4$ without and with different concentrations of bark resin of *Schinus molle* at 20°C, (a) Nyquist, (b) Bode, and (c) phase-angle representations

plots (Figure 2c), increasing the concentration of the inhibitor indicated an increasing trend in inhibitive behavior due to adsorption of the metal surface of more inhibitor molecules at higher concentrations. Furthermore, the depression of phase angle at the relaxation frequency occurs with decreasing of inhibitor concentration, which indicated the decrease of capacitive response with the decrease of inhibitor concentration. Such a phenomenon could be attributed to higher corrosion activity at low concentrations of inhibitors.[48,49]

The obtained impedance data were fitted to the electrical equivalent circuit diagram given in Figure 3a to model the pipeline steel/solution interface in the absence and presence of the inhibitor. The circuit consists of the solution resistance $R_s$, the charge transfer resistance $R_t$, the constant phase element (CPE), the inductive elements, $R_L$ and $L$.[50] The use of a CPE is required for modeling the frequency dispersion generally related to the surface heterogeneity.[48,51]

An excellent fit with this model was obtained for all experimental data. As an example, the Nyquist and Bode plots of both experimental and simulated data of pipeline steel in 0.5 M sulfuric acid containing 1 g/L of BRSM are shown in Figure 3b,c. It is clear that the measured impedance plot is in accordance with that calculated by the used equivalent circuit model. This means that the equivalent circuit model suggested in Figure 3a could reasonably represent the charge transfer and metal/solution interface features related to the corrosion process of API5L X70 pipeline steel in 0.5-M sulfuric acid solution containing different concentrations of BRSM. The impedance function of the CPE is described as follows[52]:

$$Z_{CPE} = Y_0^{-1}(j\omega)^{-n}, \tag{3}$$

where $Y_0$ is the magnitude of the CPE, $\omega$ is the angular frequency, $j$ is the imaginary root, and $n$ is the deviation parameter relating to the phase shift representing the microscopic fluctuation of the metal surface. The CPE can display an inductor ($n = -1$), resistor ($n = 0$), capacitor ($n = 1$), or Warburg impedance ($n = 0.5$). The use of CPE rather than a pure capacitor resulted in the non-ideal dielectric of the inhomogeneous electrode surface.[53,54] The double-layer capacitance ($C_{dl}$) was calculated using the following equation[55]:

$$C_{dl} = Y_0(2\pi f_{max})^{n-1}, \tag{4}$$

where $f_{max}$ is the frequency at which the imaginary component of the impedance is maximum.

The Nyquist plots are significantly changed after addition of inhibitor and the impedance of the inhibited system increased with inhibitor concentration (Figure 2a). On increasing the inhibitor concentration, the $R_{ct}$ value increased and the inhibiting power was higher (Table 1). The maximum inhibitive effect and the highest charge transfer resistance have been found at a BRSM concentration of 1.0 g/L. A high-charge transfer resistance is associated with a slower corroding system. On the contrary,

**TABLE 1** Electrochemical impedance parameters for API5L X70 in 0.5 M $H_2SO_4$ solution in the absence and the presence of bark resin of *Schinus molle* at 20°C

| System/concentration | $R_s$ ($\Omega$ cm$^2$) | $Y_0$ ($\mu\Omega \cdot S^n \cdot cm^{-2}$) | $n$ | $R_t$ ($\Omega$ cm$^2$) | $L$ (H cm$^2$) | $R_L$ ($\Omega$ cm$^2$) | $C_{dl}$ ($\mu$F/cm$^2$) | $\eta_{EIS}$ (%) |
|---|---|---|---|---|---|---|---|---|
| Blank | 4.44 | 230.10 | 0.88 | 20.96 | 45.19 | 182.80 | 100.51 | – |
| 0.20 g/L | 4.66 | 120.40 | 0.86 | 31.00 | 45.00 | 244.00 | 48.82 | 32 |
| 0.50 g/L | 4.62 | 116.70 | 0.85 | 38.00 | 47.00 | 280.00 | 45.92 | 45 |
| 1.00 g/L | 4.40 | 105.90 | 0.85 | 56.00 | 47.00 | 283.10 | 43.14 | 63 |
| 2.00 g/L | 4.65 | 105.20 | 0.84 | 55.97 | 45.00 | 290.00 | 40.37 | 63 |

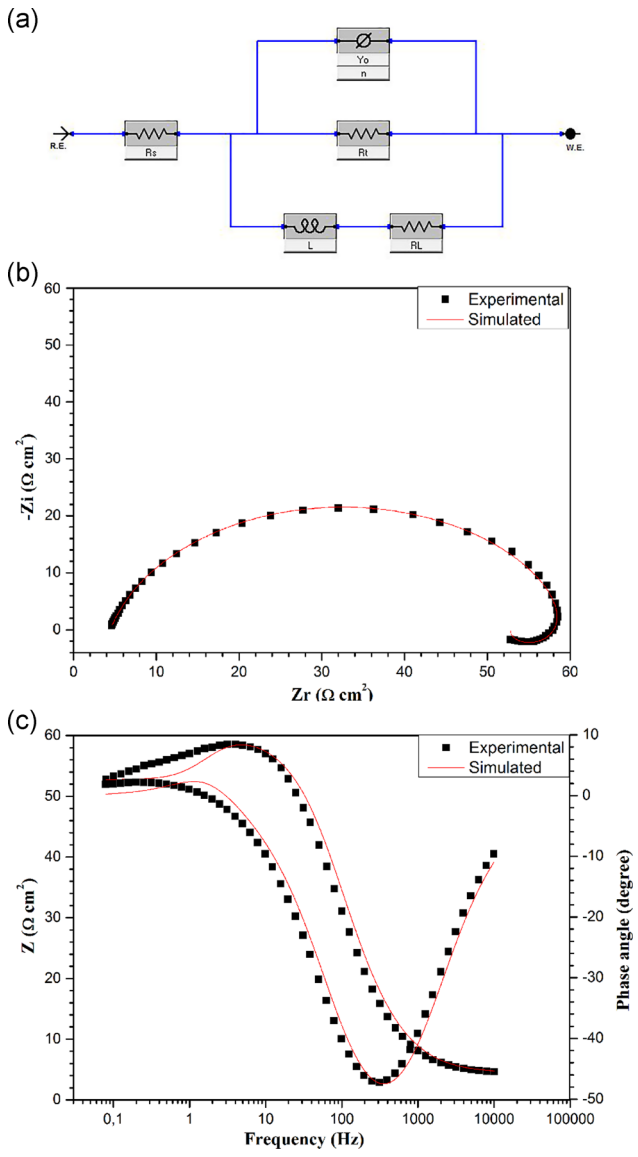


**FIGURE 3** (a) Equivalent circuit used to fit the impedance data, together with the (b) Nyquist, and (c) Bode plots of experimental data and simulated data, recorded for API5L X70 pipeline steel in 0.5 M $H_2SO_4$ containing 1.0 g/L bark resin of *Schinus molle* [Color figure can be viewed at wileyonlinelibrary.com]

when increasing the concentration of the BRSM compounds, $C_{dl}$ values tend to decrease and the inhibition efficiency increases (Table 1). The decrease in $C_{dl}$ values, resulting from local dielectric constant decrease and/or from the increase of the thickness of the electrical double layer, suggests that these molecules act via adsorption at the metal/solution interface.[56,57]

These observations clearly bring out that (a) the corrosion of pipeline steel in 0.5 M sulfuric acid is controlled by a charge transfer process and (b) the corrosion inhibition occurs through the adsorption of the compounds on the steel surface. Their values of inhibition efficiency given in Table 1 show that inhibition efficiency increases with an increase in the concentration of BRSM with the highest value of 63% obtained at BRSM concentration of 1.0 g/L.

### 3.1.2 | PDP measurements

Figure 4 shows the polarization curves for API5L X70 pipeline steel in 0.5-M sulfuric acid solution in the absence and presence of various concentrations of BRSM. It is clear that the presence of BRSM causes a marked decrease in the corrosion rate, that is, it bodily shifts both the cathodic and anodic curves to lower currents but with different extents. This implies that both the hydrogen evolution and anodic iron dissolution reactions of API5L X70 pipeline steel corrosion are inhibited. This may be ascribed to adsorption of BRSM over the corroding surface. The displacement in $E_{corr}$ ($\Delta E_{corr}$) between in the absence and presence of the inhibitor, were less than 85 mV. Therefore, the inhibitor was defined as a mixed-type.[53,58] Table 2 lists important corrosion parameters such as the free-corrosion potential ($E_{corr}$), corrosion current density ($I_{corr}$), the slope of the cathodic branch ($b_c$), and slope of the anodic branch ($b_a$).

The results indicate the cathodic Tafel slope ($b_c$) for pipeline steel in the absence and presence of inhibitor does not change significantly indicating that the BRSM does not change the mechanism of the hydrogen

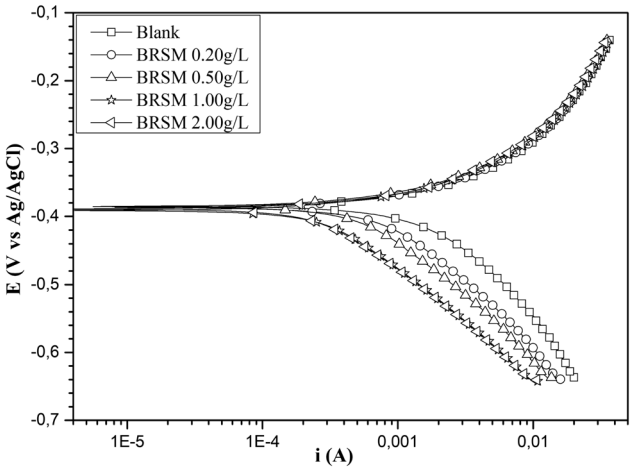


**FIGURE 4** Polarization curves for API5L X70 in 0.5-M $H_2SO_4$ solution without and with different concentrations of bark resin of *Schinus molle* (BRSM) at 20°C

evolution reaction, and the corrosion is rather inhibited by blocking of the iron surface by simple adsorption process.[26,59] It is clear that inhibition efficiency increases with an increase in the concentration of the inhibitor with the highest value of 62% obtained at BRSM concentration of 1.0 g/L. Good agreement with electrochemical impedance spectroscopy is obtained.

### 3.1.3 | Adsorption isotherm and standard adsorption free energy

In the present study, several adsorption isotherms were assessed, and the Langmuir adsorption isotherm was found to give the best description of the adsorption behavior of the studied inhibitor (Figure 5). A correlation between surface coverage ($\theta = \eta_{EIS}\%/100$) and the concentration of inhibitor ($C$) in the electrolyte can be represented by the Langmuir adsorption isotherm.[60]

$$\frac{C}{\theta} = \frac{1}{K_{ads}} + C, \tag{5}$$

where $K_{ads}$ is the constant of adsorption. Plots of $C/\theta$ with $C$ at 20°C yield a straight line with slope values close to 1. From the values of the adsorption constant, $K_{ads}$, the standard free energy of adsorption $\Delta G^{o}_{ads}$ is determined using the following equation[61–63]:

$$\Delta G^{o}_{ads} = -RT \ln(1 \times 10^{6} K_{ads}), \tag{6}$$

where $1 \times 10^{6}$ is the concentration of water molecules expressed in mg/L, $R$ is the universal gas constant and $T$ is the absolute temperature. The values of $\Delta G^{o}_{ads}$ and $K_{ads}$ are listed in Table 3. The $K_{ads}$ value may be taken as a measure of the strength of the adsorption forces between the inhibitor molecules and the metal surface.[35] Generally, values of $\Delta G^{o}_{ads}$ up to −20 kJ/mol are consistent with electrostatic interaction between charged molecules and a charged metal (which indicates physical adsorption), whereas those more negative than −40 kJ/mol involves charge sharing or transfer from the inhibitor components to the metal surface to form a coordinate type of bond (which indicates chemisorption).[64,65] In the present study, the value of $\Delta G^{o}_{ads} = -19.63$ kJ/mol indicates that the adsorption of BRSM on API5L X70 pipeline steel surface involves physical adsorption.

## 3.2 | Inhibition of iodide ions

Figure 6 shows the polarization curves of API5L X70 pipeline steel immersed in 0.5-M sulfuric acid solution in the absence and presence of different concentrations of KI at 20°C. The addition of KI decreases sharply the rates of the evolution of hydrogen and the dissolution of the pipeline steel in the 0.5-M sulfuric acid solution. By comparing the polarization curves in the absence and presence of various concentrations of KI, it is observed that an increase in the KI concentration shifts slightly the corrosion potential ($E_{corr}$) in the positive direction and reduced both anodic and cathodic current densities. In addition, the results in Table 4 reveal that the

**TABLE 2** Potentiodynamic polarization parameters for API5L X70 in 0.5-M $H_2SO_4$ solution in the absence and the presence of bark resin of *Schinus molle* at 20°C

| System/Concentration | $E_{corr}$ (mV) | $I_{corr}$ (μA) | $-b_c$ (mV/dec) | $b_a$ (mV/dec) | $\eta_{pol}$ (%) |
|---|---|---|---|---|---|
| Blank | −383.01 | 1,572.68 | 199.20 | 109.80 | – |
| 0.20 g/L | −386.41 | 1,115.73 | 217.70 | 94.80 | 29 |
| 0.50 g/L | −386.63 | 907.65 | 217.70 | 92.20 | 42 |
| 1.00 g/L | −404.72 | 600.57 | 197.20 | 90.80 | 62 |
| 2.00 g/L | −403.62 | 595.66 | 196.88 | 89.98 | 62 |

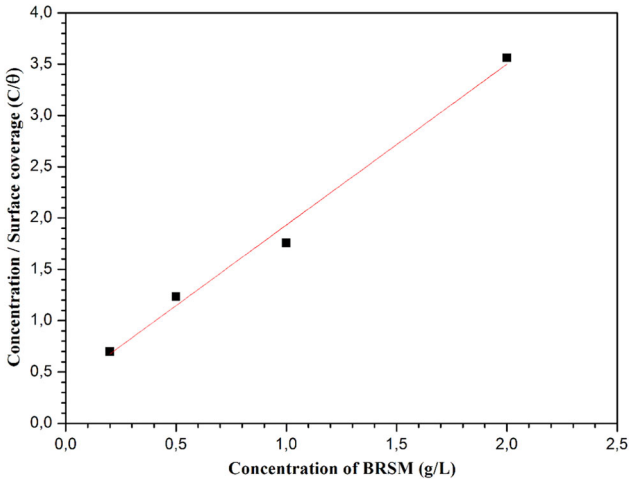


**FIGURE 5** Langmuir adsorption isotherm for bark resin of *Schinus molle* (BRSM) on API5L X70 in 0.5-M $H_2SO_4$ solution at 20°C [Color figure can be viewed at wileyonlinelibrary.com]

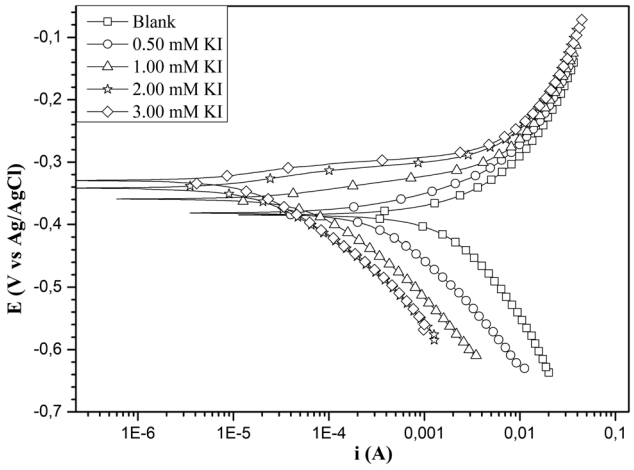


**FIGURE 6** Polarization curves for API5L X70 in 0.5-M $H_2SO_4$ solution without and with different concentrations of KI at 20°C

presence of KI in the 0.5-M sulfuric acid solution inhibits significantly both the anodic and cathodic processes.

Figure 7 presents the impedance response of API5L X70 pipeline steel in 0.5-M sulfuric acid solution with and without different concentrations of KI. The obtained electrochemical parameters are listed in Table 5. As can be seen from Figure 7 and Table 5, the charge transfer resistance increased with increasing the concentrations of KI and the protection efficiency was also improved simultaneously. The bigger semicircle of 2 mM KI in Figure 7 shows that a higher concentration of KI has better corrosion inhibition. The resistance and protection efficiency values can reach upto 1,080 $\Omega\,cm^2$ and 98%, respectively, when mild steel was immersed in 0.5-M sulfuric acid solution in the presence of 2 mM KI, indicating excellent inhibition effect.

## 3.3 | Synergistic effect of BRSM with iodide ions

### 3.3.1 | Electrochemistry measurements

Figure 8 shows the polarization curves of API5L X70 pipeline steel immersed in 0.5-M sulfuric acid solution containing various concentrations of BRSM in the presence of 2 mM KI. The calculated electrochemical parameters are listed in Table 6. As can be seen from Figure 8 and Table 6, the corrosion current density decreases sharply and corrosion potential shifts to a more positive direction after the addition of KI, whereas the inhibition efficiency enhances greatly after the addition of KI, which suggests that the adsorption protective layer tends to be more complete and stable on the electrode surface than BRSM alone in 0.5-M sulfuric acid solution.

The investigated BRSM/iodide ion system can be classified into the anodic, cathodic or mixed type of inhibitors depending upon the shift in the $E_{corr}$ values of inhibited metallic specimens with respect to the $E_{corr}$ values of the uninhibited metallic specimen. The BRSM/iodide ion system showed the maximum variation in the values of $E_{corr}$ of 62 mV. Less than 85 mV shift in the values of $E_{corr}$ suggests that the BRSM/iodide ion system acts as a mixed-type corrosion inhibitor. In addition, the BRSM/iodide ion system causes a significant decrease in the rate of both anodic metallic dissolution and cathodic hydrogen evaluation processes.

EIS measurements were undertaken using a fixed concentration of KI (2.0 mM) combined with different concentrations of BRSM (0.2, 0.5, and 1.0 g/L), for assessing the synergistic effect of the BRSM/iodide ion system on the corrosion inhibition of API5L X70 pipeline steel in 0.5 M sulfuric acid at 20°C. Figure 9 shows the Nyquist plots of pipeline steel in 0.5 M sulfuric acid solution at 20°C containing the BRSM/iodide ion system. The results clearly show a distinct synergistic effect of the BRSM/iodide ion system on the corrosion behavior of pipeline steel compared to the blank acid solution in the absence and the presence of BRSM alone.

**TABLE 3** Parameters of Langmuir adsorption isotherm for API5L X70 in 0.5-M $H_2SO_4$ solution containing bark resin of *Schinus molle* at 20°C

| Isotherm mode | Linear correlation coefficient | Slope | $K_{ads}$ (L/g) | $\Delta G^{\circ}_{ads}$ (kJ/mol) |
|---|---|---|---|---|
| Langmuir | 0.99541 | 1 | 2.75 | −19.63 |

**TABLE 4** Potentiodynamic polarization parameters for API5L X70 in 0.5-M $H_2SO_4$ solution in the absence and the presence of KI at 20°C

| System/Concentration | $E_{corr}$ (mV) | $I_{corr}$ (μA) | $-b_c$ (mV/dec) | $b_a$ (mV/dec) | $\eta_{pol}$ (%) |
|---|---|---|---|---|---|
| Blank | −383.01 | 1,572.68 | 199.20 | 109.80 | – |
| 0.50 mM | −388.43 | 531.15 | 185.3 | 82.1 | 66 |
| 1.00 mM | −365.11 | 188.39 | 172.2 | 42.72 | 88 |
| 2.00 mM | −357.94 | 90.68 | 166.8 | 36.15 | 94 |
| 3.00 mM | −328.09 | 88.84 | 148.66 | 34.27 | 94 |

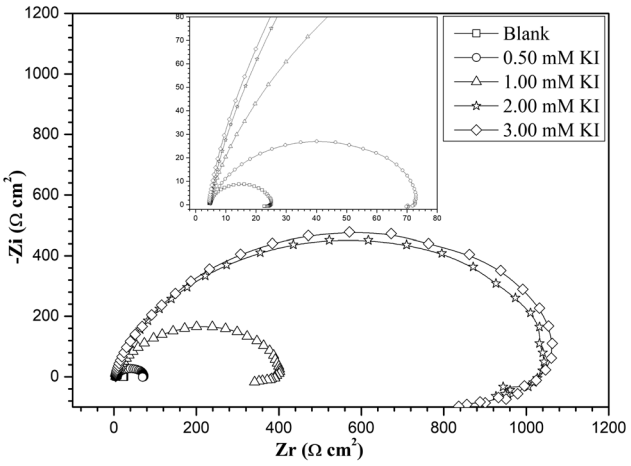


**FIGURE 7** Electrochemical impedance spectroscopy plots for API5L X70 in 0.5 M $H_2SO_4$ solution without and with different concentrations of KI at 20°C

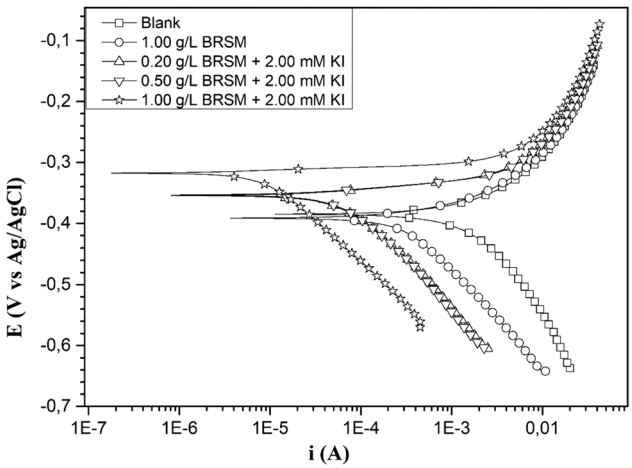


**FIGURE 8** Polarization curves for API5L X70 in 0.5-M $H_2SO_4$ solution containing 1.0 g/L bark resin of *Schinus molle* (BRSM) and BRSM/iodide ion system at 20°C

In comparison with the BRSM alone, the diameters of the semicircles in Nyquist plot (Figure 9) increase after the addition of different concentrations of BRSM in 0.5 M sulfuric acid containing 2.0 mM KI, yielding higher values of $R_t$ than that observed with BRSM alone in 0.5 M sulfuric acid.

Examination of Figure 9 (Nyquist plot) also revealed that the complex plane impedance consists of one capacitive loop at high frequencies and one inductive loop at low-frequency values (that is, two-time constants) for the curves obtained in the presence of the BRSM/iodide ion system. The equivalent circuit shown in Figure 3a was used to fit the experimental data obtained from the impedance measurements, and the corresponding electrochemical parameters are listed in Table 7.

The results in the Table 7 show that addition of 2 mM KI to different concentrations of BRSM (0.2, 0.5, and 1.0 g/L) increased $R_t$ at a maximum value of 1,440.96 Ω $cm^2$ in the presence of the BRSM/iodide ion system (1 g/L BRSM + 2 mM KI), whereas $R_t$ value is 56 Ω $cm^2$ only in the presence of 1 g/L BRSM (Table 7). Also, $C_{dl}$ decreased from 43.14 μF/$cm^2$ for 1 g/L BRSM to

**TABLE 5** Electrochemical impedance parameters for API5L X70 in 0.5 M $H_2SO_4$ solution in the absence and the presence of KI at 20°C

| System/concentration | $R_s$ (Ω $cm^2$) | $Y_0$ (μΩ·$S^n$·$cm^{-2}$) | $n$ | $R_t$ (Ω $cm^2$) | $L$ (H $cm^2$) | $R_L$ (Ω $cm^2$) | $C_{dl}$ (μF/$cm^2$) | $\eta_{EIS}$ (%) |
|---|---|---|---|---|---|---|---|---|
| Blank | 4.44 | 230.10 | 0.88 | 20.96 | 45.19 | 182.80 | 100.51 | – |
| 0.50 mM | 4.83 | 119.30 | 0.83 | 70.00 | 100.00 | 648.70 | 44.85 | 70 |
| 1.00 mM | 4.49 | 49.87 | 0.85 | 422.00 | 748.00 | 2,722.00 | 24.96 | 95 |
| 2.00 mM | 4.54 | 33.93 | 0.88 | 1,080.00 | 4,481.00 | 5,649.00 | 21.22 | 98 |
| 3.00 mM | 4.20 | 30.00 | 0.90 | 1,098.00 | 4,977.00 | 5,680.00 | 20.76 | 98 |

**TABLE 6** Potentiodynamic polarization parameters for API5L X70 pipeline steel in 0.5 M $H_2SO_4$ at 20°C without and with bark resin of *Schinus molle* (BRSM) and BRSM/iodide ion system

| System/Concentration | $E_{corr}$ (mV) | $I_{corr}$ (μA) | $-b_c$ (mV/dec) | $b_a$ (mV/dec) | $\eta_{pol}$ % |
|---|---|---|---|---|---|
| Blank | −383.01 | 1,572.68 | 199.20 | 109.80 | – |
| 1.00 g/L BRSM | −404.72 | 600.57 | 197.20 | 90.80 | 62 |
| 0.20 g/L BRSM + 2.00 mM KI | −358.375 | 112.55 | 180.6 | 27.6 | 93 |
| 0.50 g/L BRSM + 2.00 mM KI | −358.434 | 77.38 | 184.2 | 26.3 | 95 |
| 1.00 g/L BRSM + 2 mM KI | −321.63 | 10.35 | 141.2 | 10.2 | 99 |

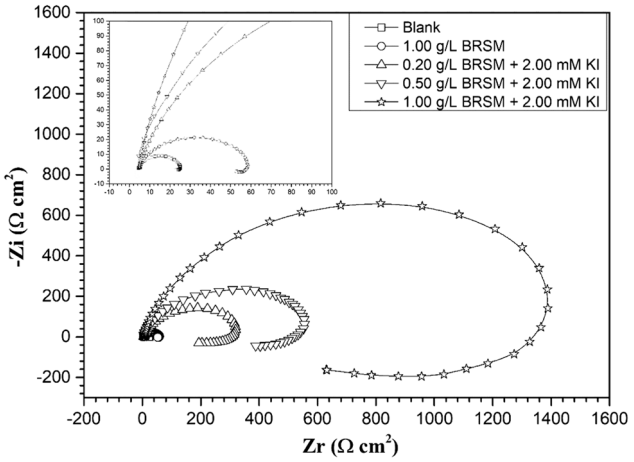


**FIGURE 9** Electrochemical impedance spectroscopy plots for API5L X70 in 0.5-M $H_2SO_4$ solution containing 1.0 g/L bark resin of *Schinus molle* (BRSM) and BRSM/iodide ion system at 20°C

15.30 μF/cm² in the presence of the BRSM/iodide ion system (1 g/L BRSM + 2 mM KI), and the inhibition efficiency values can reach 99%. It must be noted that the results obtained from polarization curves and impedance spectra follow the same trend and are in close agreement.

### 3.3.2 | Adsorption isotherm and standard adsorption free energy

With the objective of evaluating the mode of adsorption of the BRSM/KI system on API5L X70 pipeline steel in 0.5 M sulfuric acid, Langmuir, Temkin, and Frumkin adsorption isotherms were evaluated. According to Equation (5), the Langmuir isotherm is the best fitting for the data, as shown in Figure 10.

It is found that the slope is very close to 1 which indicates the adsorption of BRSM/iodide ion system inhibitor on the API5L X70 pipeline steel surface in 0.5 M sulfuric acid obeys the Langmuir adsorption isotherm. The value of $K_{ads}$ can be calculated from the intercept of straight lines $C/\theta$ with the $y$-axis and the $\Delta G^{o}_{ads}$ value was calculated using Equation (6). The linear regression parameters are listed in Table 8.

In the present study, the value of $\Delta G^{o}_{ads}$ (−26.85 kJ/mol) is found to be within the range of −40 to −20 kJ/mol; this probably means that the adsorption of BRSM/iodide ion system on API5L X70 pipeline steel surface involves both physical adsorption and chemical adsorption.

### 3.3.3 | Synergism parameter

Experimental results acquired in this study showed that the addition of iodide ions to the solution containing BRSM increases the inhibition efficiency and the degree of surface coverage. This behavior can be assigned to the synergistic effect between KI and BRSM. To confirm the veracity of the existence of the synergism phenomenon between KI and BRSM, the synergism parameter was evaluated using the equation initially proposed by

**TABLE 7** Electrochemical impedance (EIS) parameters for API5L X70 pipeline steel in 0.5 M $H_2SO_4$ at 20°C without and with bark resin of *Schinus molle* (BRSM) and BRSM/iodide ion system

| System/Concentration | $R_s$ (Ω cm²) | $Y_0$ (μΩ·S$^n$·cm$^{-2}$) | $n$ | $R_t$ (Ω cm²) | $L$ (H cm²) | $R_L$ (Ω cm²) | $C_{dl}$ (μF/cm²) | $\eta_{EIS}$ % |
|---|---|---|---|---|---|---|---|---|
| Blank | 4.44 | 230.10 | 0.88 | 20.96 | 45.19 | 182.80 | 100.51 | – |
| 1.00 g/L BRSM | 4.40 | 105.90 | 0.85 | 56.00 | 47.00 | 283.10 | 43.14 | 63 |
| 0.20 g/L BRSM + 2.00 mM KI | 4.73 | 46.07 | 0.87 | 320.90 | 392.60 | 610.80 | 25.29 | 93 |
| 0.50 g/L BRSM + 2.00 mM KI | 4.66 | 48.09 | 0.86 | 550.10 | 317.10 | 696.10 | 21.26 | 96 |
| 1.00 g/L BRSM + 2.00 mM KI | 4.50 | 22.94 | 0.89 | 1,440.96 | 820.00 | 2,576.00 | 15.30 | 99 |

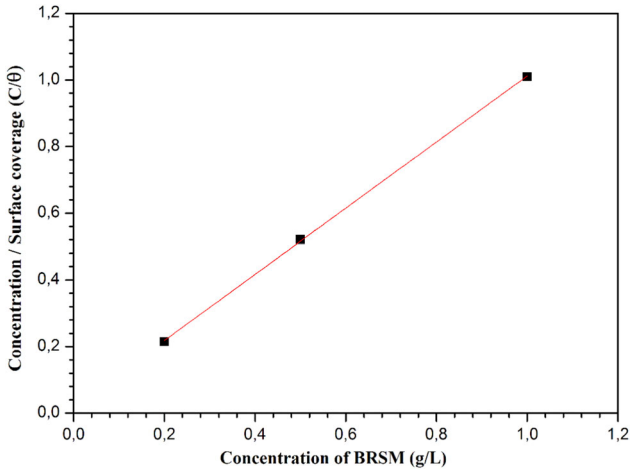


**FIGURE 10** Langmuir adsorption isotherm for API5L X70 in 0.5-M $H_2SO_4$ solution containing 2.0 mM KI combined with different concentrations of bark resin of *Schinus molle* (BRSM) [Color figure can be viewed at wileyonlinelibrary.com]

Aramaki and Hackermann in 1964 and used by some authors.[66–68]

$$S_1 = \frac{1 - I_{1+2}}{1 - \grave{I}_{1+2}}, \tag{7}$$

where $I_{1+2} = I_1 + I_2$, $I_1$ is the inhibition efficiency of the iodide ions, $I_2$ is the inhibition efficiency of BRSM, $\grave{I}_{1+2}$ is the measured inhibition efficiency for the BRSM in combination with the iodide ions. Given that BRSM and KI have no effect on each other and are adsorbed at the metal/solution interface independently, then, $S_1$ is equal to 1. Alternatively, synergistic effects manifest when $S_1 > 1$ and antagonistic effects prevail at $S_1 < 1$.[69,70] The calculated values of the synergism parameter are displayed in Table 9.

From Table 9, it is seen that the values of $S_1$ for all the concentrations of BRSM studied are greater than unity, which indicates that there is a true synergism between BRSM and KI in 0.5 M sulfuric acid.

There are three possible models for inhibitor adsorption with the aid of halide ions: (a) the adsorption of the halide ion which then attracts the inhibitor molecule to the metal; (b) exchange of adsorption site by halide ions and organic ions (competitive adsorption); and (c) co-adsorption of inhibitor and halide ions.[71,72] A combination of these models is also feasible. From the results obtained in this study, the observed synergistic effect may suggest that the first model is applicable. The KI is first adsorbed onto the metal surface and the BRSM molecules are then adsorbed onto the top of the already chemisorbed layer of KI, thus providing greater surface coverage and improved inhibition efficiency.

## 3.4 | SEM–EDX analysis

Figure 11 shows the SEM images and EDX spectra obtained for API5L X70 pipeline steel after immersion in 0.5 M sulfuric acid at 20°C for 72 hr in the absence and presence of 1.0 g/L BRSM and 1.0 g/L BRSM + 2.0 mM KI. The elemental composition (wt%) of the steel specimens in different test environments is given in Table 10. The pipeline steel surface before immersion is relatively smooth (Figure 11a) and shows an intense Fe peak in the EDX spectrum corresponding to 96.47 wt% (Table 10). Exposure of the pipeline steel surface to the 0.5-M sulfuric acid solution caused strong damage with general corrosion and severity of pitting in the absence of the BRSM inhibitor, as evident in Figure 11b. It is obvious from the EDX spectra in Figure 11b that the pipeline steel surface was hydrated with sulfate ions; the presence of an intense peak with 13.70 wt% (Table 10) supports this claim.

In the presence of 1.0 g/L BRSM (Figure 11c), the sample has a smooth surface compared with that of the samples immersed in 0.5 M sulfuric acid with some small pitting. Besides this, the wt% of Fe, which reduced from 96.47 to 51.48% on exposure to the corrosive environment, increased in the BRSM-inhibited solution to 63.17%, indicating the protection of pipeline steel offered by BRSM inhibitor.

**TABLE 8** Parameters of Langmuir adsorption isotherm for API5L X70 in 0.5-M $H_2SO_4$ solution containing 2.0 mM KI combined with different concentrations of bark resin of *Schinus molle*

| Isotherm mode | Linear correlation coefficient | Slope | $K_{ads}$ (L/g) | $\Delta G^{\circ}_{ads}$ (kJ/mol) |
|---|---|---|---|---|
| Langmuir | 0.99994 | 0.99225 | 50.71 | −26.85 |

**TABLE 9** Synergism parameters of API5L X70 pipeline steel in 0.5-M $H_2SO_4$ solution at 20°C

| | Synergism parameter ($S1$) | |
|---|---|---|
| System/Concentration | EIS method | PDP method |
| 0.20 g/L BRSM + 2.00 mM KI | 1.40 | 1.32 |
| 0.50 g/L BRSM + 2.00 mM KI | 1.50 | 1.43 |
| 1.00 g/L BRSM + 2.00 mM KI | 1.64 | 1.58 |

Abbreviations: BRSM, bark resin of *Schinus molle*; EIS, electrochemical impedance spectroscopy; PDP, potentiodynamic polarization.

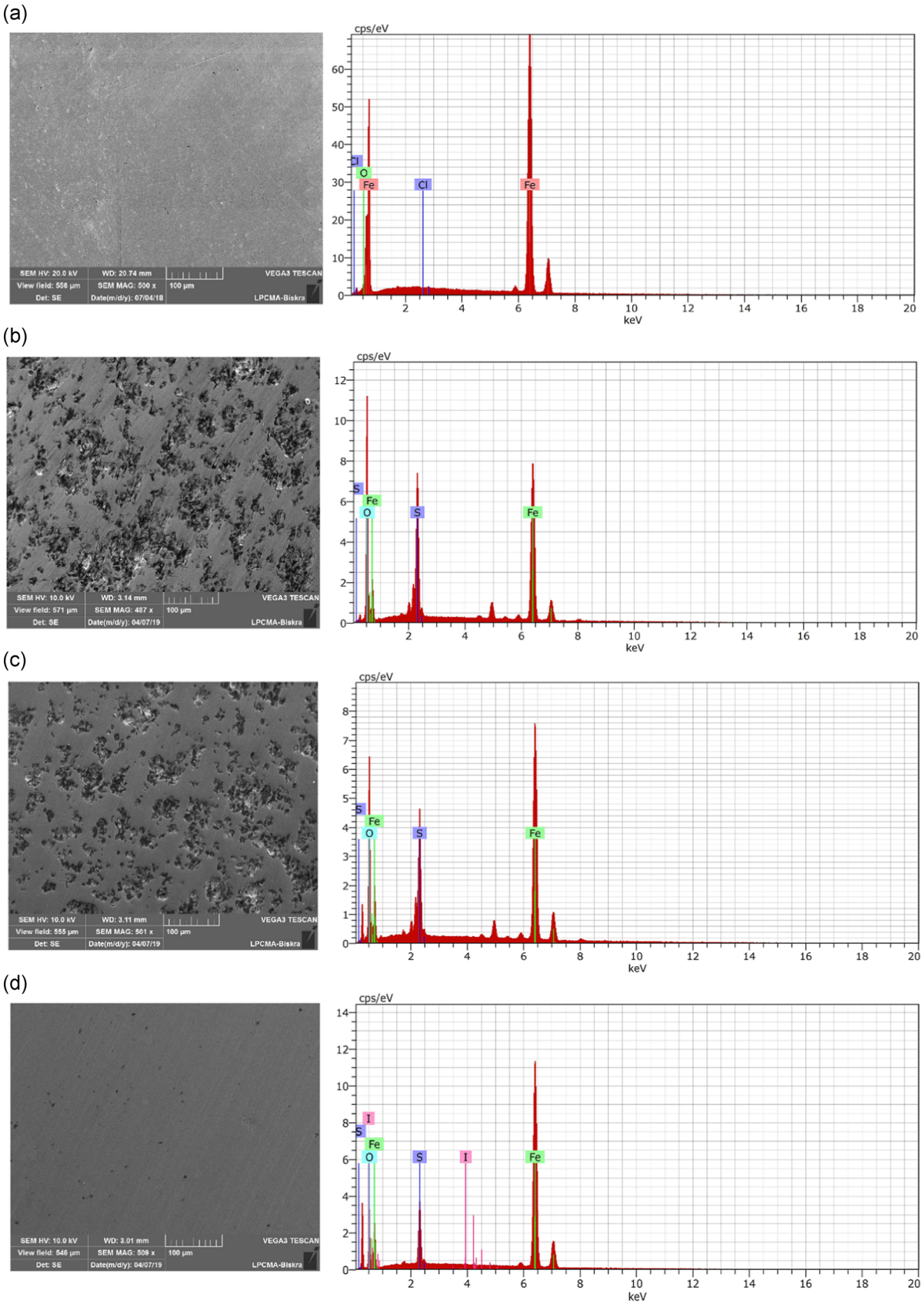


**FIGURE 11** SEM–EDX spectra of API5L X70 surface after 72 hr of immersion at 20°C. (a) Polished sample without immersion, (b) 0.5 M $H_2SO_4$, (c) 0.5 M $H_2SO_4$ + 1.0 g/L BRSM, (d) 0.5 M $H_2SO_4$ + 1.0 g/L + BRSM + 2.0 mM KI. BRSM, bark resin of *Schinus molle*; EDX, energy-dispersive X-ray; SEM, scanning electron microscopy [Color figure can be viewed at wileyonlinelibrary.com]

**TABLE 10** Elemental composition (wt%) obtained from the energy-dispersive X-ray spectra for API5L X70 pipeline steel immersed in 0.5 M $H_2SO_4$ at 20°C without and with bark resin of *Schinus molle* (BRSM) and BRSM/iodide ion system

| Elements | Steel | Steel in $H_2SO_4$ | Steel in $H_2SO_4$ + BRSM | Steel in $H_2SO_4$ + BRSM + KI |
|---|---|---|---|---|
| Fe | 96.47 | 51.48 | 63.17 | 82.25 |
| O | 3.53 | 34.82 | 25.44 | 10.49 |
| S | – | 13.70 | 11.39 | 6.99 |
| I | – | – | – | 0.26 |

However, a smoother surface and no damage were observed in Figure 11d compared to the image in Figure 11c and the higher wt% of Fe (82.25%) in the acid solution containing the BRSM/iodide ion system confirms the electrochemical results. The appearance of the I peak from EDX spectra in Figure 11d confirms the adsorption of the additives on the pipeline steel surface.

## 4 | CONCLUSIONS

PDP measurements, electrochemical impedance spectroscopy, and SEM–EDX were used to study the corrosion inhibition of API5L X70 pipeline steel in 0.5-M sulfuric acid solution using BRSM/KI system as an eco-friendly inhibitor.

The principal conclusions are as follows:

1. The inhibition efficiency of BRSM increases considerably after addition of KI, from 63% of BRSM alone to 99% of the BRSM/iodide ion system.
2. The PDP studies show that BRSM alone and the BRSM/iodide ion system act as a mixed-type inhibitor in sulfuric acid.
3. The adsorption of BRSM alone and BRSM/iodide ion system on the pipeline steel surface in sulfuric acid solution obeys the Langmuir adsorption isotherm.
4. The values of the synergistic parameter are superior to unity showing the corrosion protection brought about by BRSM in combination with the iodide ions is synergistic in nature and cooperative adsorption between halides and BRSM dominates over competitive adsorption.
5. The standard adsorption free energy ($\Delta G^{\circ}_{ads}$) indicates that the adsorption of BRSM involves physical adsorption. However, probably physical and chemical adsorption is proposed from the trend ($\Delta G^{\circ}_{ads}$) of which is more negative for the BRSM/iodide ion system.
6. The analysis of the pipeline steel surface after 72 hr of immersion in 0.5-M sulfuric acid solution by SEM-EDX revealed pitting corrosion of steel surface in the presence of BRSM, whereas in the presence of the BRSM/iodide ion system, no attack on the steel surface was observed.

## ACKNOWLEDGMENTS

The authors acknowledge funding from the General Directorate of Scientific Research and Technological Development, Algeria.

## ORCID

*Mounir Djellab* http://orcid.org/0000-0003-4540-292X
*Hamza Bentrah* http://orcid.org/0000-0002-9199-317X

## REFERENCES

[1] A. L. Chong, J. I. Mardel, D. R. MacFarlane, M. Forsyth, A. E. Somers, *ACS Sustainable Chem. Eng.* **2016**, *4*, 1746.
[2] M. Mobin, M. Rizvi, L. O. Olasunkanmi, E. E. Ebenso, *ACS Omega* **2017**, *2*, 3997.
[3] M. Finšgar, J. Jackson, *Corros. Sci.* **2014**, *86*, 17.
[4] D. A. Winkler, M. Breedon, P. White, A. E. Hughes, E. D. Sapper, I. Cole, *Corros. Sci.* **2016**, *106*, 229.
[5] D. Yang, Y. Ye, Y. Su, S. Liu, D. Gong, H. Zhao, *J. Cleaner Prod.* **2019**, *229*, 180.
[6] M. Messali, H. Lgaz, R. Dassanayake, R. Salghi, S. Jodeh, N. Abidi, O. Hamed, *J. Mol. Struct.* **2017**, *1145*, 43.
[7] K. Azzaoui, E. Mejdoubi, S. Jodeh, A. Lamhamdi, E. Rodriguez-Castellón, M. Algarra, A. Zarrouk, A. Errich, R. Salghi, H. Lgaz, *Corros. Sci.* **2017**, *129*, 70.
[8] M. M. Solomon, H. Gerengi, S. A. Umoren, N. B. Essien, U. B. Essien, E. Kaya, *Carbohydr. Polym.* **2018**, *181*, 43.
[9] H. Bentrah, Y. Rahali, A. Chala, *Corros. Sci.* **2014**, *82*, 426.
[10] S. A. Umoren, A. A. AlAhmary, Z. M. Gasem, M. M. Solomon, *Int. J. Biol. Macromol.* **2018**, *117*, 1017.
[11] M. M. Solomon, S. A. Umoren, I. I. Udosoro, A. P. Udoh, *Corros. Sci.* **2010**, *52*, 1317.
[12] M. M. Solomon, H. Gerengi, S. A. Umoren, *ACS Appl. Mater. Interfaces* **2017**, *9*, 6376.
[13] M. V. Fiori-Bimbi, P. E. Alvarez, H. Vaca, C. A. Gervasi, *Corros. Sci.* **2015**, *92*, 192.
[14] S. A. Umoren, I. B. Obot, A. Madhankumar, Z. M. Gasem, *Carbohydr. Polym.* **2015**, *124*, 280.
[15] G. Babaladimath, B. Vishalakshi, S. T. Nandibewoor, *Mater. Chem. Phys.* **2018**, *205*, 171.
[16] A. E. Elkholy, F. El-Taib Heakal, A. M. Rashad, K. Zakaria, *J. Pet. Sci. Eng.* **2018**, *166*, 263.
[17] A. Biswas, S. Pal, G. Udayabhanu, *Appl. Surf. Sci.* **2015**, *353*, 173.

[18] M. Mobin, M. Basik, J. Aslam, *J. Mol. Liq.* **2018**, *263*, 174.
[19] H. Lgaz, I.-M. Chung, R. Salghi, I. H. Ali, A. Chaouiki, Y. El Aoufir, M. I. Khan, *Appl. Surf. Sci.* **2019**, *463*, 647.
[20] M. Mobin, M. A. Khan, M. Parveen, *J. Appl. Polym. Sci.* **2011**, *121*, 1558.
[21] M. Bello, N. Ochoa, V. Balsamo, F. López-Carrasquero, S. Coll, A. Monsalve, G. González, *Carbohydr. Polym.* **2010**, *82*, 561.
[22] S. John, A. Salam, A. M. Baby, A. Joseph, *Prog. Org. Coat.* **2019**, *129*, 254.
[23] M. M. Solomon, H. Gerengi, T. Kaya, S. A. Umoren, *Int. J. Biol. Macromol.* **2017**, *104*, 638.
[24] Á. F. Szőke, G. S. Szabó, Z. Hórvölgyi, E. Albert, L. Gaina, L. M. Muresan, *Carbohydr. Polym.* **2019**, *215*, 63.
[25] C. Jeyaprabha, S. Sathiyanarayanan, G. Venkatachari, *Electrochim. Acta* **2006**, *51*, 4080.
[26] A. Khamis, M. M. Saleh, M. I. Awad, *Corros. Sci.* **2013**, *66*, 343.
[27] E. E. Oguzie, Y. Li, F. H. Wang, *J. Colloid Interface Sci.* **2007**, *310*, 90.
[28] A. M. Ridhwan, A. A. Rahim, A. M. Shah, *Int. J. Electrochem. Sci.* **2012**, *7*, 8091.
[29] I. B. Obot, A. Madhankumar, *Mater. Chem. Phys.* **2016**, *177*, 266.
[30] S. A. Umoren, O. Ogbobe, I. O. Igwe, E. E. Ebenso, *Corros. Sci.* **2008**, *50*, 1998.
[31] I. B. Obot, *Port. Electrochim. Acta* **2009**, *27*, 539.
[32] M. Heydari, M. Javidi, *Corros. Sci.* **2012**, *61*, 148.
[33] P. C. Okafor, Y. Zheng, *Corros. Sci.* **2009**, *51*, 850.
[34] G. R. Malca-García, L. Hennig, M. L. Ganoza-Yupanqui, A. Piña-Iturbe, R. W. Bussmann, *Rev. Bras. Farmacogn.* **2017**, *27*, 67.
[35] H. Taoui, H. Bentrah, A. Chala, M. Djellab, *Mater. Corros.* **2019**, *70*, 511.
[36] S. A. Umoren, I. B. Obot, *J. Adhes. Sci. Technol.* **2014**, *28*, 2054.
[37] M. Abdallah, B. Jahdaly, M. Sobhi, A. Ali, *Int. J. Electrochem. Sci.* **2015**, *10*, 4482.
[38] S. A. Umoren, Z. M. Gasem, I. B. Obot, *Anti-Corros. Methods Mater.* **2015**, *62*, 19.
[39] M. Lebrini, M. Lagrenée, H. Vezin, M. Traisnel, F. Bentiss, *Corros. Sci.* **2007**, *49*, 2254.
[40] R. Sadeghi Erami, M. Amirnasr, S. Meghdadi, M. Talebian, H. Farrokhpour, K. Raeissi, *Corros. Sci.* **2019**, *151*, 190.
[41] K. K. Anupama, K. Ramya, A. Joseph, *J. Mol. Liq.* **2016**, *216*, 146.
[42] R. Mehdaoui, A. Khelifa, A. Khadraoui, O. Aaboubi, A. Hadj Ziane, F. Bentiss, A. Zarrouk, *Res. Chem. Intermed.* **2015**, *42*, 5509.
[43] A. Farahi, F. Bentiss, C. Jama, M. A. El Mhammedi, M. Bakasse, *J. Alloys Compd.* **2017**, *723*, 1032.
[44] M. Cui, S. Ren, Q. Xue, H. Zhao, L. Wang, *J. Alloys Compd.* **2017**, *726*, 680.
[45] B. Qian, J. Wang, M. Zheng, B. Hou, *Corros. Sci.* **2013**, *75*, 184.
[46] S. A. Haladu, S. A. Umoren, S. A. Ali, M. M. Solomon, *Int. J. Electrochem. Sci.* **2017**, *12*, 9061.
[47] B. Zhang, C. He, C. Wang, P. Sun, F. Li, Y. Lin, *Corros. Sci.* **2015**, *94*, 6.
[48] H. Hamani, T. Douadi, M. Al-Noaimi, S. Issaadi, D. Daoud, S. Chafaa, *Corros. Sci.* **2014**, *88*, 234.
[49] P. Singh, V. Srivastava, M. A. Quraishi, *J. Mol. Liq.* **2016**, *216*, 164.
[50] M. Djellab, H. Bentrah, A. Chala, H. Taoui, *Mater. Corros.* **2019**, *70*, 149.
[51] R. Solmaz, *Corros. Sci.* **2014**, *79*, 169.
[52] G. Sığırcık, D. Yildirim, T. Tüken, *Corros. Sci.* **2017**, *120*, 184.
[53] Y. Qiang, S. Zhang, B. Tan, S. Chen, *Corros. Sci.* **2018**, *133*, 6.
[54] N. Yilmaz, A. Fitoz, ÿ Ergun, K. C. Emregül, *Corros. Sci.* **2016**, *111*, 110.
[55] Y. Qiang, S. Zhang, S. Yan, X. Zou, S. Chen, *Corros. Sci.* **2017**, *126*, 295.
[56] S. Zehra, M. Mobin, J. Aslam, M. Parveen, *J. Adhes. Sci. Technol.* **2017**, *32*, 317.
[57] G. Khan, W. J. Basirun, A. B. B. M. Badry, S. N. Kazi, P. Ahmed, S. M. Ahmed, G. M. Khan, *Int. J. Electrochem. Sci.* **2018**, *13*, 12420.
[58] Y. Liang, C. Wang, J. Li, L. Wang, J. Fu, *Int. J. Electrochem. Sci.* **2015**, *10*, 8072.
[59] E. Alibakhshi, M. Ramezanzadeh, G. Bahlakeh, B. Ramezanzadeh, M. Mahdavian, M. Motamedi, *J. Mol. Liq.* **2018**, *255*, 185.
[60] G. Salinas-Solano, J. Porcayo-Calderon, L. M. Martinez de la Escalera, J. Canto, M. Casales-Diaz, O. Sotelo-Mazon, J. Henao, L. Martinez-Gomez, *Ind. Crops Prod.* **2018**, *119*, 111.
[61] P. Roy, P. Karfa, U. Adhikari, D. Sukul, *Corros. Sci.* **2014**, *88*, 246.
[62] M. M. Solomon, S. A. Umoren, *J. Adhes. Sci. Technol.* **2015**, *29*, 1060.
[63] M. M. Solomon, S. A. Umoren, A. U. Israel, I. G. Etim, *Pigm. Resin Technol.* **2016**, *45*, 280.
[64] P. Muthukrishnan, B. Jeyaprabha, P. Prakash, *Arab. J. Chem.* **2017**, *10*, S2343.
[65] M. Salah, L. Lahcène, A. Omar, H. Yahia, *Int. J. Ind. Chem.* **2017**, *8*, 263.
[66] B. J. Usman, S. A. Umoren, Z. M. Gasem, *J. Mol. Liq.* **2017**, *237*, 146.
[67] Z. Zhang, N. Tian, W. Zhang, X. Huang, L. Ruan, L. Wu, *Corros. Sci.* **2016**, *111*, 675.
[68] W. Zhang, H. J. Li, A. Wang, C. Ma, Z. Wang, H. Zhang, Y. C. Wu, *Mater. Corros.* **2019**, *70*, 2303.
[69] A. A. Farag, T. A. Ali, *J. Ind. Eng. Chem.* **2015**, *21*, 627.
[70] P. Mourya, P. Singh, R. B. Rastogi, M. M. Singh, *Appl. Surf. Sci.* **2016**, *380*, 141.
[71] S. A. Umoren, M. M. Solomon, *J. Ind. Eng. Chem.* **2015**, *21*, 81.
[72] S. A. Umoren, Y. Li, F. H. Wang, *Corros. Sci.* **2010**, *52*, 1777.

**How to cite this article:** Djellab M, Bentrah H, Chala A, Taoui H, Kherief S, Bouamra B. Synergistic effect of iodide ions and bark resin of *Schinus molle* for the corrosion inhibition of API5L X70 pipeline steel in $H_2SO_4$. *Materials and Corrosion*. 2020;1–13.
https://doi.org/10.1002/maco.202011533

Received: 2 April 2018 | Accepted: 4 July 2018
DOI: 10.1002/maco.201810203

ARTICLE

Materials and Corrosion

# Synergistic effect of halide ions and gum arabic for the corrosion inhibition of API5L X70 pipeline steel in $H_2SO_4$

**Mounir Djellab** | **Hamza Bentrah** | **Abdelouahad Chala** | **Hicham Taoui**

Laboratoire de Physique des couches minces et applications, Université de Biskra, Biskra, Algérie

**Correspondence**
Mounir Djellab, Laboratoire de Physique des couches minces et applications, Université de Biskra, B.P. 145, Biskra R.P. 07000, Algérie.
Email: mounircorrsci@gmail.com

This paper aims to increase the inhibition efficiency of gum arabic (GA) for the corrosion of API5L X70 pipeline steel in sulfuric acid through the addition of halide ions (potassium iodide [KI], potassium chloride [KCl], and potassium bromide [KBr]). The synergistic effect of GA and halide ions has been studied using potentiodynamic polarization curves, electrochemical impedance spectroscopy, and surface analysis by scanning electron microscope (SEM). The results show that substantial corrosion inhibition (99%) using 2 g $L^{-1}$ GA and 0.5 mM KI can be obtained in synergistic manner. The adsorption of GA in combination with iodide ions follows Langmuir adsorption isotherm. GA combined with KI acts as a mixed-type inhibitor in sulfuric acid.

**KEYWORDS**
API5L X70 pipeline steel, EIS, gum arabic, iodide ions, sulfuric acid, synergistic effect

## 1 | INTRODUCTION

Carbon steel is the most commonly used material for transmission pipelines in the gas and oil industry, and may be subjected to different acidic environments. Sulfuric acid is employed in many service environments such as pickling, cleaning of boilers, de-scaling, and acidization of oil well.[1,2] In order to reduce the undesirable carbon steel dissolution by these processes and as the most effective and economic method, corrosion inhibitors are widely employed.[3,4] The new generation of environmental regulation requires the replacement of toxic inhibitors with non-toxic inhibitors.[5] In view of this, many alternative ecofriendly corrosion inhibitors have now been developed. The most common class of environment friendly inhibitor for different metal-environment systems is natural products.[6–8] The use of natural polymeric structures, derived from extracts of leaves or seeds, as green corrosion inhibitors is receiving strong preference.[9] The reviews of the literature on several polymers as corrosion inhibitors of carbon steel in hydrochloric acid solution were recently published.[3,9–11] They showed that all the reported polymers were found to be more efficient in hydrochloric acid than in sulfuric acid for the corrosion inhibition of carbon steel. Indeed, gum arabic (GA) and pectin act as a good inhibitor for the corrosion of carbon steel in 1 M hydrochloric acid and the inhibition efficiency increases with the inhibitor concentration but it is almost constant with rise in temperature and the maximum value is 93% at 4 g $L^{-1}$ GA[3] and 94% at 2 g $L^{-1}$ pectin.[9] The polyacrylamide grafted guar gum is reflected as a good corrosion inhibitor for mild steel in 1 M hydrochloric acid with 90% inhibition efficiency.[12] However, in sulfuric acid, the results obtained show different behavior. Carboxymethyl cellulose (CMC) acts as inhibitor for mild steel in sulfuric acid and the inhibition efficiency was found to increase with increase in CMC concentration (the maximum value is 64% at 0.5 g $L^{-1}$ CMC) but decreased with rise in temperature.[13] The inhibition efficiency of GA at 30, 40, 50, and 60 °C in 0.1 M sulfuric acid is respectively 21.9%, 25.9%, 32.9%, and 37.9%, and for polyethylene glycol at the same temperatures is 16.6%, 32.3%, 36.3%, and 40.2%.[14] Several modifications have been done in recent days in an attempt to enhancing the effectiveness of polymers as metal corrosion inhibitors. One of such modifications is the addition of halide ions to polymer compounds. It has been reported that

  

addition of iodide ion to tannic acid in 0.1 M sulfuric acid,[15] to polyacrylamide,[16] and polyaspartic[17] in 0.5 M sulfuric acid could synergistically upgrade the inhibition efficiency from moderate to over 90% protection of the studied mild steel. But in other studies, the synergy between polymers and halide ions did not yield satisfactory results concerning the inhibition efficiency for carbon steel in sulfuric acid. Indeed, the synergy between exudate gum from pachylobus edulis and halide ions[18] shows that the inhibition efficiency at 30, 40, 50, and 60 °C is respectively 58%, 48%, 39%, and 31% for KCl, and 60%, 52%, 40%, and 35% for KBr, and 65%, 53%, 43%, and 41% for KI. The study of Umoren et al.[14] is the only report on corrosion inhibition of mild steel in sulfuric acid involving the synergy between GA and halide ions, but the overall results were not encouraging because the inhibition efficiency at 30, 40, 50, and 60 °C was respectively 21%, 35%, 37%, and 38% for KCl, and 31%, 40%, 44%, and 47% for KBr, and 39%, 55%, 57%, and 59% for KI.

In the work reported here, the influence of halide ions on the corrosion inhibition of API5L X70 pipeline steel using GA in 0.5 M sulfuric acid at 30 °C was investigated. An attempt had also been made to elucidate the mechanism of the corrosion inhibition in the polymer-halide systems.

## 2 | EXPERIMENTAL

### 2.1 | Material

The industrial purpose of the study has guided the choice of the API 5L X70 pipeline steel which is used widely in the oil and gas industry. The working electrodes (API5L X70 pipeline steel), for electrochemical experiments, were cut into $3 \times 3 \times 1$ cm, with the following chemical composition (weight percentage): C 0.12 max, Mn 1.68 max, Si 0.27 min, P 0.012 max, S 0.005 max, Cr 0.051 max, Ni 0.04 max, Nb 0.033 max, Ti 0.03 max, and the balance Fe. The samples were mounted in the electrochemical cell, and the surface area of each electrode exposed to the electrolyte was 2.85 $cm^2$. Exposed surface of each sample was prepared by wet grinding with silicon carbide abrasive papers (grade 320–500–600–800), rinsed with distilled water and degreased with acetone.

### 2.2 | Medium

The aggressive solution of 0.5 M sulfuric acid was prepared by dilution of AR grade 95% sulfuric acid with distilled water.

### 2.3 | Inhibitor

Dried GA powder, exuded by Acacia Senegal trees, was selected for the present study.

### 2.4 | Electrochemical techniques

Two electrochemical techniques, namely, potentiodynamic polarization and electrochemical impedance spectroscopy, were used to study the synergistic effect between halide ions and GA, in 0.5 M sulfuric acid. Electrochemical measurements were performed using a Gamry Ref 3000 with Echem 6.0 operating software.

A Gamry para cell with a standard three-electrode configuration consisting of a standard Ag/AgCl electrode (the potential of Ag/AgCl electrode is the same of the saturated calomel electrode and equal to 240 mV vs. NHE) and graphite were used as the reference and counter electrode respectively, while the sample acted as the working electrode. The working electrode was connected with a copper wire on the backside and installed in customized Teflon assembly and exposed on the solution side to about 2.85 $cm^2$ working area. All experiments were performed in stagnant aerated solutions at 30 °C. The working electrode was immersed in a test solution for 1 h until a stable open circuit potential was attained. The analyses were performed using Echem Analyst commercial software developed by Gamry. Potentiodynamic polarization studies were carried out from the cathodic potential of −0.25 V to anodic potential of +0.25 V with respect to the corrosion potential ($E_{corr}$) at a scan rate of 0.5 mV $s^{-1}$. The linear Tafel segments of the anodic and cathodic curves were extrapolated to corrosion potential to obtain the corrosion current densities ($I_{corr}$). Because of the presence of a degree of nonlinearity in the Tafel slope part of the obtained polarization curves, the Tafel constants were calculated as a slope of the points after ($E_{corr}$) by ±80 mV.

The values of inhibition efficiency $\eta_{pol}$ were calculated using the following equation:

$$\eta_{pol}\ \% = \frac{I_{corr} - I_{corr}(inh)}{I_{corr}} \times 100 \qquad (1)$$

where $I_{corr}$ and $I_{corr}(inh)$ represent corrosion current density values without and with inhibitor, respectively.

Electrochemical impedance spectroscopy (EIS) was carried out at OCP in the frequency range of 20 kHz to 50 mHz using a 10 mV peak-to-peak voltage excitation. Inhibition efficiency $\eta_{EIS}$ is calculated on the basis of the equation:

$$\eta_{EIS}\ \% = \frac{R_t - \acute{R}_t}{R_t} \times 100 \qquad (2)$$

where $\acute{R}_t$ is charge transfer resistance value in 0.5 M sulfuric acid, and $R_t$ is charge transfer resistance value in the presence of GA or GA plus halides.

## 2.5 | Surface analysis

### 2.5.1 | Surface study by scanning electron microscopy (SEM)

In order to examine the changes in surface morphology of the API5L X70 pipeline steel, the electrodes were immersed in a solution of 0.5 M sulfuric acid containing 2 g $L^{-1}$ GA without and with the optimal concentration of halide ions (obtained from electrochemical experiments). After 96 h waiting time, the electrodes were removed from the cells and dried. An electron microscope, TESCAN VEGA3, was used for SEM study.

# 3 | RESULTS AND DISCUSSION

## 3.1 | Inhibition by gum arabic

### 3.1.1 | Electrochemical impedance spectroscopy measurements

The impedance data recorded on API5L X70 pipeline steel immersed in 0.5 M sulfuric acid solution without and with different concentrations of GA are shown in Figure 1 in (a) Nyquist, (b) Bode modulus, and (c) Bode phase angle representations. Inspection of the plots revealed that the shape of Nyquist plots in the absence and presence of inhibitor is similar which indicates an unchanged mechanism of corrosion. The Nyquist plots instead of ideal semicircles are found to be depressed. This depressed form of semicircles has been attributed to the inhomogeneity of the electrode surface arising from surface roughness or interfacial phenomena.[19] The Nyquist plots reveal that each impedance diagram consists of a large capacitive loop at high frequencies (HF) and an inductive loop at low frequencies (LF) both in the absence and presence of inhibitor. The presence of two time constants for iron dissolution at $E_{corr}$ in the absence of inhibitors has been reported in the literature.[20,21] The HF capacitive loop could be attributed to the double layer capacity in parallel with the charge transfer resistance ($R_t$). The LF inductive loop may be originated from the relaxation process obtained by adsorption species as $H^+_{ads}$ and $SO_4^{-2}$ on the surface of the metal. It may also be attributed to the re-dissolution of the passivated surface at low frequencies.[17] Figure 2a shows simulated and experimentally generated impedance diagrams for API5L X70 pipeline steel immersed in 0.5 M sulfuric acid solution in the presence of 2 g $L^{-1}$ GA. Excellent fit with this model was obtained for all experimental data. From the figure, it is very clear that the measured impedance plot is in accordance with the one calculated by the equivalent circuit. The circuit consists of the solution resistance Rs, the charge transfer resistance $R_t$, the constant phase element (CPE), the inductive elements, RL, and L. For the description of a frequency independent phase

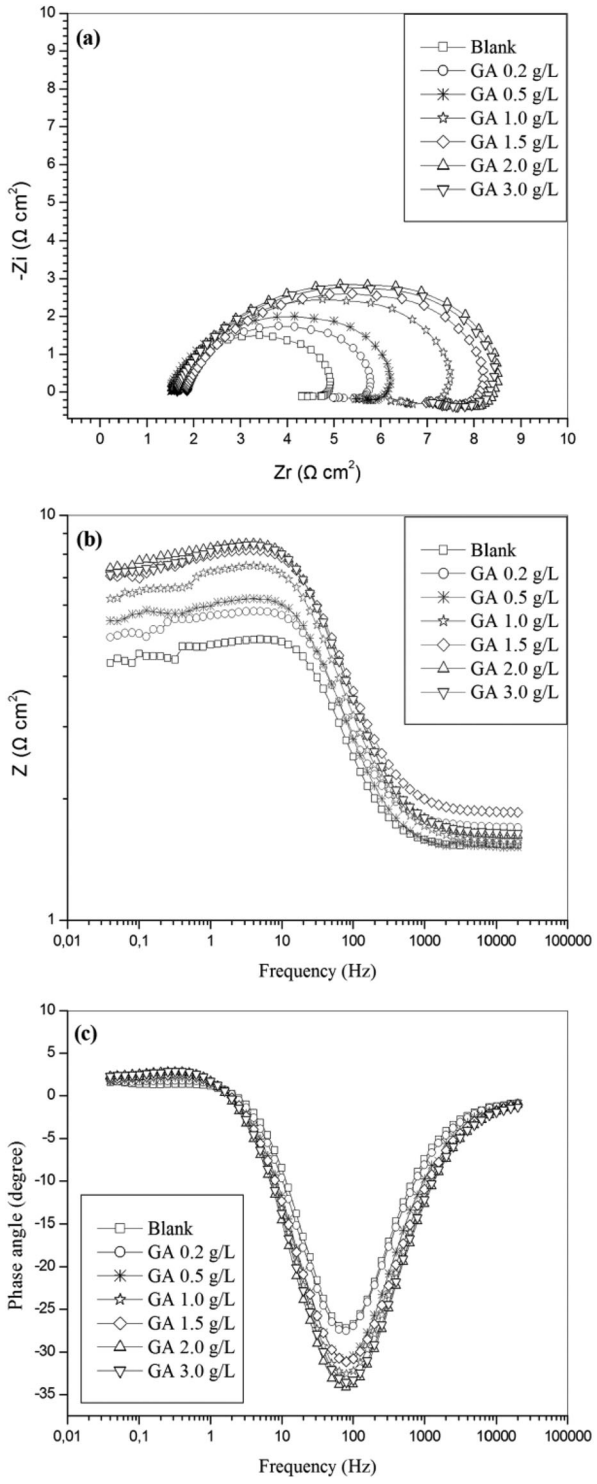


**FIGURE 1** EIS plots for API5L X70 pipeline steel in 0.5 M $H_2SO_4$ without and with different concentrations of GA at 30 °C, (a) Nyquist, (b) Bode modulus, and (c) Bode phase angle representations

shift between an applied AC potential and its current response, a constant phase element (CPE) is used. CPE is an element whose impedance value is a function of the frequency and whose phase is independent of the frequency and its impedance is defined as[22,23]:

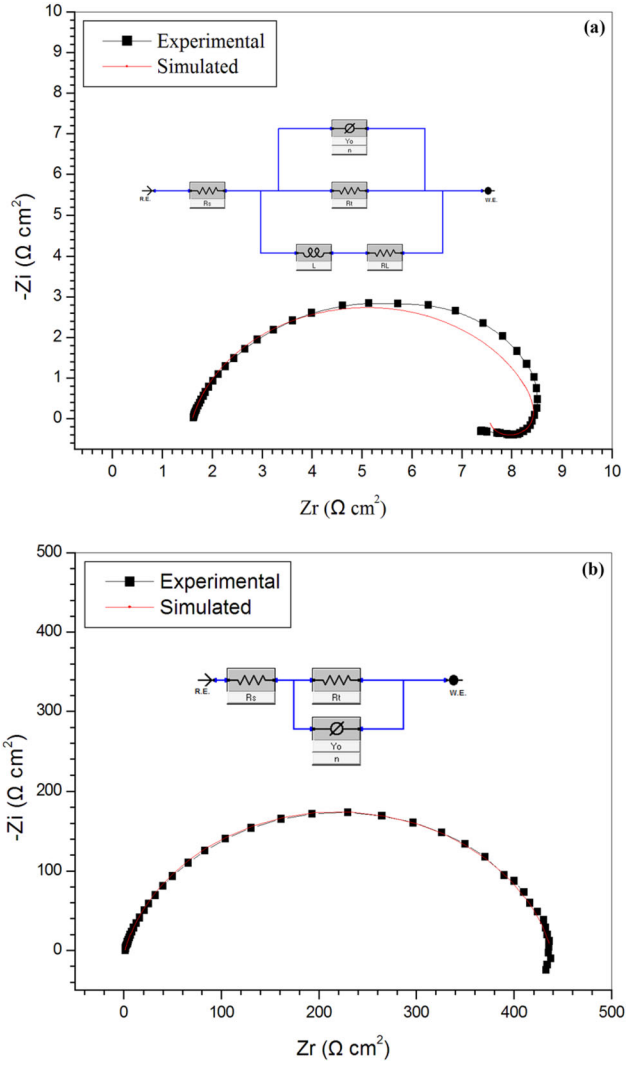


**FIGURE 2** Nyquist plots of experimental data and simulated data, together with the equivalent circuit used to fit the impedance data, recorded for API5L X70 pipeline steel in 0.5 M $H_2SO_4$ containing (a) 2 g $L^{-1}$ GA and (b) 2 g $L^{-1}$ GA + 0.75 mM KI. [Color figure can be viewed at wileyonlinelibrary.com]

$$Z_{CPE} = Y_0^{-1}(j\omega)^{-n} \quad (3)$$

where $Y_0$ is a proportional factor that indicates the combination of properties related to both the surfaces and electroactive species independent of frequency; $j$ is imaginary number; $\omega$ is the angular frequency, and $\omega$ equal to $2\pi f$, where f is the frequency; and n has the meaning of a phase shift and is related to a slope of the log |Z| versus log f plots and usually is in the range 0.5 and 1.

The double layer capacitance $C_{dl}$ was calculated using Eq. (4) [24,25]:

$$C_{dl} = Y0(2\pi f_{max})^{n-1} \quad (4)$$

where $f_{max}$ is the frequency at which the imaginary component of the impedance is maximum.

Examination of the impedance plots clearly shows that the introduction of GA affected the impedance responses of the system (steel/sulfuric acid); notably an increase in the diameter of the semicircle (Figure 1a), impedance modulus of the interface at the low frequency region (Figure 1b). Also the phase angle plots (Figure 1c) show a wide peak. Similar results were obtained by Refs. [26,27].

The values of the electrochemical parameters derived from Nyquist plots are given in Table 1.

It can be observed that the values of $R_t$ increase while the values of $C_{dl}$ decrease with increase in concentration of GA. The decrease in $C_{dl}$ on the introduction of GA to the acid solution indicates the presence of a protective layer that covers the surface of the electrode. The adsorption of GA on the API5L X70 pipeline steel surface decreases $C_{dl}$ because they displaced the water molecules and other ions that were originally adsorbed on the surface. With higher concentration of inhibitor (GA), either the thickness of the protective layer or the surface coverage by inhibitor increased due to more inhibitor electrostatically adsorbed on the electrode surface.[17,28] The values of inhibition efficiency given in Table 1 show that inhibition efficiency increases with increase in concentration of GA with the highest value of 52% obtained at GA concentration of 2 g $L^{-1}$.

### 3.1.2 | Potentiodynamic polarization measurements

The kinetics of the anodic and cathodic reactions occurring on API5L X70 pipeline steel surface in 0.5 M sulfuric acid

**TABLE 1** Electrochemical impedance parameters for API5L X70 in 0.5 M $H_2SO_4$ solution in the absence and the presence of GA at 30 °C

| System/concentration | Rs ($\Omega$ cm$^2$) | $Y_0$ ($\mu\Omega$ $S^n$ cm$^{-2}$) | $n$ | $R_t$ ($\Omega$ cm$^2$) | $L$ (H cm$^2$) | $R_L$ ($\Omega$ cm$^2$) | $C_{dl}$ ($\mu$F cm$^{-2}$) | $\eta_{EIS}$% |
|---|---|---|---|---|---|---|---|---|
| Blank | 1.5 | 1814 | 0.90 | 3.48 | 05.00 | 30 | 1048 | – |
| 0.2 g $L^{-1}$ GA | 1.7 | 1887 | 0.87 | 4.23 | 05.00 | 27 | 924 | 17 |
| 0.5 g $L^{-1}$ GA | 1.5 | 1714 | 0.88 | 4.80 | 06.37 | 27 | 887 | 27 |
| 1 g $L^{-1}$ GA | 1.5 | 1833 | 0.83 | 6.25 | 05.00 | 30 | 721 | 44 |
| 1.5 g $L^{-1}$ GA | 1.8 | 1593 | 0.84 | 6.66 | 05.60 | 30 | 662 | 48 |
| 2 g $L^{-1}$ GA | 1.6 | 1654 | 0.83 | 7.28 | 06.10 | 31 | 650 | 52 |
| 3 g $L^{-1}$ GA | 1.6 | 1662 | 0.83 | 7.20 | 05.00 | 31 | 654 | 52 |

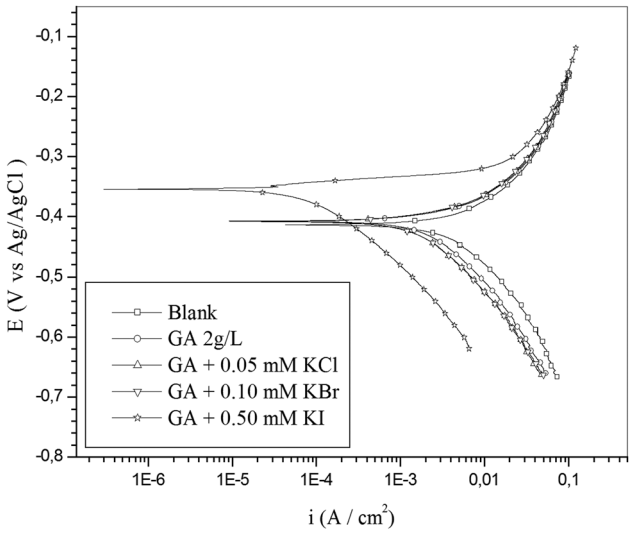


**FIGURE 3** Polarization curves for API5L X70 in 0.5 M $H_2SO_4$ solution containing 2 g $L^{-1}$ GA and GA combined with the optimal concentrations of halides at 30 °C

solutions in the absence and the presence of 2 g $L^{-1}$ GA was investigated using potentiodynamic polarization measurements (Figure 3). Inspection of the figure revealed that addition of GA causes a decrease in the corrosion rate, that is, shifts both the anodic and cathodic curves to lower values of current densities. This implies that both the hydrogen evolution and anodic iron dissolution reactions of API5L X70 pipeline steel corrosion are inhibited. This may be ascribed to adsorption of GA over the corroding surface. The values of corrosion current densities ($I_{corr}$), corrosion potential $E_{corr}$, the cathodic Tafel slope (bc), and anodic Tafel slope (ba) obtained from the polarization curves are listed in Table 2. The results in the table indicate that corrosion current density decreases markedly in the presence of GA compared to the blank solution. It is also observed that the presence of GA does not shift $E_{corr}$ remarkably; therefore, GA could be regarded as a mixed-type inhibitor. It is clear that inhibition efficiency increases with increase in concentration of GA and the highest inhibition efficiency of 50% was obtained. Good agreement with electrochemical impedance spectroscopy is obtained.

### 3.1.3 | Adsorption isotherm and standard adsorption free energy

The understanding of isotherms that describe the adsorption behavior of a corrosion inhibitor is an important part of present work, as this can provide information to the nature of the interaction between the metal and inhibitor. In the present study, several adsorption isotherms were assessed, and the Langmuir adsorption isotherm was found to give the best description of the adsorption behavior of the studied inhibitor (Figure 4). A correlation between surface coverage ($\theta = \eta_{EIS}\%/100$) and the concentration of inhibitor (C) in electrolyte can be represented by the Langmuir adsorption isotherm.[29–31]

$$\frac{C}{\theta} = \frac{1}{K_{ads}} + C \tag{5}$$

where $K_{ads}$ is constant of adsorption. Plots of C/θ with C at 30 °C yield straight line with slope values close to 1. From the values of the adsorption constant, Kads, the standard free energy of adsorption $\Delta G^{\circ}_{ads}$ is determined using the following equation[12,32,33]:

$$\Delta G^{\circ}_{ads} = -RT \ln(1 \times 10^6 K_{ads}) \tag{6}$$

where $1 \times 10^6$ is the concentration of water molecules expressed in mg $L^{-1}$, $R$ is the universal gas constant and $T$ is the absolute temperature. The values of $\Delta G^{\circ}_{ads}$ and $K_{ads}$ are listed in Table 3. $K_{ads}$ value may be taken as a measure of the strength of the adsorption forces between the inhibitor molecules and the metal surface.[10,34] $K_{ads}$, in the present study, is relatively low (1,2 L $g^{-1}$) when compared with other studies of a good inhibitor in sulfuric acid solution for corrosion of steel, Tagetes erecta (Marigold flower) extract.[2] This explains why the GA is a moderate inhibitor in sulfuric acid solution. In previous study,[3] with the same inhibitor (gum arabic), but in 1 M hydrochloric acid solution for API 5L X42 pipeline steel, the values of $K_{ads}$ were 10.03, 8.7, 8.4, and 7.9 L $g^{-1}$ at 25, 35, 45, and 65 °C, respectively, where the values of the inhibition efficiency were almost good and constant (the maximum value is 93%) with increasing the temperature. Generally, values of $\Delta G^{\circ}_{ads}$ up to −20 kJ $mol^{-1}$

**TABLE 2** Potentiodynamic polarization parameters for API5L X70 in 0.5 M $H_2SO_4$ solution containing 2 g $L^{-1}$ GA and GA combined with the optimal concentrations of halides at 30 °C.

| System/ concentration | $E_{corr}$ (mV) | $I_{corr}$ (μA $cm^{-2}$) | −bc (mV $dec^{-1}$) | ba (mV $dec^{-1}$) | $\eta_{pol}$ % |
|---|---|---|---|---|---|
| Blank | −414 | 4570 | 171 | 103 | – |
| GA 2g $L^{-1}$ | −407 | 2306 | 155 | 59 | 50 |
| GA + 0.1 mM KBr | −408 | 2055 | 135 | 46 | 57 |
| GA + 0.1 mM KCl | −407 | 1401 | 132 | 42 | 62 |
| GA + 0.5 mM KI | −354 | 91 | 120 | 15 | 98 |

**TABLE 3** Parameters of Langmuir adsorption isotherm for API5L X70 in 0.5 M $H_2SO_4$ solution containing GA at 30 °C.

| Isotherm mode | Linear correlation coefficient | $K$ ($L\,g^{-1}$) | $\Delta G°_{ads}$ ($kJ\,mol^{-1}$) |
|---|---|---|---|
| Langmuir | 0.99536 | 1.2 | −17.87 |

are consistent with electrostatic interaction between charged molecules and a charged metal (which indicates physical adsorption) while those more negative than $-40\,kJ\,mol^{-1}$ involves charge sharing or transfer from the inhibitor components to the metal surface to form a coordinate type of bond (which indicates chemisorption).[35,36] In the present study, the value of $\Delta G°_{ads}$ is $-17.87\,kJ\,mol^{-1}$ indicating that the adsorption of GA on API5L X70 pipeline steel surface involves physical adsorption.

## 3.2 | Synergism of GA with halide ions

### 3.2.1 | Effect of halide ions

The effect of halide ions on inhibitive action of GA in 0.5 M sulfuric acid solution was investigated by electrochemical impedance spectroscopy by adding different concentrations of halide ions and fixing the concentration of inhibitor at $2\,g\,L^{-1}$ (the optimal concentration of GA) and the impedance data are shown in Figure 5 for KBr, Figure 6 for KCl, and Figure 7 for KI. The impedance parameters are listed in Table 4.

The $R_t$ value for $2\,g\,L^{-1}$ GA is $7.28\,\Omega\,cm^2$ and $\eta_{EIS}$ is about 52%. While $R_t$ in presence of combined inhibitor GA + 0.1 mM KBr is $11.18\,\Omega\,cm^2$, GA + 0.1 mM KCl is $12.50\,\Omega\,cm^2$, and GA + 0.5 mM KI is $284\,\Omega\,cm^2$ and corresponding values of inhibition efficiency obtained by

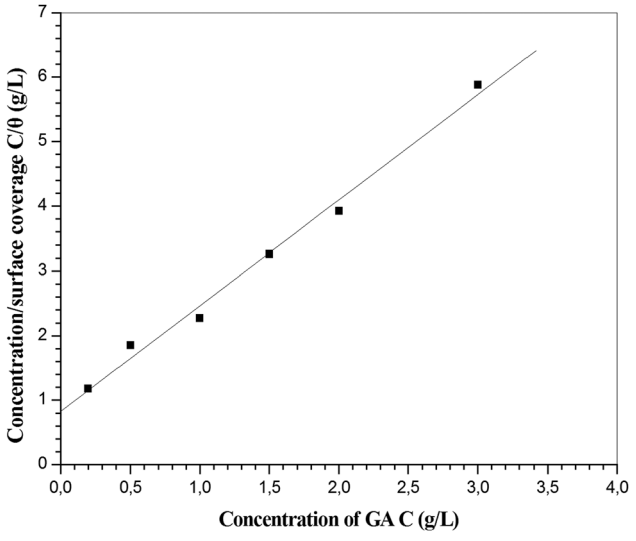


**FIGURE 4** Langmuir adsorption isotherm for GA on API5L X70 in 0.5 M $H_2SO_4$ solution at 30 °C

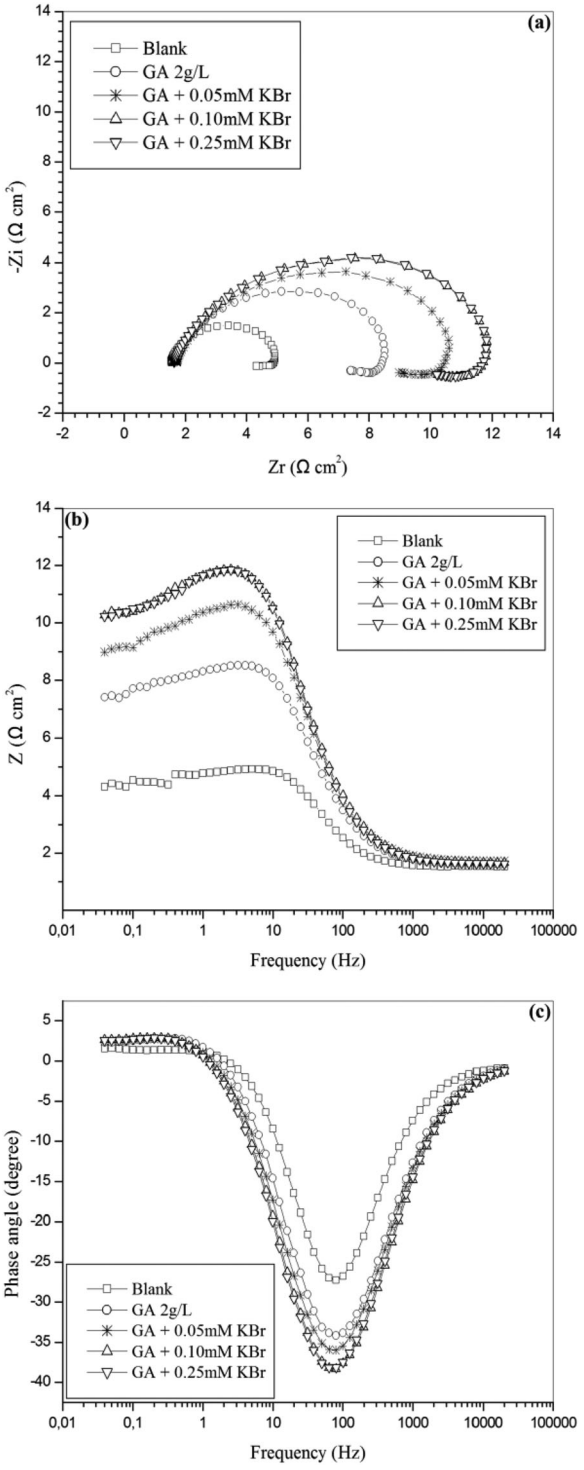


**FIGURE 5** Electrochemical impedance plots for API5L X70 in 0.5 M $H_2SO_4$ solution containing $2\,g\,L^{-1}$ GA and GA + KBr mixtures at 30 °C, (a) Nyquist, (b) Bode modulus, and (c) Bode phase angle representations

EIS method are 69%, 72%, and 99%, respectively. The $C_{dl}$ value of $2\,g\,L^{-1}$ GA is $650\,\mu F\,cm^{-2}$ and it reduces to 648, 587, and $104\,\mu F\,cm^{-2}$ by the addition of 0.1 mM KBr, 0.1 mM KCl, and 0.5 mM KI, respectively. These results reveal the existence of synergism between GA and halide

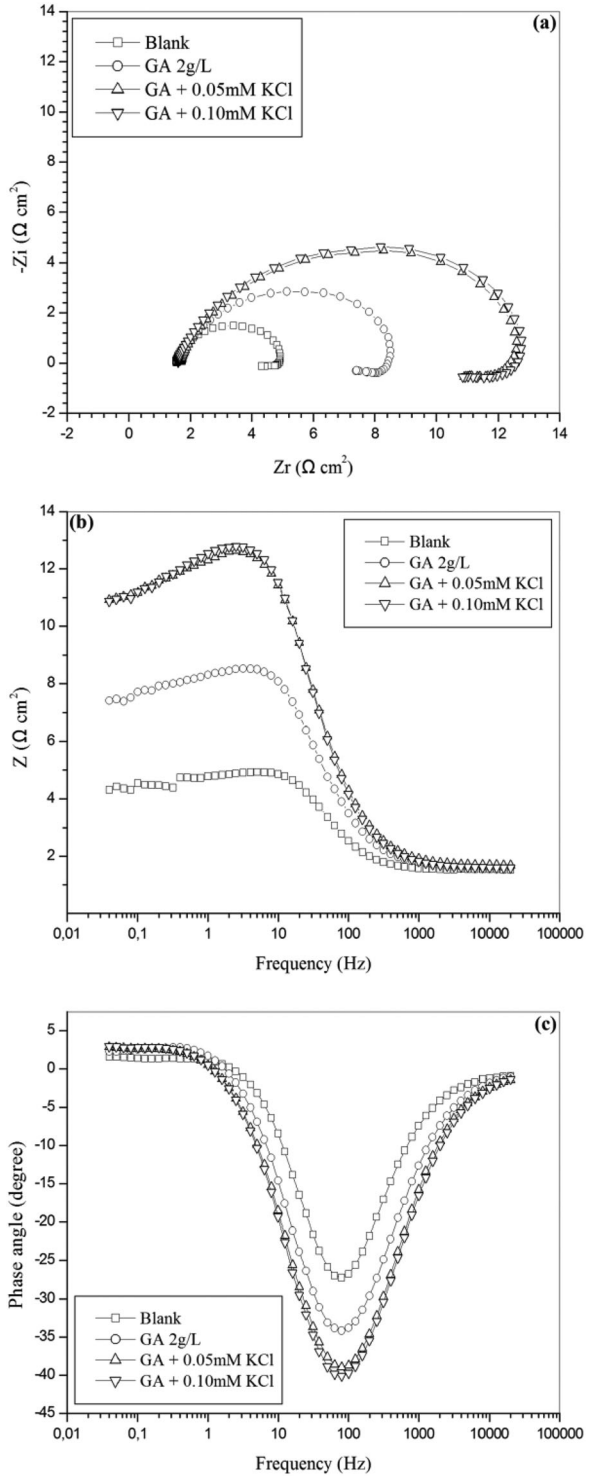


**FIGURE 6** Electrochemical impedance plots for API5L X70 in 0.5 M $H_2SO_4$ solution containing 2 g $L^{-1}$ GA and GA + KCl mixtures at 30 °C, (a) Nyquist, (b) Bode modulus, and (c) Bode phase angle representations

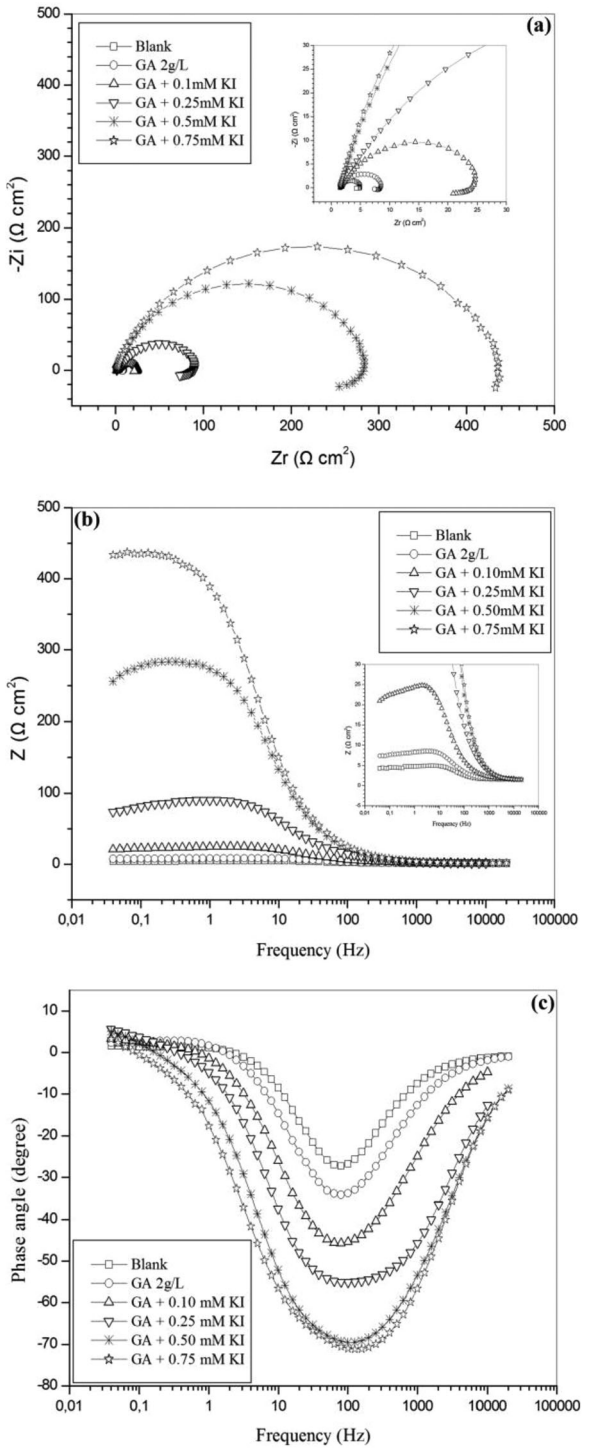


**FIGURE 7** Electrochemical impedance plots for API5L X70 in 0.5 M $H_2SO_4$ solution containing 2 g $L^{-1}$ GA and GA + KI mixtures at 30 °C, (a) Nyquist, (b) Bode modulus, and (c) Bode phase angle representations

ions. Meanwhile electronegativity and atomic radii of halide ions could be attributed to the variation in protection efficiency of GA in presence of different halides. Electronegativity decreases from $Cl^-$ to $I^-$ ($Cl^- = 3$, $Br^- = 2.8$, $I^- = 2.5$), while atomic radius increases from $Cl^-$ to $I^-$ ($Cl^- = 90$ pm, $Br^- = 114$ pm, $I^- = 135$ pm).[14] The best synergistic effect between GA and halide ions was found for the iodide ion ($\eta_{EIS} = 99\%$), and on other hand the inhibition efficiency of bromide ion and chloride ion is almost the same ($\eta_{EIS} = 69\%$ for $Br^-$ and $\eta_{EIS} = 72\%$ for $Cl^-$). The

**TABLE 4** Electrochemical impedance parameters for API5L X70 in 0.5 M $H_2SO_4$ solution containing 2 g $L^{-1}$ GA and GA combined with different concentrations of halides at 30 °C.

| System/concentration | Rs ($\Omega$ $cm^2$) | $Y_0$ ($\mu$ $\Omega$ $S^n$ $cm^{-2}$) | $n$ | $R_t$ ($\Omega$ $cm^2$) | $L$ (H $cm^2$) | $R_L$ ($\Omega$ $cm^2$) | $C_{dl}$ ($\mu$ F $cm^{-2}$) | $\eta_{EIS}$ % |
|---|---|---|---|---|---|---|---|---|
| Blank | 1.5 | 1814 | 0.90 | 3.48 | 05.00 | 30 | 1048 | – |
| 2 g $L^{-1}$ GA | 1.6 | 1654 | 0.83 | 7.28 | 06.10 | 31 | 650 | 52 |
| GA + 0.05 mM KBr | 1.7 | 1795 | 0.80 | 09.85 | 05.00 | 35 | 653 | 64 |
| GA + 0.10 mM KBr | 1.6 | 1703 | 0.80 | 11.18 | 05.80 | 37 | 648 | 69 |
| GA + 0.25 mM KBr | 1.6 | 1769 | 0.80 | 11.30 | 05.00 | 37 | 643 | 69 |
| GA + 0.50 mM KBr | 1.6 | 1865 | 0.80 | 10.52 | 06.00 | 39 | 678 | 67 |
| GA + 0.05 mM KCl | 1.6 | 1490 | 0.81 | 12.10 | 05.00 | 40.00 | 570 | 71 |
| GA + 0.10 mM KCl | 1.5 | 1534 | 0.81 | 12.50 | 05.00 | 40.00 | 587 | 72 |
| GA + 0.25 mM KCl | 1.6 | 1801 | 0.81 | 10.30 | 05.00 | 35.00 | 670 | 66 |
| GA + 0.50 mM KCl | 1.6 | 1784 | 0.80 | 10.03 | 05.00 | 36.00 | 649 | 65 |
| GA + 0.10 mM KI | 1.6 | 1064 | 0.78 | 25.50 | 19.00 | 100 | 385 | 86 |
| GA + 0.25 mM KI | 1.4 | 504 | 0.75 | 107 | 50.00 | 230 | 179 | 96 |
| GA + 0.50 mM KI | 1.4 | 170 | 0.86 | 284 | – | – | 104 | 99 |
| GA + 0.75 mM KI | 1.4 | 163 | 0.85 | 436 | – | – | 100 | 99 |

large ionic radii and low electronegativity compared to other halide ions lead to specific adsorption of iodide ions on the metal surface.[37]

The polarization behaviour for API5L X70 pipeline steel in the presence of 2 g $L^{-1}$ GA along with 0.1 mM KBr, 0.1 mM KCl, and 0.5 mM KI is depicted in Figure 3 and the corrosion kinetic parameters obtained from these curves are given in Table 2. From Table 2, it is seen that the corrosion current density is reduced from 4570 $\mu A\ cm^{-2}$ in the free acid solution to 2306 $\mu A\ cm^{-2}$ in the presence of 2 g $L^{-1}$ GA. These values were further reduced to 2055 $\mu A\ cm^{-2}$ for 0.1 mM KBr, 1401 $\mu A\ cm^{-2}$ for 0.1 mM KCl, and 91 $\mu A\ cm^{-2}$ for 0.5 mM KI. Also inhibition efficiency was upgraded from 50% obtained for 2 g $L^{-1}$ GA alone to 57%, 62%, and 98% for 0.1 mM KBr, 0.1 mM KCl, and 0.5 mM KI, respectively. Good agreement with electrochemical impedance spectroscopy is obtained. Thus combination of GA and KI was selected for further studies.

### 3.2.2 | Synergistic effect of GA with iodide ions

In order to assess the effect of iodide ions additive on the corrosion inhibition of GA for API5L X70 pipeline steel in 0.5 M sulfuric acid solution, electrochemical impedance spectroscopy measurements were undertaken using a fixed concentration of GA (2 g $L^{-1}$) combined with different concentrations of KI (0.1–0.75 mM). The impedance response from these systems is depicted in Figure 7, representing, respectively, the Nyquist, Bode, and the phase angle plots. The results clearly show a distinct effect of the iodide ions additive on the corrosion behavior of API5L X70 pipeline steel compared to the blank acid solution in the absence and the presence of GA alone. In comparison with the GA alone, the size of the semicircle in Nyquist plot (Figure 7a), the impedance of the interface in Bode plot (Figure 7b), and the maximum phase angle in (Figure 7c) all increase on the addition of iodide ions to GA and further increase is observed as the concentration of iodide ion increases. Examination of Figure 7a (Nyquist plot) also revealed that the complex plane impedance consists of one capacitive loop at high frequencies and one inductive loop at low frequency values (that is, two time constants) for the curves obtained for the blank, GA alone, GA + 0.1 mM KI and GA + 0.25 mM KI. However, in the presence of high concentrations of KI (0.5 and 0.75 mM), the inductive loop disappears and the Nyquist plots for GA in combination with 0.5 and 0.75 mM KI systems have only one depressed semicircle, corresponding to one time constant in the Bode plots. The capacitive loop may arise from the time constant of the electrical double layer and the charge transfer resistance while the inductive loop may originate from the relaxation of adsorbed intermediates (in the blank medium) or the adsorption of the inhibiting species (in the presence of inhibitor).[16,38] The existence of the capacitive loops and disappearance of the low frequency inductive loops compared with the Nyquist diagram in the 0.5 M sulfuric acid solutions in absence and presence of GA could be related to the gradual replacement of water molecules and/or hydroxyl ions by halide ions on the surface of the metal and consequently reducing the active sites necessary for the coupled dissolution reaction, involving hydroxyl ions as proposed by Barcia et al.[39] for iron in sulphate-chloride system. Similar view is also held by Bartos et al.[40] for iron in hydrochloric acid and by Okafor et al.[21] for mild steel in sulfuric acid solutions.

Two equivalent circuits shown in Figure 2 were used to fit the experimental data obtained from the impedance measurements. Figure 2 was used for the impedance data characterized by two and one time constants, respectively, and the corresponding electrochemical parameters are listed in Table 4. The results in the table show that addition of iodide ions to 2 g $L^{-1}$ GA increased the charge transfer resistance ($R_t$) from 7.28 Ω $cm^2$ to 25–436 Ω $cm^2$ for 0.1–0.75 mM KI concentration. Also the double layer capacitance ($C_{dl}$) decreased from 650 μF $cm^{-2}$ for 2 g $L^{-1}$ GA to 385, 179, 104, and 100 μF $cm^{-2}$ on addition of 0.1, 0.25, 0.5, and 0.75 mM KI, respectively, to 2 g $L^{-1}$ GA solution. Inhibition efficiency was also found to be upgraded from 52% in the presence of 2 g $L^{-1}$ GA to 86–99% on addition of varying concentrations of (0.1–0.75 mM) KI to 2 g $L^{-1}$ GA solution. The improved inhibition efficiency caused by the addition of iodide ions to GA is due to synergistic effect.

From Figure 3 and Table 2, the corrosion potential ($E_{corr}$) was observed to shift toward more noble potentials with addition of 0.5 mM KI to 2 g $L^{-1}$ GA solution. This shift indicates that inhibitor molecules are more adsorbed on the anodic sites resulting in an inhibition of the anodic reactions. Generally, if the displacement in $E_{corr}$ is >85 mV with respect to $E_{corr}$ in uninhibited solution, the inhibitor can be seen as a cathodic or anodic type.[41,42] In our study the displacement is 60 mV, which indicates that the blend inhibitor GA + 0.5 mM KI acts as a mixed-type inhibitor in sulfuric acid.

In order to evaluate mode of adsorption of GA and combined inhibitor GA + KI on API5L X70 pipeline steel in 0.5 M sulfuric acid, Langmuir, Temkin, and Frumkin adsorption isotherms were evaluated. According to Eq. (5), the Langmuir isotherm is the best fitting for the data, as shown in Figure 8.

It is found that the slope is very close to 1 which indicates the adsorption of GA in combination with KI on API5L X70 pipeline steel surface in 0.5 M sulfuric acid obeys Langmuir adsorption isotherm. The value of $K_{ads}$ can be calculated from intercept of straight lines C/θ axis and the $\Delta G°_{ads}$ value was calculated using Eq. (6). The linear regression parameters are listed in Table 5.

In the present study, the value of $\Delta G°_{ads}$ (−32.49 kJ $mol^{-1}$) is found to be within the range −40 to −20 kJ $mol^{-1}$; probably means that the adsorption of GA combined with KI on API5L X70 pipeline steel surface involves both physical adsorption and chemical adsorption.

The extent of synergism between iodide ions and GA molecules has been analyzed by estimating the synergism parameter $S_1$ which is given by Aramaki and Hackermann in 1964 and used by some authors.[43,44]

$$S_1 = \frac{1 - I_{1+2}}{1 - \grave{I}_{1+2}} \quad (7)$$

Where $I_{1+2} = I_1 + I_2$, $I_1$ is the inhibition efficiency of the iodide ions, The value of inhibition efficiency of 0.5 mM KI for pure iron in 0.5 M sulfuric acid was 84%,[16] and in other study was 78%,[45] $I_2$ is the inhibition efficiency of GA, $\grave{I}_{1+2}$ is the measured inhibition efficiency for the GA in combination with the iodide ions. $S_1$ approaches unity when no interaction between the inhibitor molecules exists, while $S_1 > 1$ indicates a synergistic effect. In case of $S_1 < 1$, antagonistic behavior prevails which may lead to competitive adsorption. The $S_1$ was 1.31 for 0.50 mM KI in presence of 2 g $L^{-1}$ GA in 0.5 M sulfuric acid, suggesting the synergistic action of iodide ions with GA.

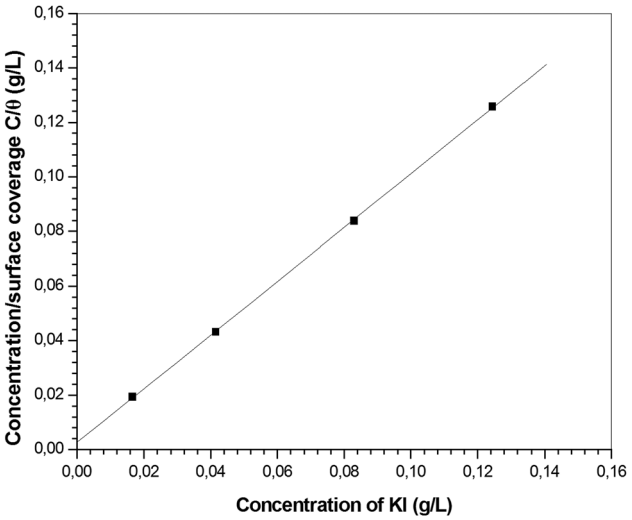


**FIGURE 8** Langmuir adsorption isotherm for API5L X70 in 0.5 M $H_2SO_4$ solution containing 2 g $L^{-1}$ GA combined with different concentrations of KI

### 3.2.3 | Explanation for synergistic effect between gum arabic and iodide ions

First, in sulfuric acid solution, the charge of the metal surface can be determined from the value of $E_{corr}$-$E_{q=0}$ (zero charge potential).[46] The $E_{q=0}$ of iron is −550 mV versus SCE.[47] In the present system, the value of $E_{corr}$ obtained in 0.5 M sulfuric acid is −414 mV versus Ag/AgCl and equal to −414 mV versus SCE. So the steel surface charges positive charge in sulfuric acid solution because of $E_{corr}$-$E_{q=0}$ (zero charge potential) >0. Second, when KI is added into the solution, it will be hydrolyzed to form iodide ion. Because the API5L X70 pipeline steel surface has extra positive charges in blank solution from $E_{q=0}$ analysis, $I^-$ will be firstly adsorb on the metal surface. Third, the interfacial activity of GA is

**TABLE 5** Parameters of Langmuir adsorption isotherm for API5L X70 in 0.5 M $H_2SO_4$ solution containing 2 g $L^{-1}$ GA combined with different concentrations of KI

| Isotherm mode | Linear correlation coefficient | Slope | K (L $g^{-1}$) | $\Delta G°_{ads}$ (kJ $mol^{-1}$) |
|---|---|---|---|---|
| Langmuir | 0.99995 | 0.98657 | 397 | −32.49 |

attributed to their amphiphilic nature since the polysaccharide fractions are highly water soluble, containing hydroxyl functional group (—OH), and carboxyl functional group (—COOH),[48] whereas the protein rich fraction is responsible for their hydrophobic behavior.[49] In acid solution, the carbonyl oxygen (C═O) may be protonated and the molecule exists as a polycation. So GA will form positively charged molecules in sulfuric acid solution.[13] Since the anions of $I^-$ could be specifically adsorbed on the steel surface, thereby given rise to negatively charged steel surface. The formation of positively charged protonated species facilitates adsorption of the compound on the metal surface through electrostatic interaction between the GA molecule and the steel surface (physisorption).

## 3.3 | SEM analysis

Figure 9 presents the surface morphology of polished steel and samples after immersion in 0.5 M sulfuric acid for 96 h in the absence and presence of $2\,g\,L^{-1}$ GA, $2\,g\,L^{-1}$ GA + 0.1 mM KCl, $2\,g\,L^{-1}$ GA + 0.1 mM KBr, and $2\,g\,L^{-1}$ GA + 0.5 mM KI. Figure 9b shows that API5L X70 pipeline steel surface was strongly damaged with deep cavities in the absence of the inhibitor. In presence of $2\,g\,L^{-1}$ GA (Figure 9c), $2\,g\,L^{-1}$ GA + 0.1 mM KCl (Figure 9d), and $2\,g\,L^{-1}$ GA + 0.1 mM KBr (Figure 9e) the samples have smoother surface compared with that of the samples immersed in 0.5 M sulfuric acid with few small notches (pitting corrosion). No damages are observed in the

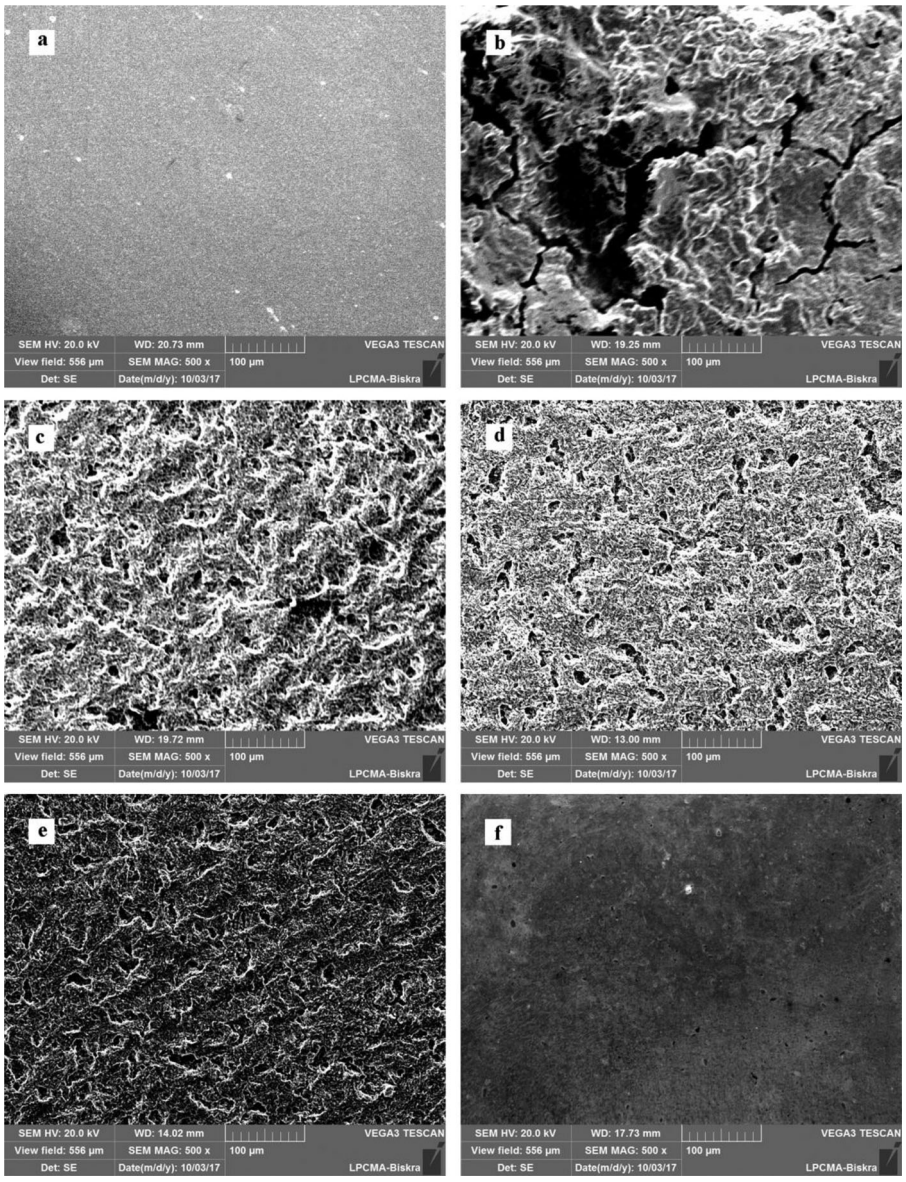


**FIGURE 9** Scanning electron micrographs of API5L X70 surface after 96 h immersion at 30 °C. (a) polished sample without immersion, (b) 0.5 M $H_2SO_4$, (c) 0.5 M $H_2SO_4$ + 2 g $L^{-1}$ GA, (d) 0.5 M $H_2SO_4$ + 2 g $L^{-1}$ GA + 0.1 mM KBr, (e) 0.5 M $H_2SO_4$ + 2 g $L^{-1}$ GA + 0.1 mM KCl, and (f) 0.5 M $H_2SO_4$ + 2 g $L^{-1}$ GA + 0.5 mM KI

micrograph after the addition of 2 g/L GA + 0.5 mM KI to the 0.5 M sulfuric acid solution (Figure 9f). This indicates that the combination of GA and KI hinders the dissolution of iron and thereby reduces the rate of corrosion, and it reveals good protection against corrosion. The less damage of API5L X70 pipeline steel surface when dipped in 0.5 M sulfuric acid containing GA and KI (Figure 9f) might be due to the specific adsorption of iodide ions on the steel which facilitates the adsorption of GA molecules.

## 4 | CONCLUSIONS

The main conclusions are:

1. Synergistic effect was observed between GA and the halides. The best synergistic effect between GA and halide ions was found for the iodide ion, while chloride and bromide ions were in the second place with almost the same degree.
2. The addition of iodide ions enhances the inhibition efficiency of GA significantly, from 52% to 99%.
3. The adsorption of GA alone and in combination with iodide ions on API5L X70 pipeline steel surface in sulfuric acid solution follows Langmuir adsorption isotherm.
4. The potentiodynamic polarization data indicate that GA combined with KI acts as a mixed-type inhibitor in sulfuric acid.
5. The standard adsorption free energy ($\Delta G^{\circ}_{ads}$) indicates that the adsorption of GA involves physical adsorption. While probably physical and chemical adsorption is proposed from the trend of ($\Delta G^{\circ}_{ads}$) which is more negative for the GA combined with KI.
6. The results of EIS indicate that in the presence of high concentrations of KI (from 0.5 mM), the inductive loop disappears and the Nyquist plots for GA in combination with KI systems have only one depressed semicircle, corresponding to one capacitive loop.

## ACKNOWLEDGMENTS

We would like to thank Prof. Dr. Alda Simoes, Miss K. Chafia and Mr. Samir, for their help.

## ORCID

*Mounir Djellab* http://orcid.org/0000-0003-0541-9217

## REFERENCES

[1] A. F. S. Abdul Rahiman, S. Sethumanickam, *Arab. J. Chem.* **2017**, *10*, S3358.
[2] P. Mourya, S. Banerjee, M. M. Singh, *Corros. Sci.* **2014**, *85*, 352.
[3] H. Bentrah, A. Chala, M. Djellab, Y. Rahali, H. Taoui, *Anti-Corr. Methods Mater.* **2017**, *64*, 409.
[4] F. Y. Cui, L. Guo, S. T. Zhang, *Mater. Corros.* **2014**, *65*, 1194.
[5] L. Guo, S. T. Zhang, W. P. Li, G. Hu, X. Li, *Mater. Corros.* **2014**, *65*, 935.
[6] S. Hooshmand Zaferani, M. Sharifi, D. Zaarei, M. R. Shishesaz, *J. Environ. Chem. Eng.* **2013**, *1*, 652.
[7] P. E. Alvarez, M. V. Fiori-Bimbi, A. Neske, S. A. Brandán, C. A. Gervasi, *J. Indus. Eng. Chem.* **2018**, *58*, 92.
[8] C. Kamal, M. G. Sethuraman, *Mater. Corros.* **2014**, *65*, 846.
[9] M. V. Fiori-Bimbi, P. E. Alvarez, H. Vaca, C. A. Gervasi, *Corros. Sci.* **2015**, *92*, 192.
[10] H. Bentrah, Y. Rahali, A. Chala, *Corros. Sci.* **2014**, *82*, 426.
[11] K. Azzaoui, E. Mejdoubi, S. Jodeh, A. Lamhamdi, E. Rodriguez-Castellón, M. Algarra, A. Zarrouk, A. Errich, R. Salghi, H. Lgaz, *Corros. Sci.* **2017**, *129*, 70.
[12] P. Roy, P. Karfa, U. Adhikari, D. Sukul, *Corros. Sci.* **2014**, *88*, 246.
[13] M. M. Solomon, S. A. Umoren, I. I. Udosoro, A. P. Udoh, *Corros. Sci.* **2010**, *52*, 1317.
[14] S. A. Umoren, O. Ogbobe, I. O. Igwe, E. E. Ebenso, *Corros. Sci.* **2008**, *50*, 1998.
[15] Y. Hao, L. A. Sani, T. Ge, Q. Fang, *Corros. Sci.* **2017**, *123*, 158.
[16] S. A. Umoren, Y. Li, F. H. Wang, *Corros. Sci.* **2010**, *52*, 1777.
[17] B. Qian, J. Wang, M. Zheng, B. Hou, *Corros. Sci.* **2013**, *75*, 184.
[18] S. A. Umoren, U. F. Ekanem, *Chem. Eng. Commun.* **2010**, *197*, 1339.
[19] M. Kissi, M. Bouklah, B. Hammouti, M. Benkaddour, *Appl. Surf. Sci.* **2006**, *252*, 4190.
[20] S. A. Umoren, Y. Li, F. H. Wang, *Corros. Sci.* **2010**, *52*, 2422.
[21] P. C. Okafor, Y. Zheng, *Corros. Sci.* **2009**, *51*, 850.
[22] A. Zarrouk, B. Hammouti, T. Lakhlifi, M. Traisnel, H. Vezin, F. Bentiss, *Corros. Sci.* **2015**, *90*, 572.
[23] W. Li, L. Hu, Z. Tao, H. Tian, B. Hou, *Mater. Corros.* **2011**, *62*, 1042.
[24] X. Li, S. Deng, H. Fu, *Corros. Sci.* **2012**, *62*, 163.
[25] M. A. Hegazy, *J. Mol. Liq.* **2015**, *208*, 227.
[26] S. A. Umoren, *J. Mol. Liq.* **2016**, *219*, 946.
[27] F. G. Liu, M. Du, J. Zhang, M. Qiu, *Corros. Sci.* **2009**, *51*, 102.
[28] J. Zhao, G. Chen, *Electrochim. Acta.* **2012**, *69*, 247.
[29] D. M. Basak, M. M. Erman, K. Gülfeza, Y. Birgül, *Anti-Corr. Methods Mater.* **2016**, *63*, 369.
[30] L. Lin, P. Xiaona, X. Jinjuan, Q. Jianhua, *Anti-Corr. Methods Mater.* **2015**, *62*, 353.
[31] B. M. Prasanna, B. M. Praveen, H. Narayana, T. V. Venkatesha, *Anti-Corr. Methods Mater.* **2016**, *63*, 47.
[32] M. M. Solomon, S. A. Umoren, *J. Adhes. Sci. Technol.* **2015**, *29*, 1060.
[33] M. M. Solomon, S. A. Umoren, A. U. Israel, I. G. Etim, *Pigm. Resin Technol.* **2016**, *45*, 280.
[34] M. A. Ameer, A. M. Fekry, *Int. J. Hydrogen Energy.* **2010**, *35*, 11387.
[35] P. Muthukrishnan, B. Jeyaprabha, P. Prakash, *Arab. J. Chem.* **2017**, *10*, S2343.
[36] M. Salah, L. Lahcène, A. Omar, H. Yahia, *Int. J. Indus. Chem.* **2017**, *8*, 263.
[37] Z. A. Iofa, V. V. Batrakov, B. Cho Ngok, *Electrochim. Acta* **1964**, *9*, 1645.

[38] M. S. Morad, A. A. O. Sarhan, *Corros. Sci*. **2008**, *50*, 744.
[39] O. E. Barcia, O. R. Mattos, *Electrochim. Acta*. **1990**, *35*, 1601.
[40] N. H. M. Bartos, *J. Electrochem. Soc*. **1992**, *139*, 3428.
[41] X. Li, S. Deng, H. Fu, *Corros. Sci*. **2009**, *51*, 1344.
[42] E. S. Ferreira, C. Giacomelli, F. C. Giacomelli, A. Spinelli, *Mater. Chem. Phys*. **2004**, *83*, 129.
[43] B. J. Usman, S. A. Umoren, Z. M. Gasem, *J. Mol. Liq*. **2017**, *237*, 146.
[44] Z. Zhang, N. Tian, W. Zhang, X. Huang, L. Ruan, L. Wu, *Corros. Sci*. **2016**, *111*, 675.
[45] S. S. C. Jeyaprabha, S. Muralidharan, G. Venkatachari, *J. Braz. Chem. Soc*. **2006**, *17*, 61.
[46] D. P. Schweinsberg, V. Ashworth, *Corros. Sci*. **1988**, *28*, 539.
[47] S. Deng, X. Li, *Corros. Sci*. **2012**, *55*, 407.
[48] S. S. Banerjee, D.-H. Chen, *J. Hazard. Mater*. **2007**, *147*, 792.
[49] A. Grein, B. C. da Silva, C. F. Wendel, C. A. Tischer, M. R. Sierakowski, A. B. D. Moura, M. Iacomini, P. A. J. Gorin, F. F. Simas-Tosin, I. C. Riegel-Vidotti, *Carbohydr. Polym*. **2013**, *92*, 312.

**How to cite this article:** Djellab M, Bentrah H, Chala A, Taoui H. Synergistic effect of halide ions and gum arabic for the corrosion inhibition of API5L X70 pipeline steel in $H_2SO_4$. *Materials and Corrosion*. 2018;1–12.
https://doi.org/10.1002/maco.201810203

# Anti-Corrosion Methods and Materials

The influence of temperature on the corrosion inhibition of API 5L X42 pipeline steel in HCl medium by gum arabic

Hamza Bentrah, Abdelouahad Chala, Mounir Djellab, Youssouf Rahali, Hicham Taoui,

# The influence of temperature on the corrosion inhibition of API 5L X42 pipeline steel in HCl medium by gum arabic

*Hamza Bentrah*
Department of Mechanical Engineering, University of Biskra, Biskra, Algeria
*Abdelouahad Chala*
Department of Materials Science, University of Biskra, Biskra, Algeria, and
*Mounir Djellab, Youssouf Rahali and Hicham Taoui*
Department of Mechanical Engineering, University of Biskra, Biskra, Algeria

**Abstract**

**Purpose** – This paper aims to investigate the influence of temperature (25-65°C) on the adsorption and the inhibition efficiency of gum arabic (GA) for the corrosion of API 5L X42 pipeline steel in 1M HCl.

**Design/methodology/approach** – Inhibition behaviour on steel in HCl has been studied in relation to the concentration of the inhibitor and the temperature using potentiodynamic polarization curves and electrochemical impedance spectroscopy. Thermodynamic parameters of adsorption were calculated from the viewpoint of adsorption theory.

**Findings** – The results show that at a temperature range from 25 to 65°C, GA was a good inhibitor for API 5L X42 pipeline steel, and its inhibition efficiency was significantly stable. The maximum inhibition efficiency (93 per cent) is obtained at 4 g $L^{-1}$. In absence and presence of GA, there is almost no change in the corrosion mechanism regardless of the temperature. The adsorption of GA on steel surface is an exothermic process. The adsorption of GA involves physical adsorption.

**Practical implications** – The use of GA as an eco-friendly corrosion inhibitor is practical for carbon steel in HCl.

**Originality/value** – The stability of inhibition efficiency of GA at a temperature range from 25 to 65°C could find possible applications in acid pickling, industrial acid cleaning and acid descaling.

**Keywords** EIS, Corrosion inhibitors, API 5L X42 pipeline steel, Gum arabic, Hydrochloric acid, Thermodynamic parameters

**Paper type** Research paper



## 1. Introduction

Acid solutions are used extensively in industries such as acid pickling, industrial acid cleaning, acid descaling and oil well acidizing, leading to serious metallic corrosion. The most commonly used acids are HCl, $H_2SO_4$, $HNO_3$, HF, citric acid, formic acid and acetic acid. HCl is most widely used solvent for water-side deposits on steels. The concentration and temperature vary from 5 to 15 per cent and 50 to 80°C. Per example, it is used preferably not above 65°C to remove calcium carbonate scale (Garverick, 1994).

The use of inhibitors in acid solutions is one of the most economical and practical methods of reducing corrosive attack on metals. For an inhibitor treatment to be effective, it should meet certain criteria, such as:

- It must protect the entire metal from corrosion.
- Low concentrations of the inhibitor must be effective.
- The inhibitor must be effective under a wide range of conditions such as pH, temperature, heat flux and water quality.
- It should not produce deposits on the metal surface that impede heat transfer.
- The treatment must be environmentally acceptable toxicity for discharge.
- It must prevent formation of carbonate and sulfate scales.
- It must combat biological activity due to microorganisms (Sastri, 2012).

The effect of temperature on corrosion is a complex function. A change in temperature can affect kinetics and mechanism of metal dissolution and oxide formation and adsorption and desorption. Thus, change in temperature can:

- increase the corrosion inhibition [aqueous coffee ground extracts (Torres *et al.*, 2011), aqueous garlic peel extract (de Assunção Araújo Pereira *et al.*, 2012), Phyllanthus amarus extracts (Okafor *et al.*, 2008), the extract of Salvia officinalis leaves (Soltani *et al.*, 2012)];
- decrease the corrosion inhibition [acidic lignin (Yahya *et al.*, 2015), *Thymus satureioides* essential oils (Bammou *et al.*, 2010), marigold flower extract (Mourya *et al.*, 2014),

The current issue and full text archive of this journal is available on Emerald Insight at: **www.emeraldinsight.com/0003-5599.htm**

Anti-Corrosion Methods and Materials
64/4 (2017) 409–417

[DOI 10.1108/ACMM-11-2016-1734]

Received 26 November 2016
Accepted 16 March 2017

seed extract of *Psidium guajava* (Kumar *et al.*, 2011), mustard seed extract (Umoren, 2016a), date palm (*Phoenix dactylifera*) leaf extract (Umoren *et al.*, 2015)]; or

- have no effect on corrosion inhibition [bipyrazole derivative (Hmamou *et al.*, 2015)].

In continuation of our research for finding natural organic compounds with high corrosion inhibition efficiency (Bentrah *et al.*, 2014), the present paper deals with the temperature effect on the effectiveness of gum arabic (GA) as a green inhibitor against the corrosion of API 5L X42 pipeline steel in 1M HCl at a temperature range from 25 to 65°C.

## 2. Experimental

### 2.1 Material

The test material was API 5L X42 pipeline steel in the form of disc shape, with the following chemical composition (weight percentage): C 0.2 max, Mn 1.18 max, Si 0.1 min, P 0.025 max, S 0.01 max, Cr 0.4 max, Ni 0.4 max, Nb 0.035 max, Ti 0.02 max and the balance Fe. The samples were mounted in Teflon and had a surface area of 0.785 $cm^2$. Exposed surface of each sample was prepared by wet grinding with silicon carbide abrasive papers (grade 320–500–600–800), rinsed with distilled water and degreased with acetone.

### 2.2 Medium

The concentration of the corrosive medium was 1M prepared from AR grade 37 per cent HCl. All preparations were made using distilled water.

### 2.3 Inhibitor

Dried GA powder, exuded by *Acacia Senegal* trees, was selected for the present study.

### 2.4 Electrochemical techniques

Two electrochemical techniques, namely, potentiodynamic polarization and electrochemical impedance spectroscopy (EIS), were used to study the corrosion behaviour of API 5L X42 pipeline steel, without and with GA, in 1M HCl. All experiments were performed in the one-compartment cell with three electrodes connected to a Radiometer PGZ301 potentiostat with Volta Master 4 software. The working electrode (WE) was carbon steel. Platinum disc was used as the counter electrode, and a saturated calomel electrode (SCE) coupled to a fine Luggin capillary was used as the reference electrode. Before measurement, the WE was immersed in test solution at open circuit potential (OCP) for 1 h to be sufficient to attain a stable state.

The potential of potentiodynamic polarization curves was started from a potential of −700 to −300 mV vs SCE at a sweep rate of 0.3 mV $s^{-1}$. Corrosion current density Icorr ($\mu$A $cm^{-2}$) was calculated from Stern–Geary equation (Gu *et al.*, 2013):

$$I_{corr} = \frac{|b_a| \times |b_c|}{2.3 \times (|b_a| + |b_c|) \times Rp}, \quad (1)$$

where $b_c$ and $b_a$ are the cathodic and anodic Tafel slopes, respectively, and $R_p$ is the polarization resistance ($\Omega$ $cm^2$). Because of the presence of a degree of nonlinearity in the Tafel slope part of the obtained polarization curves, the Tafel constants were calculated as a slope of the points after Ecorr by ±50 mV. The values of inhibition efficiency $\eta_{pol}$ was calculated using the following equation:

$$\eta_{pol}\ \% = \frac{Icorr - Icorr\ (inh)}{Icorr} \times 100, \quad (2)$$

where $I_{corr}$ and $I_{corr\ (inh)}$ represent corrosion current density values without and with inhibitor, respectively. The surface coverage ($\theta$) is defined by $\eta_{pol}$ per cent/100.

EIS was carried out at OCP in the frequency range from 20 kHz to 50 mHz using a 10 mV peak-to-peak voltage excitation. Inhibition efficiency $\eta_{EIS}$ is calculated on the basis of the equation:

$$\eta_{EIS}\% = \frac{Rt - \acute{R}t}{Rt} \times 100 \quad (3)$$

where Rt and $\acute{R}t$ are charge transfer resistances values in the presence and absence of GA, respectively.

## 3. Results and discussion

### 3.1 Effect of temperature on corrosion kinetics of API 5L X42 pipeline steel with and without gum arabic

The kinetic parameters for steel in 1M HCl solution at 25°C, 35°C, 45°C and 65°C in the absence and presence of GA are given in Table I and Table II. Table I shows the respective kinetic parameters including corrosion current density ($I_{corr}$), corrosion potential ($E_{corr}$), cathodic Tafel slope ($b_c$), anodic Tafel slope ($b_a$), polarization resistance $R_p$ and inhibition efficiency obtained from potentiodynamic polarization method ($\eta_{pol}$). Table II shows the impedance parameters including charge transfer resistance $R_t$, double-layer capacitance Cdl and inhibition efficiency obtained from the EIS method ($\eta_{EIS}$). The potentiodynamic polarization curves and Nyquist plots for API 5L X42 pipeline steel in 1M HCl without and with different concentrations of GA at 25°C are available in a previous study (Bentrah *et al.*, 2014).

#### *3.1.1 Effect of temperature on the mechanism of steel dissolution without gum arabic*

From Table I, the corrosion rate (Icorr) increases with temperature. The increase was more than 15 times from 25 to 65°C. From Figure 1(a), it is clear that with increasing temperature, the anodic and cathodic curves were observed to shift to a higher current density, i.e. an increase in the corrosion rate. The parallel cathodic Tafel lines suggested that the temperature does not modify the hydrogen evolution mechanism and the reduction of $H^+$ ions at the steel surface, which occurs mainly through a charge transfer mechanism. From Table II, the charge transfer resistance (Rt) decreases and the double-layer capacitance (Cdl) increases with increasing the temperature, i.e. an increase in the corrosion rate of steel. From Figure 1(b), the Nyquist plots are characterized by one capacitive semicircle with the centers below the real axis, showing that the corrosion process was charge transfer controlled in HCl corrosive medium

**Table I** Corrosion parameters obtained from potentiodynamic polarization method for API 5L X42 pipeline steel in 1 M HCl containing various concentrations of Gum Arabic at different temperatures

| T (°C) | C (g $L^{-1}$) | Ecorr (mV) | Icorr ($\mu$A $cm^{-2}$) | ba (mV $dec^{-1}$) | −bc (mV $dec^{-1}$) | Rp ($\Omega$ $cm^2$) | $\eta_{EIS}$ (%) |
|---|---|---|---|---|---|---|---|
| **25** | 0 | −503 | 501 | 89 | 116 | 43.7 | – |
| | 0.1 | −493 | 275 | 66 | 99 | 62.6 | 43 |
| | 0.5 | −491 | 90 | 69 | 113 | 205 | 82 |
| | 1 | −495 | 63 | 81 | 119 | 315 | 87 |
| | 2 | −480 | 34 | 77 | 129 | 560 | 93 |
| | 4 | −480 | 33 | 79 | 106 | 600 | 93 |
| **35** | 0 | −453 | 1,293 | 79 | 98 | 14.7 | – |
| | 0.1 | −459 | 684 | 59 | 98 | 23.4 | 47 |
| | 0.5 | −451 | 284 | 57 | 93 | 54 | 78 |
| | 1 | −461 | 170 | 65 | 89 | 96 | 86 |
| | 2 | −463 | 126 | 70 | 109 | 147 | 90 |
| | 4 | −474 | 85 | 64 | 95 | 195 | 93 |
| | 5 | −483 | 88 | 65 | 96 | 190 | 93 |
| **45** | 0 | −440 | 2,226 | 81 | 108 | 9 | – |
| | 0.1 | −445 | 1,254 | 57 | 94 | 12.3 | 43 |
| | 0.5 | −446 | 514 | 57 | 94 | 30 | 77 |
| | 1 | −453 | 265 | 52 | 95 | 55.1 | 88 |
| | 2 | −467 | 215 | 71 | 98 | 83.1 | 90 |
| | 4 | −472 | 144 | 51 | 104 | 103.4 | 93 |
| | 5 | −477 | 137 | 53 | 100 | 110 | 93 |
| **65** | 0 | −448 | 7,760 | 81 | 119 | 2.7 | – |
| | 0.1 | −446 | 4,324 | 75 | 111 | 4.5 | 44 |
| | 0.5 | −438 | 2,018 | 58 | 133 | 8.7 | 74 |
| | 1 | −449 | 1,010 | 55 | 142 | 17.5 | 87 |
| | 2 | −442 | 0695 | 56 | 134 | 24.7 | 91 |
| | 4 | −463 | 0546 | 64 | 141 | 35 | 93 |
| | 5 | −462 | 538 | 66 | 139 | 35.2 | 93 |

(Umoren, 2016a). Good agreement between EIS and potentiodynamic polarization curves is obtained.

*3.1.2 Effect of temperature on the corrosion inhibition of steel by gum arabic*

In a previous work (Bentrah *et al.*, 2014), we noticed that at 25°C, when the concentration of GA is less than 2 g $L^{-1}$, the inhibition efficiency increases sharply with an increase in concentration, while a further increase causes no appreciable change in performance. This behaviour applies to the rest of the temperatures, except 4 g $L^{-1}$ of GA. It is apparent from Table I that with increasing temperature, the corrosion current density ($I_{corr}$) increases, the polarization resistance ($R_p$) decreases and the values of inhibition efficiency of GA are nearly constant ($\eta_{pol}$ = 93 per cent). GA inhibitor efficiency is temperature-independent. From Figures 2(a), (c) and (e) and Figure 3(a), in the presence of GA with increasing temperature, the slight change of both bc and ba in acid solution indicates that the corrosion mechanism of steel does not change.

As shown in Figures 2(b), (c) and (f) and Figure 3(b), with increasing temperature in inhibited 1M HCl solutions, the impedance spectra exhibit one single capacitive loop, which indicates that the corrosion of steel is mainly controlled by the charge transfer process (Zarrouk *et al.*, 2015, Hegazy *et al.*, 2012). The shape is maintained in the temperature range studied, indicating that there is almost no change in the corrosion mechanism regardless of the temperature. It is noted that these capacitive loops are not perfect semicircles which can be attributed to different physical phenomena such as roughness and homogeneities of the solid surfaces, impurities, grain boundaries and distribution of the surface active sites (Behpour *et al.*, 2010). The values of inhibition efficiency obtained by EIS are nearly constant in the temperature range studied ($\eta_{EIS}$ = 93 per cent). Good agreement between EIS and potentiodynamic polarization curves is obtained.

### 3.2 Activation energy calculations

The activation energy (Ea) values for the corrosion of API 5L X42 pipeline steel in the absence and presence of different concentrations of GA were calculated using Arrhenius equation (Shukla and Quraishi, 2010):

$$\log (I_{corr}) = \left(\frac{-Ea}{2.303RT}\right) + A, \quad (4)$$

where R is the universal gas constant, T is the experimental temperature, A is the pre-exponential factor and Icorr is corrosion rate calculated by equation (1). A plot [Figure 4(a)] of log($I_{corr}$) versus 1/T gives a straight lines with the slope of –Ea/2,303R, from which the activation energies were calculated and are listed in Table III.

**Table II** Corrosion parameters obtained from electrochemical impedance spectroscopy method for API 5L X42 pipeline steel in 1 M HCl containing various concentrations of Gum Arabic at different temperatures

| T (°C) | C (g $L^{-1}$) | Cdl ($\mu$F) | Rt ($\Omega$ $cm^2$) | $\eta_{pol}$ (%) |
|---|---|---|---|---|
| **25** | 0 | 148.0 | 43.6 | – |
| | 0.1 | 109.2 | 61.5 | 41 |
| | 0.5 | 89.7 | 209 | 79 |
| | 1 | 65.8 | 315 | 86 |
| | 2 | 34.8 | 560 | 92 |
| | 4 | 32.8 | 600 | 93 |
| **35** | 0 | 341 | 16 | – |
| | 0.1 | 220 | 26 | 38 |
| | 0.5 | 198 | 42 | 62 |
| | 1 | 151 | 84.5 | 81 |
| | 2 | 105 | 146 | 89 |
| | 4 | 90 | 176 | 91 |
| | 5 | 81 | 198 | 91 |
| **45** | 0 | 471 | 8.2 | – |
| | 0.1 | 279 | 13.4 | 38 |
| | 0.5 | 196 | 31.4 | 74 |
| | 1 | 169 | 59 | 86 |
| | 2 | 113 | 91 | 91 |
| | 4 | 96 | 109 | 92 |
| | 5 | 85 | 123 | 93 |
| | 0 | 821 | 2.7 | – |
| **65** | 0.1 | 569 | 4 | 32 |
| | 0.5 | 471 | 8.2 | 67 |
| | 1 | 236 | 17.4 | 84 |
| | 2 | 150 | 25.7 | 89 |
| | 4 | 111 | 36.4 | 93 |
| | 5 | 114 | 36.6 | 93 |

The enthalpy of activation ($\Delta H^*$) and the entropy of activation ($\Delta S^*$) for the corrosion of steel in HCl were obtained by applying the transition-state equation (Ostovari *et al.*, 2009):

$$\log \frac{I_{corr}}{T} = \left[\log\left(\frac{R}{hN}\right) + \left(\frac{\Delta S^*}{2,303R}\right)\right] - \left(\frac{\Delta H^*}{2,303RT}\right), \quad (5)$$

where h is the Planck's constant and N is the Avogadro's number. Figure 4(b) shows a plot of $\log(I_{corr}/T)$ versus 1/T. Straight lines are obtained with a slope of $\Delta H^*/2.303R$, and from the intercepts of $\log(I_{corr}/T)$-axis, $\Delta S^*$ values were calculated and are given in Table III. The values of Ea generally in the studied range of GA concentration are higher for the inhibited solutions than for the uninhibited solutions, indicating an inhibitive action for the inhibitor by increasing the energy barrier for the corrosion process, emphasizing on the electrostatic character of the inhibitor's adsorption (physisorption) on the steel surface (Solomon *et al.*, 2010; Noor and Al-Moubaraki, 2008). The values of Ea are larger than the analogous values of $\Delta H^*$, indicating that the corrosion process must involve a gaseous reaction, simply the hydrogen evolution reaction, associated with a decrease in the total reaction volume. Moreover, for all systems, the average value of the difference Ea − $\Delta H^*$ is about 2.6 kJ $mol^{-1}$, which is approximately around the average value of RT (2.69 kJ $mol^{-1}$), where T is in the range of the experimental temperatures, indicating that the corrosion process is a unimolecular reaction and is characterized by the following equation (Noor, 2007):

**Figure 1** (a) Potentiodynamic polarization curves and (b) Nyquist plots for API 5L X42 pipeline steel in 1 M HCl without GA at 25, 35, 45 and 65°C

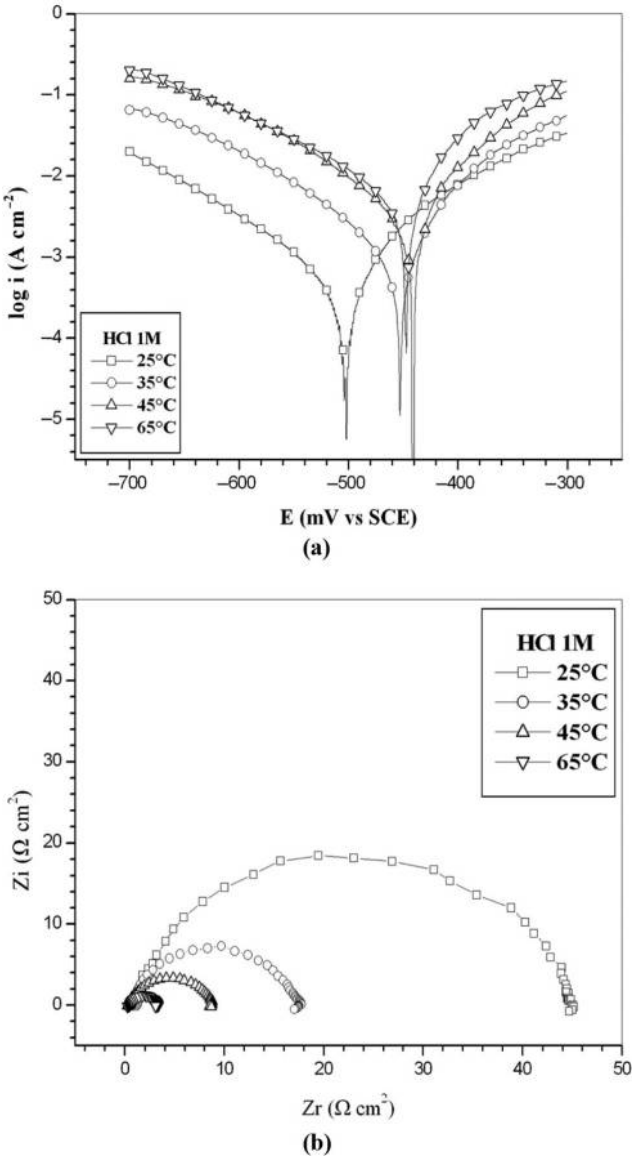


$$Ea - \Delta H^* = RT. \quad (6)$$

The positive signs of the enthalpy ($\Delta H^*$) reflected the endothermic nature of the steel dissolution process and indicated that the dissolution of steel was difficult (Hegazy *et al.*, 2012). The values of entropy of activation ($\Delta S^*$) are large and negative both in the uninhibited and inhibited systems, which implies that the activated complex in the rate determining step represents an associated rather than dissociation step, meaning that a decrease in disorder takes

**Figure 2** Potentiodynamic polarization curves and Nyquist plots for API 5L X42 pipeline steel in 1 M HCl with different concentrations of GA at 35, 45 and 65°C

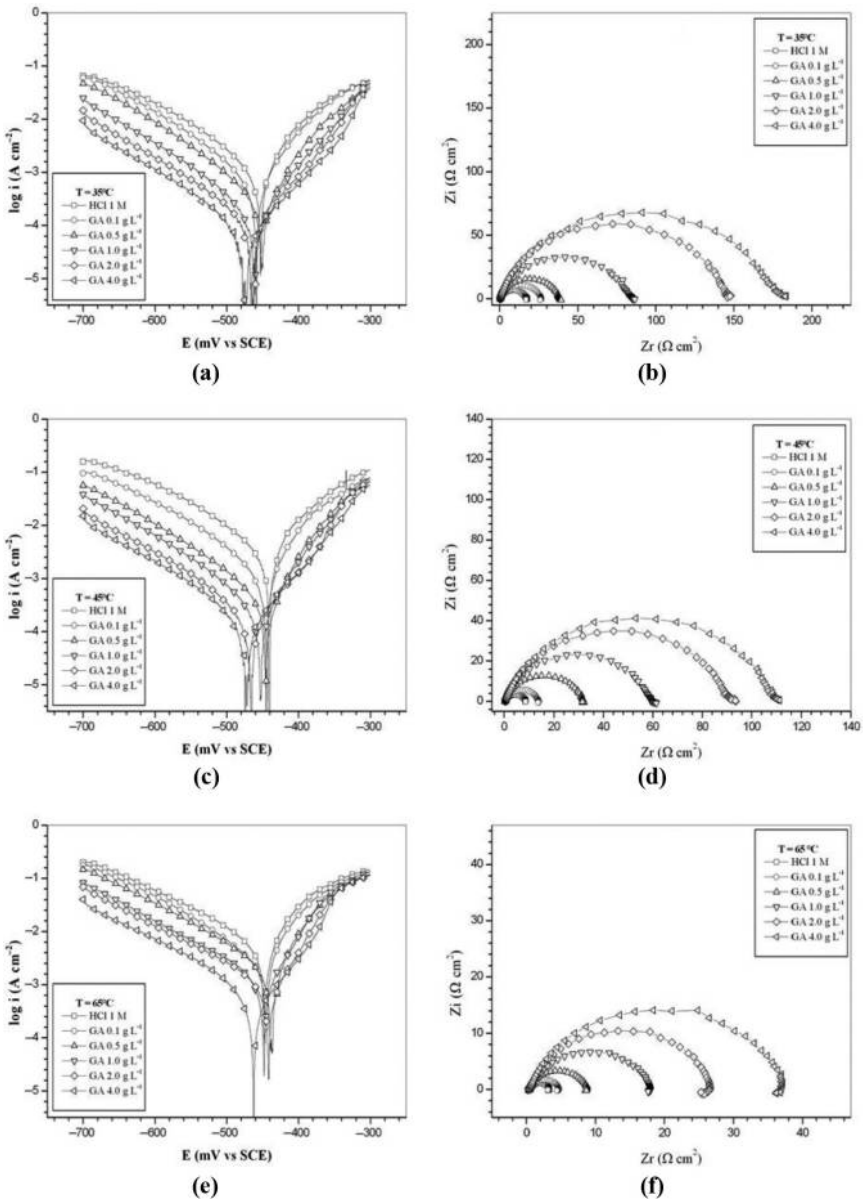


place on going from reactants to the activated complex. Thus, a greater degree of orderliness appears during its transformation from reactant to activated complex (Solomon *et al.*, 2010).

### 2.3 Adsorption isotherm behaviour

Basic information dealing with the interaction between the inhibitor molecule and metal surface can be provided by adsorption isotherm. In the present study, several adsorption isotherms were assessed, and the Langmuir adsorption isotherm was found to give the best description of the adsorption behaviour of the studied inhibitor. A correlation between surface coverage ($\theta = \eta_{pol}$ per cent/100) and the concentration of inhibitor (C) in electrolyte can be represented by the Langmuir adsorption isotherm (El Azzouzi *et al.*, 2016).

$$\frac{C}{\theta} = \frac{1}{K_{ads}} + C, \tag{7}$$

where $K_{ads}$ is constant of adsorption. Plots of $C/\theta$ with C at 25°C, 35°C, 45°C and 65°C yield a straight line with slope values very close to 1 (Figure 5).

From the values of the adsorption constant, $K_{ads}$, the standard free energy of adsorption ($\Delta G^{\circ}_{ads}$) are determined using the following equation (Roy *et al.*, 2014, Umoren, 2016b):

$$\Delta G^{\circ}_{ads} = RT \ln (1 \times 10^3 K_{ads}), \tag{8}$$

where $1 \times 10^3$ is the concentration of water molecules expressed in g $L^{-1}$, R is the universal gas constant and T is

**Figure 3** (a) Potentiodynamic polarization curves and (b) Nyquist plots for API 5L X42 pipeline steel in 1 M HCl with 4 g $L^{-1}$ GA at 25, 35, 45 and 65°C

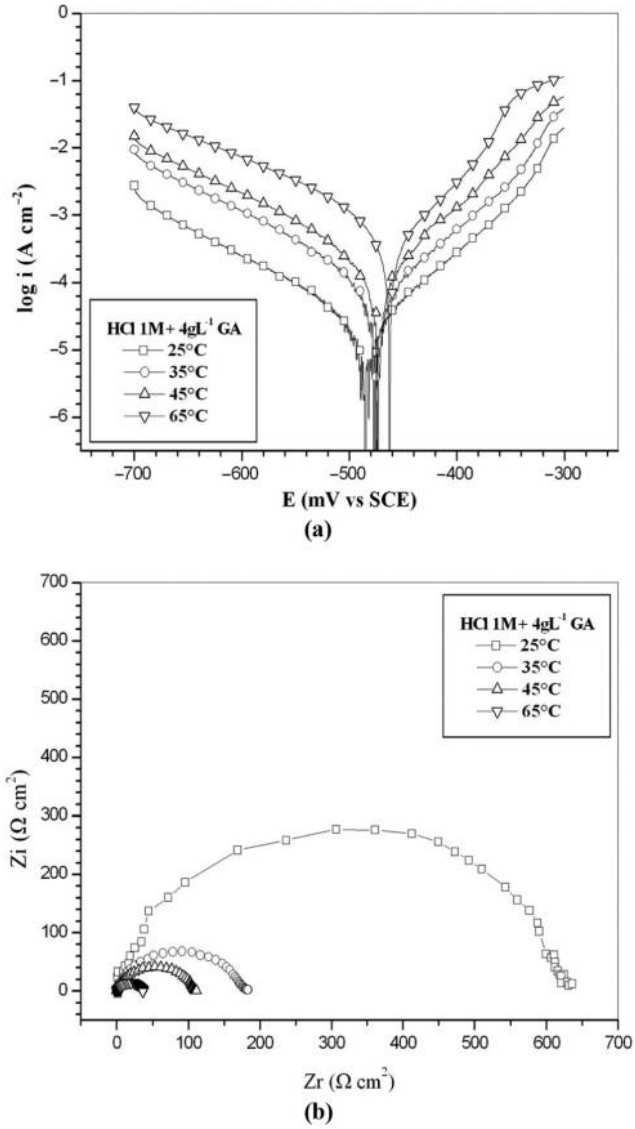


**Figure 4** (a) Arrhenius plots of log($I_{corr}$) versus 1/T at different concentrations of Gum Arabic; (b) Transition-state plots of log($I_{corr}$/T) versus 1/T in 1 M HCl in absence and presence of various concentrations of Gum Arabic

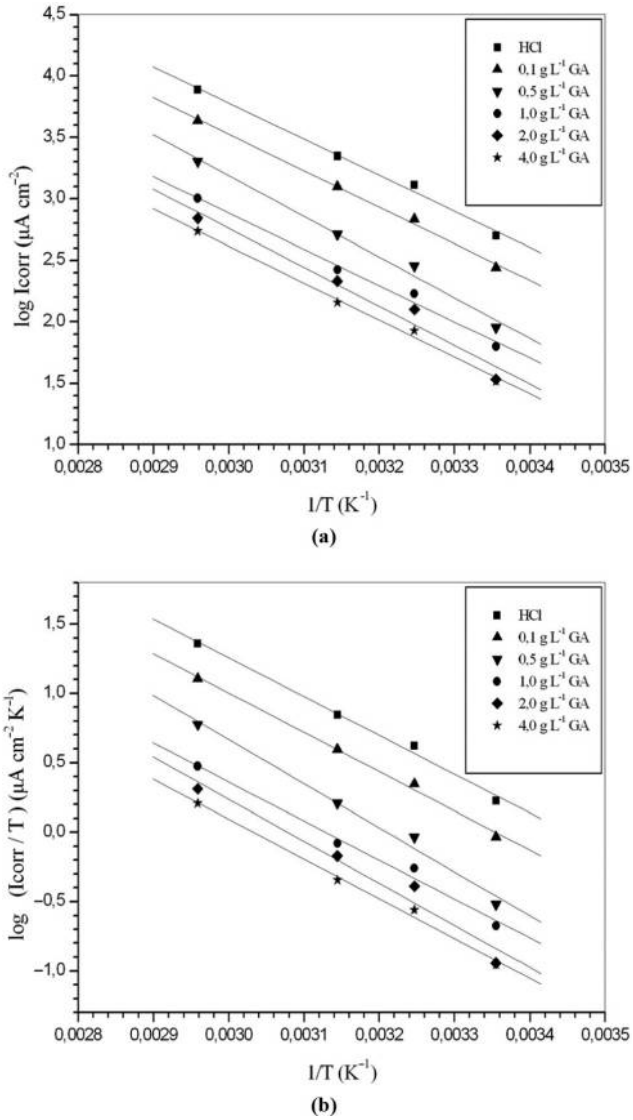


the absolute temperature. The values of $\Delta G^{\circ}_{ads}$ and $K_{ads}$ are listed in Table IV. The negative values of $\Delta G^{\circ}_{ads}$ indicate the stability of the adsorbed layer on the steel surface and spontaneity of the adsorption process.

Tang *et al.* (2003) reported that it was difficult for the inhibitor (neutral red) to adsorb onto the steel surface when the $\Delta G^{\circ}_{ads}$ increases with an increase in temperature; this phenomenon once again indicated that the adsorption was unfavorable with increasing experimental temperature as the result of the desorption of inhibitor from the steel surface. It was commonly believed that simple adsorption on bare surface was generally an exothermic process which was accompanied by a decrease in $\Delta G^{\circ}_{ads}$. In this case, the same results were obtained. The standard adsorption enthalpy ($\Delta H^{\circ}_{ads}$) could be calculated on the basis of Van't Hoff equation:

**Table III** The values of activation parameters Ea, $\Delta H^*$ and $\Delta S^*$ for API 5L X42 pipeline steel in 1 M HCl in the absence and presence of different concentrations of Gum Arabic

| C (g $L^{-1}$) | Ea (KJ $mol^{-1}$) | $\Delta H^*$(KJ $mol^{-1}$) | $\Delta S^*$(J $mol^{-1}K^{-1}$) |
|---|---|---|---|
| **0** | 56.1 | 53.5 | −51 |
| **0.1** | 56.8 | 54.1 | −54 |
| **0.5** | 63 | 60.7 | −56 |
| **1** | 56.4 | 53.7 | −67 |
| **2** | 60.6 | 58 | −57 |
| **4** | 57.5 | 54.8 | −69 |

**Figure 5** Langmuir isotherm adsorption mode of GA on the API 5L X42 pipeline steel surface in 1 M HCl at (a) 25°C, (b) 35°C, (c) 45°C and (d) 65°C

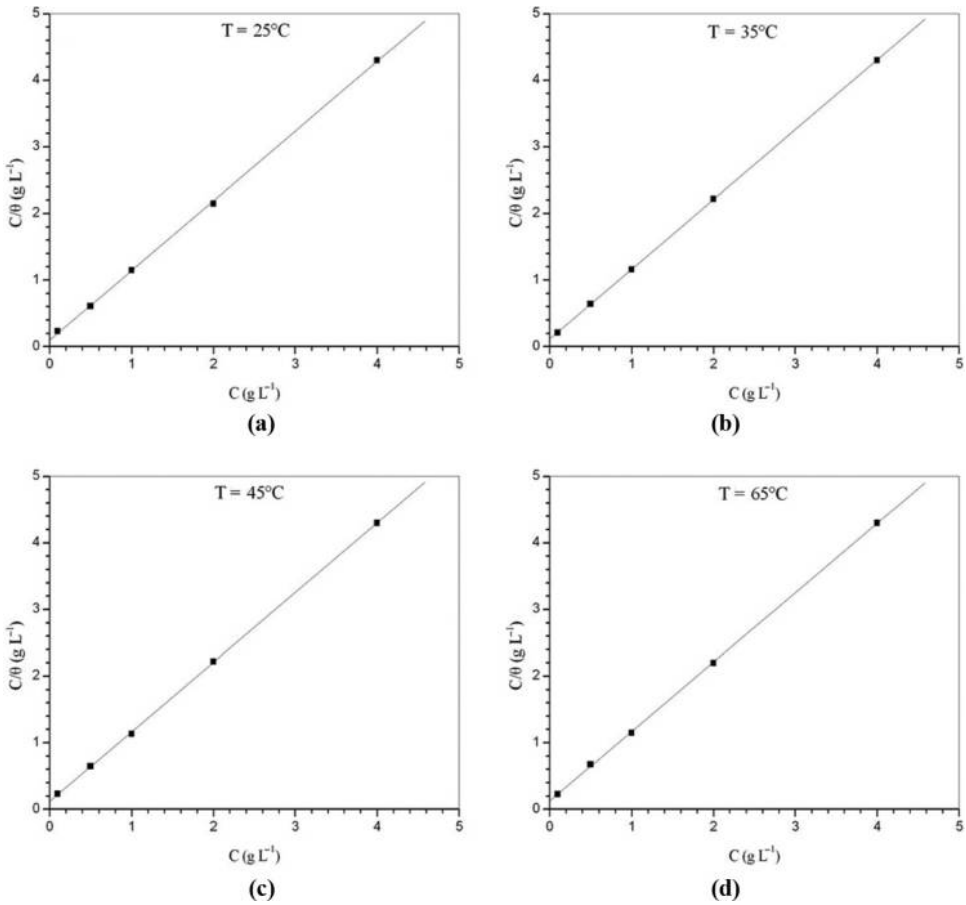


$$\frac{d \ln K_{ads}}{dT} = \frac{\Delta H^{\circ}_{ads}}{RT^2}, \tag{9}$$

where R is the gas constant, T the absolute temperature and $K_{ads}$ is the adsorptive equilibrium constant. Equation (9) can also be changed as follows:

$$\ln K_{ads} = \frac{-\Delta H^{\circ}_{ads}}{RT} + D, \tag{10}$$

where D is integration constant. It should be noted that $-\Delta H^{\circ}_{ads}/R$ is the slope of the straight line $\ln K_{ads}$ versus 1/T according to equation (10). $\Delta H^{\circ}_{ads}$ is calculated from the slope.

**Table IV** Adsorption parameters for Gum Arabic calculated from Langmuir adsorption isotherm for API 5L X42 pipeline steel in 1 M HCl solution at 25-65°C

| T (°C) | $K_{ads}$(L $g^{-1}$) | $\Delta G^{\circ}_{ads}$ (kJ/mol) | $\Delta H^{\circ}_{ads}$ (kJ/mol) | $\Delta S^{\circ}_{ads}$ (J/mol k) | Coefficient de régression linéaire de $\Delta G^{\circ}_{ads}$ |
|---|---|---|---|---|---|
| **25** | 10.03 | −22.8 | −4.6 | 61 | 0.999 |
| **35** | 8.7 | −23.2 | | 60.3 | 0.999 |
| **45** | 8.4 | −23.8 | | 60.3 | 0.999 |
| **65** | 7.9 | −25.2 | | 60.9 | 0.999 |

With the obtained both parameters of $\Delta G^{\circ}_{ads}$ and $\Delta H^{\circ}_{ads}$, the standard adsorption entropy ($\Delta S^{\circ}_{ads}$) can be calculated using the following thermodynamic basic equation:

$$\Delta S^{\circ}_{ads} = \frac{\Delta H^{\circ}_{ads} - \Delta G^{\circ}_{ads}}{T}. \tag{11}$$

The values of $\Delta H^{\circ}_{ads}$ and $\Delta S^{\circ}_{ads}$ are listed in Table IV.

The positive values of $\Delta S^{\circ}_{ads}$ mean that the adsorption process is accompanied by an increase in entropy, which is the driving force for the adsorption of inhibitor onto the carbon steel surface (Hegazy *et al.*, 2012). Bentiss *et al.* (2005) reported that if $\Delta H^{\circ}_{ads} > 0$, then adsorption is chemisorption, and if $\Delta H^{\circ}_{ads} < 0$, then it can be either physisorption or chemisorption. Further, in the exothermic process, physisorption can be distinguished from chemisorption on the basis of the magnitude of $\Delta H^{\circ}_{ads}$. For physisorption, the enthalpy of adsorption is usually less than 40 kJ $mol^{-1}$, and for chemisorption, it is greater than 100 kJ$mol^{-1}$ (Zarrouk *et al.*, 2016). Results show that the enthalpy of adsorption is small and negative (−4.6 kJ$mol^{-1}$), which means that the adsorption is physisorption.

It is worthwhile to note that when the inhibition efficiency increases with the elevated temperature, chemisorption may play a major role during the adsorption process of inhibitor on

steel surface (Oguzie *et al.*, 2004; Liao *et al.*, 2016), which does not involve conformity with the present study.

## 4. Conclusions

The main conclusions are as follows:

- GA acts as a good inhibitor for the corrosion of API 5L X42 pipeline steel in 1M HCl, and the inhibition efficiency increases with the inhibitor concentration, but it is almost constant with rise in temperature, and the maximum value is 93 per cent at 4 g $L^{-1}$ GA. GA inhibitor efficiency is temperature-independent.
- Results of polarization and EIS studies suggest that in absence and presence of GA, there is almost no change in the corrosion mechanism regardless of the temperature.
- The values of $\Delta G^{\circ}_{ads}$ decrease (becomes more negative) with an increase in temperature, and the negative value of $\Delta H^{\circ}_{ads}$ indicates the occurrence of an exothermic process.
- The values of Ea and $\Delta H^{\circ}_{ads}$ indicate that the adsorption of GA involves physical adsorption.
- Langmuir adsorption isotherm was found to give the best description of the adsorption behaviour of the studied inhibitor at a temperature range from 25 to 65°C.

## References

Bammou, L., Chebli, B., Salghi, R., Bazzi, L., Hammouti, B., Mihit, M. and Idrissi, H. (2010), "Thermodynamic properties of thymus satureioidesessential oils as corrosion inhibitor of tinplate in 0.5 M HCl: chemical characterization and electrochemical study", *Green Chemistry Letters and Reviews*, Vol. 3 No. 3, pp. 173-178.

Behpour, M., Ghoreishi, S.M., Mohammadi, N., Soltani, N. and Salavati-Niasari, M. (2010), "Investigation of some Schiff base compounds containing disulfide bond as HCl corrosion inhibitors for mild steel", *Corrosion Science*, Vol. 52 No. 12, pp. 4046-4057.

Bentiss, F., Lebrini, M. and Lagrenée, M. (2005), "Thermodynamic characterization of metal dissolution and inhibitor adsorption processes in mild steel/2,5-bis(n-thienyl)-1,3,4-thiadiazoles/hydrochloric acid system", *Corrosion Science*, Vol. 47 No. 12, pp. 2915-2931.

Bentrah, H., Rahali, Y. and Chala, A. (2014), "Gum Arabic as an eco-friendly inhibitor for API 5L X42 pipeline steel in HCl medium", *Corrosion Science*, Vol. 82, pp. 426-431.

de Assunção Araújo Pereira, S.S., Pêgas, M.M., Fernández, T.L., Magalhães, M., Schöntag, T.G., Lago, D.C., de Senna, L.F. and D'Elia, E. (2012), "Inhibitory action of aqueous garlic peel extract on the corrosion of carbon steel in HCl solution", *Corrosion Science*, Vol. 65, pp. 360-366.

El Azzouzi, M., Aouniti, A., Tighadouin, S., Elmsellem, H., Radi, S., Hammouti, B., El Assyry, A., Bentiss, F. and Zarrouk, A. (2016), "Some hydrazine derivatives as corrosion inhibitors for mild steel in 1.0M HCl: weight loss, electrochemichal, SEM and theoretical studies", *Journal of Molecular Liquids*, Vol. 221, pp. 633-641.

Garverick, L. (1994), *Corrosion in the Petrochemical Industry*, ASM International.

Gu, K., Lv, L., Lu, Z., Yang, H., Mao, F. and Tang, J. (2013), "Electrochemical corrosion and impedance study of SAE1045 steel under gel-like environment", *Corrosion Science*, Vol. 74, pp. 408-413.

Hegazy, M.A., Hasan, A.M., Emara, M.M., Bakr, M.F. and Youssef, A.H. (2012), "Evaluating four synthesized Schiff bases as corrosion inhibitors on the carbon steel in 1M hydrochloric acid", *Corrosion Science*, Vol. 65, pp. 67-76.

Hmamou, D.B., Salghi, R., Zarrouk, A., Zarrok, H., Touzani, R., Hammouti, B. and El Assyry, A. (2015), "Investigation of corrosion inhibition of carbon steel in 0.5M $H_2SO_4$ by new bipyrazole derivative using experimental and theoretical approaches", *Journal of Environmental Chemical Engineering*, Vol. 3, pp. 2031-2041.

Kumar, K.P.V., Pillai, M.S.N. and Thusnavis, G.R. (2011), "Seed extract of Psidium Guajava as ecofriendly corrosion inhibitor for carbon steel in hydrochloric acid Medium", *Journal of Materials Science & Technology*, Vol. 27 No. 12, pp. 1143-1149.

Liao, L.L., Mo, S., Lei, J.L., Luo, H.Q. and Li, N.B. (2016), "Application of a cosmetic additive as an eco-friendly inhibitor for mild steel corrosion in HCl solution", *Journal of Colloid and Interface Science*, Vol. 474, pp. 68-77.

Mourya, P., Banerjee, S. and Singh, M.M. (2014), "Corrosion inhibition of mild steel in acidic solution by Tagetes erecta (Marigold flower) extract as a green inhibitor", *Corrosion Science*, Vol. 85, pp. 352-363.

Noor, E.A. (2007), "Temperature effects on the corrosion inhibition of mild steel in acidic solutions by aqueous extract of fenugreek leaves", *International Journal of Electrochemical Science*, Vol. 2, pp. 996-1017.

Noor, E.A. and Al-Moubaraki, A.H. (2008), "Thermodynamic study of metal corrosion and inhibitor adsorption processes in mild steel/1-methyl-4[4′(-X)-styryl pyridinium iodides/hydrochloric acid systems", *Materials Chemistry and Physics*, Vol. 110, pp. 145-154.

Oguzie, E.E., Unaegbu, C., Ogukwe, C.N., Okolue, B.N. and Onuchukwu, A.I. (2004), "Inhibition of mild steel corrosion in sulphuric acid using indigo dye and synergistic halide additives", *Materials Chemistry and Physics*, Vol. 84, pp. 363-368.

Okafor, P.C., Ikpi, M.E., Uwah, I.E., Ebenso, E.E., Ekpe, U.J. and Umoren, S.A. (2008), "Inhibitory action of phyllanthus amarus extracts on the corrosion of mild steel in acidic media", *Corrosion Science*, Vol. 50 No. 8, pp. 2310-2317.

Ostovari, A., Hoseinieh, S.M., Peikari, M., Shadizadeh, S.R. and Hashemi, S.J. (2009), "Corrosion inhibition of mild steel in 1 M HCl solution by henna extract: a comparative study of the inhibition by henna and its constituents (Lawsone, Gallic acid, α-d-Glucose and Tannic acid)", *Corrosion Science*, Vol. 51, pp. 1935-1949.

Roy, P., Karfa, P., Adhikari, U. and Sukul, D. (2014), "Corrosion inhibition of mild steel in acidic medium by polyacrylamide grafted Guar gum with various grafting percentage: effect of intramolecular synergism", *Corrosion Science*, Vol. 88, pp. 246-253.

Sastri, V.S. (2012), *Green Corrosion Inhibitors: Theory and Practice*, Wiley.

Shukla, S.K. and Quraishi, M.A. (2010), "The effects of pharmaceutically active compound doxycycline on the corrosion of mild steel in hydrochloric acid solution", *Corrosion Science*, Vol. 52 No. 7, pp. 314-321.

Solomon, M.M., Umoren, S.A., Udosoro, I.I. and Udoh, A.P. (2010), "Inhibitive and adsorption behaviour of carboxymethyl cellulose on mild steel corrosion in sulphuric acid solution", *Corrosion Science*, Vol. 52 No. 4, pp. 1317-1325.

Soltani, N., Tavakkoli, N., Khayatkashani, M., Jalali, M.R. and Mosavizade, A. (2012), "Green approach to corrosion inhibition of 304 stainless steel in hydrochloric acid solution by the extract of Salvia officinalis leaves", *Corrosion Science*, Vol. 62, pp. 122-135.

Tang, L., Mu, G. and Liu, G. (2003), "The effect of neutral red on the corrosion inhibition of cold rolled steel in 1.0 M hydrochloric acid", *Corrosion Science*, Vol. 45 No. 10, pp. 2251-2262.

Torres, V.V., Amado, R.S., de Sá, C.F., Fernandez, T.L., Riehl, C.A.d.S., Torres, A.G. and D'Elia, E. (2011), "Inhibitory action of aqueous coffee ground extracts on the corrosion of carbon steel in HCl solution", *Corrosion Science*, Vol. 53, pp. 2385-2392.

Umoren, S.A. (2016a), "Biomaterials for corrosion protection: evaluation of mustard seed extract as eco-friendly corrosion inhibitor for X60 steel in acid media", *Journal of Adhesion Science and Technology*, Vol. 30 No. 17, pp. 1858-1879.

Umoren, S.A. (2016b), "Polypropylene glycol: a novel corrosion inhibitor for ×60 pipeline steel in 15 per cent HCl solution", *Journal of Molecular Liquids*, Vol. 219, pp. 946-958.

Umoren, S.A., Gasem, Z.M. and Obot, I.B. (2015), "Date palm (Phoenix dactylifera) leaf extract as an eco-friendly corrosion inhibitor for carbon steel in 1M hydrochloric acid solution", *Anti-Corrosion Methods and Materials*, Vol. 62, pp. 19-28.

Yahya, S., Othman, N.K., Daud, A.R., Jalar, A. and Ismail, R. (2015), "The influence of temperature on the inhibition of carbon steel corrosion in acidic lignin", *Anti-Corrosion Methods and Materials*, Vol. 62, pp. 301-306.

Zarrouk, A., Hammouti, B., Lakhlifi, T., Traisnel, M., Vezin, H. and Bentiss, F. (2015), "New 1H-pyrrole-2,5-dione derivatives as efficient organic inhibitors of carbon steel corrosion in hydrochloric acid medium: electrochemical, XPS and DFT studies", *Corrosion Science*, Vol. 90, pp. 572-584.

Zarrouk, A., Zarrok, H., Ramli, Y., Bouachrine, M., Hammouti, B., Sahibed-dine, A. and Bentiss, F. (2016), "Inhibitive properties, adsorption and theoretical study of 3,7-dimethyl-1-(prop-2-yn-1-yl)quinoxalin-2(1H)-one as efficient corrosion inhibitor for carbon steel in hydrochloric acid solution", *Journal of Molecular Liquids*, Vol. 222, pp. 239-252.

## Corresponding author

**Hamza Bentrah** can be contacted at: hamzacorrsci@gmail.com

**الملخص:**

تتميز مثبطات التآكل المستخدمة في الصناعة البترولية بكونها مواد سامة ومسرطنة وباهظة الثمن بالإضافة إلى صعوبة تحللها بعد الاستخدام، حاليا تتركز الدراسات في هذا المجال على إيجاد بدائل تتميز بـ : انعدام السمية، قابلية التحلل الحيوي، رخيصة الثمن و متوفرة من مصادر متجددة ، تتوفر جميع هذه الصفات في المركبات العضوية الطبيعية. من اجل ذلك، أنجزت دراسة فاعلية التثبيط لمادة راتنج الفلفل البيروفي *(BRSM)* كمثبط تآكل الفولاذ *API 5L X70* في حمض كلور الماء *(HCl)* وحمض الكبريت *($H_2SO_4$)* باستخدام تقنيات الكهروكيميائية وتقنيات تحليل السطح بواسطة جهاز المسح الالكتروني SEM. أيضا، تمت دراسة التضافر بين ايون اليود *(KI)* والمثبط *(BRSM)*. تبين النتائج أن المثبط يعمل كمثبط مختلط مع كفاءة تثبيط تصل الى 94% في وسط حمض كلور الماء و70% في وسط حمض الكبريت. ادمصاص مثبط (BRSM) على سطح الفولاذ يتبع ادمصاص لانغمير الحراري. تبين نتائج تحليل السطح كفاءة تثبيط عالية لراتنج الفلفل البيروفي على سطح الفولاذ *(API 5L X70)*. يوجد توافق كبير بين نتائج التقنيات الكهروكيميائية ونتائج تحليل السطح.

**الكلمات المفتاحية :**

مثبط بيئي للتآكل، راتنج الفلفل البيروفي، الفولاذ، تقنيات الكهروكيميائية، مجهر المسح الالكتروني، حمض.

**Abstract:**

Corrosion inhibitors used in the petroleum industry are characterized as toxic, carcinogenic, and expensive materials in addition to the difficulty of their decomposition after use. Currently, studies in this field are focused on finding alternatives characterized by: non toxicity, biodegradability, low price and availability from renewable sources. All these properties are available in natural organic compounds. Therefore, a study was conducted about the inhibition efficiency of the Bark Resin of Shinus Molle (BRSM) as an API 5L X70 steel corrosion inhibitor in hydrochloric acid and sulfuric acid by using electrochemical techniques and surface analysis (SEM). Also, the synergetic effect between the iodine ion (KI) and the inhibitor (BRSM) has been studied. The results show that the inhibitor acts as a mixed inhibitor with an inhibition efficiency of 94% in the hydrochloric acid and 70% in the sulfuric acid medium. The adsorption of BRSM inhibitor on steel surface follows Langmuir isotherm adsorption. The surface analysis results also show a high inhibition efficiency of the bark resin of Shinus molle on the steel surface (API 5L X70).Therefore, there is a great agreement between the results of electrochemical techniques and the results of surface analysis.

**Keywords:**

Eco-friendly inhibitor, bark resin of Shinus molle, API 5L X70 steel, electrochemical techniques, SEM, acid.

**Résumé :**

Les inhibiteurs de corrosion utilisés dans l'industrie pétrolière sont considérés comme des matériaux toxiques, cancérigènes et coûteux en plus de la difficulté de leur décomposition après utilisation. Actuellement, les études dans ce domaine se basent sur la recherche d'alternatives caractérisées par: la non toxicité, la biodégradabilité, pas cher et la disponibilité à partir de sources renouvelables. Toutes ces propriétés sont disponibles dans les composés organiques naturels. Par conséquent, une étude a été menée sur l'efficacité inhibitrice de la *Bark Resine of Shinus Molle (BRSM)* en tant qu'inhibiteur de corrosion de l'acier API 5L X70 dans l'acide chlorhydrique et l'acide sulfurique en utilisant des techniques électrochimiques et une analyse de surface (MEB). De plus, l'effet synergique entre l'ion iode (KI) et l'inhibiteur (BRSM) a été étudié. Les résultats montrent que l'inhibiteur agit comme un inhibiteur mixte avec une efficacité inhibitrice de 94% dans l'acide chlorhydrique et 70% dans le milieu acide sulfurique. L'adsorption de l'inhibiteur BRSM sur la surface en acier suit l'adsorption isotherme de Langmuir. Les résultats de l'analyse de surface montrent également une grande efficacité d'inhibition de la résine d'écorce de Shinus molle sur la surface de l'acier (API 5L X70). Ainsi, il existe un grand accord entre les résultats des techniques électrochimiques et les résultats de l'analyse de surface.

**Mots clé:**

Inhibiteur écologique, *Bark Resine of Shinus Molle (BRSM)*, acier API 5L X70, techniques électrochimique, MEB, acide.